Proceedings of the Workshop on Directional Acoustic Sensors

Sponsored by the

**Naval Undersea Warfare Center Division
and
Office of Naval Research**

**17-18 April 2001
Newport, Rhode Island**

**Prepared by
Naval Undersea Warfare Center
Division Newport
1176 Howell Street
Newport, RI 02841**

**Dr. Benjamin A. Cray
Naval Undersea Warfare Center
Division Newport**

**Dr. Roy C. Elswick
Office of Naval Research**

Report Documentation Page	*Form Approved* *OMB No. 0704-0188*

Public reporting burden for the collection of information is estimated to average 1 hour per response, including the time for reviewing instructions, searching existing data sources, gathering and maintaining the data needed, and completing and reviewing the collection of information. Send comments regarding this burden estimate or any other aspect of this collection of information, including suggestions for reducing this burden, to Washington Headquarters Services, Directorate for Information Operations and Reports, 1215 Jefferson Davis Highway, Suite 1204, Arlington VA 22202-4302. Respondents should be aware that notwithstanding any other provision of law, no person shall be subject to a penalty for failing to comply with a collection of information if it does not display a currently valid OMB control number.

1. REPORT DATE **18 APR 2001**	2. REPORT TYPE **Proceedings**	3. DATES COVERED **17-04-2001 to 18-04-2001**

4. TITLE AND SUBTITLE **Proceedings of the Workshop on Directional Acoustic Sensors**	5a. CONTRACT NUMBER
	5b. GRANT NUMBER
	5c. PROGRAM ELEMENT NUMBER
6. AUTHOR(S) **Benjamin Cray; Roy Elswick; Gerald D'Spain; Thomas Gabrielson; Manuel Silvia**	5d. PROJECT NUMBER
	5e. TASK NUMBER
	5f. WORK UNIT NUMBER
7. PERFORMING ORGANIZATION NAME(S) AND ADDRESS(ES) **Naval Undersea Warfare Center, Division Newport,1176 Howell Street,Newport,RI,02841-1708**	8. PERFORMING ORGANIZATION REPORT NUMBER
9. SPONSORING/MONITORING AGENCY NAME(S) AND ADDRESS(ES) **Naval Undersea Warfare Center, 1176 Howell Street, Newport, RI, 02842-1708**	10. SPONSOR/MONITOR'S ACRONYM(S) **NUWC**
	11. SPONSOR/MONITOR'S REPORT NUMBER(S)

12. DISTRIBUTION/AVAILABILITY STATEMENT
Approved for public release; distribution unlimited

13. SUPPLEMENTARY NOTES
NUWC2015

14. ABSTRACT
The Workshop on Directional Acoustic Sensors provided a forum for the technical exchange of ideas and experience in the use of directional acoustic sensors for undersea applications. Researchers from academia, industry, and government research laboratories presented their current work on the theory, design, and application of various types of directional acoustic sensors. This workshop, which was held in Newport, Rhode Island, builds upon the 1995 Workshop on Acoustic Particle Velocity Sensors??? by addressing progress and new theories in the area of multi-component directional acoustic sensors.

15. SUBJECT TERMS
multi-component directional acoustic sensors; directional acoustical sensors

16. SECURITY CLASSIFICATION OF:			17. LIMITATION OF ABSTRACT	18. NUMBER OF PAGES	19a. NAME OF RESPONSIBLE PERSON
a. REPORT **unclassified**	b. ABSTRACT **unclassified**	c. THIS PAGE **unclassified**	**Same as Report (SAR)**	**160**	

Standard Form 298 (Rev. 8-98)
Prescribed by ANSI Std Z39-18

FOREWORD*

The *Workshop on Directional Acoustic Sensors* provided a forum for the technical exchange of ideas and experience in the use of directional acoustic sensors for undersea applications. Researchers from academia, industry, and government research laboratories presented their current work on the theory, design, and application of various types of directional acoustic sensors. This workshop, which was held in Newport, Rhode Island, builds upon the 1995 Workshop on Acoustic Particle Velocity Sensors[†] by addressing progress and new theories in the area of multi-component directional acoustic sensors.

Twelve invited papers were presented during the two-day workshop. A poster session was also conducted in which various organizations presented overviews of specific directional sensor applications. Spirited discussions explored issues important in the development and application of directional sensors. Several of the invited papers pointed out the Taylor expansion representation of the acoustic field, the first three terms of which represent the scalar, vector, and tensor (or dyadic) components of the field, referred to by some as zero-, first-, and second-order tensor components. Topics ranged from system noise characteristics of sensors measuring these components to the signal processing of their outputs. Studies on the mechanical design and mounting of various forms of these sensors were described. Some designs comprised acoustic motion-sensors, whereas others are essentially fixed-sensors that measure gradients of various order acoustic components. Other papers provided results of current and past research on the use of these sensors in various applications: ocean acoustics; hull-mounted and towed-sonar arrays; and deployed acoustic sensors (i.e., DIFAR systems). Development plans and application results of forming certain combinations of these acoustic sensor orders were also presented, including the use of acoustic intensity probes in sound scattering measurements. New transduction materials (single crystals) were also described, showing promise for advancing the performance and design of vector and higher-order acoustic sensors.

---

*The following proceedings papers were published "as is" and were not reviewed or edited by the Workshop Committee.

[†]"Acoustic Particle Velocity Sensors: Design, Performance, and Applications," *AIP Conference Proceedings 368*, Mystic, Connecticut, 1995, M. J. Berliner and J. F. Lindberg (eds.), American Institute of Physics Press, New York, 1996.

It is hoped that these proceedings* will stimulate further research in this engaging area of underwater acoustics. Directional acoustic sensors show considerable potential for enhancing undersea acoustic measurements in a variety of commercial and military applications. Much work remains to realize the full promise of these versatile sensors.

Dr. Benjamin A. Cray, NUWC
Workshop Co-Chairman

Dr. Roy C. Elswick, ONR
Workshop Co-Chairman

A workshop speaker, Dr. Boris Aronov, Chief Scientist at BTech Acoustics, Inc., and Research Professor of Acoustics at the University of Massachusetts, Dartmouth, describes the features of a directional acoustic sensor component currently being evaluated for underwater applications.

Scientists and engineers with a broad range of experience and interests discussed the design and use of directional acoustic sensors for ocean observations and organic sensing applications.

---

*Bookmark and thumbnail views are available under the Window menu to aid the electronic reading of this *Adobe Acrobat* document. (Please note that this document was prepared for screen optimization.)

WORKSHOP ON DIRECTIONAL ACOUSTIC SENSORS

Welcoming Remarks:
> **Dr. Richard Nadolink**, Naval Undersea Warfare Center Division
> **Dr. James McEachern**, Office of Naval Research

Speakers:

Dr. Gerald D'Spain, Scripps Institute of Oceanography:
> *Directional Underwater Acoustic Sensor Work at the Marine Physical Laboratory*

Dr. Thomas Gabrielson, ARL, Pennsylvania State University
> *Design Problems and Limitations in Directional Sensors*

Dr. Benjamin Cray, Naval Undersea Warfare Center Division
> *Directional Acoustic Receivers: Signal and Noise Characteristics*

Dr. Manuel Silvia, SITTEL Corporation
> *Signal Processing Considerations for a General Class of Directional Acoustic Sensors*

Dr. James McConnell, Acoustech Corporation
> *Development of a Pressure-Acceleration Underwater Acoustic Intensity Probe*

Dr. Gerald Lauchle, Pennsylvania State University
> *Acoustic Intensity Scattered from an Elliptic Cylinder*

Mr. Mike Higgins, RDA, Inc.
> *DIFAR System Overview*

Dr. Richard Keltie, North Carolina State University
> *Vector Sensor Modeling and Support Bracket Design*

Dr. David Brown, University of Massachusetts, Dartmouth
Dr. Boris Aronov, University of Massachusetts, Dartmouth, and BTECH Acoustics
> *Acoustic Pressure Gradient Sensors: Motion and Fixed Types*

Dr. Paul Wlodkowski and **Dr. Fred Schloss**, Wilcoxon Research
> *Advanced in Acoustic Particle Velocity Sensorics*

Mr. P. David Baird, EDO Corporation
> *EDO Directional Acoustic Sensor Technology*

Dr. Bruce Abraham, Anteon Corporation
> *Directional Hydrophones in Towed System*

NUWC Overview

Presented by:
Dr Richard H Nadolink

Chief Technology Officer
Naval Undersea Warfare Center
Division Newport

01-NUWC-GRA/0080U.M1   0321-TLW

NUWC

Entire Undersea Warfare System for all Submarine Missions

Tactical Warfare System for Surface Ship USW

OUR REASON FOR BEING
- Understand technical implications of military problems
- Help industry successfully develop appropriate products
- Determine that responsible solutions are delivered
- Ensure rapid response to critical Fleet needs
- Lay foundation for Navy after next

BY PROVIDING
- Connectivity between warfighter and technical community
- Technical competency for integrity of total warfighting system
- Full access to our intellectual and facility resources
- Close liaison with industry and academia

Nation's only asset dedicated to undersea warfare

01-NUWC-GRA/0080U.M2   0321-TLW

Key Player Throughout the Entire Life Cycle

NAVSEA

Research & Development

Prototyping

Undersea Warfare Analysis

INNOVATION

Fleet Support

Test & Evaluation

Systems Development

Acquisition Support
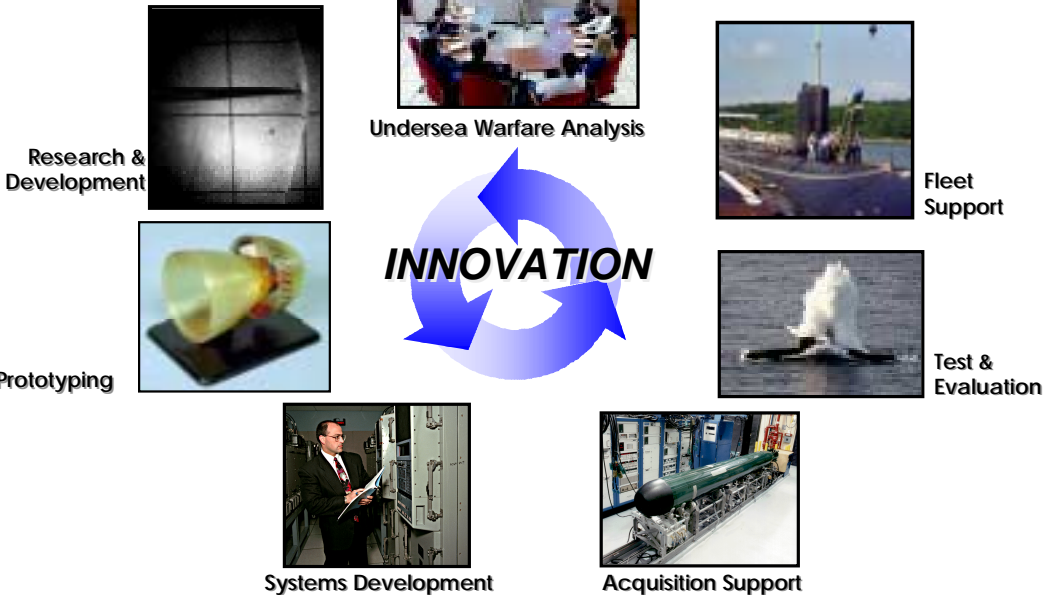
We support 60 years of undersea technology

Our Customer Base

NAVSEA

Spectrum of Customers

- **Fleet**
- **Program and resource sponsors**
  - NAVSEA, PEOs, CNO, SPAWAR
- **Scientific sponsors**
  - (e.g., ONR, DARPA)
- **Intelligence community**
  - (e.g., ONI)
- **Defense industry**
  - (e.g., EB, Boeing)
- **Non-defense industry**
- **Foreign Navies**
  - (e.g., Australia, UK, Germany)

We are a NWCF Activity

- **Customers decide where to buy products and services**
- **NUWC is accountable for efficient delivery of products and services**

By Resource Sponsor

17% N091 T&E and Tech Reqmt

2% N6 SPAWAR

5% Other

65% Submarine Warfare Division N77

11% N76 Surface Warfare
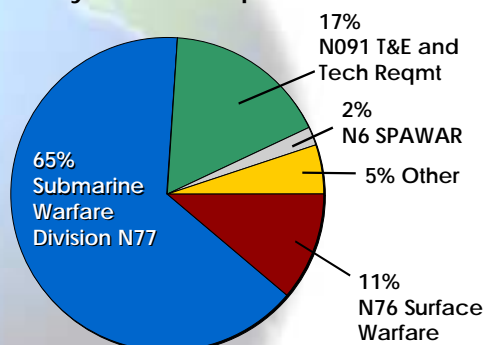
$673M Direct (FY00)

Provide best value to our customers

Our People

Bar chart:
- FY92: Total Onboard ~4300, S&E Onboard ~2800 (57% S&E)
- FY99: Total Onboard ~2800, S&E Onboard ~1900 (64% S&E)
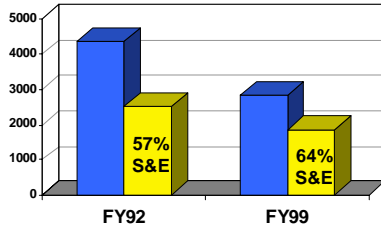
Legend: Total Onboard | S&E Onboard

Pie chart:
- Engineers/Scientists (67%)
- Professional Admin. (16%)
- Tech Support (9%)
- Clerical (4%)
- Admin. Support (3%)
- Wage Grade (1%)
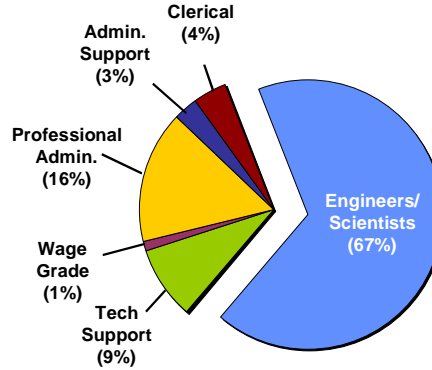
42% of our S&E have advanced degrees

FY00
Civilian   2643
Military   29

CAPABILITIES IN USW

Spheres of Excellence (labeled circles):
- Submarine Combat and Combat Control Systems
- Undersea Weapons, UUVs, Targets, Launchers and CMs
- Submarine/Surface Ship USW Surveillance
- Submarine-Unique Communications, ESM and Electro-optics
- Undersea Warfare Modeling And Analysis
- Undersea Tactical Ranges

Center: **Since 1984 — EXCELLENCE**

Capabilities list:
- Acoustic sensors, transducers, and arrays
- Signal processing
- Structural acoustics
- Information processing
- Torpedo and UUV propulsion and signature control
- Weapon systems targeting and control
- Submarine electromagnetics, antennas, electro-optics and communications
- Undersea vehicle guidance and control
- Hydrodynamics
- Ocean physics
- Undersea range technology
- Warfare modeling, simulation and analysis
- Large scale numerical modeling and analysis
- System engineering/cost & operational effectiveness analysis
- Undersea materials technology (metrology)

Spheres of Excellence = Core S&T Competencies
NUWC maintains special expertise, facilities, and equipment in
15 technical disciplines to ensure "world class" capability.

Towed Array Technology (R)Evolution
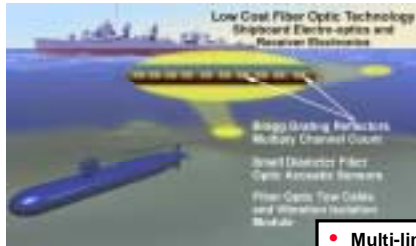
- Low Cost
- Commonality
- Wide Acoustic Bandwidth
- High Dynamic Range
- Immunity to EMI

6.3a ADVANCED TECHNOLOGY DEMONSTRATION

- Multi-line
- Adaptive Beamforming
- Array Element Location
- Array Motion Compensation
- Low Tension Handling Technology

1990s

6.2 EXPLORATORY DEVELOPMENT

- High Speed Low Self-Noise Arrays
- Small Diameter Arrays
- Digital Telemetry
- Array Shape Estimation
- Hydrodynamic Aperture Formation
- Passive Localization

1980s

6.1 RESEARCH

- Flow Noise Models
- Identification of Noise Mechanisms

1970s

ONR VERTICAL S&T INTEGRATION FOR MULTIPLATFORMS

01-NUWC-GRA/0264U.M8

The Undersea Superiority of Tomorrow's Fleet Resides with Us Today

Vector Sensor Workshop
Newport, RI 17 - 18 April 2001

James McEachern

ONR321 SS

Sensors, Sources and Arrays

703-696-6462

mceachj@onr.navy.mil

Vector Sensor Workshop

- The sensors
- The signal
- The noise
- The Payoff?
- *The Way Forward...*

Vector Sensors

- DIFAR sonobuoys -

  " over 2 million served…"

  – HPA evolved to velocity sensors
  – 10 Hz dp/dx over 1.5M aperture
    - element matching vs bearing accuracy
    - packaging volume limitation
  – Pressure & pressure gradient,
  – Pressure & particle velocity
  – Pressure & particle acceleration

Higher Order Sensors
pressure isn't everything...

  – Higher order acoustic sensors
    - Exploit additional acoustic parameters
    - Larger apparent aperture
      – 1st product theorem
      – more gain per unit length
    - Intensity/ vector sensors
      – detect energy flow
      – sense reactive signal
      – reverb suppression?
      – DI ~ 3 to 4.7 dB
    - Strain rate/tensor sensors
      – DI = 9.5 dB
  – Applications & application issues

p-u dot type ...
acoustic vector
sensor

Measures
three (3)
components of
the acoustic
intensity
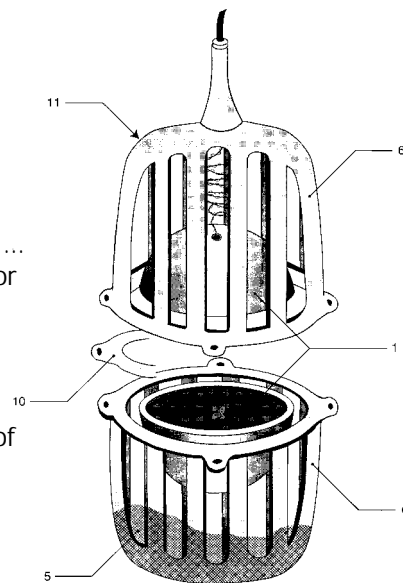
Sensor Issues

- Infer $q_{\text{order } n}$ from order (n-1) sensors
- N^{th} order sensor { p; dp/dx; du/dx }
  - Array of $(N-1)^{th}$ order sensors
  - "Monolithic" tensor sensor ?

acoustic tensor sensor

Each corner is a 3-axis velocity probe

"monolithic" tensor sensor
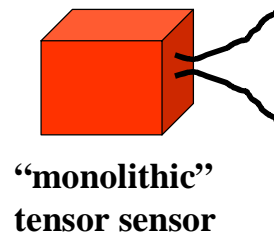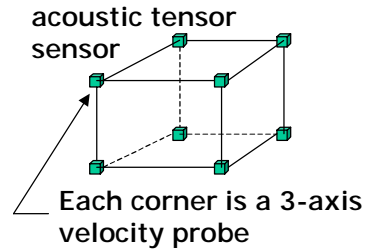
Higher Order Parameters
Interrelationship & the Environment

- p,u, du/dt, du/dx, *I*
- phase relationships
- Noise
  - •u noise
  - •phase noise
  - •strain rate noise
- correlation
  - •temporal
  - •spatial
  - •auto-
  - •cross-

Phase between Pressure and Velocity in x-direction (ka=20,a=1,b=0.2,angle=60)
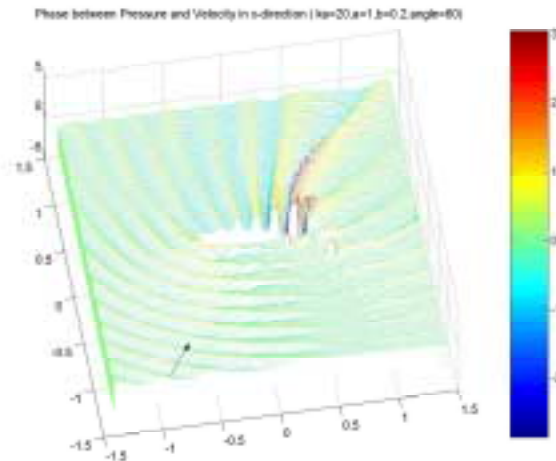
Phase between *p* and u_x for 60-deg. incidence.

G.C. Lauchle, 2001

Interesting Questions… *(we hope)*

- What phenomena to measure?
- What sensors to use?
- How do we build the sensors?
- What are the sensor characteristics?
- How do we use the data?
- What is the nature of the signal and noise data in the tensor domain?
- Are there signal and noise discriminators?

Vector Sensor Workshop

Objectives

- Status of acoustic vector sensor research

   What do we know about acoustic vector sensors?

- Areas for future research

   What are the interesting issues in:
   – *vector sensors*
   – *higher order acoustic parameters*

Directional Underwater Acoustic Sensor Work at the Marine Physical Lab

Gerald L. D'Spain
William S. Hodgkiss
Marine Physical Laboratory
Scripps Institution of Oceanography
San Diego, California 92152

Directional Underwater Acoustic Sensor Work

at the Marine Physical Lab

Gerald L. D'Spain and William S. Hodgkiss

Marine Physical Laboratory
Scripps Institution of Oceanography
San Diego, CA 92152

ABSTRACT

Several sensor systems that simultaneously measure the underwater acoustic pressure and particle velocity fields ("vector sensors") have been designed and deployed at sea by the Marine Physical Laboratory over the past few decades. These systems include the set of 12 freely drifting, neutrally buoyant Swallow floats, the 16-element vertical DIFAR (actually "TRIFAR") array, and a set of moored, flow-shielded DIFAR sonobuoy systems for measuring nearshore acoustics. In addition, standard Navy DIFAR 53D sonobuoys have been deployed in many experiments. Examples of the measurements made by these sensor systems are presented to illustrate their scientific usefulness. The framework for the analysis of the data is provided both by the energetics of acoustic fields and by array processing with single-spatial-point measurements. Special emphasis here is placed on the reactive acoustic intensity, i.e., the energy flux required to support the spatial structure in the acoustic field. Ideas for extending the vector sensor concept to a new "tensor sensor" also are presented.

INTRODUCTION

The purpose of this paper is to summarize work done at the Marine Physical Lab (MPL) in directional acoustic sensors. Sect. I briefly describes some of the ocean acoustic vector sensor systems designed, built, and/or deployed at sea by MPL. The basic equations and approach used in the analysis of the directional sensor data are presented in Sect. II. Sect. III contains a brief overview of some of the scientific results obtained with the use of vector sensor data. At-sea data from four different directional sensor systems deployed in four different ocean acoustics experiments are presented. The ideas behind, and the benefits of, a new design "tensor sensor" are discussed in Sect. IV. We hope to be able to build such a system in the near future. Finally, a few concluding remarks are given in Sect. V.

I. OVERVIEW OF MPL VECTOR SENSOR SYSTEMS

A. Freely Drifting Swallow Floats

The Swallow floats are autonomous, neutrally buoyant sensor systems that simultaneously measure the three components of acoustic particle velocity and acoustic pressure in the 0.3 to 20 Hz frequency band. They drift freely along with the prevailing ocean current to reduce contamination from relative flow past the sensor, a well-known problem with measurements in the infrasonic band from fixed sensor systems. Fig. 1 shows a schematic drawing of a Swallow float. In addition to the infrasonic acoustic sensors (i.e., the infrasonic hydrophone below the glass sphere, the 3-component geophone assembly on the underside of the north pole of the glass sphere, and the compass inside the sphere at the south pole used to orient the horizontal geophone components), each float was equipped with an 8 kHz hydrophone system to provide acoustic localization capability. Further details on the system hardware can be found in Ref. 1.

B. The Vertical "DIFAR" Array

MPL's vertical DIFAR array, re Fig. 2, is composed of 16 elements with an inter-element spacing of 15 m. Each of the elements contains three orthogonally-oriented geophones to measure acoustic particle velocity and a hydrophone to measure pressure. Each element also contains a flux-gate compass for

measuring the orientation of the horizontal geophones, a programmable high-frequency data acquisition for acoustic element localization, a preamp with programmable gain from 0 to 120 dB, and a 16-bit A/D converter that provides additional dynamic range. The data sampling rate is programmable to either 150, 300, 600, 1200, or 2400 samples/sec. Data collected to date were sampled at 600 samples/sec, providing an effective data bandwith of 10-270 Hz. Additional details on the vertical DIFAR array hardware are contained in Ref. 2.

C. Nearshore Moored DIFAR Sonobuoys

As part of MPL's Adaptive Beach Monitoring program, a set of 8 standard Navy SSQ 53D DIFAR sonobuoys, provided by the Naval Air Warfare Center, were modified for long-term moored deployments in very shallow water (less than 50 m). Their purpose was to measure the directional properties of the nearshore underwater ambient sound field as a function of range offshore, starting just outside the surf zone. The DIFAR sensor in each unit was suspended by an elastic rubber tube within a bottom-mounted, hemispherical flow shield. The multiplexed sensor signal was transmitted up an electrical cable to the RF transmitter mounted on a surface float where it was RF telemetered to the shore-based recording facility. The surface float also contained sufficient battery power for continuous 3-5 day operation. System design was based heavily on one developed by researchers at the Applied Research Lab, University of Texas at Austin [3].

Another sensor system whose data are presented in Sect. IIIC is a variant of the moored DIFAR sonobuoy system. Referred to as the "OSZM" (Outside-Surf-Zone Mooring), it transmitted its data by electromechanical cable deployed through the surf zone to a land-based recording facility rather than by RF telemetry. The cable also allowed electrical power to be transmitted to the mooring, thus eliminating the need for battery replacement. More importantly, instead of a water-column DIFAR sensor, its sensor package was composed of three orthogonally-oriented geophones and a hydrophone mounted on a flat metal plate. The plate was diver-deployed directly on the ocean bottom just outside the surf zone. Since the geophones measured the three components of sediment motion rather than those of the water column, the system does not classify as a directional underwater acoustic sensor *per se*. However, the unconsolidated sand layer covering the ocean bottom acts nearly like a fluid. Therefore, underwater acoustic signal processing techniques can be applied to these data, as demonstrated in Sect. IIIC.

D. Standard U.S. Navy DIFAR Sonobuoys

A final sensor system whose data are presented in Sect. IIIB is the standard U.S. Navy DIFAR sonobuoy. Not only are these systems a critical part of the Navy's air ASW effort [4], but they can be a valuable tool in ocean acoustics scientific studies (e.g., [5]). These ingenious sensor systems provide a benchmark against which newer underwater acoustic directional sensors are judged.

II. THEORETICAL FRAMEWORK

The theoretical basis for all results presented in this paper is a set of four fundamental equations. The first is the conservation of linear momentum under the linear acoustic approximation,

$$\rho_0(\underline{x}) \frac{\partial \underline{v}(\underline{x},t)}{\partial t} + \nabla p(\underline{x},t) = 0 \tag{1}$$

The ambient density is $\rho_0(\underline{x})$ and the acoustic field variables, $\underline{v}(\underline{x},t)$ and $p(\underline{x},t)$, are the particle velocity and pressure, respectively. The linearized conservation of mass with the equation of state embedded in it is

$$\frac{\partial p(\underline{x},t)}{\partial t} + \kappa_s(\underline{x}) \nabla \cdot \underline{v}(\underline{x},t) = 0 \tag{2}$$

The fluid properties, i.e., the adiabatic incompressibility $\kappa_s(\underline{x})$ and the density, are assumed to be fixed in time over the time scales of acoustic signal propagation. Deviations from an ideal fliud (e.g., viscous dissipation) are assumed negligible. These two equations contain all the physics needed for this paper. They hold in regions where no acoustic sources exist.

An important implication of Eq. (1) is that if the acoustic pressure field is measured (or otherwise known) everywhere within a given region of space, the corresponding acoustic particle velocity field can be derived everywhere within this region. That is, measurement of acoustic particle velocity adds no new information beyond that available from spatially distributed measurements of pressure.

The third equation, which provides the basis for array processing with measurements at a single point in space, is an expression of Taylor's theorem. Applying this theorem to the acoustic pressure field in a region about the measurement point, $\underline{x}_o$, where no acoustic sources exist, gives

$$p(\underline{x},t) = p(\underline{x}_o,t) + \nabla p(\underline{x}_o,t) \cdot \Delta\underline{x} + \frac{1}{2}\Delta\underline{x}^T \left[\begin{array}{c}\text{Matrix of} \\ \text{2nd Derivatives}\end{array}\right]_{\underline{x}_o} \Delta\underline{x} + \cdots \tag{3}$$

where $\Delta\underline{x} \equiv \underline{x} - \underline{x}_o$.

Finally, the acoustic strain rate, a second-rank tensor denoted by $[\dot{\varepsilon}]$ and which is used in the concept of a "tensor sensor" presented in Sect. IV, is equal to

$$[\dot{\varepsilon}](\underline{x},t) = \nabla\underline{v}(\underline{x},t) \tag{4}$$

This expression assumes that the spatial gradients of the fluid ambient density are negligible so that the acoustic particle velocity field is curl-free (i.e., $\nabla \times \underline{v} = 0$).

By combining Eqs. (1) and (2) to eliminate particle velocity, the acoustic wave equation in pressure can be derived. Alternatively, the equations can be transformed from first order to second order in the acoustic variables to obtain expressions that characterize the energetics of acoustic fields [6,7]. Just as two types of energy density exist in a sound field (potential and kinetic), two types of energy flux occur. One, the "active" intensity, describes the net transport of acoustic energy through the medium. In a monotone sound field, it is proportional to the spatial gradient of the wave field phase. The second type of energy flow, the "reactive" intensity, is proportional to the spatial gradient of the pressure autospectrum (or potential energy density). It is required to support the spatial structure of the field. Its existence and importance is the reason that ocean acoustic fields cannot, in general, be modeled as the superposition of uncorrelated plane wave arrivals.

The two energy densities and the individual components of the active and reactive intensities appear in the 4x4 data cross spectral matrix formed from vector sensor ("combined receiver") data. The properties of the 3x3 particle velocity sub-cross spectral matrix can be analyzed in terms of the polarization of acoustic particle motion [7,8]. Therefore, all cross spectral matrix terms have basic physical significance.

III. SOME RESULTS OF AT-SEA MEASUREMENTS

A. Vector Array Processing

The Taylor series expansion of the acoustic pressure field given in Eq. (3) says that the measurement of acoustic pressure and its higher-order spatial derivatives at a single point in space is equivalent to the measurement of acoustic pressure in a volume about the measurement point. Therefore, the techniques used in beamforming with spatially distributed pressure measurements can be applied to single point measurements of pressure and its spatial derivatives. In particular, since Eq. (1) shows that acoustic particle velocity at a given frequency is proportional to the first order spatial gradient of pressure, then high resolution beamforming techniques can be used with simultaneous pressure and particle velocity measurements. Application of minimum variance (Capon [9]) as well as conventional beamforming techniques to these types of single point measurements were discussed in Refs. 10 and 11 (see also [12,13]). As an example, a comparison of the results of using conventional beamforming (CBF) and adaptive beamforming (ABF) at a source tow frequency of 225 Hz with data from all properly-operating channels of the Vertical DIFAR Array is presented in Fig. 3 (from a combination of Figs. 5 and 6 of [10]). The elevation angle is plotted along the vertical axis, with negative angles indicating downward-pointing beams, and the azimuth, in degrees clockwise from true north, is given along the horizontal axis. These data were collected when the towed source was located 23° east of north.

Most of the dark-colored areas in the figure are due to the bottom-bounce arrival, predicted from numerical modeling to be the most predominant arrival at this range. Vertically-aliased replicas of this arrival also occur because the array element spacing of 15 m represents more than two acoustic wavelengths at 225 Hz. The horizontal resolution of the ABF method is superior to that using conventional DIFAR processing in this case since the signal-to-noise ratio (SNR) was large.

To combine the data from DIFAR elements spaced over an interval of depth in the water column, a number of approaches can be taken. For the results presented in Fig. 3, a conventional delay-and-sum beamforming in the vertical direction first was performed. The delay-and-summing was done with the time series from sensors of the same type; that is, all the pressure time series were delay-and-summed, then the vertical geophone data were delay-and-summed, and so on. This initial step created, in effect, the four-component time series for an equivalent single DIFAR element with extended vertical aperture corresponding to each vertical look direction. Then, conventional Bartlett processing (upper panel) and minimum variance Capon processing (lower panel) were applied to the four-component, delayed-and-summed time series.

An attempt to perform global Capon processing, i.e., estimating and inverting the full 64 x 64 cross spectral matrix, failed due to the problem of correlated arrivals from different vertical directions. Correlated arrivals result in a non-negligible reactive energy flux which is the cause of the problem. Real ocean acoustic wave fields in most cases cannot be modeled as the superposition of uncorrelated plane wave arrivals.

As discussed in Ref. 11, the distance, Δx, that the pressure field can be extrapolated from the measurement point with a given error and with an expansion to a given order is dependent upon the degree of spatial variability of the pressure field. The maximum spatial variability in any direction at a given frequency cannot exceed that determined by the acoustic wavelength, at least for non-evanescent acoustic fields. Otherwise, the velocity of the energy flow required to support the spatial structure would exceed the speed of sound in the fluid, which is physically impossible. Therefore the effective spatial aperture of a single point array is related to the acoustic wavelength, rather than being determined by a fixed inter-element spacing as with conventional arrays. Thus, single point arrays are frequency-adaptive; their effective aperture decreases with increasing frequency. The result of this property is that the plane wave response (or beampattern) for single point arrays is independent of frequency. This result also implies that grating lobes do not exist; spatial aliasing cannot occur since a sampling in space is not being performed.

The phenomenon of superdirectivity is directly related to the Taylor series expansion of the pressure field. That is, superdirectivity arises for a spatially distributed hydrophone array when the directivity index is maximized as a function of the element weights, and the interelement spacing becomes smaller than half the acoustic wavelength [14]. One can show that, as the ratio of the interelement spacing to the acoustic wavelength approaches zero, the weights for a "linear point array" approach the finite difference approximations to the spatial derivatives of pressure given in Eq. (3). The instability that results when the weights become large and of opposite sign can be avoided by the use of alternative transduction methods suggested by the physical interpretation of the spatial derivatives of pressure, e.g., when the measurement of a component of acoustic particle velocity replaces the measurement of pressure at two closely-spaced points.

Note that high resolution beamforming techniques have been applied to single point measurements of other wave fields, e.g., the estimation of ocean surface gravity wave directional spectra from "pitch-and-roll" buoys [15].

B. Bioacoustics

In 1996, the Marine Physical Lab conducted an experiment just south of San Miguel Island bordering the Santa Barbara Channel as part of its Marine Mammal Vocalization program. The purpose of this ONR-sponsored program was to study the natural calling behavior of large baleen whales (blue, fin, and humpback whales) and to investigate how their calls could be used as loud, low-frequency sources of opportunity to determine properties of the ocean environment. During one period, recordings of vocalizing blue whales were made simultaneously by a vertical line array of 48 hydrophones and a freely drifting, standard Navy SSQ 53B sonobuoy. Fig. 4 shows a 5-min spectrogram from the omnidirectional component of the DIFAR sonobuoy. Two characteristic Type A calls (the second call after the start of the 5-

min period and the one at the 4-min mark) and 6 Type B calls with high SNR (17-Hz FM sweeps and associated higher harmonics) are present. The issue is to determine the number and locations of animals contributing to this sequence of calls. If more than one individual is vocalizing, an interesting question is how, if at all, calling behavior is altered by the presence of other calling animal(s).

The 5 min of data from the sonobuoy were divided into consecutive 5-sec blocks and the average active intensity per frequency within each block was calculated. (Sonobuoy data permit only the horizontal component of active intensity to be determined). The upper panel in Fig. 5 shows a plot of the horizontal active intensity in a 2.4-Hz-wide bin centered at 51 Hz as it evolved over the 5-min period. The 51-Hz bin contains the energy in the 3rd harmonic of the Type B calls and little of the energy from the Type A calls. The figure was created by plotting the sequential average active intensity vector estimates consecutively head to tail, starting at the origin of the compass. The beginning and end of each vector is indicated by a small "x" (as are the 10° intervals on the outer compass circle). The plot clearly shows that the first two B calls created net energy flux in the WNW direction, 180° from the source to the ESE (approximate bearing of 120°). The third B call generates energy flow to the SE, indicating a second vocalizing animal to the NW (bearing 340°). The final three Type B calls created progressively weaker flux to the ENE, in the same direction as the first two calls. Therefore, two animals appear to be the sources of the Type B calls, one to the NW and a second, more "talkative" one to the ESE.

The corresponding plot for the 91 Hz bin, which contains the energy from the Type A calls but no Type B energy, is shown in the lower panel in Fig. 5. The 91 Hz bin also contains energy from a spectral line (re Fig. 4), radiated by the R/P FLIP, the platform from which the experiment was conducted. Upon deployment from FLIP, the sonobuoy drifted almost due north, towards San Miguel Island away from FLIP. The 91-Hz energy flow at the beginning of the 5-min period, and at other times when neither of the Type A signals were present, is to the north in the direction away from FLIP. The first Type A signal interrupts this northward flow by creating flux to the SE, away from a source at bearing 335°. It most likely was created by the same animal that generated the third Type B call in the previous figure. The second A call clearly is coming from the same direction as the more "talkative" animal from the previous figure. Therefore, two animals most likely are contributing to the calling sequence in Fig. 4.

Range and depth estimates of these two calling animals, determined by matched-field processing with the vertical hydrophone array data, are discussed on pp. 1291-1292 and presented in Fig. 8 of Ref. 16.

These DIFAR sonobuoy data demonstrate one great benefit of such systems; they allow measurement of the directionality of very low frequency signals. DIFAR sonobuoys along with DIFAR demultiplexing systems and display units, are beginning to be routinely used in marine mammal acoustics studies [17].

C. Seismology

Earthquake-generated T phase arrivals have been recorded in almost every Swallow float deployment. Association of these arrivals with specific events was accomplished by calculating the travel times to epicentral locations of major events posted in earthquake bulletins and comparing the listed origin times with those predicted from the Swallow float data. Agreement of the two origin times typically was within a few secs. An example of a Swallow float recording of an earthquake is presented in Ref. 6. During the IONEX 92 experiment, over 50 aftershocks from a subduction zone event off Crete were recorded [18]. In addition, several aftershocks of the 1992 Lander's earthquake in southern California were recorded during a vertical DIFAR array deployment in the southern California Bight region.

Another source of land-based seismic signals that can couple into the water column is shown in Fig. 6. Offshore underwater sounds from these tracked vehicles operating on land were recorded during MPL's Adaptive Beach Monitoring program. As an example, the adaptive plane wave beamforming results over the 30-70 Hz frequency band as a function of time during the transit of four such tracked vehicles downcoast along the beach is shown in Fig. 7 [19]. These results were obtained from data collected by a 2D hydrophone array on the ocean bottom 1.5 km offshore. The beach, to the NE from the array deployment site, runs NW-SE at this site. The directionality indicated by the acoustic results agrees well with visual observations during the experiment.

Data collected over this same time period by the OSZM's bottom-mounted geophone/hydrophone package (Sect. IC) were processed using acoustic vector intensity techniques, similar to the approach used for the blue whale calls in Fig. 5. The horizontal projection of the active intensity component integrated across the bands from 34 to 56 Hz ("x") and from 64 to 70 Hz (triangles) as a function of time over the same time period as Fig. 7 is shown in Fig. 8. For the 34-56 Hz band, the background energy flow before the start of the vehicle run is from the southwest to the northeast. The start of the run resulted in flow to the south, which evolves into a flow to the southwest as the vehicles traveled down the beach. The majority of the flow in this lower band occurs in a more southerly direction than that in the higher frequency band. The latter is dominated by flow 180° away from the bearing to the coastline, corresponding to the location where the vehicles passed through CPA. Whereas the 64-to-70-Hz flow continues to evolve towards a westerly direction as the vehicles proceeded downcoast, it does not do so in the lower frequency band. Although changes in land-to-water coupling characteristics may play a role, these frequency band differences are probably due to the fact that the frequency content of the vehicle signals shifted to higher frequencies as they increased speed upon reaching the open part of the beach. Results of adaptive beamforming with the hydrophone array data over these two frequency bands separately are consistent with those in Fig. 8.

As the previous results illustrate, the geophone/hydrophone package clearly provides useful information on the time-evolving directionality of the land vehicle sounds. It does so without the need to know the phase velocity of the arriving energy since the individual sensor channels are located at a single point in space. To obtain the broadband adaptive plane wave beamforming results in Fig. 7, the phase velocity as a function of frequency first had to be measured. The phase velocity in this case is a strong function of frequency since the received energy is carried by the lowest order normal mode which is near cutoff at these low frequencies in these very shallow waters [19].

D. Physical Acoustics

Dislocations are places in the acoustic field where the amplitude goes to zero and the total field phase becomes undetermined [20]. Although they are curious features of the field in their own right, they may also be sensitive indicators of fluctuations in the environment [21]. Three candidate dislocations in the pressure field are indicated by vertical dashed lines in Fig. 9. The solid curve is the acoustic pressure spectrum and the dotted curve is the vertical component particle velocity spectrum. These data were collected by a Swallow float deployed at nearly 1600 m depth during the 1990 NATIVE 1 experiment near the Blake Plateau in the northwest Atlantic Ocean. Those in Fig. 9 were obtained during a 2.7-hour period (record number along the abscissa is a measure of time) as the source, transmitting a 7.0 Hz tone, was towed out to distance of nearly 19 km.

At a dislocation in the pressure field, not all the correponding particle velocity components will be zero. That is, although the pressure field amplitude may be zero, its spatial gradient, upon which the particle velocity also depends, will not be unless the field amplitude is negligible throughout a finite volume (i.e., a shadow zone rather than dislocation). Fig. 9 shows that at many of the pressure field minima, the vertical geophone component spectrum actually attains a local maximum.

The vector properties of acoustic intensity can be used to determine what happens in the neighborhood of a dislocation. The directions of the active and reactive intensities change quickly in such regions. In particular, the radial component of reactive intensity changes sign in passing by a dislocation. Also, the magnitude of the reactive intensity becomes large since greater energy flow is required to support the existence of the acoustic hole. In addition, acoustic particle motion near a dislocation is strongly non-rectilinear since the active and reactive flow directions become misaligned (discussed below).

Fig. 10 shows plots of the projections of the intensity vectors in the radial/vertical plane (radial in the forward direction is the direction 180° away from the source) over a 15-min period (20 records) about the first pressure field minimum, occurring at record 996 in Fig. 9. The active intensity (upper panel) is dominated mostly by the horizontal component, representing the direction of net flux of energy down the waveguide. However, near the candidate dislocation at record 996, the radial active intensity component decreases significantly so that net flux occurs predominantly in the vertical direction. Also, in passing by this location, the vertical active intensity component flips from the downward to the upward direction. The

lower panel of Fig. 10 shows the corresponding reactive intensity. It is mostly vertical since the spatial structure in ocean waveguides typically is significantly greater in that direction than in the radial. The reactive intensity can vary wildly in places where the spatial variations in the pressure field are very small, as near the beginning of the 20-record period. Of interest here, however, is how both the radial and vertical reactive intensity components flip in direction at record 996. The behavior of the two types of energy flow seen in Fig. 10 is consistent with that expected near a dislocation.

The polarization of the particle motion in a way combines the information contained in the active and reactive intensity components. As discussed in Ref. 8 (see pp. 218-219 of [7] for derivation), the following relationship exists between the two types of vector acoustic intensity and the imaginary components of the 3x3 particle velocity data cross spectral matrix:

$$\text{Im}\left\{ [\mathbf{S_v}](f) \right\} = \frac{\underline{C}_{p\underline{v}}(f) \times \underline{Q}_{p\underline{v}}(f)}{S_p(f)} \tag{5}$$

This relationship can be used to define the following two nondimensional measures of the "degree of circularity" of the particle motion:

$$\Theta_1 \equiv 2\, \frac{\underline{C}_{p\underline{v}}(f) \times \underline{Q}_{p\underline{v}}(f)}{S_p(f)\sum S_{v_j}(f)} \tag{6a}$$

and

$$\Theta_2 \equiv 2\, \frac{\text{Im}\left\{ [\mathbf{S_v}](f) \right\}}{\sum S_{v_j}(f)} \tag{6b}$$

Purely circular motion results in a value for Θ of ± 1, with the sign distinguishing between prograde and retrograde directions, and purely rectilinear motion has a value of zero. These two measures of the degree of circularity are plotted in Fig. 11 over the same time period as in Fig. 9; Eq. (6a) is plotted with a dotted curve and Eq. (6b) with a solid curve. Both measures agree extremely well over the full duration of the source tow. As indicated by the vertical dashed line at record 996 in Fig. 11, the particle motion reverses from being nearly perfectly circular in one direction to circular motion in the opposite direction. Again, this result is consistent with that expected in the neighborhood of a dislocation.

These and additional results on possible dislocations in Swallow float data were presented at the most recent Acoustical Society of America meeting [22].

IV. "TENSOR" SENSOR

To increase the directivity index (DI; defined as the array gain of a single plane wave in an isotropic noise field) for a conventional, spatially distributed pressure sensor array, more sensors at the appropriate spacing simply are added (assuming spatial coherence of the signal across the increased array aperture). For an array that theoretically exists at a single point in space, an increase in DI is obtained by making measurements of increasingly higher order spatial derivatives of the acoustic pressure field. Pressure is a scalar quantity, equivalent to a tensor of rank zero. The gradient of pressure is a vector quantity, a first rank tensor, and the gradient of a vector is a 2nd rank tensor.

A physical interpretation of the term at second order in the Taylor series expansion in Eq. (3) is given by Eq. (4). That is, for an acoustic field in an otherwise stationary fluid, the spatial gradient of the acoustic particle velocity is equal to the acoustic rate of strain. The concept of strain rate usually appears in fluid mechanics with reference to viscous dissipation. However, a sound field causes all kinds of spatial distortions of the fluid medium from its ambient state so that strain rate also is a useful concept in acoustics.

Results of investigating the benefits of measuring the quantities out to second order in the Taylor series expansion were presented in [13] and summarized in [11]. The investigation involved both the

beamforming properties of a "tensor sensor" and the vector and tensor properties of the terms in the data cross spectral matrix in the context of the energetics of acoustic fields. Those results are repeated here.

A. Tensor Sensor Beamforming Properties

The beamformer output time series for a tensor sensor (originally called the "double DIFAR" in [13]) can be written as

$$d^{(2)}(\underline{x}, t) = a_o p(\underline{x}, t) + \sum_{j=1}^{3} a_j Z_j v_j(\underline{x}, t)\cos(\beta_j) + \frac{1}{2}\sum_{i=1}^{3}\sum_{j=1}^{3} b_{ij} W_{ij} \dot{\varepsilon}_{ij}(\underline{x}, t)\cos(\beta_i)\cos(\beta_j) \tag{7}$$

where $\dot{\varepsilon}_{ij}$ is the ij-th term in the 2nd rank strain rate tensor, $[\dot{\varepsilon}]$, the Z_j's and W_{ij}'s are conversion factors (not necessarily purely real), the $\cos(\beta_j)$'s are the direction cosines, and the a_j's are b_{ij}'s are arbitrary weights. Different approaches to beamforming can be defined by determining the arbitrary weights in various ways. The conventional beamforming approach sets the weights to fixed and "equal" (properly normalized) values. The standard DIFAR beamformer with a cardioid beampattern (re the dashed curve in Fig. 12b) is an example of this approach. It provides a DI of 4.8 dB, has a main lobe width (defined by the 3-dB down points) of 131°, has no side lobes and just one null.

Alternatively, the weights can be determined under various optimization criteria. For example, they can be determined so that the DI is maximized. A DIFAR beamformer at first order has a maximum DI of 6 dB, a main lobe width of 105°, a single side lobe of level -6 dB (180° from direction of maximum sensitivity), and 2 nulls. The plane wave response of this beamformer is plotted as a dotted curve in Fig. 12a. In comparison, a tensor sensor has a maximum DI of 9.5 dB, a main lobe width of 65 deg, side lobe level of -9.5 dB, and 4 nulls. The resulting plane wave response having maximum DI is shown as the solid curve in Fig. 12a. The solid curve in Fig. 12b is the tensor sensor beampattern that results from applying the constraint that a null exist 180° from the direction of maximum sensitivity. It has a maximum DI of 9.0 dB, a main lobe width of 70°, side lobes that are 13.0 dB down in level, and 3 nulls.

A second optimization approach is to determine the weights using a data-adaptive approach of minimizing the beamformer output variance under various constraints (e.g., Capon processing). Fig. 13 shows the results of a tensor sensor simulation in which the acoustic field is created by four sources having the following combination of directions of arrival (DOA) and signal-to-noise ratios (SNR); (DOA: 0°, SNR: 12 dB), (DOA: 45°, SNR: 9 dB), (DOA: 180°, SNR: 6 dB), and (DOA: 270°, SNR: 3 dB). The solid curve is the beamformer output using the conventional beamforming approach and the dotted curve shows the Capon processor output. The presence of 4 sources is clearly indicated in the Capon results since this processor has some control over the direction in which it steers its nulls.

B. Energetics of the Cross Spectral Matrix

By using tensor and vector algebra and the fundamental physical laws expressed in Eqs. (1) and (2), relationships between the various quantities in the tensor sensor 10x10 data cross spectral matrix can be derived. This approach is exactly the same used to derive the vector properties of the two components of acoustic intensity. One property of the acoustic pressure/strain rate tensor is

$$p\,[\dot{\varepsilon}] = \nabla(p\underline{v}) + \frac{\partial}{\partial t}\left\{\frac{1}{2}\rho_o(\underline{v})(\underline{v})\right\} \tag{8}$$

Also, it can be shown using the strain energy function that the trace of $p\,[\dot{\varepsilon}]$ (i.e., the sum of the diagonal elements) yields the conservation of acoustic energy equation. For stationary, stochastic fields in the frequency domain:

$$\text{Re}\left\{S_{p\,[\dot{\varepsilon}]}(f)\right\} = \nabla\underline{C}_{p\underline{v}}(f) \tag{9}$$

Therefore, the cross spectrum between the acoustic pressure and the acoustic rate of strain provides information on the local spatial heterogeneity of the active acoustic intensity. Likewise, a property of the velocity/strain rate second rank tensor is

$$\rho_o \underline{v} \cdot [\dot{\underline{\varepsilon}}] = \nabla \{K.E.D.\} \tag{10}$$

where "K.E.D." signifies the kinetic energy density.

The existence of relationships between some of the terms in the tensor sensor data cross spectral matrix implies that they do not provide entirely independent information on the acoustic field. However, these relationships provide a way of quality checking the data from such systems. We hope to have the opportunity to build a prototype tensor sensor in the near future.

An interesting question is - do high quality ocean acoustic strain rate sensor systems already exist in nature [23]?

V. CONCLUSIONS

A sensor, or array of sensors, that simultaneously measures acoustic pressure and the three components of acoustic particle velocity adds no new information to what can be obtained by a set of spatially distributed pressure measurements. However, vector and "tensor" sensors have some distinct advantages; they are more compact in size, can be easier to deploy, and do not suffer from those errors introduced by element location uncertainty or uncertainty in the phase speed of propagation across the array aperture. They may be the only practical way of obtaining directional properties of the underwater acoustic field at infrasonic frequencies. In addition, a single point vector or tensor sensor has a beam pattern that is independent of frequency, making it convenient for broadband studies. Finally, the terms in these sensors' data cross spectral matrices are of basic physical significance so that results often are more easily interpreted and insights more readily obtained.

The greatest challenge in this field is making high quality ocean acoustic measurements with these types of sensor systems. Motion-induced self noise is a particularly vexing problem.

Finally, the beautiful and complicated interference patterns displayed by real ocean acoustic fields rely upon the reactive energy flow for their existence. Such patterns, which contain very useful information on source location and environmental properties, are completely absent in fields that can be modeled as the superposition of uncorrelated plane wave arrivals.

ACKNOWLEDGMENTS

REFERENCES

[1]   G. L. D'Spain, W. S. Hodgkiss, and G. L. Edmonds, "The simultaneous measurement of infrasonic acoustic particle velocity and acoustic pressure in the ocean by freely drifting Swallow floats," IEEE J. Oceanic Eng. 16 (2), 195-207 (1991).

[2]   J. C. Nickles, G. L. Edmonds, R. A. Harriss, F. H. Fisher, W. S. Hodgkiss, J. Giles, and G. L. D'Spain, "A vertical array of directional acoustic sensors," Oceans '92, Newport, Rhode Island, 340-345 (1992).

[3]   M. B. Bennett, L. A. Thompson, P. T. Eisman, and K. C. Focke, "Moored data buoy for shallow water acoustic studies," Appendix A of "Shallow Water Passive Technology - Broadband Correlation Studies; SWAMP II Operations and Preliminary Results" by K. C. Focke and S. K. Mitchell, ARL Tech. Rept. ARL-TR-92-6, Applied Research Labs, Univ. of Texas at Austin (1992).

[4] G. W. Wolf, "U.S. Navy sonobuoys - Key to antisubmarine warfare," Sea Technology, 41-44, Nov. (1998).

[5] O. B. Wilson, S. N. Wolf, and F. Ingenito, "Measurements of acoustic ambient noise in shallow water due to breaking surf," J. Acoust. Soc. Am. 78 (1), 190-195 (1985).

[6] G. L. D'Spain, W. S. Hodgkiss, and G. L. Edmonds, "Energetics of the deep ocean's infrasonic sound field," J. Acoust. Soc. Am. 89 (3), 1134-1158 (1991).

[7] G. L. D'Spain, "The energetics of the ocean's infrasonic sound field," Ph.D. thesis, University of California, San Diego (1990).

[8] G. L. D'Spain, "Polarization of acoustic particle motion in the ocean and its relation to vector acoustic intensity," Proc. 2nd Int'l Workshop on Acoustical Engin. and Technol., Harbin, China, 149-164 (1999).

[9] J. Capon, "High-resolution frequency-wavenumber spectrum analysis," Proc. IEEE 57 (8), 1408-1418 (1969).

[10] G. L. D'Spain, W. S. Hodgkiss, G. L. Edmonds, J. C. Nickles, F. H. Fisher, and R. A. Harriss, "Initial analysis of the data from the vertical DIFAR array," Oceans '92, Newport, Rhode Island, 346-351 (1992).

[11] G. L. D'Spain, "Relationship of underwater acoustic intensity measurements to beamforming," Canadian Acoust. 22 (3), 157-158 (1994).

[12] G. L. D'Spain and W. S. Hodgkiss, "Array processing with acoustic measurements at a single point in the ocean," J. Acoust. Soc. Am. 91 (4), 2364 (1992).

[13] G. L. D'Spain and W. S. Hodgkiss, "Further comments on beamforming with acoustic measurements at a single point in the ocean," J. Acoust. Soc. Am. 93 (4), 2375 (1993).

[14] R. L. Pritchard, "Maximum directivity index of a linear point array," J. Acoust. Soc. Am. 26 (6), 1034-1039 (1954).

[15] J. Oltman-Shay and R. T. Guza, "A data-adaptive ocean wave directional spectrum estimator for pitch and roll type measurements," J. Phys. Oceano. 14, 1800-1810 (1984).

[16] A. M. Thode, G. L. D'Spain, and W. A. Kuperman, "Matched-field processing and geoacoustic inversion of blue whale vocalizations," J. Acoust. Soc. Am. 107 (3), 1286-1300 (2000).

[17] M. McDonald and J. A. Hildebrand, private communication (2000), C. Greene, private communication (2000), J. Barlow, private communication (2000).

[18] F. Desharnais, and G. L. D'Spain, "Acoustic intensity measurements with Swallow floats", Canadian Acoust. 22 (3), 159-160 (1994).

[19] G. L. D'Spain, L. P. Berger, W. A. Kuperman, W. S. Hodgkiss, L. M. Dorman, and W. A. Gaines, "Observations of land vehicle activity and other land-based sounds with offshore underwater acoustic arrays", accepted for publ. in J. Acoust. Soc. Am. (2000).

[20] J. F. Nye and M. V. Berry, "Dislocations in wave trains," Proc. R. Soc. Lond. A. 336, 165-190 (1974).

[21] A. A. Zhuravlev, I. K. Kobozev, Yu. A. Kravtsov, V. G. Petnikov, V. A. Popov, and A. Yu. Shmelev, "Dislocation tomography of the ocean: a new acoustical diagnostic method," Acoustical Physics 39 (4), 404-405 (1993) (Akust. Zh. 39, 761-762).

[22] G. L. D'Spain, D. P. Williams, and W. A. Kuperman, "Energetics of dislocations in ocean acoustic fields," J. Acoust. Soc. Am. 108 (5), 2543 (2000).

[23] G. L. D'Spain and P. A. Lepper, "Localizing marine animals and how marine animals might localize sound," J. Acoust. Soc. Am. 108 (5), 2541 (2000).

FIGURE CAPTIONS

Figure 1. Schematic of an MPL Swallow float.

Figure 2. Schematic of 2 elements of MPL's 16-element, 225-m-aperture, Vertical DIFAR Array.

Figure 3. Comparison of conventional and adaptive (Capon) processing at 225 Hz from at-sea data collected by the Vertical DIFAR Array in 1991.

Figure 4. 5-min spectrogram from the omnidirectional component of a 53B DIFAR sonobuoy deployed during MPL's 1996 Marine Mammal Vocalization experiment.

Figure 5. Upper panel is the horizontal active intensity at 51 Hz over the same 5-min time period and from the same DIFAR sonobuoy as in Fig. 4. Lower panel shows the corresponding result at 91 Hz.

Figure 6. Amphibious tracked vehicle ("amtrack") traveling down the beach during MPL's 1996 Adaptive Beach Monitoring experiment (ABM 96).

Figure 7. Adaptive beamforming over the 30-70 Hz frequency band during a 10-min period in ABM 96 using data from the 64-element hydrophone line array deployed quasi-parallel to the coast 1.5 km offshore in 12-m-deep water.

Figure 8. Horizontal active intensity from the OSZM data integrated over the bands from 34 to 56 Hz ("x") and from 64 to 70 Hz (triangles) as a function of time during the 10-min period shown in Fig. 7. Also plotted as a smooth curve is the north-south geophone velocity spectral density against that from the east-west component as a function of time, both integrated across the 34 to 56 Hz band.

Figure 9. Hydrophone (solid curve) and vertical geophone (dotted curve) spectral levels at 7 Hz as a function of time (20 records equals 15 min) recorded by a Swallow float at nearly 1600 m depth during source tow in the NATIVE 1 experiment.

Figure 10. Time series of the active (upper panel) and reactive (lower panel) intensities at 7 Hz over a 15-min time period about the first pressure spectral null (marked by the lefthand-most vertical dashed line) in Fig. 9. Plotted is the projection of the intensity vectors in the radial/vertical plane. The compasses in the upper right corners indicate Up, Down, Forward, and Back.

Figure 11. Degree of circularity of particle motion in the radial/vertical plane at 7 Hz over the same time period as Fig. 9.

Figure 12. 2D plane wave responses for various component weightings for first order DIFAR sensors and second order tensor sensors. In Fig. 12a, the dotted curve is for the DIFAR sensor with maximum DI of 6.0 dB and the solid curve is for the tensor sensor with maximum DI of 9.5 dB. In Fig. 12b, the 2D plane wave response for the standard DIFAR with equal component weighting (DI = 4.8 dB) is plotted with a dashed curve, and the tensor sensor with maximum DI under the constraint that a null exist in the 180° direction (DI = 9.0 dB) is plotted with a solid curve.

Figure 13. Simulation of conventional Bartlett (solid curve) and Capon (dotted curve) beamformer outputs of a tensor sensor for a field composed of four sources having directions of arrival (DOA) and signal-to-noise ratios of (DOA: 0°, SNR: 12 dB), (DOA: 45°, SNR: 9 dB), (DOA: 180°, SNR: 6 dB), and (DOA: 270°, SNR: 3 dB).
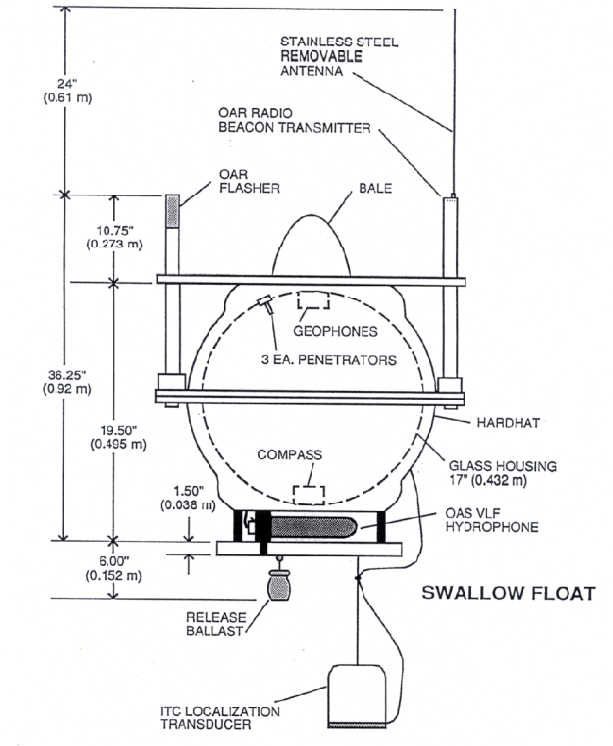
Fig. 1
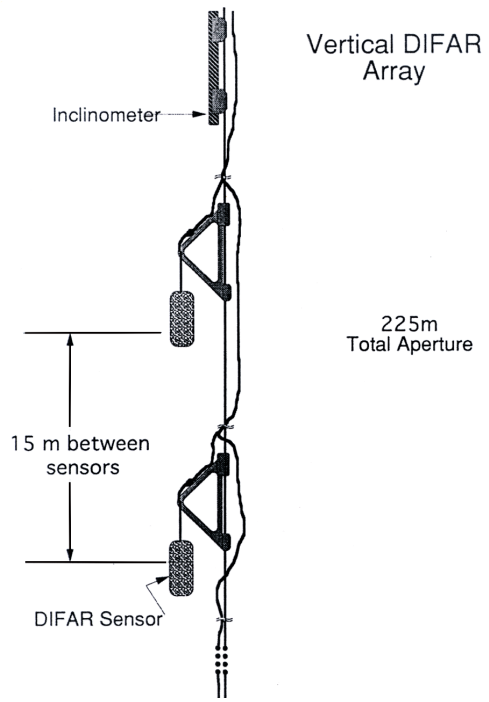
Fig. 2
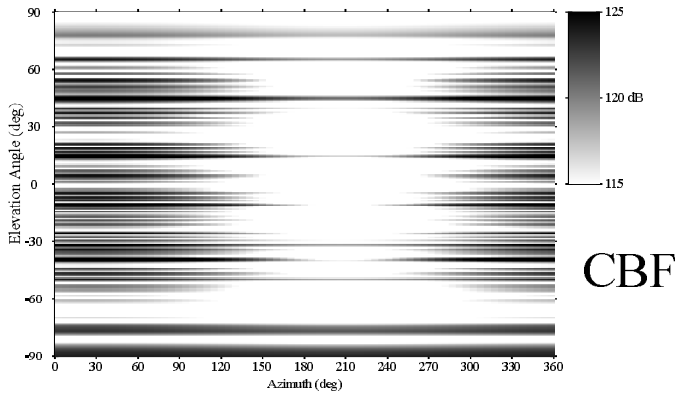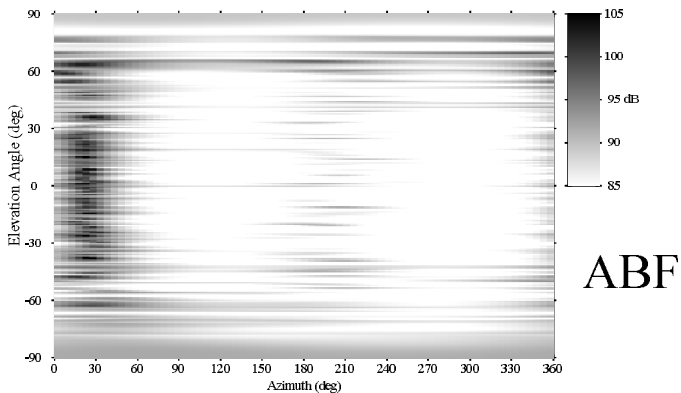
Fig. 3
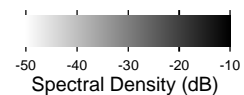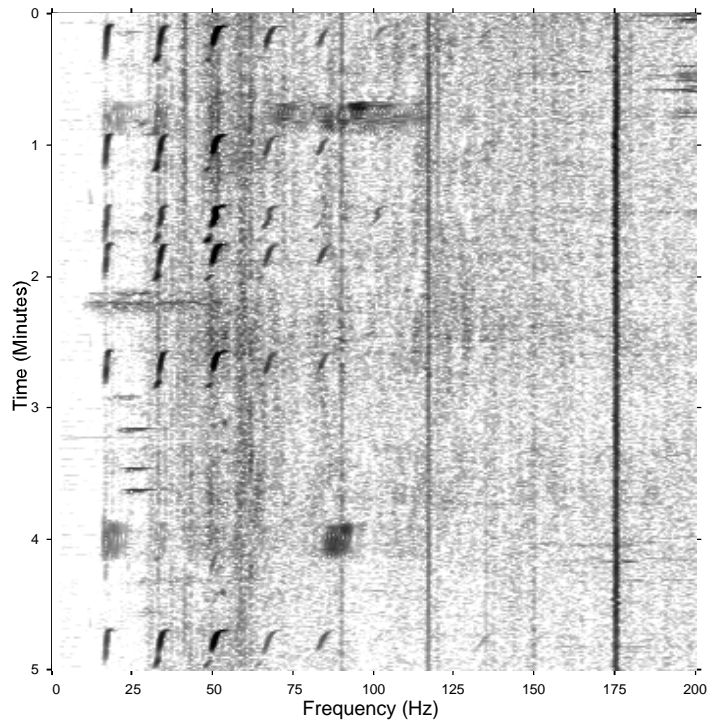
Fig. 4

MMV 96, Sono 53B Horizontal Active Intensities at 1 Freqs
5-Min Period: 1 St Blk: 1 No. Blks: 61 1st Freq: 51 Hz
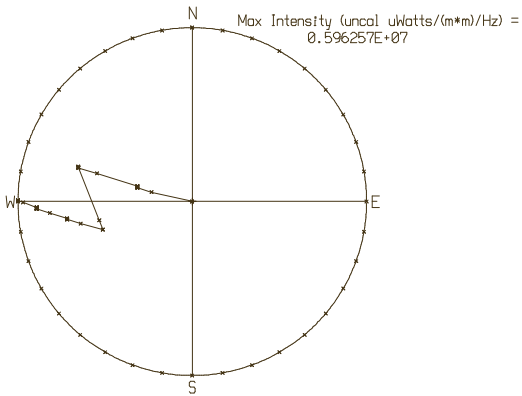
Max Intensity (uncol uWatts/(m*m)/Hz) = 0.596257E+07

MMV 96, Sono 53B Horizontal Active Intensities at 1 Freqs
5-Min Period: 1 St Blk: 1 No. Blks: 61 1st Freq: 91 Hz

Max Intensity (uncol uWatts/(m*m)/Hz) = 84078.8
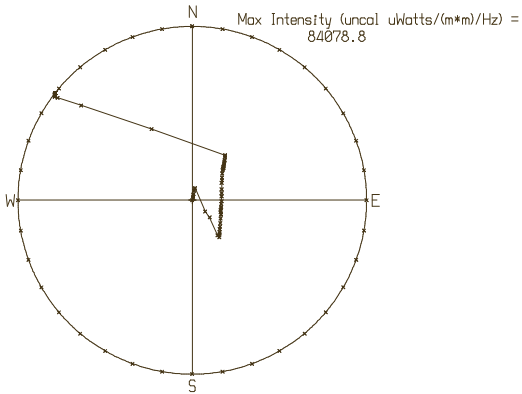
Fig. 5

Fig. 6

ABM 96 SRP NS Array JD 323 22:40
Adaptive Beamformer 30-70 Hz

Beam Density Level (dB re 1uPa^2/Hz)
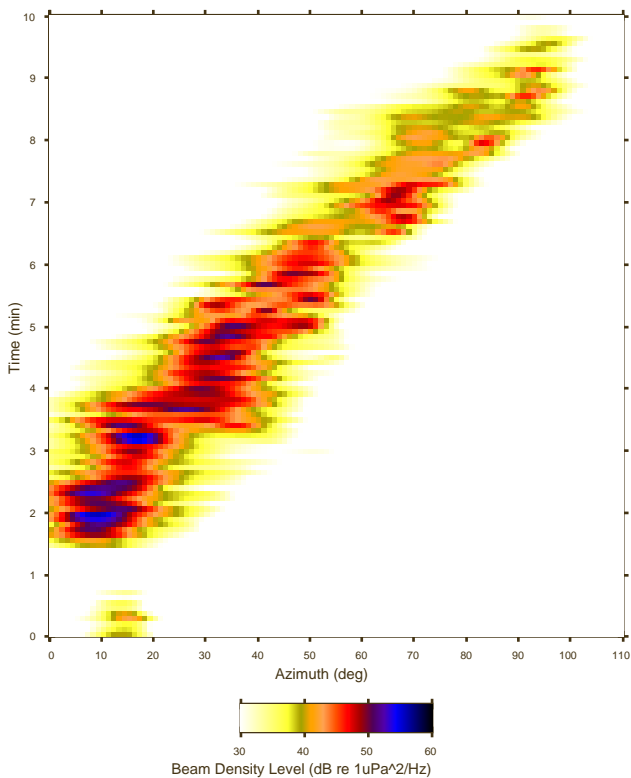
Fig. 7

ABM 96, JD 320 2240 Horiz Active Intensity, 34-56 Hz and
64-70 Hz, and Horizontal Geo Spectra 34-56 Hz
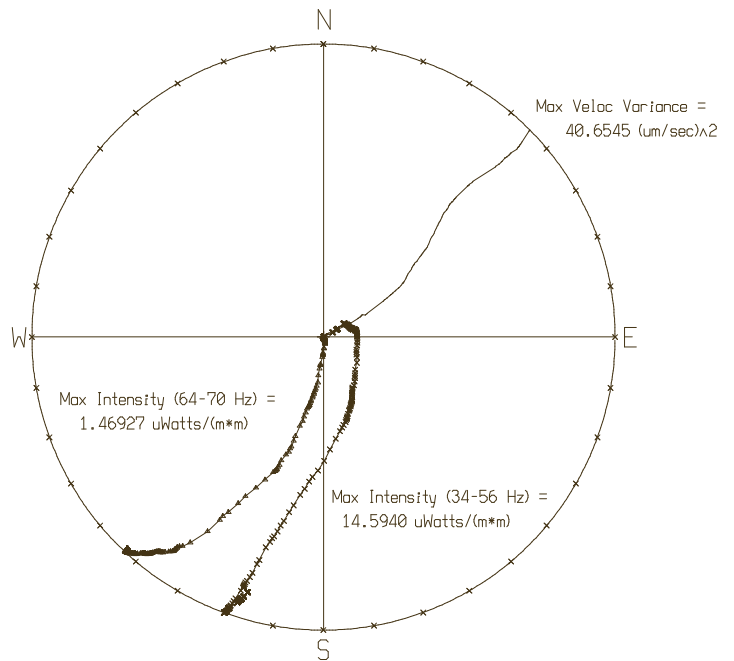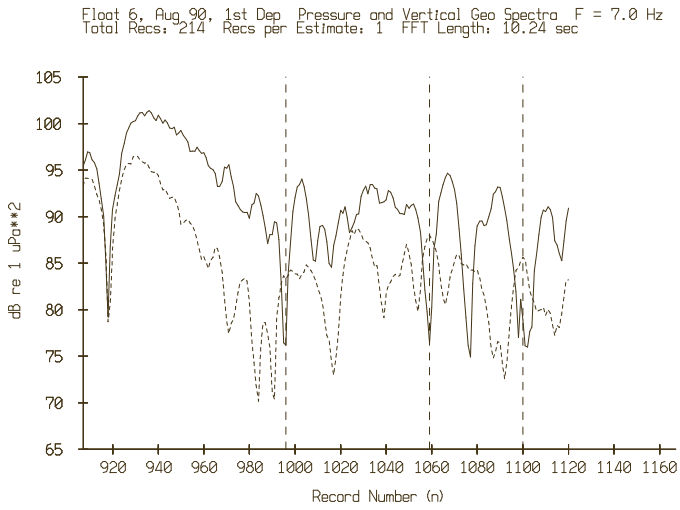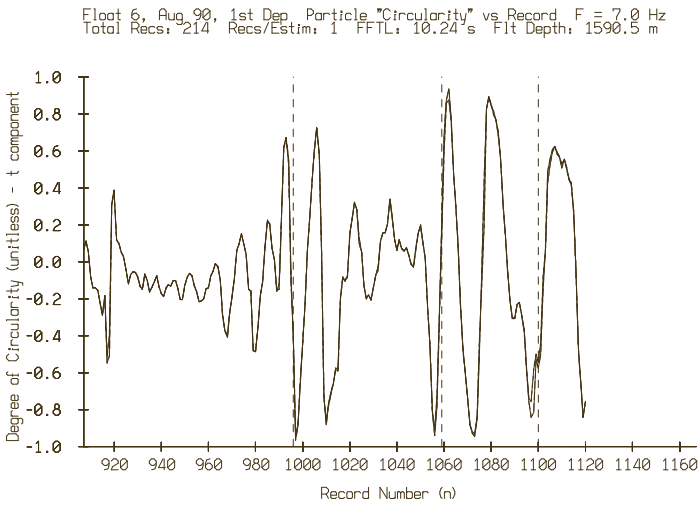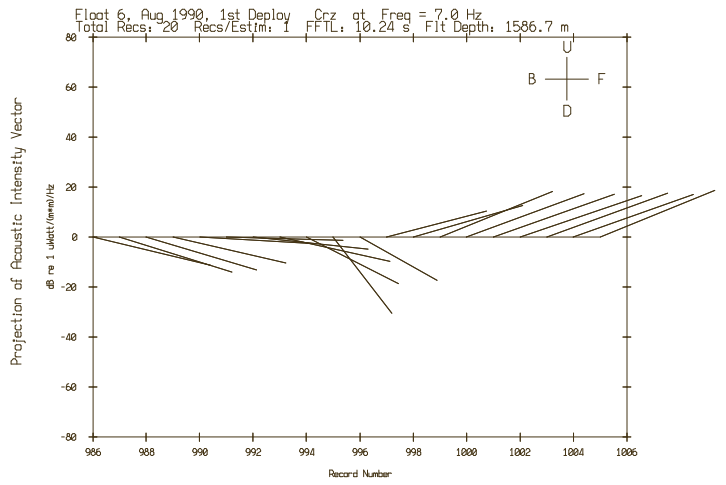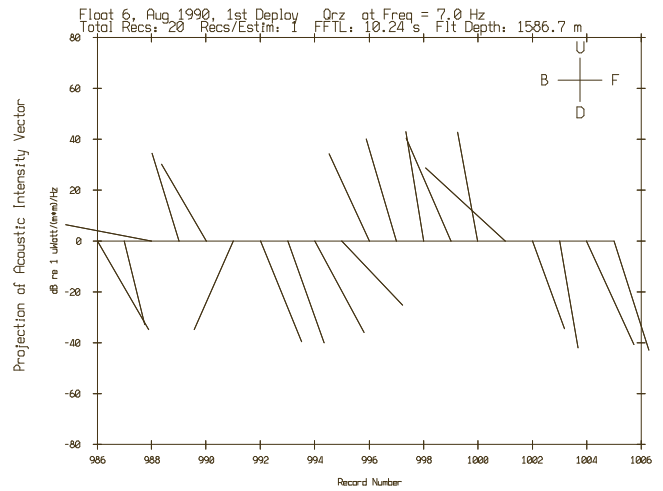
Max Veloc Variance = 40.6545 (um/sec)^2

Max Intensity (64-70 Hz) = 1.46927 uWatts/(m*m)

Max Intensity (34-56 Hz) = 14.5940 uWatts/(m*m)

Fig. 8

Fig. 9

Fig. 11

Fig. 10
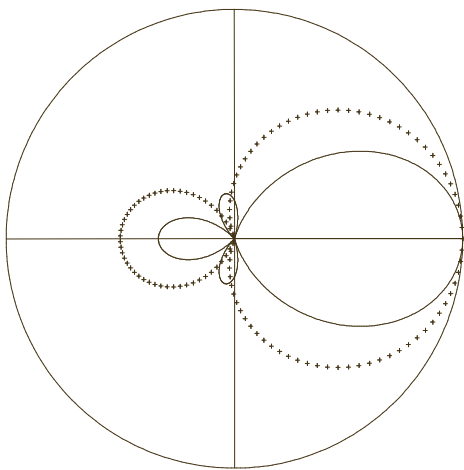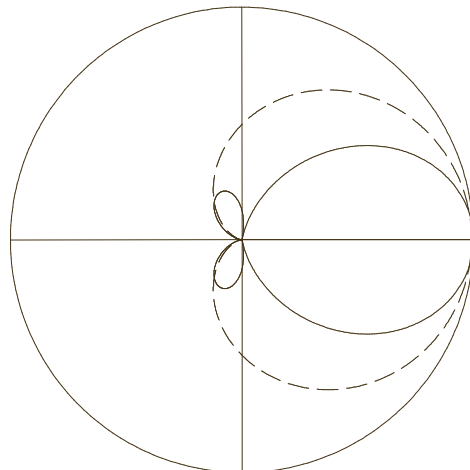
Fig. 12a

Fig. 12b
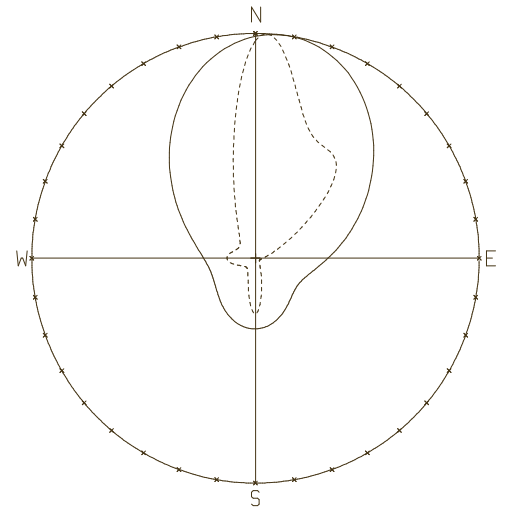
Fig. 13

Design Problems and Limitations in Vector Sensors

Thomas B. Gabrielson
Applied Research Laboratory
Pennsylvania State University
PO Box 30
State College, Pennsylvania 16804

Design Problems and Limitations in Vector Sensors

Dr. Thomas B. Gabrielson
Applied Research Laboratory
Pennsylvania State University
PO Box 30
State College, Pennsylvania 16804
tbg3@psu.edu

Abstract: Vector-based directional sensors present an effective solution to an important subset of measurement problems in underwater acoustics. There is an inherent directionality in the vector field that cannot be obtained from a pressure measurement at a single point. Inertial sensors in neutrally buoyant packages respond directly to acoustic particle motion without the dynamic-range penalty of gradient sensors; however, the conflicting requirements of supporting the sensor without interfering with its response to the acoustic field present interesting design challenges. Furthermore, their susceptibility to non-acoustic excitation makes high performance difficult to achieve in some circumstances. The gradient sensor relies on a finite-difference approximation to the pressure gradient. The elements of the gradient sensor do not need to move with the velocity field and the elements can be made much smaller allowing higher frequency operation. However, the output of a gradient sensor depends on subtraction of two nearly equal quantities, which severely limits the dynamic range. Success in the application of vector sensors depends on an understanding of their physics and their limitations.

I. INTRODUCTION

There are at least two fundamentally different approaches to achieving directional discrimination in acoustic sensors. One approach is to use arrays of single elements with their outputs combined to form beams. Such arrays are typically several wavelengths in dimension. Another approach is to measure vector properties of the acoustic field. A sensor that responds to either the local pressure gradient or the local acoustic particle velocity has an intrinsic directionality. Large-aperture arrays easily outperform individual vector sensors in degree of directionality but incur an obvious size penalty. While a great body of literature exists on the design and performance of large-aperture arrays, vector sensors are less well documented. Military and civilian applications consume millions of gradient or velocity sensors of various types, so there is a substantial body of corporate knowledge, though.

Terminology is confusing and inconsistent in the literature. In this summary paper, a sensor that responds directly to incident pressure will be called a scalar or pressure sensor. A sensor that responds directly to some vector measure of the acoustic field will be called a vector sensor. If a vector sensor measures by finite-difference approximation of the field gradient it will be called a gradient sensor; if a vector sensor responds directly to motion of the sensor body with an output directly related to acoustic displacement, velocity, or acceleration, it will be called an inertial sensor. Sometimes the terms velocity sensor and pressure-gradient sensor are used interchangeably in the literature, but this obscures the physics. The manner in which gradient and inertial sensors respond to the field is substantially different.

A short, superficial history of the development of vector sensors illustrates some of the important design issues. The ribbon microphone was one of the first widely known vector sensors. In 1931, Olson[1] describes the relationship between pressure gradient and velocity and outlines the near-field correction for the amplitude of the inferred pressure field. Two years later, Wolff and Massa[2] broach the possibility of measuring acoustic intensity from the product of velocity and pressure. A neutrally buoyant inertial sensor for underwater acoustics was built and tested in 1941 by Kendall.[3] The concepts embodied by Kendall's design are common to most inertial vector sensors used underwater since that time.

Much of the research directed toward vector sensors was funded by the US Navy toward development of air-deployed underwater sensors (as sonobuoys). For expendable sensors, the small size of the vector sensor outweighs the lower directionality in comparison to large-aperture arrays. Bauer and DiMattia,[4] supported by the Naval Air Development Center, described the design of a two-component inertial vector sensor using moving-coil transducers in 1966. The directional sonobuoy (DIFAR[5]) was approved for operational service for US Navy Maritime Patrol Aircraft by 1969. Since that time, US manufacturers alone have produced more than four million directional sonobuoys. The DIFAR sonobuoy has become the principal tool in maritime patrol activity with a high performance-to-price ratio.

One of the critical limitations of the vector sensor reached the open literature in 1977 with Keller's summary[6] of measured flow-induced noise on gradient and inertial sensors. The sensitivity to non-acoustic disturbance is much greater than for a simple pressure sensor. These measurements showed 20-dB higher flow noise on a vector sensor compared to a pressure sensor at 100 Hz for a flow speed of 0.5 knots (increasing to 70 dB higher at 10 Hz). Much of the subsequent work on vector sensors has been aimed at controlling the response to flow-induced noise.

In 1980, the vertical-line-array DIFAR (VLAD) received approval for service. This sonobuoy combined a large-aperture vertical array with a two-axis vector sensor. This sonobuoy is particularly noteworthy because the design philosophy was not to steer a narrow beam toward the intended target. Instead, it was designed to reject prevailing ambient noise. As a result, in proper application, it achieves an array gain far higher than its directivity index.

Perhaps the ultimate in low-frequency performance of an underwater vector sensor was achieved by the Marine Physical Laboratory's acoustic Swallow Float system. Also notable is the in-depth analysis of limits to performance published in 1991 by D'Spain, et al.[7] The quasi-free sensor body was incorporated in the neutrally buoyant infrasonic DIFAR sonobuoy (NBIDS) developed in the 1990's.

Several themes are evident throughout this history. The vector sensor was and is highly successful as an air-expendable instrument. The sonobuoy industry markets a two-axis vector sensor complete with RF telemetry, a sophisticated sea-surface motion isolation system, electronic magnetic compass, and military qualified air-launch-hardened package for less than $500. Perhaps the most serious shortcoming of the vector sensor is its sensitivity to motion (in the case of the inertial sensor) or to non-acoustic pressure fluctuations (in the case

of the gradient sensor). Certainly, the success of a technology in one arena does not guarantee success in every application. Success depends on careful matching of the technology to the operational requirements. Such matching can only be done through understanding both the capabilities and limitations.

What follows is a summary of some of the important lessons learned in development of vector sensors for underwater systems. The list of issues is not exhaustive nor are all the issues of equal importance but these issues should be considered whenever new applications are explored.

II. FUNDAMENTALS

Much of the potential and many of the limitations of vector sensors are clear from the fundamental equations for linear acoustic fields. Euler's equation or Newton's Law per unit volume when there is no mean flow is

$$-\nabla p \;=\; \rho \frac{\partial \vec{v}}{\partial t} \;=\; j\omega\rho\vec{v} \;. \tag{1}$$

This vector equation is actually three scalar equations. Any one of those equations shows that a measurement of one component of the pressure gradient is equivalent to a measurement of the acoustic acceleration in that direction. The term on the left represents a gradient measurement while the center term or the term on the right represents an inertial measurement (hence the distinction between gradient and inertial sensors). The two are equivalent *as long as the field is entirely acoustic in origin*; the equation is not true in general.

The equation of continuity (merged with the equation of state) is

$$-\nabla \cdot v \;=\; \frac{1}{\rho c^2}\frac{\partial p}{\partial t} \;=\; \frac{j\omega p}{\rho c^2}\;. \tag{2}$$

This is a single *scalar* equation. (Multiply Eq. 2 by $p/j\omega$ to convert it to an expression of the potential-energy density. In this form, it is clear that only simple fluid-λικε compression is accounted.) If we know all three components of the divergence of the velocity field, we can determine the pressure *as long as the field is entirely acoustic in origin*.

The curl of Euler's equation,

$$-\nabla \times \nabla p \;\equiv\; 0 \;=\; \rho \frac{\partial}{\partial t}(\nabla \times v) \;=\; j\omega\rho\,\nabla \times v \tag{3}$$

shows that the rate of change of the curl of acoustic velocity is zero *as long as the field is entirely acoustic in origin*. Since any constant component cannot contain signal information, this is equivalent to the statement that the curl of acoustic velocity is zero. This is indicative

more of a limitation in the linear acoustic approximation than it is a statement of an experimentally relevant relationship. Here is the first direct evidence that non-acoustic flows are excluded. Turbulence – a source of flow noise – is excluded by the underlying assumptions, but turbulence is critical to understanding the limits to inertial sensing in a fluid. In the derivation of the linear acoustics equations, it is assumed that there is no bulk flow or viscosity, that there is a specific equation of state entirely dependent on the acoustic compressibility of the medium, and that all quantities are small.

What we learn from these equations is that if we can measure pressure gradient we can make inferences about the acoustic particle velocity. Conversely, if we can measure acoustic particle velocity then we can make inferences about pressure. But these inferences follow Eqs. 1 and 2 only if the field is acoustic. Structure-borne vibration or turbulence (or even mean flow) can invalidate the process. Even if the field is entirely acoustic, care must be exercised regarding assumptions. We often assume, with little error, that the pressure from an acoustically small source varies as the reciprocal of distance from that source. This does not mean that it is safe to assume the same dependence for the radial component of particle velocity. While the fundamental governing equations are reliable for linear acoustic fields, other relations like $p = \rho c v$ are not valid in general and can introduce significant error (for example) in calibration or application of vector sensors. It is also important to recognize that these relations are specific to fluid media. If we introduce a medium that has any shear stiffness, we must often account for motion coupled into shear.

III. SENSOR TYPES

A. Pressure sensor

The pressure sensor produces an output that is directly related to the incident pressure. Ideally, there is no sensitivity to acceleration, so motion of the sensor body does not produce signal. This is fundamentally a point measurement. If the responsivity of the sensor could be held constant, reducing the size of the sensor would not affect the output. There is no information about direction in the pressure-sensor output. This is a scalar or "zero-dimensional" sensor.

B. Pressure-gradient sensor

Subtraction of the outputs from two elements produces a result that is directly related to the pressure gradient. The air-acoustic intensity probe functions this way as do most noise-canceling microphones. Some early directional sonobuoys used gradient measurement. The "sensor" consists of at least two pressure-sensing elements (or both sides of a single element). The elements can be rigidly fixed in space: *motion is not central to sensing*. The gradient sensor implements the finite-difference equation

$$p(x+\delta) \ - \ p(x-\delta) \ \approx \ 2\delta \frac{\partial p}{\partial x}. \tag{4}$$

The pressure difference is directly proportional to acoustic acceleration, and the magnitude of the resultant is intimately related to the separation, 2δ, between elements. This is an "aperture" sensor. Its performance is fundamentally associated with its spatial extent. Reducing the size reduces the response (whereas increasing the size increases the error) even if the element response is unchanged. This results in an unavoidable loss in dynamic range. The gradient sensor is fundamentally directional.

C. Inertial sensors

The output of an inertial sensor is directly related to the motion of the sensor body. Depending on the specific type of transduction, the output may be more nearly proportional to acceleration, velocity, or displacement, but this aspect is not fundamental. More important: *motion of the sensor body is essential*. Ideally, there is no sensitivity to pressure. The inertial measurement is fundamentally a point measurement. The size of the sensor body does not affect the response magnitude in a fundamental way (but, like the pressure sensor, does affect the output in practical ways). The inertial sensor responds to motion regardless of origin: it cannot discriminate between acoustic waves, turbulence, or structure-borne vibration.

D. Inertial gradient sensors

In analogy with pressure-gradient sensors, it is also possible to measure the spatial rate of change of the velocity field. Two inertial elements spaced some distance apart can provide one component. In contrast to the pressure-gradient, there are nine unique elements of the spatial derivative of velocity:

$$\begin{bmatrix} \dfrac{\partial v_x}{\partial x} & \dfrac{\partial v_y}{\partial x} & \dfrac{\partial v_z}{\partial x} \\[2mm] \dfrac{\partial v_x}{\partial y} & \dfrac{\partial v_y}{\partial y} & \dfrac{\partial v_z}{\partial y} \\[2mm] \dfrac{\partial v_x}{\partial z} & \dfrac{\partial v_y}{\partial z} & \dfrac{\partial v_z}{\partial z} \end{bmatrix}. \tag{5}$$

The inertial pair implements the following finite-difference equation:

$$v_x(x+\delta) \;-\; v_x(x-\delta) \;\approx\; 2\delta\frac{\partial v_x}{\partial x} \;=\; \frac{j2\delta}{\omega\rho}\frac{\partial^2 p}{\partial x^2}. \tag{6}$$

As with the pressure-gradient sensor, the output depends fundamentally on the separation between elements, and there is an unavoidable loss in dynamic range. The sum of the main diagonal elements of the derivative matrix is the divergence of the velocity field, which is directly proportional to the second time derivative of the pressure. This provides a useful test of the fidelity of the sensor system or of the acoustic nature of the field.

In a purely acoustic field, the matrix would be symmetric since symmetry is equivalent to zero curl. In many important cases of simple waves (and appropriate alignment of the reference axes with the field) all of the off-diagonal terms are zero (again providing a test of either the sensor system or the field). This would be true for a pure plane wave in any set of Cartesian coordinates or for a spherical wave in coaxial spherical coordinates. (An inertial *rotation* sensor would measure quantities related to the off-diagonal terms.)

IV. REQUIREMENTS FOR INERTIAL SENSORS

A. Fundamental requirements

By far the most important aspect of the inertial sensor is that it must move freely with the acoustic fluid motion. Furthermore,

- it must respond faithfully in magnitude and phase to the local acoustic particle velocity;
- its presence must not perturb the acoustic field or that perturbation must be correctable; and,
- it must be insensitive to or shielded from non-acoustic excitation such as turbulence in the local flow field, turbulence produced by the sensor body, vibrations conducted through the support structure, or local radiation of nearby structural vibration.

Intuition developed with pressure sensors is dangerous when applied to inertial sensors. Inertial sensors are typically far more sensitive to motion than pressure sensors.

B. Sensitivity to motion

Sensitivity to motion of a pressure hydrophone is normally given by its acceleration sensitivity, S_a. Typical acceleration sensitivity for a hydrophone[8] is of the order of one pascal per meter per second-squared. Consider a pressure hydrophone and an inertial sensor immersed in an acoustic plane wave. Assume that both are free to move with the acoustic field and that the pressure-associated output of the hydrophone and the velocity output of the inertial sensor are accurate. The pressure-equivalent signal produced by the hydrophone in response to the acoustic acceleration would be S_a times the acoustic velocity multiplied by the radian frequency, ω. The pressure-equivalent signal produced by the inertial sensor would be ρc times the acoustic velocity. The ratio of the pressure-sensor response to the velocity-sensor response is then $S_\alpha \omega / \rho c$. This ratio is $4 \cdot 10^{-6}$ at 1 Hz and $4 \cdot 10^{-3}$ at 1000 Hz. In this situation, the pressure sensor is substantially less sensitive to motion at all but very high frequency.

An important consequence is that isolation mounts developed for pressure hydrophones are entirely inadequate for inertial sensors from the standpoint of isolation from structural vibration. (And, for an inertial sensor, the mount must allow freedom of motion with the acoustic field.)

Another instructive comparison concerns the response to vertical motion. Vertical oscillatory motion is fundamentally different from horizontal motion for underwater sensors. In vertical motion, there is a potentially large pressure signal produced simply from motion in the hydrostatic pressure gradient. For an amplitude, h, of vertical motion, there is a corresponding amplitude, $\rho g h$, of pressure change. One millimeter of vertical motion corresponds to 10 *pascals* of pressure amplitude (140 dB with respect to one micropascal). The amplitude of such an oscillation with velocity, v, is v/ω.

For a pressure hydrophone and an inertial sensor undergoing the same vertical oscillation, their outputs converted to equivalent pressure can be compared. The effective pressure amplitude is $\rho g v/\omega$. The pressure-equivalent output of the velocity sensor is $\rho c v$. The ratio of pressure-sensor output to velocity-sensor output is 10^{-3} at 1 hertz or 10^{-6} at 1000 Hz. Again, the amplitude of the spurious signal is far larger on the inertial sensor than on the pressure sensor. For example, even with an excellent suspension system, it is difficult to make low-frequency vertical-axis inertial measurements with a sonobuoy.

A practical consequence of the motion sensitivity of the inertial sensor is that a complex surface-motion isolation system is a necessity for directional sonobuoys even though low cost is critical. Furthermore, any application that specifies acceleration-canceling hydrophones would be challenging to adapt to inertial sensors.

C. Multi-axis systems

If more than one component of the velocity or acceleration vector is measured at the same location, some care is required in the sensor design. The design of mounts and suspensions is particularly difficult when the sensor body must be free to move in all three axes as discussed in a separate section below. Another issue associated with multi-axis sensors is inter-element phase error. Three-axis accelerometers are commercially available and consist of a triad of orthogonal single-axis accelerometers in a single mounting block. A similar design for an underwater sensor leads to a frequency-dependent phase error in the relationship between components because the response centers of the elements are not collocated. (This phase error also exists in the commercial accelerometer, but most structural-vibration-measurement applications do not involve component-to-component phase reconstruction, so the small package size is more desirable than phase accuracy.)

If, instead of three elements, six elements are arranged so that each pair straddles a common center point, then the phase error associated with the response centers is zero. The common phase-center design is also advantageous in that the center point can be collocated with the center of mass of the sensor body. If the phase center, the center of mass, and the center of acoustic pressure are all collocated, several potential errors in fidelity can be avoided. The elements in the directional-sonobuoy sensor body have the common-centroid design (but the separate pressure hydrophone is vertically offset from the phase center of the directional elements). Another illustration of the common-centroid design is the miniature directional element shown in Fig. 1. Here, four differential capacitance elements are

arranged with a common center and connected electrically as a full bridge. There are a number of practical advantages in this design besides the common phase center.[9]
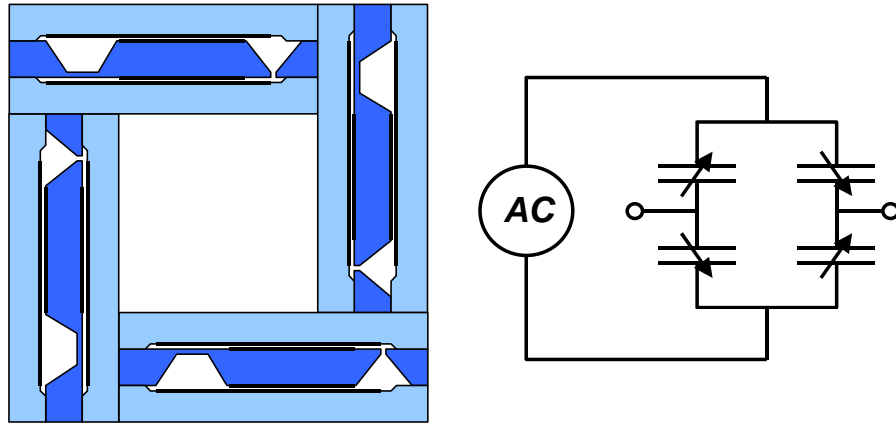
FIG. 1. Full-bridge differential-capacitance inertial sensor for two-axis operation. Each axis comprises a full bridge made from two opposing structures. The two orthogonal pairs of structures provide two-axis response with a common phase center. The structure is 7 x 7 x 3 millimeters in size. Each bridge is driven with a high-frequency AC signal and the output, modulated by the sensed acceleration, is detected synchronously.

V. REQUIREMENTS FOR PRESSURE-GRADIENT SENSORS

A. Fundamentals

The pressure-gradient sensor relies (either explicitly or implicitly) on subtraction of two nearly equal quantities. This concept is essential to its operation and is the root of its most serious limitations. The gradient sensor

- must have excellent element-to-element matching in both phase and amplitude (or have a reliable calibration and correction);
- must have low self-noise in all elements since the dynamic range is compromised fundamentally by the subtraction; and
- must not perturb the acoustic field significantly.

B. Finite differences

The magnitude of the gradient calculated by finite difference is reduced in amplitude by a factor of the order of the element separation, d, in wavelengths. Small kd (where k is the wave number) is essential for accuracy in determining the derivative but small kd also means a large reduction in dynamic range. This is completely analogous to the loss of precision in numerical finite-difference operations.

There are also phase errors associated with the orientation of the elements. A sensor designed to measure the gradient in two dimensions could be made from three elements as shown in Fig. 2. However, the phase centers of both pairs and of the equivalent monopole

are not coincident. If, instead, four elements are used, then all of the phase centers can be collocated. This construction is equivalent to using centered differences instead of one-sided differences in finite-difference computations.

FIG. 2. Two configurations for measuring the gradient in two dimensions. For the arrangement on the left, the phase centers of the two dipoles and of the equivalent pressure formed by summing all three elements are not coincident. In contrast, the phase centers for both dipoles and the equivalent pressure for the arrangement on the right are coincident. The four-sensor arrangement has zero in-plane phase error.

C. Basic dipole

The basic "dipole" element is shown in Fig. 3. This is only a true dipole for vanishingly small separation, but, in practice, its output is not essentially different than a dipole because the spacing is kept small. If the outputs from the two elements are subtracted, the resultant pressure is

$$
\begin{aligned}
p_D \quad &= \quad 2\,p_A - 2\,p_B \quad = \quad 4\,j\,p_0 \sin\!\left(\frac{k\,d}{2}\cos\theta\right). \\
&\approx \quad 2\,j\,p_0\,k\,d\,\cos\theta \qquad \left(k\,d \ll 1\right)
\end{aligned}
\tag{7}
$$
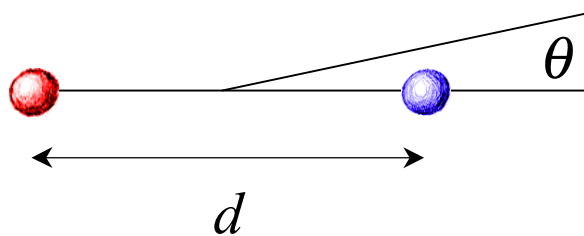
FIG. 3. Basic two-element gradient sensor. The outputs of the two elements are subtracted. For separation, d, much less than an acoustic wavelength, the system behaves as a dipole.

In order to facilitate comparison of monopole, dipole, and quadrupole sensors, a consistent normalization of four units (two for each element in this case) will be used throughout. The comparison monopole would have a scale factor of four. This normalization maintains the same effective self-noise level for each type of sensor so that the progressive loss in dynamic range is immediately evident.

Of critical importance in understanding the performance of the gradient sensor is the influence of noise. Internal self-noise in the elements is normally not coherent from element to element (in contrast to ambient noise). Consequently, even though the outputs are

subtracted, the self-noise adds incoherently. For the dipole, the signal amplitude is $2\,k\,d$ while that of the monopole is 4 but the self-noise floor (with our normalization) is the same. As a result, the signal-to-noise can be poor even if each element taken independently has high signal-to-noise.

Within these constraints, three orthogonal dipoles (using six elements, for example) give all of the first-order terms in the Taylor series expansion for pressure about the measurement point and completely define the vector gradient in pressure.

The outputs of two orthogonal dipoles (and a simple pressure measurement) can be combined to form a cardioid, which can be steered in any direction by proper phasing of the two dipoles:

$$p_D \;+\; jkd\,p_M \;\approx\; 4\,j\,p_0\,kd\left[1\,+\,\cos\theta\right] \tag{8}$$

where p_M is four times p_0 to maintain the "four-unit" normalization. Notice that we retain the signal-to-noise disadvantage (kd factor). In addition, a frequency-independent phase shift of 90 degrees must be provided.

D. Basic quadrupole

If a dipole is useful, then perhaps a quadrupole is even more useful. In finite-difference form, the longitudinal quadrupole is equivalent to the second spatial derivative:

$$p\left(x+\delta\right) \;-\; 2\,p\left(x\right) \;+\; p\left(x-\delta\right) \;\approx\; 4\delta^2 \frac{\partial^2 p}{\partial x^2}\,. \tag{9}$$

The arrangement for a longitudinal quadrupole is shown in Fig. 4. If the outputs are combined as follows

$$p_Q \;=\; 2\,p_B \;-\; p_A \;-\; p_C \;=\; 2\,p_0 \;-\; 2\,p_0\cos\left(kd\cos\theta\right)$$
$$\approx\; 4\,p_0\left(\frac{kd}{2}\right)^2\cos^2\theta \qquad \left(kd \;<<\; 1\right)\,. \tag{10}$$

then we obtain an approximation to the second derivative of the field. The directivity (see Fig. 5) is sharper than the dipole, but the signal-to-noise penalty (in amplitude) goes as $(kd)^2$, so the dynamic range is seriously limited. From Fig. 5, if the single element noise is 60 dB below the signal, the dipole peak is less than 30 dB above the noise and the quadrupole would produce no directivity at all. In effect, the quadrupole sacrifices almost 70 dB of dynamic range (11 bits in a digital system) and would require an extraordinarily high element signal-to-noise ratio to estimate the second derivative accurately.
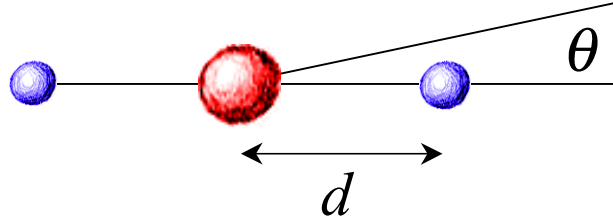
FIG. 4. Basic configuration of a three-element sensor for estimating the second space derivative. Two times the output of the center element is subtracted from the sum of the outputs of the outer elements. If *d* is much less than a wavelength, the configuration is a longitudinal quadrupole.
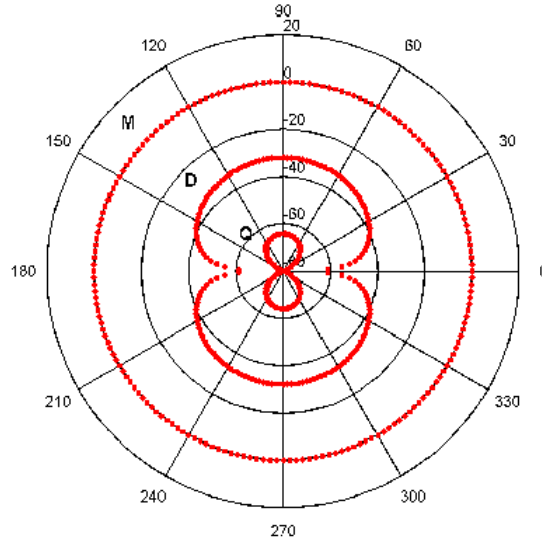
FIG. 5. Comparison of the directional response of a monopole, a dipole, and a quadrupole ($ka = 0.05$). The sensors are compared in such a way as to have equal self-noise power, so the reduction in level of the main lobe corresponds to the sacrifice in dynamic range.

One hindrance to the development of good engineering judgment in directional systems is the tendency to normalize directivity plots so that the maximum response is unity. Fig. 5 is constructed so that the self-noise floor is identical in each case and the performance penalty incurred in the finite-difference process is clearly evident. For transmitting arrays, normalization to input power produces more instructive comparisons than peak normalization. For example, comparisons between the beam patterns of the primary and difference beams in a parametric sonar done in this manner would still reveal the beam shape but also highlight the inefficiency of the process.

The signals from orthogonal quadrupoles can be combined to form a cardioid-squared pattern as follows

$$4 p_Q - 2 j k d\, p_D + (k d)^2 p_M \;\approx\; 4 p_0 (k d)^2 [1 + \cos\theta]^2 \tag{11}$$

which can be steered to any orientation by proper phasing.

11

Because of the dynamic-range loss, the quadrupole may be completely impractical with pressure elements and second-order finite-difference construction; however, the equivalent can be formed through finite-difference combination of inertial sensor outputs (see Eq. 6). This approach avoids the harsh $(kd)^2$ dynamic-range penalty *but introduces the motional sensitivity of the inertial sensor that is exacerbated by the finite-difference operation*.

VI. COMPARISON OF GRADIENT AND INERTIAL SENSORS

A. Inertial sensors

The sensor output is directly related to acceleration (or velocity or displacement), and good dynamic range is readily achievable. The effective noise floor of an inertial sensor can usually be designed to be far below that of an equivalent gradient sensor. However,

- the sensor body must be free to respond accurately to the acoustic wave;
- it must be protected from non-acoustic disturbances;
- it is difficult to miniaturize sufficiently to make good measurements at high frequency; and,
- it is difficult to isolate sufficiently to make good measurements at low frequency.

B. Pressure-gradient sensors

The elements of the gradient sensor can be compact and rigidly fixed in space. The elements

- must be well matched in both phase and amplitude, or some provision for calibration and correction must be made;
- must have low self noise; and,
- must have a large basic dynamic range to compensate for the subsequent loss in range associated with the finite-difference operation.

VII. SUSPENSIONS

A. Basic requirements

Suspensions are critical to proper operation of inertial sensors much more so than for pressure or pressure-gradient sensors so the focus here is on inertial sensors. The fundamentals of inertial-sensor suspensions have been covered in detail elsewhere[10] so only a brief summary of the basics is presented. Fundamentally, the suspension

- must have a natural frequency well below the intended range of operation;
- must fix the time-average position and orientation of the sensor body;
- must permit movement of the sensor body with the acoustic field;

- must isolate the sensor from structure-borne vibration;
- must not distort the response of the sensor either in magnitude, phase, or apparent angle; and
- must withstand operational shock.

In order to categorize various systems, we will consider both the dimensionality of the sensor and the number of position and orientation constraints. Since pressure sensing produces a scalar measure of the field, that will be called a "zero-dimensional" measurement. A single-axis vector probe constitutes a one-component measurement and so on to three dimensions of measurement. More dimensions can be defined for inertial-gradient sensors, but we can decompose these higher order systems into sets of one-, two-, or three- component sensors insofar as suspension design is concerned. We will not discuss mounting zero-dimension sensors further.

Since the suspension must support the sensor in some repeatable position, it imposes constraints at least on the time-averaged position. There are six degrees of freedom for such support: three axes of translation and three axes of rotation. Depending on the application, it may not be necessary to constrain all six degrees of freedom.

B. One-component sensors

If the vector sensor is intended to measure only one component of the field, the suspension design is straightforward with a number of practical variants. The ribbon microphone and the modern air-acoustic intensity probes are examples of one-component sensors. Presently under commercial development[11] are inertial velocity sensors with compact suspensions of spiral-cut leaf springs. By making use of the fact that low stiffness is not required in directions orthogonal to the sense axis, the suspension is much more space effective and durable. Such a suspension introduces anisotropy, which can have consequences for reconstruction of the acoustic field.

Single-axis sensors embedded in compliant coatings rely on the characteristics of the coating for suspension. Freedom of motion along the sense axis depends on the relatively low shear stiffness of the coating. Perpendicular to the sense axis and in the plane of the coating, the compressional elastic properties of the coating material are important. If the compressional stiffness is close to that of water and the boundaries are far removed, then reasonable isotropy and, therefore, fidelity in one dimension is possible. Two varieties of single-component suspension (and one type of two-component suspension) are shown in Fig. 6.

C. Two-component sensors

In underwater acoustics, two-component sensing is far more common than any other type. For two-component sensors, the third axis can be used as a "stiff" support axis. This results in a robust suspension with a very low resonance frequency in either sense direction. The sonobuoy (see Fig. 6) uses a uniaxial support: a weight hangs below the sensor body and pulls the connecting cable taut between sensor body and whatever is above the sensor body.

This taut-line suspension is very weak for small transverse displacements, so the sensor body is free to follow the acoustic motion with good fidelity above the transverse resonance. There are three translational constraints but only two rotational constraints. Rotation about the support axis is not constrained. Instead, a magnetic compass is used to stabilize the azimuthal orientation electronically.

Good low-frequency performance is difficult to obtain with any inertial sensor because the amplitudes of the corrupting excitations tend to increase with decreasing frequency. The sonobuoy suspension is designed to isolate from vertical and horizontal surface motion but it cannot remove steady horizontal flow that results from current shear. Consequently, there is some irreducible level of flow past the sensor body that results in flow-induced noise.
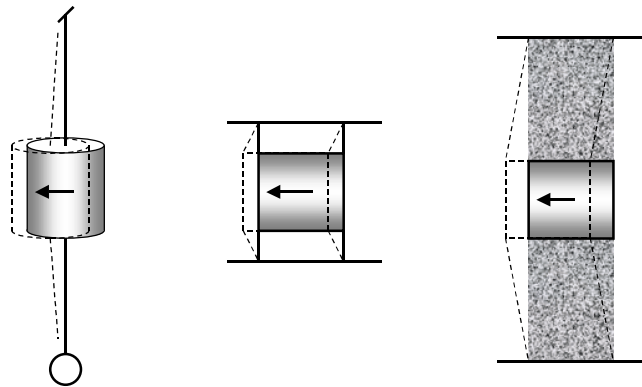
FIG. 6. Primary varieties of velocity-sensor suspension. The suspended (sonobuoy) two-component sensor is shown on the left. A sensor supported by mechanical springs at each end is shown in the center, and a sensor embedded in a compliant suspension material is shown on the right.

D. Three-component sensors

Three-component sensors with six-degree-of-freedom constraint are difficult to build with reasonable size. Probably the best known three-component sensor system is the Swallow Float[12] system. This system has only one translational constraint provided by buoyancy adjustment for stability in the ocean density profile. Two rotational constraints are imposed by shifting the center of mass below the center of buoyancy; rotation about the vertical axis is unconstrained. By relaxing the translational constraint, exceptional low-frequency performance is obtained.

In order for a system like the Swallow Float to reach vertical equilibrium in a density gradient, the body must be significantly less compressible than the fluid. As a result, the body will scatter the local acoustic field substantially if the frequency of operation approaches $ka = 1$.

Another approach for three-component sensing is to stage single-component sensors in nested suspensions. This is difficult to accomplish without a serious volume penalty.

A third technique is to embed the sense-element cluster in a compliant, elastic material. Special care must be exercised in the design of the shear stiffness and the external mounts, however. If the design relies on shear stiffness to control the suspension resonance, the mount must be designed to avoid any axis being constrained by compression of the material since the compressional modulus is normally much higher. With such a system, it is extremely difficult to avoid considerable anisotropy in the suspension.

E. Symmetry And Anisotropy

The fundamental tenet of suspension design is that the primary resonance of the suspension should be well below the lowest frequency of interest. While this is straightforward to achieve in one- and two-component vector sensors, it can be very difficult to achieve in practical three-component sensors. If all of the fundamental resonances are not well below the frequency of operation, then we must consider the effects of three-dimensional anisotropy in the suspension on the signals produced by the sensor.

For example, the suspension used in the sonobuoy directional package has resonances with respect to horizontal displacements that are very low, but the resonance with respect to vertical displacement can be in the band of interest. This anisotropy affects the fidelity of the sensor response with respect to the vertical component. In the sonobuoy application, accurate resolution of the vertical component is immaterial. The anisotropy, in this case, only serves to increase the apparent level of signals at low frequency over that that would be produced by a perfect horizontal-component sensor.

However, this anisotropy would be problematic if it were necessary to sense the vertical component with the same suspension. Not only would the isolation be poor, but also the vertical sensor would be overly constrained and the vector resultant would have the wrong direction. The Swallow Float and the neutrally buoyant infrasonic DIFAR sonobuoy with their quasi-free "suspensions" circumvent this problem but only by incurring substantial limitation in employment.

A soft polymeric material can be used as a suspension if the restoring force is arranged to be through shear in the polymer. If the polymer body is fixed at two diametrically opposite points, then shear is the operative restoring force for displacement perpendicular to the support axis. However, along the support axis, the restoring force is compression/extension. The modulus may be much higher for compression/extension, so it is more difficult to keep this resonance low. Consequently, the isolation may be much worse and the motion more restricted for the sensor aligned along the support axis. Clearly, this also results in anisotropy in the overall suspension scheme and distortion of angle of arrival. In evaluating such systems, it is vital to test the sensor for arrivals from all directions. If it is only evaluated for arrivals perpendicular to the support axis (for example), problems can go undetected. The sensor should be tested in its eventual mount and should be evaluated for all directions of arrival not only with respect to the sensor elements but also with respect to the

mount. (It is also necessary to measure the excitation of the mount itself to avoid confusing sensor suspension problems with problems associated with laboratory fixtures.)

Interesting problems can also arise when periodic arrays of single-component sensors are embedded in a compliant layer. The suspension problems for a single sensor are not essentially different from those discussed above, but the periodic array adds a complication. The interaction of the sensor bodies through either shear or compressional coupling in the compliant layer introduces effective bulk properties to the layer. The periodic structure introduces "conduction bands" and "stop bands" for propagation through the layer. Coincidence between wave numbers in the material and incident tangential wave numbers for acoustic waves produces strong coupling. The conduction/stop band structure can make this coupling complicated and introduce spurious structure to the vector sensor output.

VIII. PERFORMANCE LIMITS

There are many limits to performance in any sensor technology. We have already discussed problems associated with response to non-acoustic disturbance and limitations imposed by suspensions. Here, a few additional problems are summarized. As is the spirit throughout this paper, this is not an exhaustive list. The intent is to ensure that several important considerations are not ignored in the design, development, and application of vector sensors.

A. Noise

Sensor self-noise can limit the performance of a system dramatically. Those noise components associated with the basic sensor structure, materials, or first-stage electronics should never be overlooked even if they have been ignored successfully in the past. These components are generally uncorrelated from sense element to sense element and, as such, are straightforward to account in a performance budget. The impact of such noise on dipole and quadrupole sensors was discussed above. In short, these noise components should not be compared to the omnidirectional ambient-noise level to determine their importance. The more array gain desired from the system or the more dynamic range sacrificed by finite difference, the further below ambient these noise sources must be.

Vector sensors are particularly susceptible to flow noise. Flow noise is noise associated with relative motion between the sensor body and the fluid in which it is immersed. Flow noise may consist of pre-existing turbulence advected past the sensor body by the relative flow, or it may consist of turbulence produced by the presence of the body in the flow. In either case, there is a non-acoustic field to which the sensor responds. The effects of flow noise can be reduced by increasing the effective sensor size (with a wind-screen, a flow shield, or many sensors connected together). In any case, though, the overall sense dimension must be small enough to respond properly to the local acoustic field. If the correlation distance of the turbulence is much smaller than an acoustic wavelength, extra sensor dimension provides

some averaging over the flow disturbances. Combining the outputs of several closely spaced elements is common practice in towed arrays of pressure hydrophones.

Any motion transmitted from a structure to the sensor will also produce a signal that is not associated with the incident acoustic field. One of the critical aspects of suspension design is transmissibility or vibration isolation.

For a "good" sensor design, the ocean ambient should control the achievable performance rather than the sensor noise, flow noise, or structure-borne noise. Consideration of the effects of ambient noise is difficult, though, because the ambient-noise field is complicated. Even in the deep ocean, the ambient is strongly anisotropic; in important shallow-water areas, the anisotropy can be extreme. In order to facilitate calculations, it is often assumed that the ambient noise is isotropic. However, unless the frequency is above 50 kHz or so, ocean ambient (particularly in shallow water) can be strongly anisotropic and this will affect performance predictions. Performance numbers obtained using the assumption of isotropic noise are neither upper nor lower limits to ultimate performance. In some cases, considerable performance improvement can be obtained by exploiting the anisotropy of the noise field.[13]

B. Fidelity of response

If the suspension has been designed well, then its influence on the acoustic performance of the sensor should be negligible. However, the sensor itself can corrupt the received signal. Although many lab measurements and calibration focus on the magnitude response of sensors, the phase response is often more important in determining the eventual system performance.

Consider, for example, a single-degree-of-freedom accelerometer that might be used in an inertial sensor. Conventional wisdom suggests designing the Q to be rather small so that the response is "flat" over as wide a band of frequency as possible. Such a design philosophy results in substantial phase error well below the resonance. While, in principle, these phase errors can be calibrated and removed, the success of such a correction process relies on the stability of the resonance frequency as well as on the stability of the damping. Small shifts in the resonance frequency (which would be difficult to detect from an examination of the magnitude response) can produce substantial phase changes even a decade below the resonance.

A higher Q system results in much smaller in-band phase error. Shifts in the resonance frequency or damping (temperature dependence, for example) have reduced effect away from the resonance. Since phase errors usually create more problems in array beamforming or in vector component resolution (particularly for gradient sensors), the higher Q design is important. The price of the higher Q is that the system must handle a larger dynamic range of signals.

An often-overlooked aspect of the phase response results from the low-frequency roll-off. The lower edge of the pass band for a piezoelectric sensor (for example) is normally set by the relationship between the sensor capacitance and the input resistance of the first stage preamplifier. This is a *single-pole filter* so the effects of phase extend well into the pass band and are only as stable as the element values in the filter.

C. Calibration and operation in the "near" field

Often, it is assumed that acoustic pressure is equal to the fluid density times the fluid sound speed times the acoustic particle velocity but this is only true in certain circumstances (most commonly a plane-wave field). In "free-field" calibration, the range between source and receiver is often such that kr is not very large. For comparison calibration (for example) of two pressure sensors, the near-field details are unimportant. However, for comparison of pressure sensors and inertial sensors a correction is required.

If the source is small with respect to a wavelength, then it can be treated as a simple source. If we use Euler's equation to find the relationship between pressure and particle velocity using the pressure field produced by a simple source, we find that the normalized ratio is

$$\frac{\rho c v_r}{p} = 1 - j\frac{1}{kr}. \tag{12}$$

For $kr = 12$ (almost three meters at 1000 Hz), the phase is still 5 degrees different from the simplistic plane-wave assumption.

While it is simple to remove this correction from measured data, it is often useful to measure the phase relationship as a function of source-receiver separation. The tangent of the measured phase (with the phase bias error subtracted) as a function of kr should be a straight line. By iterative fitting, the phase bias can be determined and the quality of the calibration can be assessed. Departures from the expected straight-line behavior should be suspect.

REFERENCES

1. H. F. Olson, "Mass controlled electrodynamic microphones: the ribbon microphone," J. Acoust. Soc. Am. **3**, 56-68, 1931.

2. I. Wolff and F. Massa, "Use of pressure gradient microphones for acoustical measurements," J. Acoust. Soc. Am. **4**, 217-234, 1933.

3. C. B. Leslie, J. M. Kendall, and J. L. Jones, "Hydrophone for measuring particle velocity," J. Acoust. Soc. Am. **28**, 711-715, 1956.

4. B. Bauer and A. DiMattia, "Moving-coil pressure-gradient hydrophone," J. Acoust. Soc. Am. **39**, 1264(A), 1966.

5. DIFAR is a shortening of Directional LOFAR. LOFAR retains little of its original derivation (Low-Frequency Analysis and Ranging) and has come to mean the generic single-hydrophone sonobuoy.

6. B. D. Keller, "Gradient hydrophone flow noise," J. Acoust. Soc. Am. **62**, 205, 1977. Also, R. A. Finger, L. A. Abbagnaro, and B. B. Bauer, "Measurements of low-velocity flow noise on pressure and pressure gradient hydrophones," J. Acoust. Soc. Am. 65, 1407-1412, 1979.

7. G. L. D'Spain, W. S. Hodgkiss, and G. L. Edmonds, "The simultaneous measurement of infrasonic acoustic particle velocity and acoustic pressure in the ocean by freely drifting Swallow floats," IEEE J. Oceanic Engineering **16**, 195-207, 1991.

8. Sensor Technology Limited, P.O. Box 97, Collingwood, Ontario, Canada L9Y 3Z4.

9. T. B.Gabrielson, "Design, Development, and Evaluation of a Microfabricated Underwater Acoustic Velocity Hydrophone," ARL Technical Report TR 00-001, Applied Research Laboratory Penn State, August 2000.

10. T. B. Gabrielson, D. L. Gardner, and S. L. Garrett, "A simple neutrally buoyant sensor for direct measurement of particle velocity and intensity in water," J. Acoust. Soc. Am. **97**, 2227-2237, 1995. Also, reference 9.

11. Acoustech Corporation, P.O. Box 139, State College, PA 16804.

12. See reference 7.

13. M. J. Buckingham, "On the Response of Steered Vertical Line Arrays to Anisotropic Noise," Proc. Royal Society of London **A367**, 539-547, 1979.

Directional Acoustic Receivers:
Signal and Noise Characteristics

Benjamin A. Cray
Submarine Sonar Department
Naval Undersea Warfare Center Division
Newport, Rhode Island 02841

Directional Acoustic Receivers: Signal and Noise Characteristics

Benjamin A. Cray
Submarine Sonar Department
Naval Undersea Warfare Center Division
Newport, Rhode Island 02841

Abstract: Calculations are presented that demonstrate that a single highly directive acoustic receiver can have a directivity index of up to 9.5 dB. This compares to a directivity index (N_{DI}) of 6 dB for an acoustic vector sensor; a single pressure sensor is omnidirectional and has no directivity. In addition to measuring pressure (p) and particle velocity (u,v,w), as in a vector sensor, the highly-directive acoustic receiver measures also the three gradients of acoustic particle velocity ($\partial u/\partial x, \partial v/\partial y, \partial w/\partial z$). The sum of these gradients is proportional to the instantaneous density of the acoustic field. There is a price to pay with highly directive sensors; these sensors are more sensitive to nonacoustic (subsonic) noise sources.

I. INTRODUCTION

In 1996, the Office of Naval Research funded a study at the Naval Undersea Warfare Center to compare the benefits of a vector-sensing passive sonar array to a conventional pressure-sensing array.[1] This initial investigation showed that directivity and self-noise gains could be realized when vector sensors are used in place of conventional pressure-sensing hydrophones. These sensors can be used to create cardioid-directive array elements, which will provide 6.0 dB of additional directivity gain (N_{DI}) and as well as provide rejection of noise from specific directions.

Utilizing acoustic intensity measurements in submarine sonars, such as the Low Frequency Hull Array, will be challenging. There are additional sonar self-noise mechanisms that are not present, or are ineffective, with conventional pressure-sensing hydrophones -- though there are many potential benefits. For example, Hickling and Morgan[2] and Wei[3] present a formulation to determine the positions of sound sources using underwater acoustic intensity measurements. The derivation considers two steady-state acoustic sources, located at arbitrary positions Q_1 and Q_2 with Cartesian coordinates (x_1, y_1, z_1) and (x_2, y_2, z_2), respectively. Two vector sensors are used to determine the sound intensity field at known positions A and B. From these measurements, it is simple to derive a set of eight nonlinear equations with eight unknowns (the coordinate positions and rms pressures of the two sources). The task then is to solve this system of equations; the authors investigated a possible solution via polynomial continuation.

II. SIGNAL GAIN IN ISOTROPIC NOISE

The directivity index (N_{DI}) of an array (or directional sensor) is defined as a decibel measure of the improvement in the signal-to-noise ratio (SNR) that a beamformed array

(or sensor) provides in an ideal isotropic noise field with a perfectly correlated signal, relative to an omnidirectional array element in the free field.[4] That is

$$DI = 10 Log DF = 10 Log \frac{(SNR)_{array}}{(SNR)_{omni-element}} ,$$ (1)

where DF is the directivity factor. This ratio reduces to

$$DF = \frac{4\pi B(\theta_s, \phi_s)}{\int_0^{2\pi} \int_0^{\pi} B(\theta, \phi) \sin(\phi) d\phi d\theta} ,$$ (2)

where $B(\theta_s, \phi_s)$ is the power sum of the array response steered to θ_s, ϕ_s. Hence, determining the signal gain of a directive sensor in isotropic noise reduces to evaluating the above double integral over θ, ϕ.

The directional dependence of the acoustic particle velocity components, as well as the velocity gradient components, may be obtained from the linearized momentum and continuity equations.[5] For brevity, this derivation will be omitted here.

Suppressing the harmonic time dependence and assuming a planewave amplitude of unity, the power sum of the weighted quantities can be written as[5]

$$B^{(10)}(\theta, \phi) = | w_p + w_x a + w_y b + w_z c + w_{xx} a^2 + w_{yy} b^2 + w_{zz} c^2 $$
$$+ w_{xy} ab + w_{xz} ac + w_{yz} bc |^2 ,$$ (3)

where $a(\theta, \phi) = \cos(\theta)\sin(\phi)$, $b(\theta, \phi) = \sin(\theta)\sin(\phi)$, and $c(\phi) = \cos(\phi)$, and θ, ϕ was defined in Fig. 1.

The objective now is to determine the weights that optimize the directivity expression shown in Eq. 2. It is straightforward to derive the directivity of a single omnidirectional pressure sensor. Namely, from Eqs. 2 and 3, with all weights except w_p zeroed

$$DF = \frac{4\pi(w_p^2)}{4\pi(w_p^2)} = 1.$$ (4)

As expected, the directivity index is zero and the single-pressure sensor is omnidirectional. A similar calculation for a sensor that measures only the u component of particle velocity gives

$$I = \int_0^{2\pi} \int_0^{\pi} (w_x \cos(\theta)\sin(\phi))^2 \sin(\phi) d\phi d\theta = \frac{4\pi}{3} w_x^2.$$ (5)

2
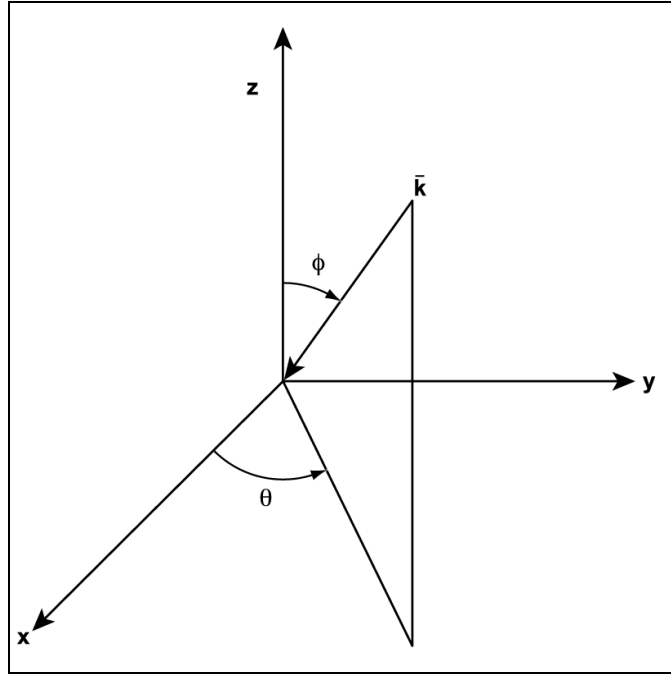
FIG. 1. Sensor coordinate system.

Upon substitution in Eq. (2),

$$DF_{(x)} = 3\cos^2(\theta_s)\sin^2(\phi_s). \tag{6}$$

Equation (6) indicates that a single velocity sensor may have a maximum directivity factor three times greater than an omnidirectional pressure sensor, that is, a gain in directivity index of 4.8 dB.

The maximum response of a vector sensor is given as

$$B^{(4)}(\theta_s, \phi_s) = \left| w_p + a(\theta_s, \phi_s)w_x + b(\theta_s, \phi_s)w_y + c(\phi_s)w_z \right|^2, \tag{7}$$

and the two-fold integral becomes

$$I = \int_0^{2\pi} \int_0^{\pi} B^{(4)}(\theta, \phi)\sin(\phi)\,d\phi\,d\theta = \frac{4\pi}{3}\left(3w_p^2 + w_x^2 + w_y^2 + w_z^2\right). \tag{8}$$

Hence, the directivity factor of a single element that measures all three components of particle velocity and acoustic pressure is

$$DF_{pv} = \frac{B^{(4)}(\theta_s, \phi_s)}{(w_p^2) + \frac{1}{3}(w_x^2 + w_y^2 + w_z^2)}. \qquad (9)$$

Maximum directivity is obtained with weights

$$w_x = 3\,a(\theta_s, \phi_s), \qquad (10)$$

$$w_y = 3\,b(\theta_s, \phi_s), \qquad (11)$$

$$w_z = 3\,c(\phi_s). \qquad (12)$$

Substituting the optimal real weights into Eq. (9) yields

$$DF_{pv} = 1 + 3\left(a(\theta_s, \phi_s)^2 + b(\theta_s, \phi_s)^2 + c(\phi_s)^2\right) = 4. \qquad (13)$$

Therefore, the maximum directivity for a single-vector sensor is DI = 10 log(4) = 6 dB, and this holds for any steering angle and frequency.

The optimal weights given in Eqs. (10) through (12) were obtained by solving for the set of weights that produced an extrema value for DF_{pv}. In practice, the procedure can be extended to determine the optimal weights for higher-order sensors, that is, the weights w_{xx}, w_{yy}, w_{zz}, w_{xy}, w_{xz}, w_{yz}. The algebra becomes cumbersome. The optimal weights for a directional sensor that measures pressure, the three components of particle velocity, and a single gradient of velocity (i.e., the weights w_p, w_x, w_y, w_z, w_{xx}) were determined. These optimal weights generate the directivity shown in Fig. 2, which is noted to be as much as 9.5 dB (or 3.5 dB greater than that of a vector sensor) along the boresight of the x-axis. Also shown are the steering directions at which the velocity gradient, u', did not provide additional gain. Not surprisingly, if the gradient v' is measured as well, the directivity increases along the boresight of the y-axis, at $\theta_s = \pm 90°$.

As with a vector sensor, it can be shown that $B^{10}(\theta_s, \phi_s)$ simplifies to a constant value (independent of sensor steering direction (θ_s, ϕ_s)) when the weights are chosen to match each component's angular response. However, it has not been determined whether such a weight set is optimal. It is believed that a highly directional sensor will achieve a constant 9.5 dB of directivity, independent of angular steering, with optimal weights.

III. NON-ACOUSTIC (SUBSONIC) NOISE SOURCES

Maidanik and Becker[6] compare the wavevector filtering characteristics of a pressure sensor to that of a single-axis velocity sensor. The sensors are assumed to be embedded in, or on, the surface of, a compliant boundary exposed to noise generated by turbulent flow. The results presented clearly demonstrate that a velocity sensor can be more sensitivity to subsonic noise sources than an omnidirectional pressure sensor.
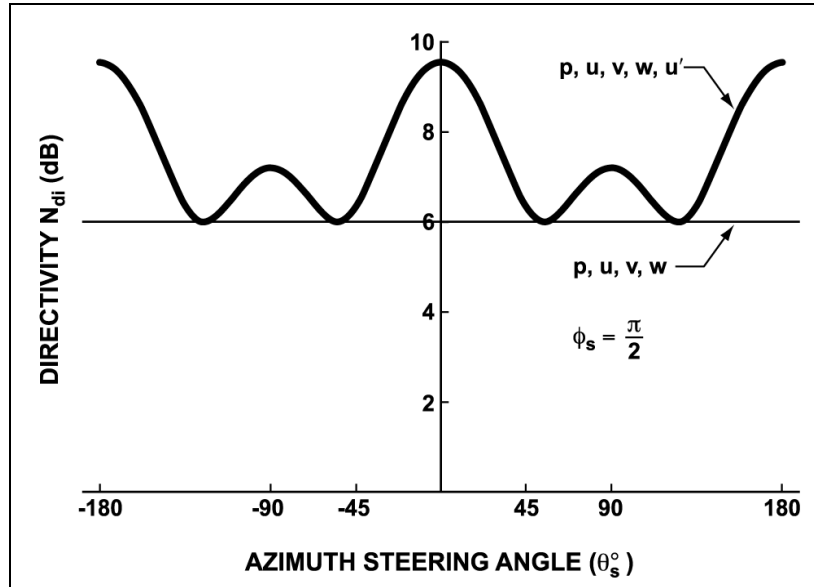
FIG. 2. Directivity of a directional sensor that measures pressure, the acoustic velocity vector, and a single gradient of velocity.

To clarify these differences, the response of a directional sensor to the flexural vibration of a fluid-loaded plate (Fig. 3) was determined. Acoustic and non-acoustic flexural waves are generated from the plate's vibration. In Fig. 4, the theoretical wavenumber response of an infinite plate, at a frequency of 1000 Hz is given. Clearly, near the surface of the plate, the predominate source of noise is centered about the plate's (flexural) wavenumber, denoted k_b. The magnitude of the flexural wavenumber, for the frequencies and plate geometries of interest here, is greater than that of the acoustic wavenumbers, and hence subsonic. These are evanescent waves that do not propagate, but decay exponentially away from the surface of the plate. In submarine sonar applications, subsonic noise sources are common.
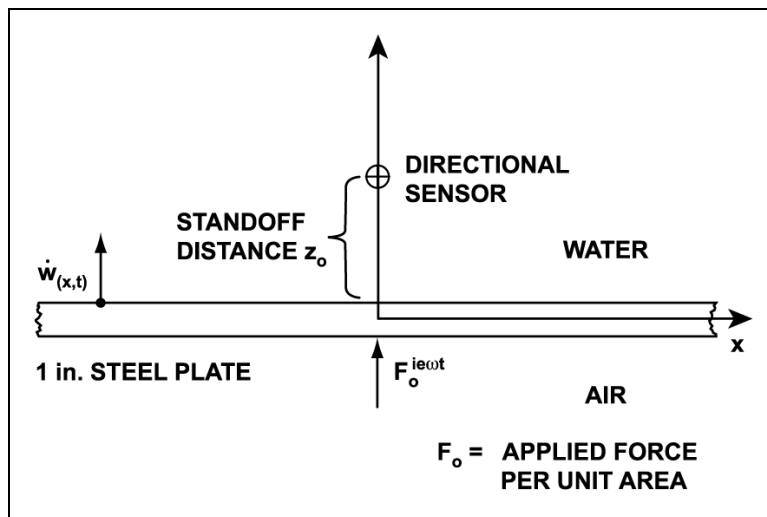
FIG. 3. Fluid-loaded plate and directional sensor configuration.
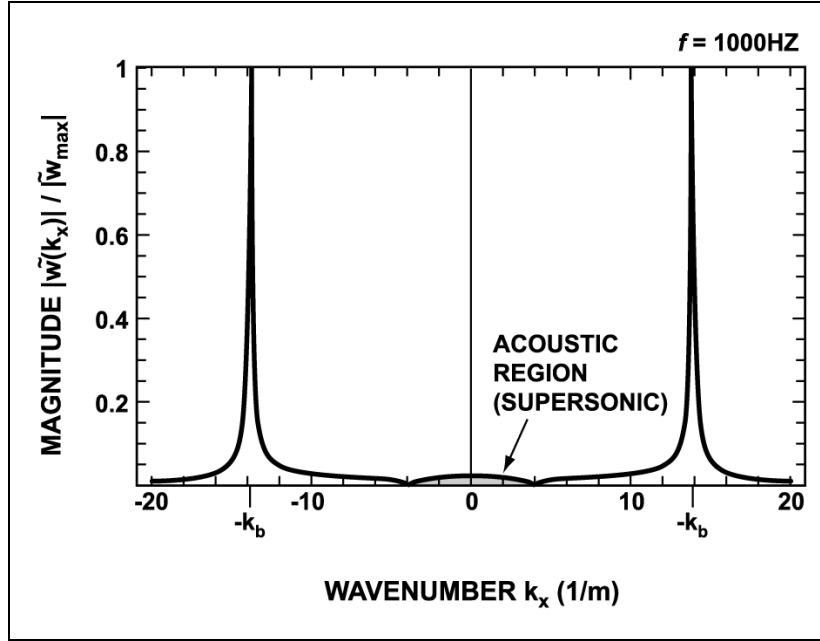
FIG. 4. Normalized magnitude response at fluid-loaded plate at 1000 Hz.

Three SNRs have been calculated, each corresponding to measurements of pressure, velocity, and the gradient of velocity. Signal is defined as a planewave, of amplitude P_o, arriving along the boresight of the z-axis. Noise is defined to be that due solely to flexural vibrations of the plate, $w(k_b)$. These ratios are written as

$$SNR_p = \left| \left(\frac{P_o}{F_o} \right) e^{ik_o z} \, e^{\sqrt{k_b^2 - k_o^2}\, z} \right| \sim \left(\frac{P_o}{F_o} \right) e^{k_b z} \quad \text{for } |k_b| \gg k_o, \tag{14}$$

$$SNR_v = \left| \left(\frac{P_o}{F_o} \right) \frac{(ik_o) e^{ik_o z} e^{\sqrt{k_b^2 - k_o^2}\, z}}{\sqrt{k_b^2 - k_o^2}} \right| \sim \left(\frac{P_o}{F_o} \right) \left(\frac{k_o}{k_b} \right) e^{k_b z} \text{ for } |k_b| \gg k_o, \tag{15}$$

$$SNR_{v'} = \left| -\left(\frac{P_o}{F_o} \right) \frac{k_b^2 \, e^{ik_o z} e^{\sqrt{k_b^2 - k_o^2}\, z}}{\sqrt{k_b^2 - k_o^2}} \right| \sim \left(\frac{P_o}{F_o} \right) \left(\frac{k_o}{k_b} \right)^2 e^{k_b z} \text{ for } |k_b| \gg k_o. \tag{16}$$

The SNRs, SNR_v and $SNR_{v'}$, at standoff distances of $z_o = 0.1$ m and $z_o = 0.3$ m, are shown in Figs. 5 and 6, respectively (where, for comparison, $P_o = F_o$). Notice that each SNR has equivalent exponential noise decay; the SNRs improve quickly with standoff. Near the plate, however, the velocity gradient sensor is much more sensitive to flexural noise, particularly at low frequency. Hence, for submarine sonar applications, additional

6

efforts will be required to mitigate against sources of subsonic self-noise with directional sensors. Viscoelastic sensor coatings (passive wavevector filters), standoff, and active filtering techniques may be necessary.
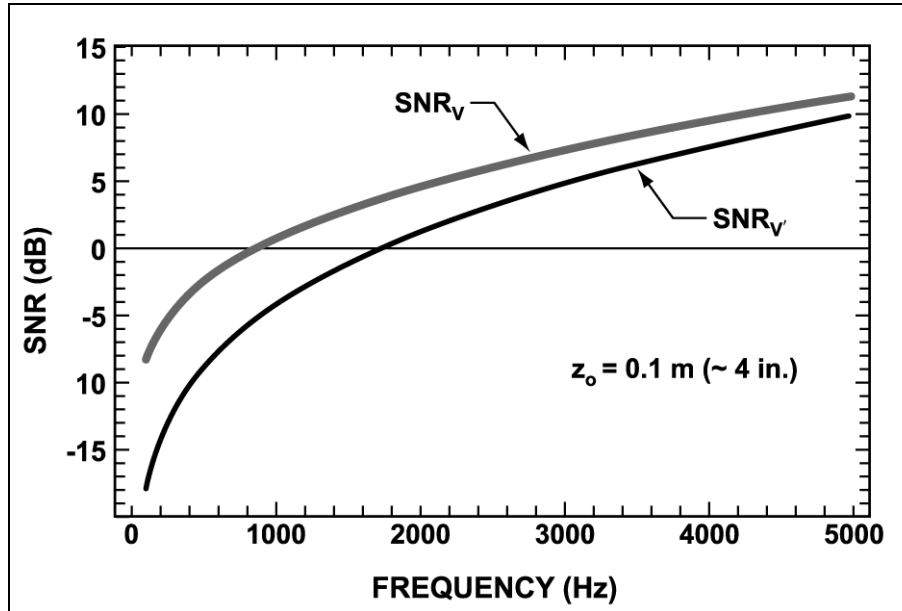
**FIG. 5. SNR for a velocity and velocity-gradient
sensor 4 in. above a steel plate.**
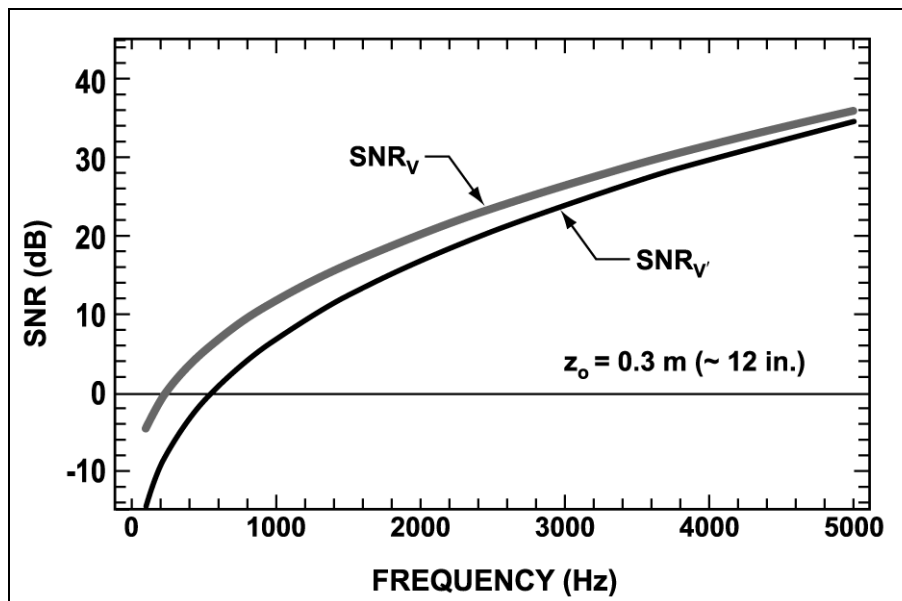
**FIG. 6. SNR for a velocity and velocity-gradient sensor
12 in. above a steel plate.**

IV. CONCLUSION

Underwater acoustic intensity measurements, along with the requisite development of directional sensors, has been an area of active research in Russia since the early 1970s. Many literature references, including textbooks, are available. Shchurov[7,8] has published over 50 academic papers, describing many aspects of the use of intensity in underwater acoustics.

In the West, less has been published in the area of underwater acoustic intensity measurements and the design of directional sensors. It is a given that directional sensors can be more susceptible to certain noise mechanisms. For example, at 600 Hz, the SNR of the velocity gradient component (Fig. 5) of a directional sensor is –5 dB below that of a conventional pressure sensor. Below 600 Hz, the deficit is even greater. Reducing a directional sensor's response to subsonic self-noise will remain a challenging task.

The gains possible, though, with this technology are significant. The point directional sensors described here have directivity gains of as much as 9.5 dB. In addition, multiple nulls may be generated within a directional sensor's angular response. These nulls can then be used to reduce signal interference, acoustic and nonacoustic sensor self-noise, and scattering and diffraction effects.

One specific goal for developing directional sensor technology is to improve the detection and localization capabilities of the AN/BSY-1 low-frequency hull array (LFHA) in SSN 688I class submarines by replacing the array's pressure sensors with directional receivers.

V. REFERENCES

1. B. A. Cray and A. H. Nuttall, A.H., "Directivity factors for linear arrays of velocity sensors," *J. Acoust. Soc. of Am.* (accepted for publication 23 March 21001).

2. R. Hickling and A. P. Morgan, "Locating sound sources with vector sound-intensity probes using polynomial continuation," *J. Acoust. Soc. Am.*, 100(1), July 1996.

3. W. Wei, Underwater Measurement of the Sound-Intensity Vector: Its Use in Locating Sound Sources, and in Measuring the Sound Power of Stationary and Living Sources, Ph. D. dissertation, University of Mississippi, 1994.

4. A. H. Nuttall and B. A. Cray, "Approximations to Directivity for Linear, Planar, and Volumetric Apertures and Arrays," NUWC-NPT Technical Report 10,798, Naval Undersea Warfare Center Division, Newport, RI, July 25, 1997.

5. B. A. Cray and V. E. Evora, "Directivity indices for combined receivers," *U.S. Navy J. of Underwater Acoustics* (accepted for publication January 2001).

6. G. Maidanik and K. J. Becker, "Primitive Comparison of the Signal-to-Noise Ratios of Pressure and Velocity Planar Arrays," NSWCCD-SIG-97/256-7030, Naval Surface Warfare Center, Carderock Division, September 1997.

7. V. A. Shchurov, "Coherent and diffusive fields of underwater acoustic ambient noise," *J. Acoust. Soc. Am.,* 90(2), Aug. 1991.

8. V. A. Shchurov and M. V. Kuyanova, "Use of acoustic intensity measurements in underwater acoustics (Modern state and prospects)," *Chinese J. of Acoustics*, **18**,(4), 1999.

Signal Processing Considerations for a General Class of Directional Acoustic Sensors

Manuel T. Silvia
Ryan E. Franklin
Dean J. Schmidlin
SITTEL CORPORATION
Research and Development Department
1206 Foothill Road
Ojai, California 93023-1727

Signal Processing Considerations for a General Class of Directional Acoustic Sensors

Dr. Manuel T. Silvia, Ryan E. Franklin, and Dr. Dean J. Schmidlin
SITTEL CORPORATION
Research and Development Department
1206 Foothill Road
Ojai, California 93023-1727

msilvia@sittelcorp.com, rfranklin@sittelcorp.com, dschmidlin@sittelcorp.com

Abstract. We consider a single acoustic sensor located at some measurement point $\vec{r}_0 = (x_0, y_0, z_0)$. A Taylor series for the scalar acoustic pressure field $p(t, \vec{r})$ about this point would include the scalar (tensor of order zero) pressure $p(t, \vec{r}_0)$ as the zero-order term, the pressure gradient/vector (tensor of order one) $\nabla p(t, \vec{r}_0)$ at the point as part of the first-order term, the dyadic (tensor of order two) $\nabla\nabla p(t, \vec{r}_0)$ at the point as part of the second order term, and so on. Using this Taylor series, we define a general class of directional acoustic sensors as follows. A scalar acoustic pressure sensor (e.g., a hydrophone) will be referred to as a directional acoustic sensor of order zero. This sensor only measures the scalar acoustic pressure $p(t, \vec{r}_0)$ at the point $\vec{r}_0$; its Taylor series about $\vec{r}_0$ assumes that the acoustic pressure field $p(t, \vec{r})$ about that point is independent of the field point $\vec{r} = (x, y, z)$. A vector acoustic pressure sensor will be referred to as a directional acoustic sensor of order one. This sensor measures both $p(t, \vec{r}_0)$ and the pressure gradient/vector $\nabla p(t, \vec{r}_0)$ at the point $\vec{r}_0$; its Taylor series about $\vec{r}_0$ assumes that the acoustic pressure field $p(t, \vec{r})$ about that point is a linear function of the field point $\vec{r}$. Similarly, a dyadic acoustic pressure sensor will be referred to as a directional acoustic sensor of order two. This sensor measures $p(t, \vec{r}_0)$, $\nabla p(t, \vec{r}_0)$ and the dyadic $\nabla\nabla p(t, \vec{r}_0)$ at the point $\vec{r}_0$; its Taylor series about $\vec{r}_0$ assumes that the acoustic pressure field $p(t, \vec{r})$ about that point is a quadratic function of the field point $\vec{r}$. It will be shown that the higher the order the directional acoustic sensor, the more directional the sensor. We also consider several signal processing methodologies for processing the outputs of this general class of directional acoustic sensors. One approach is a physics-based approach, which makes use of the acoustic intensity vector $\vec{I}(t, \vec{r}) = -p(t, r)\vec{v}(t, \vec{r})$, where $\vec{v}(t, \vec{r})$ is the acoustic particle velocity vector. In addition to the acoustic intensity vector, we introduce the useful physics-based field intensity vector $\vec{J}(t, \vec{r}) = -\dfrac{\partial p(t, \vec{r})}{\partial t}\vec{a}(t, \vec{r})$, where $\vec{a}(t, \vec{r})$ is the acoustic particle acceleration vector. Another signal processing strategy that will be discussed is a multi-channel filter approach, where the outputs of the directional acoustic sensor are considered as the inputs to a multi-channel filter, designed for some desired sensor response. It will be shown that the element beam pattern of a

directional acoustic sensor can be shaped or optimized for array gain by the use of multi-channel filtering. We close the paper with a discussion of how to perform acoustic signal processing on an array of directional acoustic sensors and provide some experimental results using real data.

I. INTRODUCTION AND HISTORICAL BACKGROUND OF DIRECTIONAL ACOUSTIC SENSORS

A <u>single</u> acoustic sensor, located at some measurement point $\vec{r}_0$, that can accurately detect and estimate the direction of arrival (DOA) from an arbitrary (narrowband or broadband) acoustic source, has always been of interest to the underwater [1], [2] and in-air [3] acoustic communities. For example, about thirty years ago, the United States Navy developed a single acoustic sensor for use in their SSQ-53 series of Directional Low-Frequency Analysis and Recording (DIFAR) sonobuoys [4]. This DIFAR sensor is composed of a single hydrophone and two orthogonal x-y accelerometers, all co-located in a single sensor package. The acoustic data out of the DIFAR sensor is basically a multi-channel time series, derived from the simultaneous measurement of the scalar acoustic pressure field at the measurement point $\vec{r}_0$, namely $p(t,\vec{r}_0)$, and the x-y components of the acoustic particle acceleration vector $\vec{a}(t,\vec{r}_0)$. By performing a temporal low-frequency Fourier analysis on the output of the scalar acoustic pressure sensor (hydrophone) or the output of a cardioid beamformer formed by a linear combination of the pressure channel and the x-y accelerometer channels, one could detect the presence of an acoustic source. By finding the unit vector associated with $\vec{a}(t,\vec{r}_0)$ and using the hydrophone as a phase reference, one could also unambiguously find the DOA of the source. In the sonobuoy community, this is called DIFAR signal processing and is generally referred to as SINE ($\sin\theta$ beam pattern for the y-axis accelerometer), COSINE ($\cos\theta$ beam pattern for the x-axis accelerometer) and OMNI (omnidirectional beam pattern for the hydrophone) processing. Based on our brief definition in the abstract, the DIFAR sonobuoy sensor is basically a two-dimensional (2-D) vector sensor or 2-D directional acoustic sensor of order one. It is important to note that the above DIFAR sensor measures the <u>exact </u>scalar acoustic pressure $p(t,\vec{r}_0)$ and the <u>exact</u> values of the x and y components of the pressure gradient $\nabla p(t,\vec{r}_0)$. The latter follows from the fact that

$$\nabla p(t,\vec{r}\,) = -\rho(\vec{r})\vec{a}(t,\vec{r}) \tag{1}$$

for linear acoustic waves propagating in an inhomogeneous acoustic medium. Here, $\rho(\vec{r})$ is the mass density of the medium at the field point $\vec{r}$. Thus, in order to know the <u>exact</u> value of the x and y components of the pressure gradient at the measurement point $\vec{r}_0$, we assume that the DIFAR sensor exactly measures the x and y components of $\vec{a}(t,\vec{r}_0)$ and knows $\rho(\vec{r})$ at the point $\vec{r}_0$. The exact value of $\nabla p(t,\vec{r}_0)$ follows from (1).

About the same time the U.S. Navy developed the DIFAR sonobuoy sensor, they also developed another 2-D directional acoustic sensor of order one called the multimode

hydrophone, which is used as a directional sensor in the AN/WLR-9 series of acoustic intercept receivers [5]. This 2-D vector sensor can be modeled by two orthogonal pressure dipoles in the x-y plane. Figure 1 gives a pictorial representation of the x and y-axis
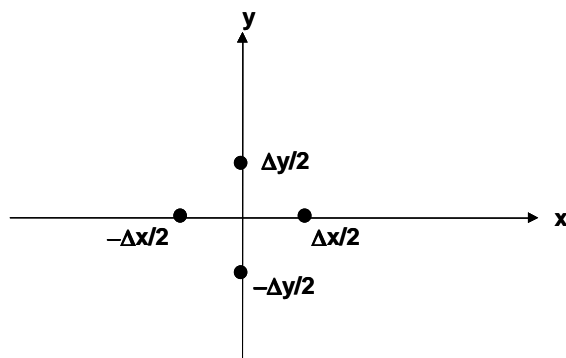
FIG. 1. The multimode hydrophone can be modeled by two orthogonal pressure dipoles in the x-y plane.

pressure dipoles. The x-axis pressure dipole consists of two scalar pressure sensors separated by a distance Δx along the x-axis. Similarly, the y-axis dipole consists of two scalar pressure sensors separated by a distance Δy along the y-axis. Unlike the DIFAR sensor, the multimode sensor cannot measure the <u>exact</u> values of the x and y components of the pressure gradient $\nabla p(t, \vec{r}_0)$, since it uses four scalar pressure sensors instead of two orthogonal accelerometers. However, we can approximate these pressure gradient components at the measurement point $\vec{r}_0 = (0,0,0)$ by using the finite difference approximations:

$$\frac{\partial p(t,0,0,0)}{\partial x} \approx \left[p\left(t, \frac{\Delta x}{2}, 0, 0\right) - p\left(t, \frac{-\Delta x}{2}, 0.0\right) \right] / \Delta x \tag{2a}$$

$$\frac{\partial p(t,0,0,0)}{\partial y} \approx \left[p\left(t, \frac{\Delta y}{2}, 0, 0\right) - p\left(t, \frac{-\Delta y}{2}, 0.0\right) \right] / \Delta y . \tag{2b}$$

Similarly, we can approximate the scalar acoustic pressure at the point $\vec{r}_0 = (0,0,0)$ by averaging the four pressure sensors; that is,

$$p(t,0,0,0) \approx \left[p\left(t, \frac{\Delta x}{2}, 0, 0\right) + p\left(t, \frac{-\Delta x}{2}, 0, 0\right) + p\left(t, \frac{\Delta y}{2}, 0, 0\right) + p\left(t, \frac{-\Delta y}{2}, 0, 0\right) \right] / 4 . \tag{3}$$

Using Eqs. (1), (2a), and (2b), we can also approximate the x-y components of the acoustic particle acceleration vector $\vec{a}(t,0,0,0)$, provided we know the mass density $\rho(\vec{r})$ at the point $\vec{r}_0 = (0,0,0)$. Referring to the previous DIFAR discussion, we see that the multimode acoustic sensor data is approximately in the same multi-channel time series

3

form as the DIFAR acoustic sensor data. Thus, in principle, we can use the SINE, COSINE and OMNI DIFAR signal processing techniques to process the outputs of the multimode hydrophone. The acoustic intercept community refers to (2b) as the SINE channel (approximate $\sin\theta$ beam pattern for the y-axis pressure dipole), (2a) as the COSINE channel (approximate $\cos\theta$ beam pattern for the x-axis pressure dipole) and (3) as the OMNI channel (omnidirectional beam pattern for (3)) and uses DIFAR-like processing to detect and estimate the DOA of acoustic emissions.

For about 30 years, researchers in the field of in-air acoustics have used directional acoustic sensors of order one (vector sensors) to estimate the magnitude and direction of the acoustic intensity vector in order to obtain the acoustic power per unit area ($Watts/m^2$) radiated by a source as a function of time t and position $\vec{r}$. Specifically, researchers at General Motors Corporation have used the instantaneous acoustic intensity vector

$$\vec{I}(t,\vec{r} = -p(t,\vec{r}))\vec{v}(t,\vec{r}) \tag{4}$$

to measure the in-air acoustic power per unit area generated by various vehicles [6]. Here, $\vec{v}(t,\vec{r})$ is the acoustic particle velocity vector, which can be obtained by performing a time integration of $-\nabla p(t,\vec{r})/\rho(\vec{r})$. It is important to note that (4) is valid for any type of linear acoustic wave propagating in an inhomogeneous acoustic medium; it does not have to be a plane wave. The magnitude of (4) gives the instantaneous acoustic power per unit area and the unit vector

$$\vec{u}(t,\vec{r}) = \frac{\vec{I}}{\left|\vec{I}\right|} \tag{5}$$

gives the instantaneous DOA of the source's radiated acoustic power.

Nehorai [7] and Shchurov [8] have done an extensive amount of research on the signal processing associated with acoustic vector sensors. For a single vector sensor, both of these researchers use the acoustic intensity vector (4) as the basis for their processing methodologies. Their basic approach is to perform a time average of (4) and use this time-averaged intensity vector to derive the corresponding unit vector, which results in the DOA estimate of the acoustic source. In this paper, we shall refer to this approach as the *acoustic intensity algorithm*. Nehorai [9] has also developed a localization algorithm for estimating the position vector of an acoustic source (range, azimuth angle and elevation angle of the source) using an arbitrary distributed array (e.g., the array does not have to be linear) of acoustic vector sensors. His approach is to first use the above acoustic intensity algorithm at each sensor location to derive a unit vector to the source relative to a specific sensor in the array. If the conditions were ideal, all the various unit vector estimates from each sensor would intersect at one point, giving the position vector of the source. In practice, when the conditions are not ideal, Nehorai uses a least-squares approach to combine all the unit vectors from each sensor to give the

'best' estimate of the source's position vector. In this paper, we shall refer to this algorithm as the *intensity-based ranging algorithm*.

Cray and Nuttall [10] have investigated linear signal processing approaches for beamforming single and multiple acoustic vector sensors that measure the acoustic pressure $p(t,\vec{r}_0)$ and the three acoustic particle velocity vector components $v_x(t,\vec{r}_0)$, $v_y(t,\vec{r}_0)$ and $v_z(t,\vec{r}_0)$. (Note that this is equivalent to measuring $p(t,\vec{r}_0)$ and $\nabla p(t,\vec{r}_0)$, using (1) to get the acoustic particle acceleration vector $\vec{a}(t,\vec{r}_0)$, then performing a time integration on $\vec{a}(t,\vec{r}_0)$ to get the acoustic particle velocity vector $\vec{v}(t,\vec{r}_0)$). Specifically, they show that by forming a linear combination of these vector sensor measurements, namely,

$$b(t,\vec{r}_0) = w_0 p(t,\vec{r}_0) + w_{1x} v_x(t,\vec{r}_0) + w_{1y} v_y(t,\vec{r}_0) + w_{1z} v_z(t,\vec{r}_0) \qquad (6)$$
$$= w_0 p(t,\vec{r}_0) + \vec{w}_1 \cdot \vec{v}(t,\vec{r}_0)$$

one can choose the real weights w_0, $\vec{w}_1 = (w_{1x}, w_{1y}, w_{1z})$ so that this single vector sensor behaves like a spatial filter. In this sense, a <u>single</u> vector sensor can perform spatial filtering or beamforming, with $b(t,\vec{r}_0)$ representing the output of the beamformer.

In this paper, we make use of the Taylor series expansion of the pressure field $p(t,\vec{r})$ about the point $\vec{r}_0$ in order to define a general class of directional acoustic sensors. (Refer to the abstract). We then investigate sensors that approximate the pressure gradient by using orthogonal pressure dipoles and finite difference approximations and show that extreme caution must be exercised when doing so. In order to deal with directional sensors that measure the pressure gradient directly (e.g., directional sensors that use accelerometers), we introduce the useful acoustic field intensity vector $\vec{J}(t,\vec{r}) = -\dfrac{\partial p(t,\vec{r})}{\partial t} \vec{a}(t,\vec{r})$, which deals <u>directly</u> with the pressure gradient or the acceleration vector. Also, because it involves the time derivative of the acoustic pressure, this field intensity vector naturally provides for equalization of an ambient acoustic pressure background, like the underwater environment, that has an acoustic noise spectrum that falls off at 6 dB per octave. We also relate the work of Cray and Nuttall to the aforementioned Taylor series expansion and generalize their concept of beamforming to the general problem of shaping the element pattern of a directional acoustic sensor. A discussion of how to beamform a practical array of directional sensors will be given. In the latter part of the paper, we provide experimental results that show the practical value of the acoustic intensity vector, the usefulness of Nehorai's ranging algorithm and how the directional sensor's spatial filtering ability could be used in a noisy environment.

II. PRESSURE GRADIENT ESTIMATION

In both the underwater and in-air communities, the pressure gradient/vector, needed for a directional acoustic sensor of order one, is found in a variety of different ways. As discussed above, one can measure the acoustic particle acceleration vector $\vec{a}(t,\vec{r}_0)$

directly and use (1) and knowledge of the mass density at the measurement point $\vec{r}_0$ to obtain a fairly accurate value of the pressure gradient $\nabla p(t, \vec{r}_0)$. Alternatively, one could measure the acoustic particle velocity vector $\vec{v}(t, \vec{r}_0)$ directly, perform a time derivative to get the acceleration vector and proceed as above to get the pressure gradient. (The accuracy of this method would depend on how well one implemented the time derivative). If one decides to use scalar pressure sensors to approximate the pressure gradient, then the finite difference approximations in (2) would have to be computed. However, great care must be exercised when approximating the pressure gradient by (2). For example, (2a) approximates the x-component of the pressure gradient at the measurement point $\vec{r}_0 = (0,0,0)$. (Refer to Fig. 1). If the pressure field was the arbitrary (narrowband or broadband) plane wave

$$p(t, \vec{r}) = f\left(t + \frac{\hat{n} \cdot \vec{r}}{c}\right), \tag{7}$$

which is assumed to be propagating toward the origin of the coordinate system in Fig. 2, then the <u>exact</u> value of the temporal Fourier transform of the pressure gradient would be
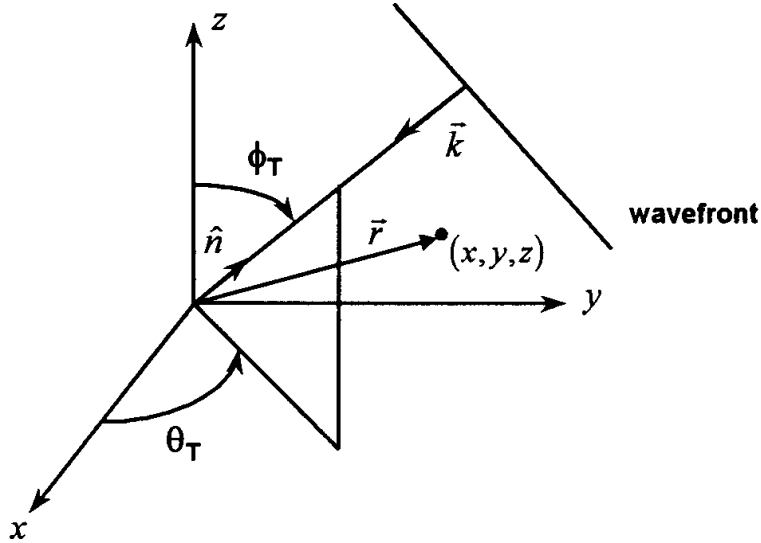
FIG. 2. The propagation of a planar wavefront towards the origin of a rectangular coordinate system.

$$\nabla P(\omega, \vec{r}) = jF(\omega)\vec{k}e^{j\vec{k}\cdot\vec{r}} = jP(\omega, \vec{r})\vec{k} . \tag{8}$$

Here, the wavenumber or propagation vector $\vec{k} = k\hat{n}$ has the magnitude $k = \omega/c = 2\pi/\lambda$ and the direction $\hat{n}$, where $\hat{n}$ is the unit vector

$$\hat{n} = \sin\phi_T \cos\theta_T \hat{x} + \sin\phi_T \sin\theta_T \hat{y} + \cos\phi_T \hat{z} . \tag{9}$$

The position vector
$$\vec{r} = x\hat{x} + y\hat{y} + z\hat{z} = r\sin\phi\cos\theta\hat{x} + r\sin\phi\cos\theta\hat{y} + r\cos\phi\hat{z} \tag{10}$$

is the vector from the origin to an arbitrary field point $\vec{r} = (x, y, z)$ in rectangular coordinates or $\vec{r} = (r\sin\phi\cos\theta, r\sin\phi\sin\theta, r\cos\phi)$ in spherical coordinates. The temporal Fourier transform of the plane wave pressure field (7) is found by using

$$P(\omega, \vec{r}) = \int_{-\infty}^{+\infty} p(t, \vec{r}) e^{-j\omega t} dt . \tag{11}$$

Now if we use (2a) to approximate the x-component of the pressure gradient at the origin (the point $\vec{r}_0 = (0,0,0)$), then the temporal Fourier transform of this approximation can be expressed as

$$\frac{\partial P(\omega, \vec{r}_0)}{\partial x} = P_x(\omega, \vec{r}_0) \approx \hat{P}_x(\omega, \vec{r}_0) = jF(\omega)\frac{2\sin\left(\pi\dfrac{\Delta x}{\lambda}\sin\phi_T\cos\theta_T\right)}{\Delta x} . \tag{12}$$

Since the <u>exact</u> value of $P_x(\omega, \vec{r}_0)$ is given by

$$P_x(\omega, \vec{r}_0) = jF(\omega)\frac{2\pi}{\lambda}\sin\phi_T\cos\theta_T , \tag{13}$$

then the fractional error in estimating the x-component of $P_x(\omega, \vec{r}_0)$ can be expressed as

$$1 - \hat{P}_x / P_x = 1 - \frac{\sin\left(\pi\dfrac{\Delta x}{\lambda}\sin\phi_T\cos\theta_T\right)}{\pi\dfrac{\Delta x}{\lambda}\sin\phi_T\cos\theta_T} = 1 - \text{sinc}\left(\pi\dfrac{\Delta x}{\lambda}\sin\phi_T\cos\theta_T\right) \tag{14}$$

Notice that (14) is frequency dependent and is valid only when the two hydrophones in the x-axis dipole (Refer to Fig. 1) are <u>exactly</u> matched in their amplitude and phase frequency responses. In practice, this is seldom the case, so we must modify our analysis to include the effects of mismatch in the frequency responses of the hydrophone and corresponding signal conditioning associated with each hydrophone in the dipole. It can be shown that when the two hydrophones of the x-axis dipole are mismatched in the magnitudes of their combined (sensor plus electronics) frequency responses, the magnitude of the fractional error in estimating the x-component of $P_x(\omega, \vec{r}_0)$ can be expressed as [11]

$$\left|1-\hat{P}_x/P_x\right|=1-\frac{\left[\delta^2+4(1+\delta)\sin^2\left(\pi\frac{\Delta x}{\lambda}\sin\phi_T\cos\theta_T\right)\right]^{\frac{1}{2}}}{\left|2\pi\frac{\Delta x}{\lambda}\sin\phi_T\cos\theta_T\right|} \, , \tag{15}$$

which is valid for $\sin\phi_T\cos\theta_T\neq0$. Here, δ is a frequency-dependent mismatch parameter defined by

$$\delta(\omega)=\left[S_1(\omega)G_1(\omega)-S_2(\omega)G_2(\omega)\right]/S_2(\omega)G_2(\omega) \, , \tag{16}$$

where $S_1(\omega)$ and $G_1(\omega)$ are the magnitudes of the frequency responses of the hydrophone and signal conditioning, respectively, for the hydrophone located on the positive x-axis (refer to Fig. 1) and $S_2(\omega)$ and $G_2(\omega)$ are the magnitudes of the frequency responses of the hydrophone and signal conditioning, respectively, for the hydrophone located on the negative x-axis. The contour plot in Fig. 3 gives the magnitude of the fractional error in estimating the x-component of the pressure gradient or the x-component of the acoustic particle acceleration vector as a function of both δ and $\Delta x/\lambda$ under the condition $\theta_T=0°$, $\phi_T=90°$. [Note that this condition is for a plane wave traveling in the negative x-direction in the x-y plane, which means that the wave hits the main response axis of the dipole or approximate accelerometer].
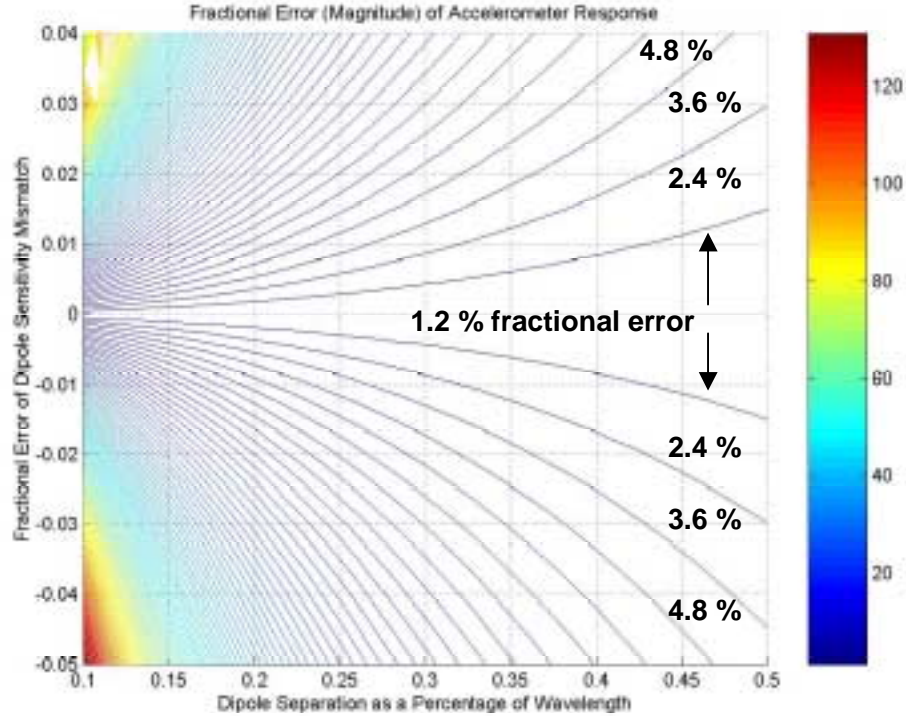
FIG. 3. Contour plot of fractional error (magnitude) as a function of δ and Δx/λ.

The mismatch parameter δ is plotted on the y-axis, $\Delta x / \lambda$ is plotted on the x-axis and each contour represents 1.2% of fractional error magnitude. For example, suppose we wanted to estimate the x-component of the pressure gradient of an acoustic field at 100 Hz using a pressure hydrophone dipole, with spacing $\Delta x = 3$ inches, with a fractional error magnitude of 10%. From Fig. 3, this implies that the amplitude sensitivities of these hydrophones must be matched better than 0.01 dB. This is very difficult to achieve in practice. If the same dipole was used to estimate the pressure gradient at 1000 Hz, 2000 Hz, and 10,000 Hz, then the amplitude sensitivities of these hydrophones must be matched better than approximately 0.03 dB, 0.04 dB, and 0.8 dB, respectively. Thus, if one had a mechanical packaging constraint to build a low-frequency, directional sensor in a small, 3-inch. diameter x 6-inch length right circular cylinder, one might consider using accelerometers or velocity sensors vice orthogonal pressure dipoles to estimate the pressure gradient.

III. TAYLOR SERIES AND DIRECTIONAL ACOUSTIC SENSORS

D'Spain [12] was the first to point out a qualitative relationship between the Taylor series expansion of the pressure field and a vector sensor. Following his observation, we consider a single acoustic sensor located at some measurement point $\vec{r}_0 = (x_0, y_0, z_0)$. A Taylor series for the scalar acoustic pressure field $p(t, \vec{r})$ about this point can be written as

$$p(t,\vec{r}) = p(t,\vec{r}_0) + (\vec{r} - \vec{r}_0) \cdot \nabla p(t,\vec{r}_0) + \frac{1}{2}(\vec{r} - \vec{r}_0) \cdot \nabla \nabla p(t,\vec{r}_0) \cdot (\vec{r} - \vec{r}_0) + \text{h.o.t.} \qquad (17)$$

The interpretation of (17) is as follows. A directional acoustic sensor is capable of extrapolating the acoustic pressure field beyond the measurement point $\vec{r}_0$ so that it actually knows this field at every point inside a sphere of radius $R = |\vec{r} - \vec{r}_0|$, where R is defined by the type of directional sensor and the error associated with the extrapolation. The Taylor series (17) is the formula used to do the wavefield extrapolation with some specified error $\varepsilon(t,\vec{r})$. For example, a directional sensor of order zero, can only measure the pressure at $\vec{r}_0$, so its estimate of the field beyond this point is $\hat{p}(t,\vec{r}) = p(t,\vec{r}_0)$ and the corresponding estimation or extrapolation error is $\varepsilon(t,\vec{r}) \equiv p(t,\vec{r}) - p(t,\vec{r}_0)$. If the error is required to be small (less than 10%), then R will be small. This implies that the aperture (2R) of a single pressure sensor is small, so by the theory of spatial Fourier transforms [13], the zero-order sensor is essentially omnidirectional. However, a sensor of order one (vector sensor) measures both the pressure and pressure gradient at $\vec{r}_0$, so its estimate of the field beyond this point is $\hat{p}(t,\vec{r}) = p(t,\vec{r}_0) + (\vec{r} - \vec{r}_0) \cdot \nabla p(t,\vec{r}_0)$ and the corresponding estimation error is

$$\varepsilon(t,\vec{r}) \equiv p(t,\vec{r}) - \hat{p}(t,\vec{r}) \qquad (18)$$
$$\varepsilon(t,\vec{r}) = p(t,\vec{r}) - [p(t,\vec{r}_0) + (\vec{r} - \vec{r}_0) \cdot \nabla p(t,\vec{r}_0)]$$

For the same error, the vector sensor will have a larger aperture than the scalar sensor, so it should be more directional. Thus, the dyadic sensor should be better than the scalar and vector sensors at estimating the field, so it should be even more directional.

We define the mean-squared error in estimating the pressure field beyond $\vec{r}_0$ by

$$MSE = \frac{1}{\pi T} \int_0^\pi \int_0^T |\varepsilon(t,\vec{r})|^2 dt d\beta \ , \tag{19}$$

where T is a suitable integration time (e.g., the temporal period of a plane wave) and β is the angle between $\hat{n}$ and $\hat{r}$. Note that $\hat{r}$ is a unit vector in the direction of $\vec{r}$. (Refer to Fig. 2). Dividing (19) by the average power in the acoustic pressure field we obtain the normalized MSE. Figure 4 shows the normalized mean-squared as a function of R/λ for the scalar, vector and dyadic sensors. For a specified normalized MSE of 10%, notice that the acoustic aperture (2R) of the scalar sensor is about $\lambda/10$, whereas the apertures for the vector and dyadic sensors are $\lambda/3$ and $\lambda/2$, respectively.
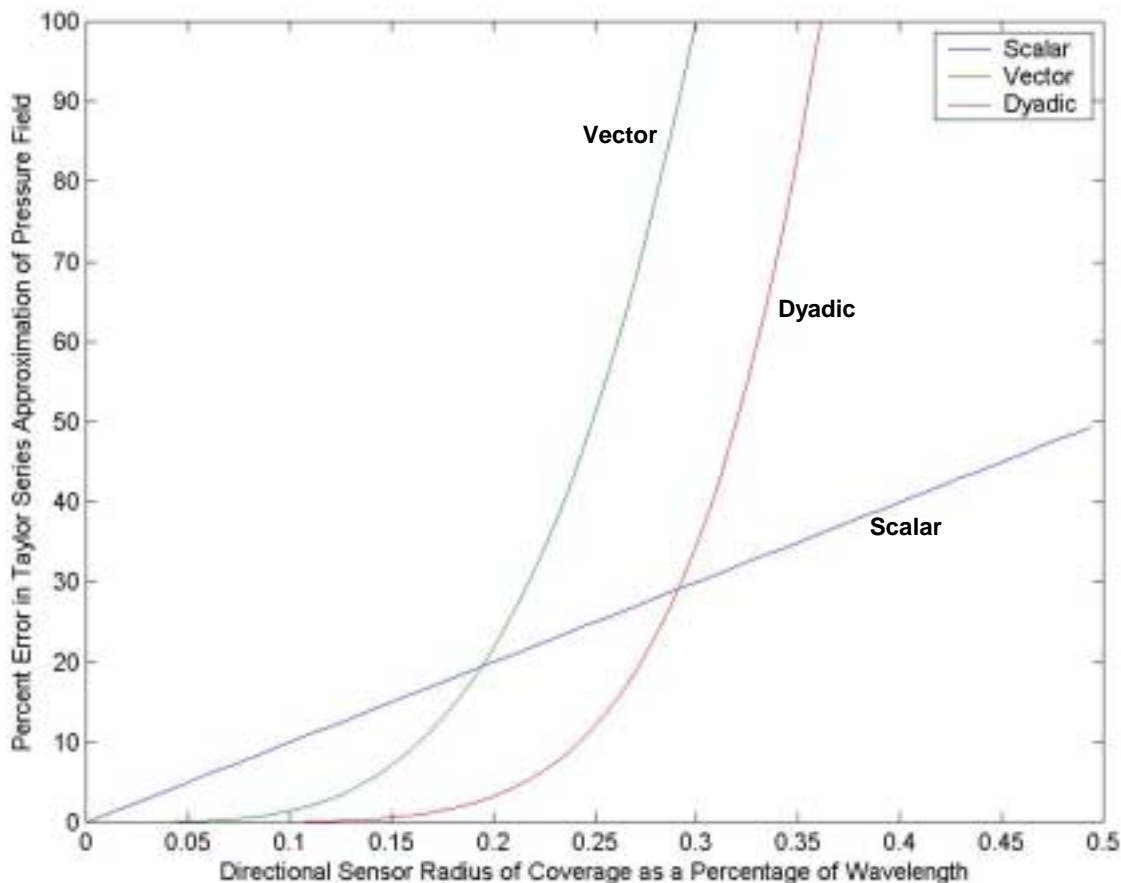
FIG. 4. Normalized mean-squared estimation error (Eq. (19)) vs. R/λ.

IV. MULTICHANNEL FILTERING AND DIRECTIONAL ACOUSTIC SENSORS

For the purposes of this section, it is convenient to deal with the temporal Fourier transform of the Taylor series (17). Rewriting (17) in the frequency domain we obtain

$$P(\omega,\vec{r}) = W_0(\omega,\vec{r})P(\omega,\vec{r}_0) + \vec{W}_1(\omega,\vec{r})\cdot\nabla P(\omega,\vec{r}_0) + \vec{W}_2(\omega,\vec{r})\cdot\nabla\nabla P(\omega,\vec{r}_0)\cdot\vec{W}_2(\omega,\vec{r}), \quad (20)$$

where we have retained only the first three terms of the series (dyadic sensor) and the weights W_0, $\vec{W}_1$ and $\vec{W}_2$ are chosen such that the right side of (20) is consistent with the Taylor series approximation of the pressure field. Specifically, $W_0 = 1$, $\vec{W}_1 = \vec{r} - \vec{r}_0$ and $\vec{W}_2 = (\vec{r} - \vec{r}_0)/\sqrt{2}$ are the only weights that allow (20) to be a Taylor series extrapolation of the pressure field by a dyadic sensor. If we pick another set of weights, we cannot be assured that (20) will be a valid Taylor series. However, this does raise the question that maybe we could select a different set of weights that might be useful for another purpose, like shaping the beam pattern of a directional sensor or finding a set of weights that results in the maximum array gain in isotropic noise. That is, the linear combination on the right side of (20) could be expressed as

$$B(\omega,\vec{r}) = W_0(\omega,\vec{r})P(\omega,\vec{r}_0) + \vec{W}_1(\omega,\vec{r})\cdot\nabla P(\omega,\vec{r}_0) + \vec{W}_2(\omega,\vec{r})\cdot\nabla\nabla P(\omega,\vec{r}_0)\cdot\vec{W}_2(\omega,\vec{r}) \quad (21)$$

where the function $B(\omega,\vec{r})$ could represent the output of a frequency domain multichannel filter with $P(\omega,\vec{r}_0)$, $\nabla P(\omega,\vec{r}_0)$ and $\nabla\nabla P(\omega,\vec{r}_0)$ as the inputs. Refer to Fig. 5 for a pictorial representation of this concept.

FIG. 5. Multichannel filtering and directional acoustic sensors.

Thus, (21) is a generalization of (20) and can be viewed as Multichannel filtering approach to directional sensors.

Following Silvia and Schmidlin, we could select the above weights in (21) to steer the beam of a vector sensor so that we have maximum sensitivity in the look direction and place a null in another direction. Further, we could select the weights so that the directional sensor produces a beam pattern that results in maximum array gain [14].

Figure 6 shows the two weight-selection criteria for the vector sensor, and Fig. 7 does the same for the case of the dyadic sensor.

105° For maximum Array gain

131° For optimum Null placement

Array gain = 6 dB

Array gain = 4.8 dB

(a)

(b)
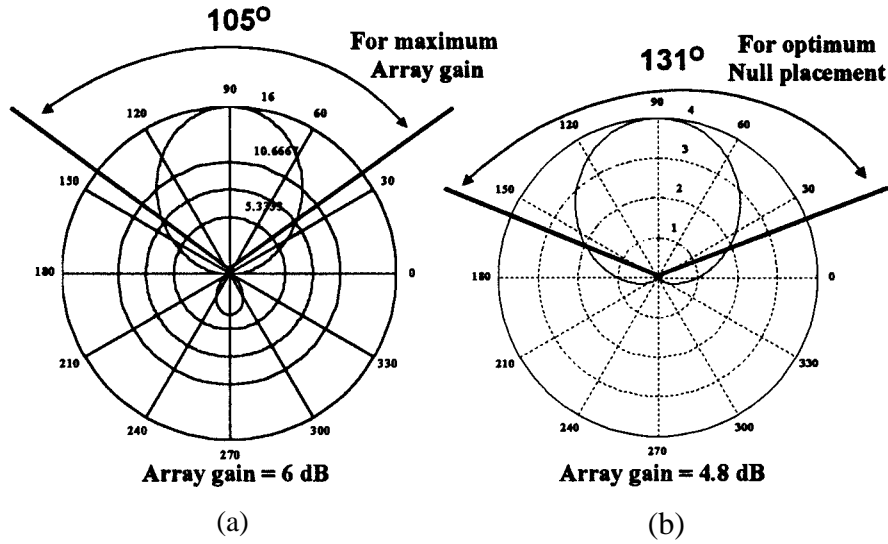
FIG. 6. Selection of weights for a vector sensor for: (a) maximum array gain, and (b) optimum null placement.

65° For maximum Array gain

94° For optimum Null placement

Array Gain = 9.5 dB

Array Gain = 7 dB

(a)

(b)
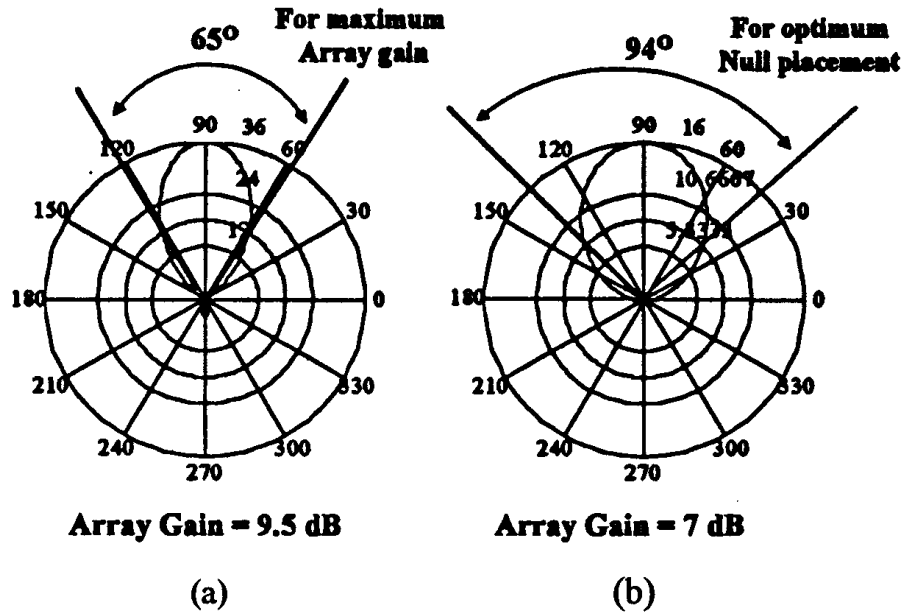
FIG. 7. Selection of weights for a dyadic sensor for: (a) maximum array gain, and (b) optimum null placement.

V. EXPERIMENTAL RESULTS

The experimental results for the acoustic intensity algorithm, intensity-based ranging algorithm, and beam steering algorithms are discussed in the oral presentation. Refer to the viewgraph material.

VI. CONCLUSIONS

We have shown that the Taylor series expansion of the pressure field provides an elegant mathematical framework for the study of directional acoustic sensors of all orders. The acoustic intensity algorithm generalizes the DIFAR and acoustic intercept receiver SINE, COSINE and OMNI signal processing. Pressure gradient estimation using orthogonal pressure dipoles must be done with caution. Multichannel filtering of the directional sensor outputs provides a useful tool for obtaining a desired sensor response. For example, the weights of the filter can be chosen to give a vector and dyadic sensor a maximum array gain relative to a pressure sensor of 6 dB and 9 dB, respectively. The higher the order the directional sensor, the more directive the sensor, as seen by the fact that a vector sensor has a minimum beamwidth of 105 degrees whereas a dyadic sensor has a minimum beamwidth of 65 degrees. Steering a vector sensor and placing nulls in the element response must also be done with caution. In summary, the proposed theoretical structure allows one to achieve up to 9.5 dB array gain by measuring the acoustic field properties, including scalar, vector and dyadic at a single point.

VII. REFERENCES

1. Donald J. Scheiber, "Directional Pressure Gradient Hydrophone," *27th Navy Symposium on Underwater Acoustics*, pp 1113-1119, Oct. 1969.

2. Marcia Mongiovi, "Low-Frequency Pressure Gradient Sensor," General Electric Corporation, Transducer Product Operation, Syracuse, NY, Patent # 3603921, 1974.

3. Robert Hickling, Wei Wei, and Richard Raspet, "Finding the direction of a Sound Source Using a Vector Sound-Intensity Probe," *J. Acoust. Soc. Am.*, Vol. 94, No. 4, pp 2408-2412, Oct. 1993.

4. Naval Air Warfare Center (NAWC), Classified Reports on the Development of the DIFAR Sensor and Related Signal Processing.

5. Naval Undersea Warfare Center, Division Newport (NUWCDIVNPT), Classified Reports on the Development of the AN/WLR-9 Acoustic Intercept Receiver and Related Signal Processing.

6. F. J. Fahy, "Measurement of Acoustic Intensity Using the Cross-Spectral Density of Two Microphone Signals," *J. Acoust. Soc. Am.*, Vol. 62, pp 1057-1059, 1977.

7. A. Nehorai and E. Paldi, "Acoustic Vector-Sensor Array Processing," *IEEE Trans. On Signal Processing*, Vol. 42, No. 9, pp 2481-2491, Sept. 1994.

8. V. A. Shchurov, "Modern State and Prospects For Use of Underwater Acoustic Intensity Measurements," Preprint. Vladivostok: Pacific Oceanological Institute FEB RAS, 44 pp., 1998.

9. M. Hawkes and A. Nehorai, "Distributed Processing for 3-D Localization Using Acoustic Vector Sensors on the Seabed or Battlefield," University of Illinois, Chicago, Electrical Engineering and Computer Science Dept., Technical Paper, 1999.

10. B. A. Cray and A. H. Nuttall, "A Comparison of Vector-Sensing and Scalar-Sensing Linear Arrays," NUWC-NPT Technical Report 10,632, 27 Jan 1997.

11. M. T. Silvia and D. J. Schmidlin, "The Effect of Using Two Pressure Sensors to Estimate One Component of the Acoustic Particle Acceleration Vector," SITTEL Technical Memorandum TM 013-2001, February 2001.

12. G. L. D'Spain, "The Vertical DIFAR Array," *presented at the Deployable Surveillance Workshop,* April 1992.

13. E. A. Robinson and M. T. Silvia, *Digital Foundations of Time Series Analysis: Volume 2: Wave Equation Space-Time Processing*, Holden-Day, Inc., San Francisco, 1981.

14. M. T. Silvia and D. J. Schmidlin, "Analysis of Vector and Dyadic Sensors," SITTEL Technical Memorandum TM 014-2001, March 2001.

Development of a Pressure-Acceleration Underwater Acoustic Intensity Probe

James A. McConnell
Acoustech Corporation
P.O. Box 139
State College, PA 16804

Development of a Pressure-Acceleration Underwater Acoustic Intensity Probe

James A. McConnell
Acoustech Corporation
P.O. Box 139
State College, PA 16804
mcconnell@acoustechcorporation.com

Abstract: An underwater acoustic intensity probe containing a hydrophone and accelerometer is described. The design process starts from first principles in which the dynamics of an accelerometer that is imbedded in a compliantly suspended sphere are evaluated using theory and experiment. The results are extended to the case of the intensity probe, which has the geometry of a right circular cylinder. Lumped parameter circuit analysis is used to assess the impact that external suspension systems and internal sensor dynamics have on the fidelity of the measurement. Experimental data is presented which shows the performance of the sensor in a standing wave field. Limitations of the sensing technology are discussed.

INTRODUCTION

The motivation for this research concerns the need to develop an underwater acoustic intensity probe that exhibits a bandwidth that extends well into the kilohertz region of the audible sound spectrum. Neutrally buoyant pressure-velocity (*p-u*) intensity probes[1,2] are very novel transducers, but are somewhat limited to frequencies below 2 kHz. The performance of the geophone is a chief limitation that sets the operational bandwidth of such probes. Accordingly, the development of a pressure-accelerometer (*p-a*) intensity probe has been pursued, although it should be stated that the concept is not new. Sykes[3] and Schloss[4] patented such devices in the mid-1960's, however, each design is relatively primitive with respect to today's technological advances. Nevertheless, the *p-a* probe described in this paper is intended for use as a diagnostic measurement tool to aid in the optimization of underwater sound projectors that are utilized by air-deployed sonobuoys.[5]   Other applications involve the combination of three orthogonal inertial sensors (e.g., either velocity or acceleration sensitive devices) in conjunction with a co-located pressure sensor. Such sensors are termed 'acoustic vector sensors' and have application to a variety of tactical acoustic sensing platforms that are operated by the U. S. Navy.

I. SPHERICAL VELOCITY/ACCELERATION SENSORS

The fidelity of underwater acoustic intensity measurements is largely dependent on the ability to determine the particle velocity with a high degree of precision. This is true for *p-u*, *p-a*, *p-p*,[6] and *u-u*[7,8] intensity probes.   To illustrate the basic physics of the problem, a spherical sensor containing an accelerometer is evaluated using theory and experiment. The object of this analysis is to quantify the effect of the sphere density, external suspension systems, and internal sensor dynamics on the fidelity of the measurement. The results are used to aid in the development of the *p-a* probe.

A. Theory

Many researchers[9-13] have derived the equation of motion for a small, unconstrained solid sphere when subjected to an acoustic plane wave in an unbounded fluid medium. The analysis shows that the velocity amplitude of the sphere is related to that of the acoustic wave by:

$$\frac{V_s}{V_o} = \frac{m_o + m_i}{m_s + m_i},$$

(1)

where V_s is the velocity amplitude of the sphere, V_o is the velocity amplitude of the acoustic wave, m_s is the mass of the sphere, m_i is the induced mass that is created as a result of the sphere translating in the fluid, and m_o is the mass of fluid having the same volume as the sphere. For the case of the sphere, the induced mass can be computed analytically in closed form and is equal to $m_o/2$. This leads to well known formulation:

$$\frac{V_s}{V_o} = \frac{3\rho_o}{2\rho_s + \rho_o}, \tag{2}$$

where ρ_o is the density of the fluid and ρ_s is the density of the sphere. It can be concluded from Eqs. (1) and (2) that a neutrally buoyant sphere has the same velocity amplitude as the incoming acoustic wave, a positively buoyant sphere responds with an amplitude that is greater than that of the acoustic wave, and a negatively buoyant sphere responds with an amplitude that is less than that of the acoustic wave. These results serve as the basis for nearly every underwater transducer that employs an inertial sensor to measure the acoustic particle velocity, or time derivatives thereof, e.g., particle acceleration.

The dynamics of the problem are somewhat different when the sphere is constrained by a compliant suspension system. Fig. 1 shows a schematic of a suspended sphere along with a lumped parameter circuit model of the system. In Fig. 1, the spring has compliance C_s and the damper has resistance R_s. The equation of motion can be inferred from the circuit and ultimately leads to the following formulation:

$$\frac{V_s}{V_o} = \frac{3\rho_o}{2\rho_s + \rho_o} \cdot \frac{1}{1 - 2j\zeta_s \dfrac{\omega_s}{\omega} - \dfrac{\omega_s^2}{\omega^2}}, \tag{3}$$

where ω is the excitation frequency, ω_s is the resonance frequency, and ζ_s is the damping factor. The resonance frequency and damping factor are further defined as $\omega_s = [(m_s + m_i) C_s]^{-1/2}$ and $\zeta_s = R_s/2(m_s + m_i)\omega_s$.
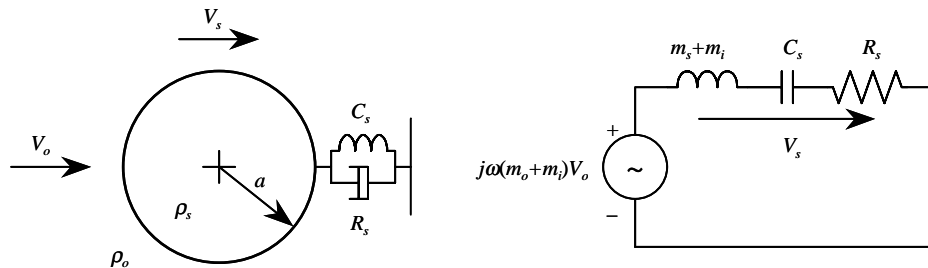
FIG. 1. Schematic of a compliantly suspended sphere undergoing rigid body translation when subjected to an acoustic plane wave. The equivalent mechanical impedance circuit is also shown.

Fig. 2 presents the result of plotting Eq. (3) versus dimensionless frequency ω/ω_s over damping factors that span two orders of magnitude. This analysis is specific to the case of neutral buoyancy. It can be inferred from the figure that about a decade above resonance, the magnitude of the sphere's motion is identical to that of the acoustic wave. The phase response, however, depends on the level of damping present in the system, and in particular, only lightly damped systems result in good phase fidelity above resonance (e.g., frequencies where the sphere exhibits little or no phase shift with respect to that of the acoustic wave). These results indicate that the motion of a lightly damped sphere can be described by Eqs. (1) and (2) at about a decade above resonance.

The dynamics of the system are further exacerbated when an inertial sensor such as a piezoceramic accelerometer or moving coil geophone is imbedded in the sphere. In either case the system can be modeled with lumped parameters to compute the open-circuit receiving response of the transducer. Figs. 3 and 4 present schematics of acceleration-based and velocity-based spherical transducers along with their corresponding lumped parameter circuit models. As before, the spheres contain an external suspension system and are subjected to an acoustic plane wave in an unbounded medium.
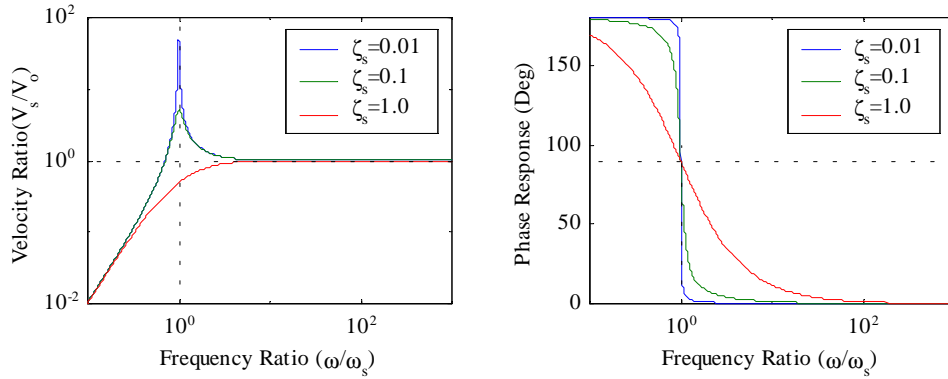
FIG. 2. Response of a compliantly suspended sphere undergoing rigid body translation when subjected to an acoustic plane wave.

In Fig. 3, m_t, C_t, and R_t are the mechanical mass, compliance, and damping of the accelerometer. The transduction constant is denoted as ϕ and C_o is the clamped capacitance. The parameters A_o, A_s, and A_t, correspond to the acceleration amplitudes of the in-coming wave, sphere, and proof-mass, respectively. Similarly, in Fig. 4, m_t, C_t, and R_t are the mechanical mass, compliance, and damping of the geophone. The transduction constant is denoted as Bl, R_e is the coil resistance, and L_e is the coil inductance. The parameter V_t corresponds to the velocity amplitude of the geophone proof-mass. The open circuit output voltage for each transducer is denoted as e_{oc}.
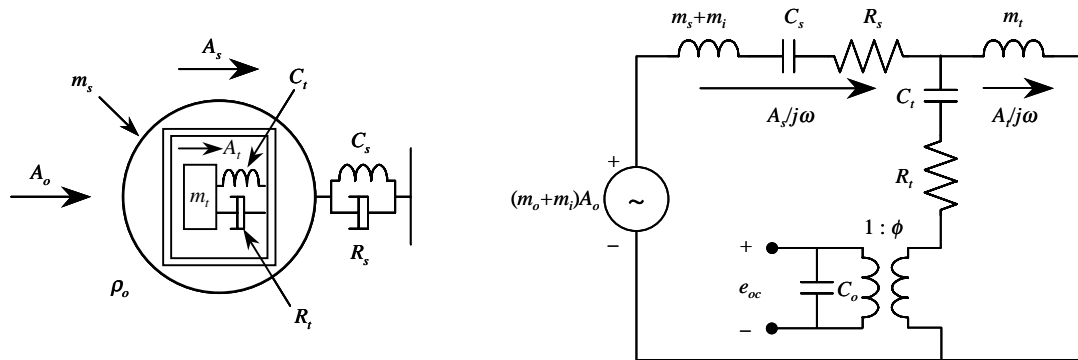
FIG. 3. Schematic of an acceleration-based spherical sensor with external suspension system. Sphere is undergoing rigid body translation as a result of acoustic plane wave excitation. The equivalent electro-mechanical impedance circuit is also shown.
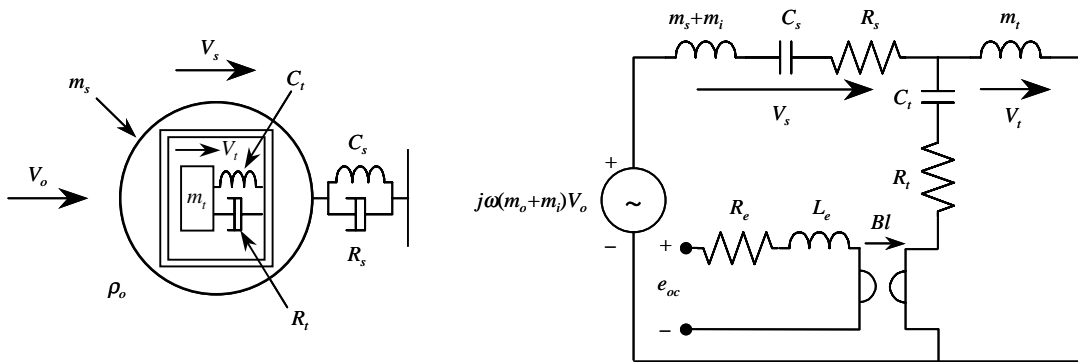
FIG. 4. Schematic of a velocity-based spherical sensor with external suspension system. Sphere is undergoing rigid body translation as a result of acoustic plane wave excitation. The equivalent electro-mechanical impedance circuit is also shown.

The open-circuit receiving response of the spherical accelerometer is determined from Fig. (3) to be $e_{oc}=\phi Z(\omega)/(j\omega)^2 C_o$. Likewise, from Fig. (4), the receiving response of the spherical geophone is determined to be $e_{oc}=BlZ(\omega)$. For both of these expressions, the term $Z(\omega)$ is defined as:

$$Z(\omega) = \frac{3\rho_o}{2\rho_s + \rho_o} \cdot \left[\left(1 - 2j\zeta_s \frac{\omega_s}{\omega} - \frac{\omega_s^2}{\omega^2} \right) \left(1 - 2j\zeta_t \frac{\omega_t}{\omega} - \frac{\omega_t^2}{\omega^2} \right) - \frac{m_t}{m_s + m_i} \left(2j\zeta_t \frac{\omega_t}{\omega} + \frac{\omega_t^2}{\omega^2} \right) \right]^{-1} \quad (4)$$

where ω_t and ζ_t are the resonance frequency and damping factor associated with the inertial transducer inside the sphere. These parameters are further defined as $\omega_t=(m_t C_t)^{-1/2}$ and $\zeta_t=R_t/2m_t\omega_t$. To assess the significance of these results, the receiving response of both transducers is plotted versus frequency $f=\omega/2\pi$. It is assumed that each sphere is lightly damped and exhibits a low resonance frequency such that $f_s=\omega_s/2\pi=5$ Hz and $\zeta_s=0.01$. It is also assumed that the resonance frequencies of the accelerometer and geophone are $f_t=\omega_t/2\pi=25$ kHz and $f_t=30$ Hz respectively, and each transducer has a damping factor of $\zeta_t=0.1$. Both spheres are assumed to be neutrally buoyant and the mass ratio $m_t/(m_s+m_i)$ is assumed to be 0.01. The results are plotted in Fig. 5 and normalized so that the magnitude of the response is unity in the pass-band. In this way, assumptions do not have to be made regarding the scalar values for ϕ, C_o, and Bl.
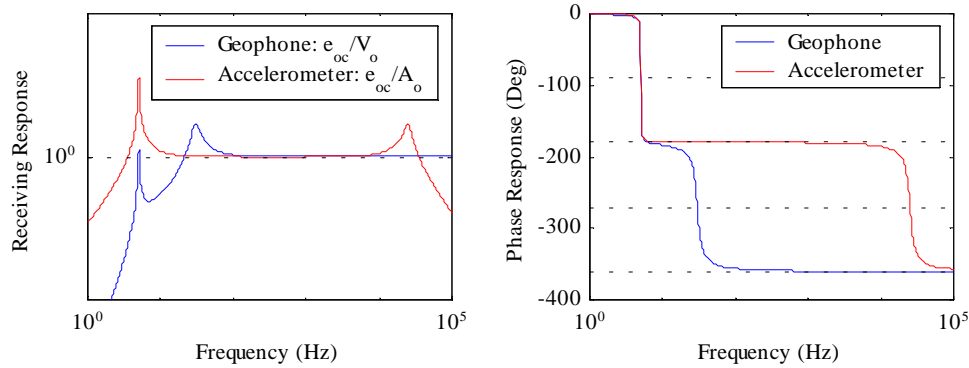
FIG. 5. Response of spherical acceleration and velocity sensors when subjected to an acoustic plane wave.

Fig. 5 shows that for each transducer, the magnitude of the response is unity in the pass-band (e.g., the region that is far removed from the resonances in the system). This figure also shows that the phase response is 'flat' within the pass-band, although a 180° phase shift is evident in the response of the accelerometer above f_s. Nevertheless, these results provide the transducer designer with some guidelines on how to design the external suspension system and select the appropriate transducer to meet the bandwidth requirements of an intensity probe.

B. Experiment

Positive, negative, and near-neutrally buoyant spherical sensors were fabricated and tested so that the theory presented in the previous section could be evaluated. More specifically, commercially available birch wood, bronze, and urethane spheres, having a diameter of 5.08 cm, were machined to incorporate an Oceana Sensor Technologies Model AP1BCN accelerometer.[14] These accelerometers have a nominal sensitivity of 10 mV/g and a mounted resonance frequency of about 25 kHz. They contain a shear-type sensing element and require constant current DC power for an internal FET based preamplifier. They are ideally suited for this application because they are designed to be imbedded into structures for vibration monitoring.

Each sensor contains a compliant spring that consists of a small inextensible tether that connects the body of the sphere to a cantilever beam. Fig. 6 shows the basic design of the sensor in its physical and lumped parameter representations. Based on the figure, the system can be modeled as a mass-loaded cantilever beam undergoing rigid body translation in the vertical direction. Now, if the internal sensor

dynamics of the accelerometer are neglected, then the lumped parameter resonance frequency of the system is predicted by[15]

$$f_s = \frac{1}{2\pi\sqrt{(m_s + m_i)C_s}} = \frac{1}{2\pi}\sqrt{\frac{3EI}{(m_s + m_i)L^3}} \quad , \tag{5}$$

where L, E, and I are the length, Young's modulus, and moment of inertia of the cantilever beam. Note that the basis for neglecting the internal sensor dynamics stems from the fact that the resonance frequency of the accelerometer is well beyond the frequency range of interest.
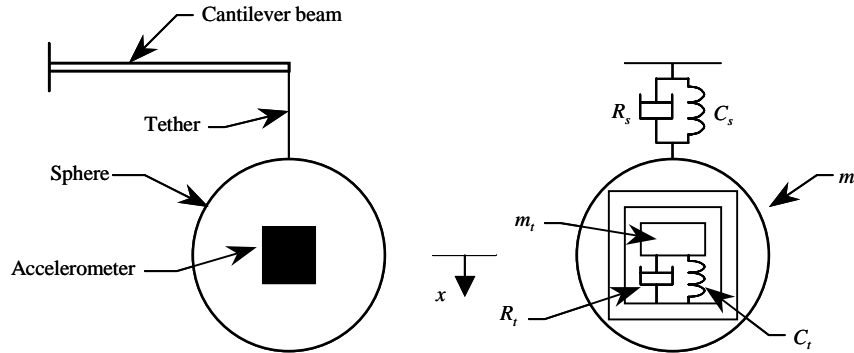
FIG. 6. Basic design of compliantly suspended spherical acceleration sensor in its physical and lumped parameter representations.

The logarithmic decrement method[16] was used to experimentally determine the resonance frequency and damping factor of each sphere. This was done by submerging the sphere inside a vertically oriented column of water and allowing it to vibrate freely once it was displaced from its equilibrium position. The transient time-series data from the accelerometer embedded within the sphere was measured using an HP 35670A dynamic signal analyzer. During the experiment the *in-situ* dimensions of the cantilever beam were measured with a micrometer. Using these parameters in conjunction with the physical properties of the beam and the sphere enabled a theoretical prediction to be made using Eq. (5). The results of the experimental and theoretical analyses are presented in Table I. It can be inferred from the table that the resonance frequencies determined by experiment are in good agreement with theory and that the spheres are lightly damped.

TABLE I. Physical properties for spherical acceleration sensors.

Sphere	Buoyancy	m_s (g)	ρ_s (g/cm^3)	$3\rho_o/(2\rho_s+\rho_o)$	Suspension	C_s (mm/N)	ζ_s[a]	f_s (Hz)[a]	f_s (Hz)[b]
Birch wood	Positive	40.0	0.58	1.39	Steel rod	4.74	0.02	8.8	8.5
Bronze	Negative	499.0	7.27	0.19	Brass strip	1.41	0.01	5.3	5.8
Urethane	Near neutral	77.5	1.13	0.92	Steel rod	10.5	0.06	4.0	4.7

[a]Experimental results, [b]theoretical results.

The second part of the experiment concerns the performance of the spheres in a standing wave field. This was done consistent with the approach taken by Gabrielson[2] in which the velocity of an inertial sensor was compared to that inferred from a reference hydrophone positioned at the same depth within a waveguide having an acoustic source at one end and a pressure-release surface at the other end. The waveguide used for this testing was made of acrylic and had an inside diameter of 10.16 cm, a length of 100 cm, and wall thickness of 3.18 mm. The walls of the waveguide are compliant, thus the sound speed is substantially reduced from the bulk speed found in open water. The sound speed was determined via experiment to be about 381 m/s.[17] This result compares favorably with theory for 'slow' waveguides.[18-22]

Fig. 7 presents a schematic of the experimental set-up and shows how the spheres and the reference hydrophone were positioned in the waveguide. A Reson TC-4013 hydrophone, having a measured sensitivity of 28.2 μV/Pa, was used as the reference standard. For each test case the measurement depth was 7.62 cm from the pressure-release surface. The sound projector at the bottom of the waveguide was a Wilcoxon Research F4 shaker that was modified to incorporate a 7.62 cm diameter aluminum piston.
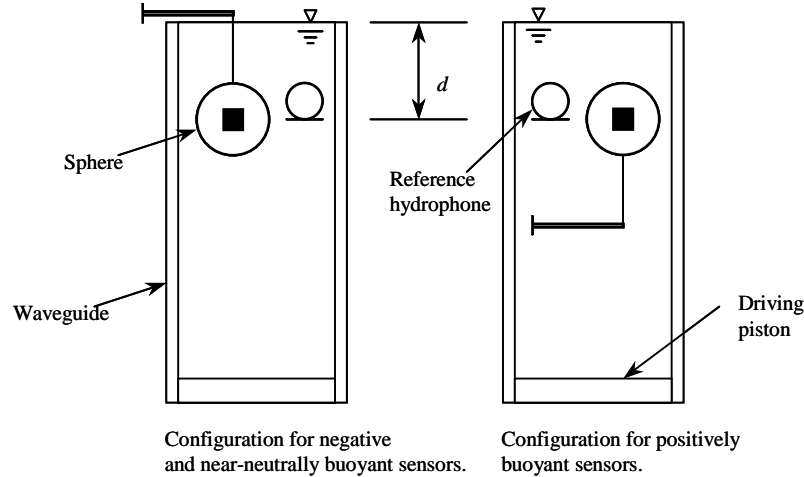
FIG. 7. Experimental set-up for tests performed in a water-filled waveguide.

Under the assumption of a loss less waveguide having a pressure release boundary condition, it can be shown that the ratio of the sphere's velocity relative to the acoustic particle velocity is

$$\frac{V_s}{V_o} = \frac{A_s}{P_o} \cdot \frac{\rho_o c \tan kd}{\omega} , \tag{6}$$

where P_o is the acoustic pressure at the measurement depth, c is the sound speed in the waveguide, k is the acoustic wave number, and d is the measurement depth. Eq. (9) was implemented by measuring the transfer function between the output voltages generated by the accelerometer in the sphere and the reference hydrophone. This was done using a HP 35670A analyzer operating in frequency response mode. The waveguide was ensonified with band-limited random noise over the 0-1600 Hz frequency range and the transfer function was measured using a 1 Hz analysis resolution, 128 rms averages, and a Hanning window. The transfer function was subsequently adjusted by the sensitivities of the transducers.

The results of the experiment are presented in Fig. 8, which compares Eqs. (2) and (6) over the 40-1000 Hz frequency range. This figure shows that the experimental data tracks well with theory, in that varying the density of the sphere causes a predictable change in the corresponding velocity amplitude. Statistical analysis of the test data revealed that, on average, the response of the spheres deviated from theory by up to 5%.
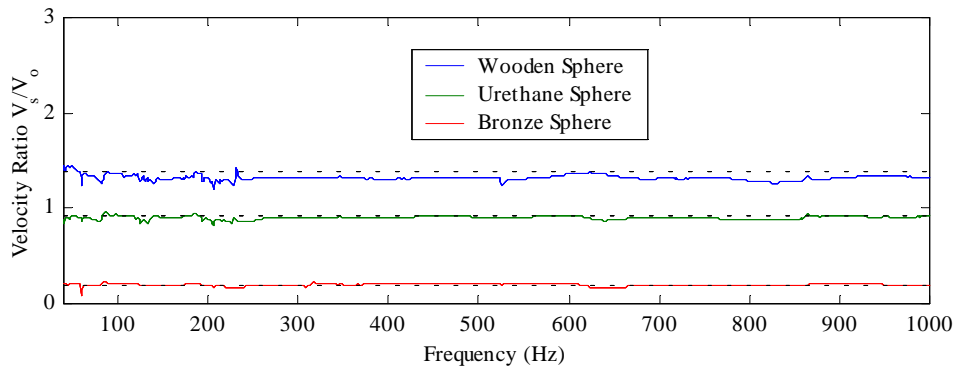
FIG. 8. Result of plotting experimental data obtained on spheres in waveguide versus theory predicted by Eq. 2. The experimental data is plotted with colored lines and the theoretical predictions are plotted as black dashed lines.

It is noted that the analysis of the data shown in Fig. 8 was limited to 40-1000 Hz because (1) the F4 shaker could not provide sufficient levels of excitation below about 40 Hz and (2) in Eq. (6), the slope of

tan *kd* changes rapidly for frequencies greater than 1000 Hz and consequently puts excruciating demands on the accuracy of the measured sound speed, depth, and knowledge of any losses in the waveguide.

II. PRESSURE-ACCELERATION INTENSITY PROBE

A. Practical intensity measurements in one dimension

For one-dimensional sound propagation having $e^{j\omega t}$ dependence, Fahy[6] defines the complex acoustic intensity spectrum at a single point in space as $C(\omega)=I(\omega)+jJ(\omega)$, where $I(\omega)$ and $J(\omega)$ are the active and reactive intensity spectra:

$$I(\omega) = \text{Re}\left\{G_{pu}(\omega)\right\} = \frac{1}{2}\text{Re}\left\{P(\omega)U(\omega)^*\right\} \tag{7}$$

$$J(\omega) = \text{Im}\left\{G_{pu}(\omega)\right\} = \frac{1}{2}\text{Im}\left\{P(\omega)U(\omega)^*\right\}. \tag{8}$$

In Eqs. (7) and (8), $G_{pu}(\omega)$ is the single-sided time-averaged rms cross-spectrum between the acoustic pressure $P(\omega)$ and the particle velocity $U(\omega)$. Intensity probes that contain discrete sensors for the independent measurement of these parameters can be used in conjunction with a standard two-channel dynamic signal analyzer to compute the quantities $I(\omega)$ and $J(\omega)$. For the case of the *p-u* probe, Eqs. (7) and (8) can be implemented directly, but for the *p-a* probe the particle velocity is computed from $A(\omega)/j\omega$, where $A(\omega)$ is the particle acceleration.

B. Design and fabrication

Two different versions of the *p-a* probe were designed, fabricated, and tested using commercial-off-the-shelf parts. The designs conform to the schematic presented in Fig. 9, which shows that the sensors are basically the same, but one contains a slotted cylindrical shell that surrounds the exterior of the probe and each employ a different type of suspension spring. The intent here is to evaluate the performance of both sensors so that the effect of the shell and the suspension springs can be quantified. An exploded view of the probe containing the slotted shell is shown in Fig. 10 and photographs of some of the prototypes are shown in Fig. 11.
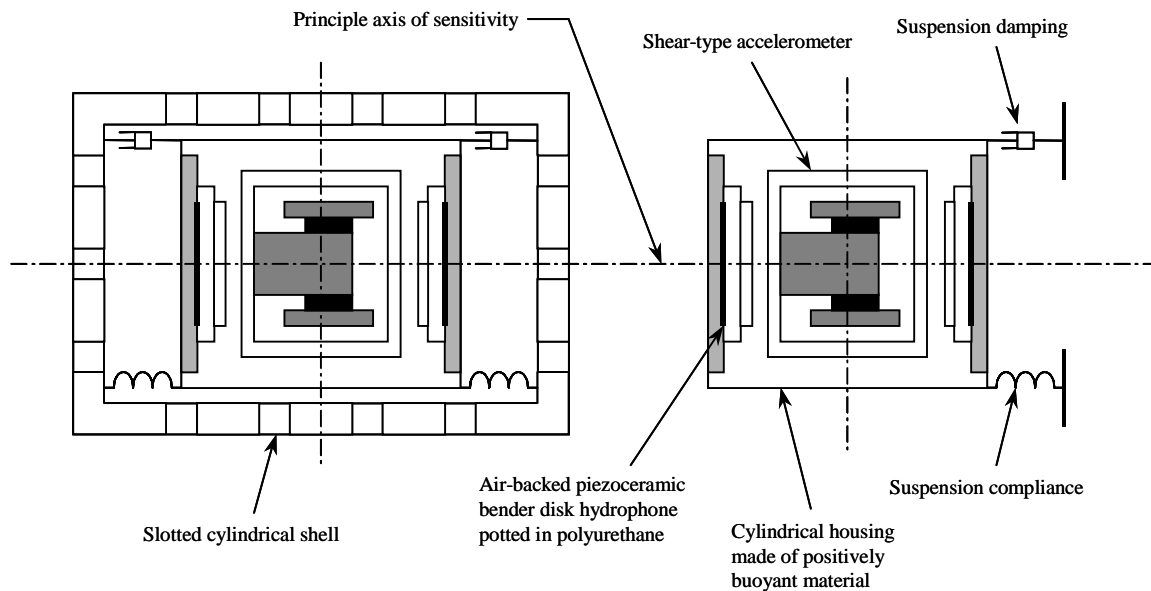
FIG. 9. Basic design concepts for the *p-a* probe. The probe on the left is compliantly suspended inside a slotted cylindrical shell. The probe on the right is of the same design but contains a different type of suspension spring.

The design of the probe is centered around embedding one bi-directional accelerometer and two omni-directional hydrophones in a cylinder of syntactic foam. The accelerometer is identical to that discussed previously in Section I. The hydrophones are air-backed piezoceramic bender disks that have a urethane coating on the side that is exposed to water. They are electrically connected in parallel to effectively measure the acoustic pressure in the geometric center of the probe where the accelerometer is located. The electrical connection also enables the hydrophones to be relatively insensitive to acceleration. The hydrophones are identical to those employed by the AN/SSQ-53D sonobuoy and have a nominal sensitivity of about –200 dB re 1 V/μPa. They exhibit an in-water resonance frequency of about 8 kHz. The electrical signals from the transducers are routed from the probe to analysis equipment via a 4-conductor shielded cable having a PVC jacket (Cooner Wire: CW2503[23]).

The cylinder is machined from a block of Syntech Materials[24] AM-24 syntactic foam, which has a nominal density of 0.384 g/cm^3. The density is selected to provide a buoyancy force that counters the weight of the fully assembled sensor. This is done, to the maximum extent practical, so that the probe is neutrally buoyant in water at 20°C. As shown in Fig. 10, the cylinder is comprised of three pieces: two end-caps and a body. Assembly steps are taken to insert the hydrophones into the end-caps and to insert the accelerometer into the body. During the final assembly step, the end-caps are inserted into the body. Epoxy resin is used to maintain the integrity of the joint. The fully assembled probe has a diameter of 2.54 cm, an aspect ratio of unity, and a mass of about 15 g. These parameters translate into an average density of about 1.17 g/cm^3, which indicates that the probe is slightly negatively buoyant.
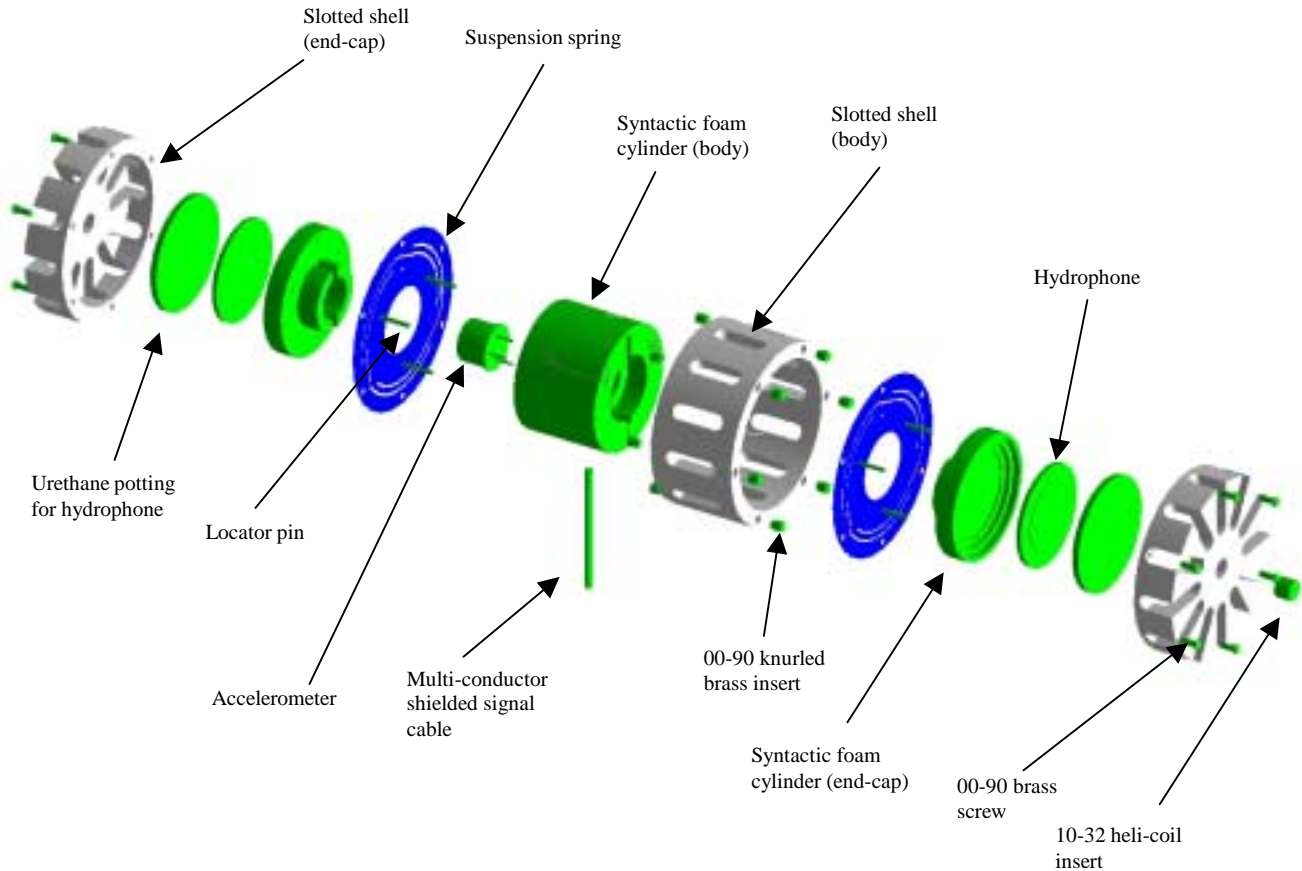
FIG. 10. Exploded view of *p-a* probe containing slotted cylindrical shell and circular leaf spring suspension.

The probe shown in Fig. 10 is compliantly suspended inside the slotted cylindrical shell using two circular leaf springs that rely on the mass-loaded cantilever beam principle. The inner and outer bolting rings of the springs are captured between the mating surfaces of the syntactic foam cylinder and the slotted cylindrical shell, respectively. Locater pins provide the alignment for the inner bolting ring and a network of 00-90 screws/inserts facilitate the alignment of the outer bolting ring. The springs are designed to be

compliant in the axial direction (e.g., the principle axis of sensitivity) and stiff in the radial direction. This is done to facilitate an in-water probe/suspension resonance frequency of about 10 Hz. The springs are photo-etched from 0.13 mm beryllium-copper shim stock.

The slotted cylindrical shell is machined from a rod of black nylon-6, whose material properties exhibit a characteristic acoustic impedance similar to that of bulk water. The shell is used to limit the axial excursions of the probe and to serve as a 'flow shield' when it is encapsulated in a nylon stocking or some other semi-porous material. The object of the flow shield is to minimize the sensor's intrinsic sensitivity to flow induced noise by displacing the turbulent boundary layer (TBL) away from the body of the probe. The TBL is created when water flows over the probe. A 10-32 heli-coil insert is installed on the flat face of the shell end-cap to provide an attachment point for an external positioning system. The shell has a diameter of 36.2 mm, a length of 34.3 mm, and a wall thickness of 3.18 mm.
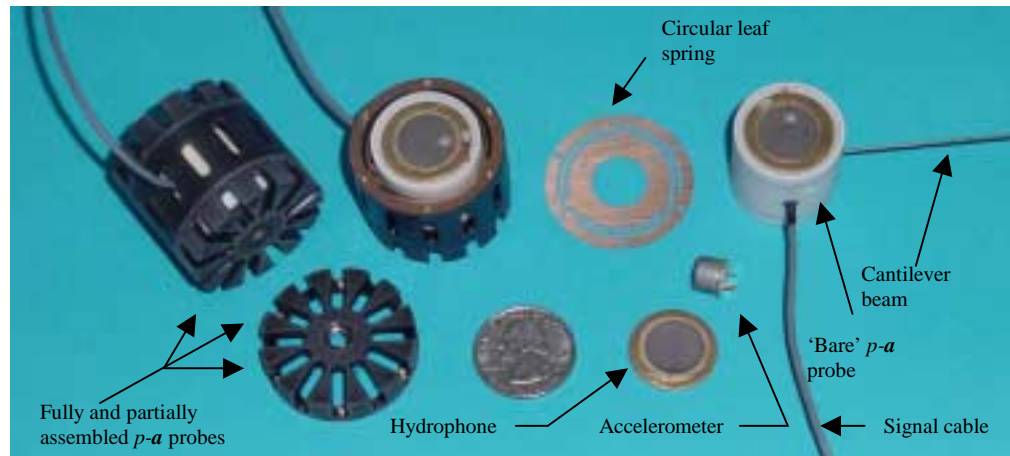
FIG. 11. Various prototype *p-a* probes and related parts.

As shown in Fig. 11, a variant of the design is simply a 'bare' probe that employs a cantilever beam as the external suspension. This embodiment is more or less designed to be consistent with the overall concepts presented in Section I. Moreover, it serves as an 'interim' design to help quantify the effects of slotted shell, circular leaf springs, and acoustic cavities that are characteristic of the other probe.

C. Experiment

Several experiments were conducted to categorize the performance of the *p-a* probe. The first concerns the notion that a properly designed *p-a* probe should have the ability to independently measure the acoustic pressure and particle acceleration without contamination. In other words, the hydrophone should be able to discriminate against acceleration and the accelerometer should be able to discriminate against pressure. An indication of whether this is occurring (or not) can be deduced by scanning a standing wave field for the locations of the nodes and antinodes. That is, a perfect standing wave exhibits pressure nodes and acceleration antinodes at the same location, and vice-versa. Also, the acoustic pressure and particle acceleration are 180° out of phase. Accordingly, the *p-a* probe (equipped with the leaf springs and slotted shell) was positioned in the 'slow' waveguide along with a Reson TC-4013 hydrophone. The waveguide was excited with a 250 Hz tone and the standing wave field was scanned over a distance of 500 mm starting from 100 mm below the pressure-release surface. Power-spectra were acquired at 5 mm increments using a HP 35670A spectrum analyzer. The data were analyzed over the 0-400 Hz frequency range using a 1 Hz analysis resolution, 16 rms averages, and a Hanning window. Fig. 12 shows the result of the experiment and presents two separate plots which show: (1) the raw uncalibrated voltage outputs from the *p-a* probe and the reference hydrophone as a function of distance, and (2) the steady-state time traces of the raw uncalibrated voltage output from the *p-a* probe at a distance 76.2 mm below the pressure-release surface. The 'raw data' is presented so that unbiased conclusions can be made without hesitation.

It can be inferred from Fig. 12 that the pressure measured by the *p-a* probe hydrophone tracks very well with that of the reference hydrophone. The figure also shows that the pressure maxima and acceleration minima are almost perfectly aligned. The spatial offset was measured to be about Δx=20 mm which translates in to a phase aberration of about $k\Delta x$=4.7°. This result was verified by computing the phase of $G_{pa}(\omega)$, in that the measured phase at 250 Hz was 175.3°, or about 4.7° away from perfect a standing wave. This latter point can be realized by viewing the time series data presented in Fig. 12. The reason for the quasi-perfect standing wave field is believed to be associated with the fact that the walls of the waveguide are compliant, not rigid, hence the wall motion radiates sound and constitutes a loss mechanism for the system. Based on these results it can be concluded that, on a relative basis, the *p-a* probe is working properly.
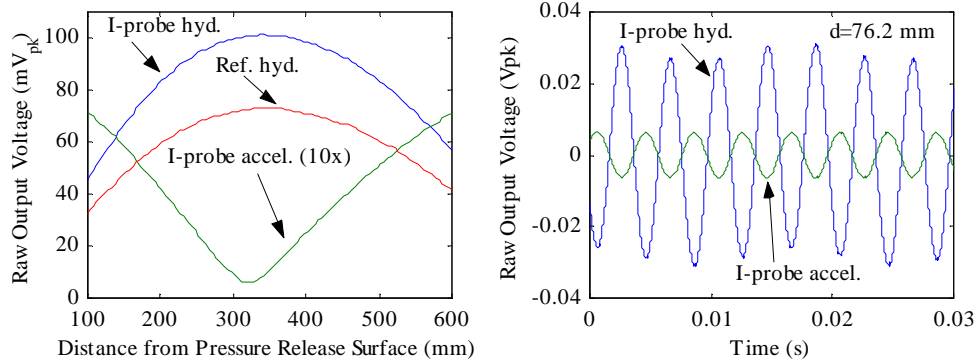
FIG. 12. Performance of *p-a* probe (equipped with leaf springs and slotted shell) in standing wave field at 250 Hz.

The second experiment concerns evaluating the performance of the accelerometer in the *p-a* probe using the approach taken for the spherical sensors in Section I. The intent here is to compare the result of Eq. (2) versus Eq. (6), however, this requires *a priori* knowledge of the induced mass for the *p-a* probe. This is an important concept because the geometry of the probe is not spherical, thus Eq. (2) is, in general, not applicable. The more general form of Eq. (1) is applicable, yet no closed form solution exists to determine the induced mass for the case of a right circular cylinder.

Accordingly, the induced mass of the *p-a* probe was measured using two different techniques. The first technique involves determining the resonance frequency of the compliantly suspended probe using the logarithmic decrement method. This was done consistent with the approach described in Section I for the spherical sensors, except the tests were performed with the probe in air and in water. Now, in order to simplify the analysis, it was assumed that the induced mass in air was zero, thus Eq. (5) can be expressed as follows:

$$m_i \cong m_c\left[\left(\frac{f_{ca}}{f_{cw}}\right)^2 - 1\right], \qquad (9)$$

where m_c is the mass of the probe and f_{ca} and f_{cw} are the fundamental mass-spring resonances of the probe in air and water, respectively.

The second technique relies on computing the in-air and in-water resonance frequencies of the hydrophone employed by the *p-a* probe. This can be realized when one considers that the induced mass is identical to the radiation mass that the hydrophone is subjected to when it is configured as a source or a receiver. In contrast to the first technique, this method serves only as an indirect way to determine the induced mass. More specifically, the mechanical mass of the hydrophone is not known, but the ratio of the resonance frequencies can be determined. This ratio should be the same as that delineated in Eq. (9), or, $f_{ha}/f_{hw}=f_{ca}/f_{cw}$, where f_{ha} and f_{hw} are the in-air and in-water resonance frequencies of the hydrophone. In this way, the second technique serves as a data quality check for the first. It is noted that the resonance frequencies of the hydrophone were determined from an electrical impedance measurement in which the transfer function between the voltage drop across the transducer and the drive current is measured.[25,26]

Prior to performing the experiments on the *p-a* probes, the first technique was validated using the bronze sphere as the test specimen. Theory predicts the induced mass to be 34.3 g (e.g., $m_i=2\pi a^3 \rho_o/3$). The experimental value was determined to be 36.9 g, which deviates from theory by 7.6%.

The results of the induced mass experiments are presented in Table II. The data obtained on the bare probe indicates that the induced mass is 9.1 g and that there is very good agreement between both techniques as evidenced by the 1% deviation in the term $(f_{ca}/f_{cw})/(f_{ha}/f_{hw})$. The data also indicates that Eqs. (1) and (2) appear to be fairly commensurate despite the differences in geometry between the cylinder and the sphere.

The results for the case of the probe with the slotted shell are mildly ambiguous, in that there was a 34% increase in the induced mass relative to the case of the bare probe, yet this did not appear to propagate into the results predicted by Eqs. (1) and (2). It is speculated that the sensitivity of these equations to values for the induced mass can be rather slight provided the probe is (near) neutrally buoyant. It is noted, however, that the 34% increase is likely to be related to the acoustic inertance of the fluid entrained in the slots.

Table II. Results of induced mass experiments performed on *p-a* probes.

Test sensor	m_c (g)	f_{ca}/f_{cw}	m_i (g)	f_{ha}/f_{hw}	$(f_{ca}/f_{cw})/(f_{ha}/f_{hw})$	$(m_o+m_i)/(m_c+m_i)$	$3\rho_o/(2\rho_c+\rho_o)^a$
Bare p-a probe	15.0	1.28	9.1	1.29	0.99	0.91	0.90
p-a probe w/slotted shell	14.9	1.39	13.7	1.16	1.20	0.92	0.90

[a] ρ_c is the average density of the fully assembled syntactic foam cylinder.

The results of the foregoing analysis are now applied to the experiments performed on the probes in which Eqs. (1) and (6) are evaluated. The bare probe was tested in the 'slow' waveguide, but the probe with the slotted shell was tested in a USRD G19 calibrator.[27] The G19 is a standing wave device made from an 10.16 cm diameter aluminum tube. The sound speed in the G19 is estimated to be about 1219 m/s.[28] The G19 was used because it was thought that the acoustic cavities in the slotted shell could resonate and consequently contaminate the measurements. Increasing the sound speed of the fluid helps to push these resonances out of the frequency range of interest.

The results of this testing are presented in Fig. 13. This figure shows that the data obtained with the bare probe is commensurate with Eq. (1) except for regions of the spectrum where spurious resonances are evident. It is speculated that the source of these resonances is associated with torsional modes and higher order transverse bending modes of the suspension spring.[29] Torsional modes are suspected because the attachment points of the cantilever beam and the signal cable are perpendicular (see Fig. 11). Thus the eccentric weight of the cable creates a torque on the probe which is ultimately transferred to the spring. Transverse bending modes are suspected because the system can be only modeled with lumped parameters for low frequencies. In other words, if the fundamental bending mode of a mass-loaded cantilever beam is 10 Hz (as is the case here), then lumped parameters should be sufficient to describe the dynamics of the system up to about a decade above resonance. Beyond this point it is reasonable to assume that higher order bending modes may become evident in the response. However, suspension springs that include an appropriate level of damping are anticipated to resolve this issue.
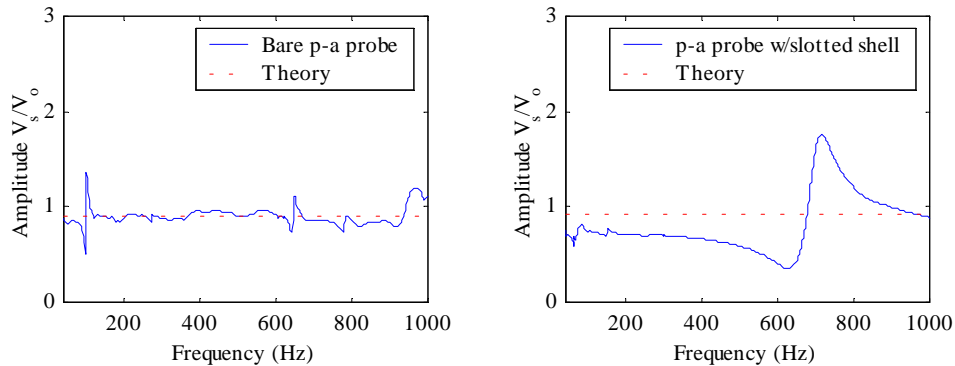
FIG. 13. Results of testing *p-a* probes to assess whether their velocity amplitude is commensurate with theory for a standing wave.

Fig. 13 also shows that the data acquired on the probe with the slotted shell does not agree with theory and appears to be controlled by a resonance response occurring at about 750 Hz. This result was repeatable over time and was also observed when another probe of the same design was tested in the G19. At the present time, the source of the resonance is unclear, although, wave effects in the suspension springs, structural modes of the slotted shell, and acoustic cavity modes of the slotted shell are all considered to be possible sources. Work is on going to resolve these issues.

III. SUMMARY AND CONCLUSIONS

The dynamics of a compliantly suspended sphere containing an accelerometer were evaluated using theory and experiment. Results show that the performance of the sensor can be predicted using lumped parameter theory, in that varying the density of the sphere causes a predictable change in the corresponding velocity amplitude. This result is specific to the pass-band, which covers the frequencies between the resonances in the system.

The results obtained for the spherical sensors were extended to the case of developing a near-neutrally buoyant *p-a* intensity probe. Two *p-a* probes were evaluated, one that was compliantly suspended in a free-flooding slotted cylindrical shell and another that employed a simple cantilever beam suspension. In essence, the only difference between the two sensors was how they were packaged. The former is far more complex than the latter.

Various tests were performed on the *p-a* probes to assess their performance in a standing wave field. The basic design appears to be viable, in that (1) the hydrophone is responsive to the acoustic pressure and discriminates against acceleration and (2) the accelerometer is responsive to the particle acceleration and discriminates against pressure.

The probe containing the simple cantilever beam suspension (e.g., the 'bare' probe) exhibited the best performance of the two probe designs that were evaluated. This occurred because an in-band resonance corrupted the data obtained on the probe that had the slotted cylindrical shell.

It is clear from this study that, novel and 'acoustically friendly' packaging concepts are critical to the successful development of *p-a* probes. This is particularly important when the probes are required to have high fidelity over a large bandwidth.

ACKNOWLEDGMENTS

REFERENCES

1. U. S. Patent 5,392,258, "Underwater Acoustic Intensity Probe", February 21, 1995.
2. T. B. Gabrielson, D. L. Gardner, and S. L. Garrett, "A Simple Neutrally Buoyant Sensor for Direct Measurement of Particle Velocity and Intensity in Water," *J. Acoust. Soc. Am.* **97**, 2227-2237 (1995).
3. U. S. Patent 3,274,539, "Transducer for Simultaneous Measurement of Physical Phenomena of Sound Wave", September 20, 1966.
4. U. S. Patent 3,311,373, "Intensity Meter, Particle Acceleration Type", March 28, 1967.
5. U. S. Government Contract N00421-98-C-1234, "Integrated Intensity Sensors and Associated Calibration System," DoD SBIR Topic No. OSD96-013 Phase II, dated September 21, 1998.
6. F. J. Fahy, *Sound Intensity*, 2*nd Ed*., (E & FN Spon, London)
7. K. J. Bastyr, G. C. Lauchle, and J. A. McConnell, "Development of a Velocity Gradient Underwater Acoustic Intensity Sensor," *J. Acoust. Soc. Am.,* **106** (6) pp. 3178-3188 (1999).
8. U. S. Patent US 6,172,940 B1, "Two Geophone Underwater Acoustic Intensity Probe", January 9, 2001.
9. E. Skudrzyk, *The Foundations of Acoustics*, Springer Publications, New York, NY (1971).

10. C. B. Leslie, J. M. Kendall, and J. L. Jones, "Hydrophone for Measuring Particle Velocity," *J. Acoust. Soc. Am.* **28**, 711-715 (1956).

11. G. K. Batchelor, *An Introduction to Fluid Dynamics*, Cambridge University Press, New York, NY (1994).

12. L. D. Landau and E. M. Lifshitz, *Fluid Mechanics*, Butterworth-Heinemann Ltd. Oxford England, Second Edition (1995).

13. N. A. Fuchs, *The Mechanics of Aerosols*, (Dover Publications, Inc., New York, 1989).

14. Oceana Sensor Technologies, Inc., 1632 Corporate Landing Parkway, Virginia Beach, VA 23454.

15. W. T. Thompson, *Theory of Vibration with Applications*, 3rd *Ed.,* (Prentice Hall, New Jersey, 1988).

16. R. K. Vierck, *Vibration Analysis* 2nd *Ed*., (Harper & Row, Publishers, New York).

17. J. A. McConnell, K J. Bastyr, and G. C. Lauchle, "Sound-speed Determination in a Fluid-filled elastic Waveguide," *J. Acoust. Soc. Am.* **105**, 1120 (A) (1999).

18. M. C. Junger and D. Feit, *Sound, Structures, and Their Interaction*, Acoustical Society of America through the American Institute of Physics, Woodbury, NY (1993).

19. J. Lighthill, *Waves in Fluids*, Cambridge University Press, New York, NY (1996).

20. J. Parmakian, *Waterhammer Analysis*, Dover Publications, New York, NY (1963).

21. T. C. Lin and G. W. Morgan, "Wave Propagation through Fluid Contained in a Cylindrical, Elastic Shell," *J. Acoust. Soc. Am.* **28**, 1165-1176 (1956).

22. R. Skalak, "An Extension of the Theory of Water Hammer," Trans. ASME **78**, 105-116 (1956)

23. Cooner Wire, 9265 Owensmouth, Chatsworth, CA 91311.

24. Syntech Materials, Inc., P. O. Box 5242, Springfield, VA 22150.

25. O. B. Wilson, *Introduction to Theory and Design of Sonar Transducers*, (Peninsula Publishing, California, 1988).

26. R. J. Bobber, *Underwater Electroacoustic Measurements*, (Peninsula Publishing, California, 1988).

27. Underwater Sound Reference Division, Naval Undersea Warfare Center Division Newport, 1176 Howell St., Newport, R I. 02841-1708.

28. J. A. McConnell, "Calibration of a Neutrally Buoyant *p-**u*** Intensity Probe," *J. Acoust. Soc. Am.* **103**, 2755(A) (1998).

29. J. A. McConnell, "Design of a Compact Suspension System for a Neutrally Buoyant Underwater Acoustic Intensity Probe," *J. Acoust. Soc. Am.* **105**, 1143-1144 (A) (1999).

Acoustic Intensity Scattered from an Elliptic Cylinder

Gerald C. Lauchle
Kang Kim
The Pennsylvania State University
Graduate Program in Acoustics and
Applied Research Laboratory
P.O. Box 30
State College, Pennsylvania 16804

Acoustic Intensity Scattered from an Elliptic Cylinder

Gerald C. Lauchle and Kang Kim

*The Pennsylvania State University, Graduate Program in Acoustics and
Applied Research Laboratory, P.O. Box 30, State College, PA 16804*

Abstract. A computational study is described where a 2-D elliptic cylinder is insonified by a plane, monochromatic acoustic wave. The elliptic cross section of the cylinder has a fineness ratio of 5:1, the incidence angle of the plane wave is $60°$ relative to the major axis of the ellipse, and $ka =$ 20, where a is the major axis of the elliptic cross section and k is the acoustic wavenumber. The calculations are performed using the finite element method of solution for partial differential equations. The MATLAB® Partial Differential Equations Toolbox was used to formulate and solve the Helmholtz equation with reflection-free conditions imposed on the computational outer boundary, and rigid conditions imposed on the surface of the scatterer. Of particular practical interest in this study is the spatial distribution of the total active acoustic intensity, i.e., the sum of the incident and scattered intensity components. Active intensity amplitude, and the phase between pressure and particle velocity, are computed and compared to pressure amplitude only. The results show that there is significant phase distortion in the forward scattered direction that could be useful in localizing objects in active bistatic operations if p-$\boldsymbol{u}$ type acoustic intensity probes were employed.

PACS numbers: 43.20.Fn, 43.30.Yj

I. INTRODUCTION

Acoustic scattering from objects is an important area of underwater acoustics. In practical applications, sound is created by a source operating under either steady-state or transient conditions; it can be radiating discrete-frequency or broadband sound. The sound scattered by the object is received by sensors located at various positions around the object. When the receiver is co-located with the source, the scattering is known as *monostatic*. When the sound is received elsewhere, the situation is called *bistatic*. Pressure hydrophones are the standard sensor used in these applications. Acoustic intensity, on the other hand is the product of acoustic pressure and acoustic particle velocity. It is a vector quantity that describes the acoustic energy per unit area per unit time that is radiated from an acoustic source, or is scattered by an object insonified by that source. It is not a traditional measure in the underwater acoustics arena, primarily because there were no reliable means, until now, to measure it. Because state-of-the-art underwater acoustic intensity vector sensors can measure the real-time phase shifts between pressure and particle velocity, a whole new area of acoustic data interpretation is now available through use of these novel sensors.

The use of intensity measurement methodology in acoustic scattering systems is not well understood at this time. Because it is very difficult to distinguish between the direct field and the scattered field in bistatic operations where the target is in the direct line between receiver and source, there is a need for research to determine whether intensity sensors offer any solution to

this problem. The primary emphasis of the research described in this paper is to determine, theoretically, the advantages, or disadvantages, of using underwater acoustic intensity sensors in underwater scattering scenarios. The issue is whether the acoustic intensity, determined by a direct measurement of the particle velocity, the pressure, and the phase between them, provides additional new information on the scattering characteristics of an object over that obtained from conventional pressure or acoustic velocity hydrophones used alone.

II. APPROACH

As sketched in Fig. 1, a rigid, 2-D elliptic cylinder is the scattering object. The scattered pressure, particle velocity, and acoustic intensity are determined from numerical solutions of the Helmholtz equation. The MATLAB® Partial Differential Equations Toolbox, that utilizes the finite element method (FEM) of computation, is used for this exercise. We concentrate on the *total* acoustic intensity distributed throughout the field. This is the complex sum of the incident intensity from an arbitrarily located distant source and the intensity scattered from the surface. It would be representative of the intensity signal measured when the sound source is broadcasting a single-frequency wave under continuous, steady-state conditions.
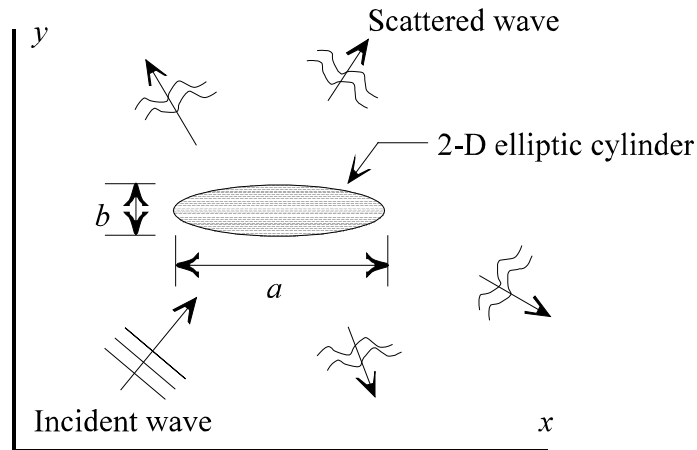
FIG. 1. Scattering of a plane wave by an elliptic cylinder.

We assume that a pressure-acoustic velocity (*p*-*u* type) intensity sensor[1] measures the field. These probes measure intensity *directly* and make no estimate of pressure or particle velocity using finite-difference solutions of either the continuity equation or the linearized Euler's equation, as is necessary in velocity-velocity[2,3] (*u*-*u*) and pressure-pressure[4] (*p*-*p*) probes, respectively. The phase between *p* (acoustic pressure) and *u* (acoustic particle velocity), or *p* and *a* (acoustic particle acceleration) is always available. These two quantities are measured at the same point in space; thus, we can determine the phase field at all locations around the scatterer.

The MATLAB® triangular mesh grid generator was used to create the scatterer and thousands of field points. We require at least 10 mesh points per acoustic wavelength. A 5:1 fineness ratio (*a/b* in Fig. 1) was selected for the elliptic cylinder. For acoustic radiation and scattering problems, the wave equation, which is hyperbolic, is solved. The incident wave is a plane wave propagating at angle θ to the major axis of the ellipse. The frequency parameter is

ka, where *k* is the acoustic wavenumber. The particle velocity is calculated using Euler's equation, which is then conjugated and multiplied by one-half the pressure to get intensity:

$$\mathbf{I} = \frac{1}{2} p \mathbf{u}^* \tag{1}$$

The real part of this expression is the *active* intensity, and the imaginary part is the *reactive* intensity. In the numerical calculations, we emphasize the magnitude of the active intensity and the phase between pressure and particle velocity.

The FEM modeling and coding were verified by comparing the numerical calculations with the theoretically exact calculations[5] of an infinitely-long, rigid cylinder insonified by a plane wave. The agreement between the two approaches was nearly perfect for *ka* = 3 and using 15 terms in the exact modal series solution.

III. RESULTS

Calculations of the active intensity and pressure due to the scattering of a plane wave by a rigid, 2-D elliptic cylinder are considered for several plane wave incidence angles and frequencies. Presented here are the results for *ka* = 20 and *θ* = 60°. Figure 2 shows the computed total pressure field. Periodic color changes represent pressure magnitude changes as the compression and rarefaction parts of the acoustic wave pass various points in space. The computational boundaries are large enough so that the patterns shown near them represent far-field patterns. The incident pressure field is described by the pattern in the vicinity of the arrow, which indicates the direction from the source. It is noted that the pattern in the forward-scattered farfield is very similar to that of the incident field. That similarity makes the detection of the elliptic cylinder in the forward-scattered direction difficult, if a pressure hydrophone is used for the sensor and if it is located in the farfield of the scatterer.

Turning our attention now to the computed intensity, Fig. 3 shows the magnitude of the active acoustic intensity field. The vectors show precisely how the acoustic energy interacts with the surface and diffracts around it to form a distorted intensity field nearly everywhere around the object. Of particular interest is how different the forward-scattered intensity field is from the incident field. This means that an intensity measurement performed in the forward-scattered direction may reveal features not identified by acoustic pressure measurements alone. Although forward-scattered highlights appear in the intensity field plots of Fig. 3, they are actually "lowlights" because the magnitudes are smaller than that of the incident intensity; i.e., the forward-scattered intensity reveals a strong shadow region.

The beam pattern expresses farfield magnitude in a polar format. The active intensity beam pattern shows little more information than the beam pattern for the total acoustic pressure, e.g., Fig. 4. Thus, simply measuring the *magnitude* of the active acoustic intensity in the farfield may not provide any advantage over measuring pressure (or particle velocity) alone. The important information is in *the phase* between the pressure and particle velocity.
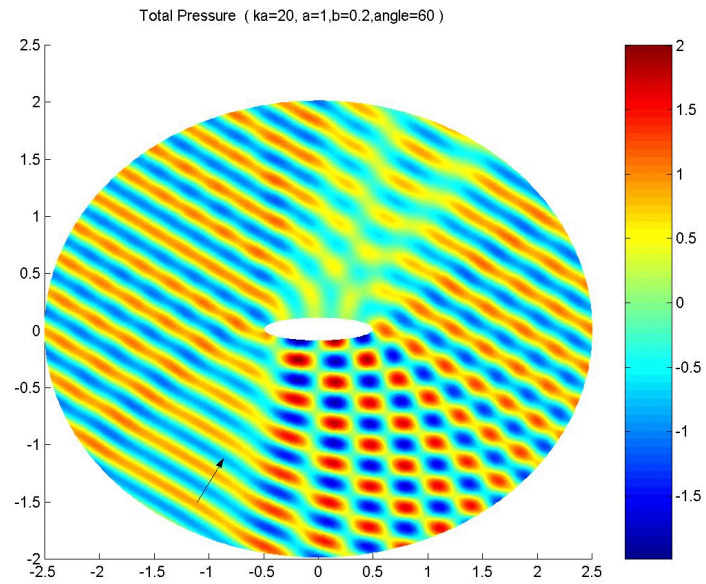
FIG. 2. Total acoustic pressure scattered by an elliptic cylinder. The source is situated in the lower left as indicated by the arrow at $\theta = 60°$.
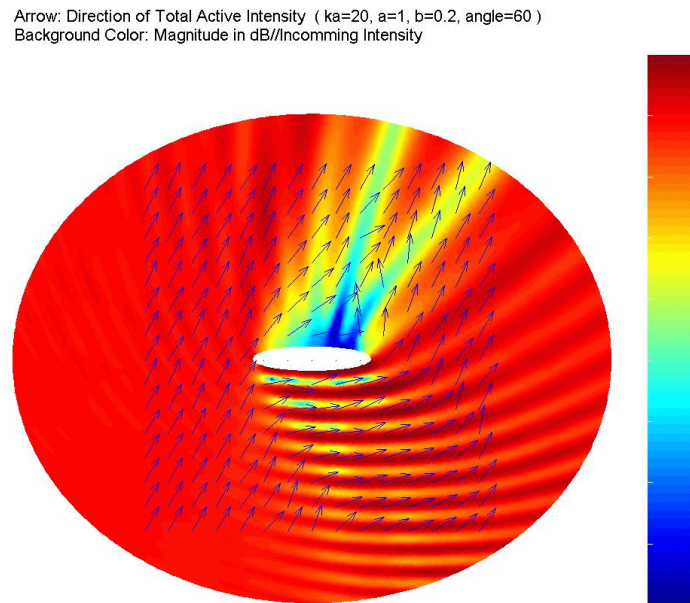
FIG. 3. Total active acoustic intensity scattered by an elliptic cylinder. The source is situated in the lower left as indicated by the origin of the vectors; $\theta = 60°$.

Beam Pattern of Total Pressure and Radial Active Intensity in dB
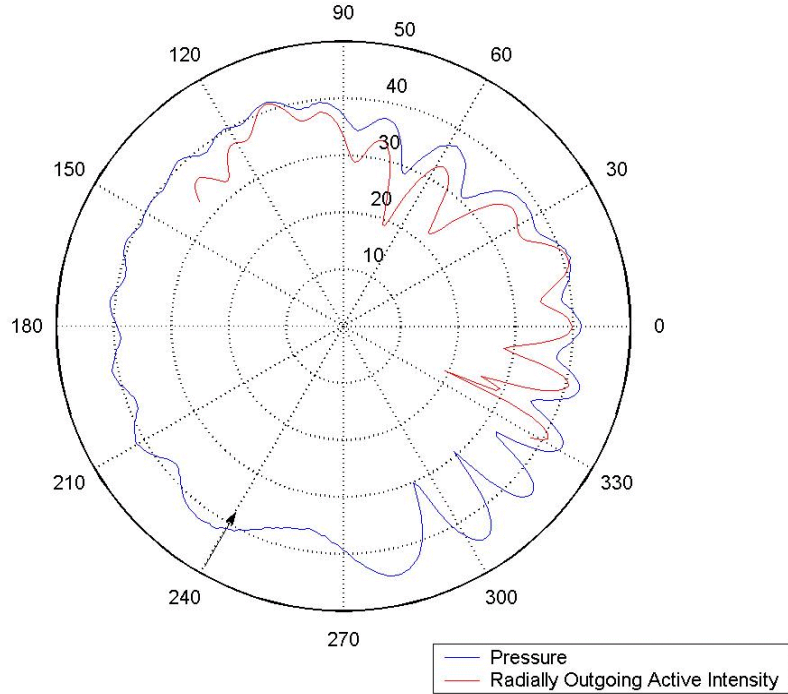
FIG. 4. Beam patterns for the magnitude of the active intensity in the forward scattered directions compared to that of the total pressure; $\theta = 60°$.

Figure 5 shows the phase (radians) between the *x*-component of the acoustic particle velocity and the pressure at all field points around the scatterer. The phase of the incident wave is simply *kr* which grows linearly with distance, *r*. The plot shows this linear growth as a sawtooth wave because the range of the phase is bounded between *(-π,π)*. A remarkable deviation from the sawtooth pattern is evident in the forward-scattered direction. This phase distortion should be easy to measure with a *p-u* or a *p-a* type underwater acoustic intensity probe. Calculations of the phase between the *y*-component of particle velocity and pressure show features and trends analogous to those of Fig. 5.

IV. CONCLUSIONS

Presented here are numerical calculations of the acoustic scattering of a plane wave by a rigid, 2-D elliptic cylinder. The particle velocity and pressure are computed and combined to form the active intensity. The interpretation of these results in terms of using intensity sensors in scattering systems is as follows. Under steady-state, pure tone source excitation in a reverberation-free environment, the total (incident + scattered) active intensity field contains valuable information in the phase between particle velocity and acoustic pressure. In the forward-scattered direction, this phase fluctuates rapidly with location suggesting that an object could be easily identified in this direction using a *p-u* type intensity probe.
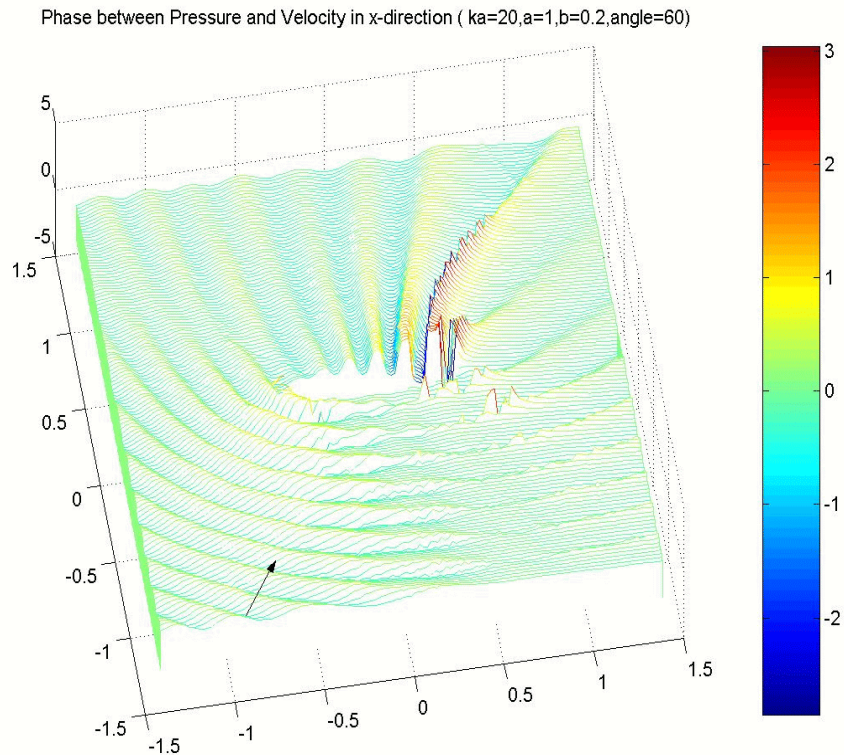
FIG. 5. Phase between the *x*-component of particle velocity and the acoustic pressure at collocated points in space during the scattering of a plane wave at 60° to an elliptic cylinder.

ACKNOWLEDGMENTS

REFERENCES

[1] T. B. Gabrielson, J. F. McEachern, and G. C. Lauchle, "Underwater acoustic intensity probe," U. S. Patent No. 5,392,258 (21 February 1995).
[2] J. A. McConnell, G. C. Lauchle, and T. B. Gabrielson, "Two-geophone underwater acoustic intensity probe," U.S. Patent No. 6,172,940 B1 (9 January 2001).
[3] K. J. Bastyr, G. C. Lauchle, and J. A. McConnell, "Development of a velocity gradient underwater acoustic intensity sensor," J. Acoust. Soc. Am. **106**, 3178-3188 (1999).
[4] K. W. Ng, "Acoustic intensity probe," U. S. Patent No. 4,982,375 (1 January 1991).
[5] E. Skudrzyk, *Foundations of Acoustics: Basic Mathematics and Basic Acoustics* (Springer-Verlag, New York and Wien, 1971).

DIFAR Systems Overview

(Presentation Synopsis)

Michael E. Higgins
RDA, Incorporated
Doylestown, Pennsylvania 18901

DIFAR System Overview
(Presentation Synopsis)

Michael E. Higgins
RDA, Incorporated
Doylestown, Pennsylvania 18901
Email: mehiggs@voicenet.com

Abstract. This brief, provided at the Directional Acoustic Sensors Workshop on 17,18 April 2001, is intended to give the attendees a description and an historical review of the Directional Frequency Analysis and Recording (DIFAR) Acoustic Subsystem, which is either currently or previously used by several Navy air antisubmarine warfare (ASW) platforms.

I. INTRODUCTION

The focus of the brief is on the directional acoustic sensors employed and how their data are handled: from its hydrophone's inputs, through the AN/SSQ-53 DIFAR sonobuoy, the radio frequency (RF) data transmission link to the monitoring aircraft, and the aircraft's DIFAR Acoustic Signal Processing and Recording Subsystems. Due to the classified nature regarding many of the details related to the DIFAR Acoustic Signal Processing Subsystems, and the requirement that the material presented at this workshop be unclassified, the description of the DIFAR subsystem provided in this brief given at the workshop, and herein, is both cursory and nonspecific in nature.

II. SUMMARY

DIFAR acoustic sensors have been in operational use by the Navy in its airborne antisubmarine warfare (ASW) platforms since 1969. They were first introduced to, and used by, the Navy's P3C Orion Aircraft. DIFAR capability has also been integrated into other air ASW platforms, such as the S2G, S3A, and S313 fixed-wing aircraft, and by the SH-60B (LAMPS), SH-60F (CV Helo), and the SH-60R (ALFS) rotary wing aircraft. The Navy's DIFAR-capable air ASW platforms, which will be in operational use for the near future, are the P3C and the SH-60R. The SH-60R helicopter is the replacement for both the SH-60B and SH-60F platforms. The SH-60R incorporates the capabilities of both the SH-60B and the SH-60F platforms, and also incorporates upgrades to the acoustic subsystems of both the SH-60B and the SH-60F.

Other DIFAR-like acoustic sensors currently in use by the Navy's air ASW platforms include the passive Vertical Line Array DIFAR (VLAD) (AN/SSQ-77), and the active/ passive DIrectional Command Activated Sonobuoy System (DICASS) (AN/SSQ-62) sonobuoy. The VLAD sensor employs a vertical line array of omnidirectional hydrophones

to form a steered beam in the vertical direction for use as the omni channel component of a composite DIFAR acoustic signal. The DICASS sensor is an active/passive DIFAR-like sonobuoy, which is used by air ASW platforms for the precise target localization and attack phases of the ASW problem.

The types of directional (i.e., pressure gradient (PG)) hydrophones used in DIFAR/ DICASS sonobuoys are listed and discussed. They include

Type 1: Ceramic vane,
Type 2: Moving coil,
Type 3: Closely spaced pairs of omnidirectional hydrophones (OHs) (which measure the integrated pressure over their surface),
Type 4: Segmented ceramic cylinder, and
Type 5: Ceramic cylinder (multimode).

Types 1 and 2 have been predominately used for passive sensor (i.e., DIFAR/VLAD) application; use of types 4 and 5 has predominated for the DICASS application. The rationale for PGH-type selection vs. sensor application and the effects of flow noise upon sensor performance are also discussed in the presentation.

The presence of fluid flow in the immediate vicinity of a PGH sensor causes local particle motion, thus acting as a nearfield source of additional acoustic noise. This effect is especially true at low frequencies, thus reducing the signal-to-noise ratio of acoustic signals arriving from distant (i.e., farfield) sources at these frequencies. When this effect is observed, the acoustic sensor is said to be "flow-noise limited" at these frequencies. As the local relative fluid flow velocity increases, the frequency below which the acoustic sensor becomes "flow-noise limited" also increases. The effect of this flow-induced noise also reduces the effective dynamic range of the sensor with respect to acoustic signals arriving from farfield sources at all frequencies. As the flow velocity is increased still further, the sensor's effective dynamic range is also further reduced, until, finally, the sensor's output becomes saturated/nonlinear, and, in effect, unusable. For these reasons, flow-noise reduction components, such as compliant hydrophone suspension systems to reduce vertical acoustic sensor motion, plus "flow socks/screens" to reduce the effects of local turbulence, are incorporated into DIFAR sonobuoy designs.

The methods employed in the DIFAR composite signal multiplexing process performed within the sonobuoy and the DIFAR composite signal demultiplexing process performed within the monitoring aircraft's acoustic signal processor are outlined and described in moderate detail within the briefing provided at the Workshop. A brief discussion of one of the methods used to compute the magnetic bearing associated with detected signals is also provided.

DIFAR System Overview

Ceramic Elements (4)

Central Mass

d_y

a

y

0

w/2

TOP SECTION VIEW

FRONT VIEW

h

Ceramic Vane Directional Hydrophone Layout

Note : Addition of an Omni Hydrophone (e.g. Ceramic Disk) to
the Central Mass unit is an example of a DIFAR Hydrophone
array used in some versions of the AN/SSQ-53 Sonobuoy

DIFAR System Overview

NEOPRENE SEPARATORS

RECEIVING ELEMENTS (DIRECTIONAL)

SONAR TRANSMITTER & OMNI CHANNEL RECEIVER

TRANSMITTING / RECEIVING ELEMENTS (OMNI)

X CHANNEL RECEIVER

Y CHANNEL RECEIVER

ELECTRODE CONFIGURATION DIRECTIONAL ELEMENT

X

Y

Example of Ceramic Cylinders (Multimode) used as Omni Hydrophones and Segmented Ceramic Cylinders used as Pressure Gradient Hydrophones in an Active / Passive array similar to that Employed by the DICASS (AN/SSQ-62) Sonobuoy

Vector Sensor Modeling and Support Bracket Design

Richard F. Keltie,
Joseph Gregory and Mark Hayes
Department of Mechanical and Aerospace Engineering
North Carolina State University
Raleigh, North Carolina 27695

Vector Sensor Modeling and Support Bracket Design

Richard F. Keltie, Professor
Joseph Gregory and Mark Hayes, Graduate Research Assistants
Department of Mechanical and Aerospace Engineering
North Carolina State University
Raleigh, North Carolina 27695

Abstract. Analytical models of a polyurethane-encapsulated accelerometer-based velocity sensor, along with its mounting bracket, are developed to determine the interaction between the various components of the sensor assembly. These models are used to understand the function of the polyurethane encapsulant and the relative effects of accelerometer buoyancy, and to optimize the design of the sensor-mounting bracket. The two primary functions of the brackets are to isolate the sensor from ship structural vibration and to provide sufficient compliance for the sensor to respond to an acoustic wave. Based on these criteria, the designs of the sensor elements and the mounting brackets are optimized. Attempts are made to correlate the model predictions with the results of recent sensor tests.

I. INTRODUCTION

The work reported in this paper deals with two topics within the conformal hull array backfit program: sensor design and operation, and a re-design of the sensor mounting brackets. It was identified early in the program that the anticipated use of velocity sensors in place of hydrophones would impose new constraints on the sensor mounting brackets. Support bracket vibration was not a significant noise source when the sensor was a pressure hydrophone, owing to the typically low acceleration sensitivities of hydrophones. The situation changes dramatically in the case of a velocity sensor, and the mount must provide significant isolation from ship structural vibration. The determination of the required amount of isolation is discussed below.

The sensor considered in this study is being designed and fabricated by EDO Corporation. Although several implementations of the sensor are being considered, most consist of a CAVES-type accelerometer encapsulated in syntactic foam to achieve neutral buoyancy. This neutrally buoyant sensor is a single-axis sensor, and three must be integrated into a single package in order to achieve a triaxial sensor. This has been accomplished by casting the sensors together using polyurethane. Part of the work reported here addressed the importance and impact of several design features of the triaxial sensor package.

II. SENSOR MODEL

In order to examine the fundamental interactions between the sensor components, a simple spherically symmetric sensor model was developed. A plane wave in the

surrounding water is incident upon the sensor package. The details of the model development are contained in a paper that is currently under review [1]. This model is an extension to the earlier work done by Leslie et al., who considered a rigid, yet neutrally buoyant, package [2].

The results of this analysis showed that at low frequencies, the entire polyurethane assembly can move essentially as a rigid body with the particle velocity of the incident wave. In this case, the sensor obviously moves with the particle velocity as well. As the frequency increases, internal dynamics involving deformation of the polyurethane are observed. For a freely suspended sensor, the first internal resonance corresponds to a nodal point at the center of the sphere – this implies a zero velocity response for the accelerometer. Alternatively, at a fixed frequency, there is a critical polyurethane coating thickness above which the internal sensor dynamics appear. This fact may be seen from Fig. 1, which shows the magnitude and phase of the ratio of sensor velocity to particle velocity as a function of frequency for the case of a relatively thick coating. Based on these results, it was deduced that the excitation of internal dynamics should be avoided in the sensor design. This conclusion indicates the need for relatively thin polyurethane coatings.
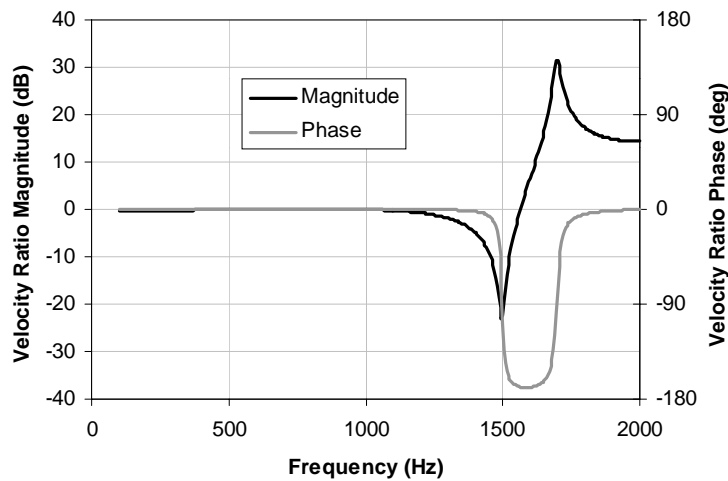
FIG. 1. Velocity ratio magnitude and phase vs. frequency for 1.0-inch diameter sensor and 1.25-inch coating.

Although in the ideal case the foam-encapsulated accelerometer is neutrally buoyant, packaging constraints sometimes make this impossible. The model was used to examine the effects of negative buoyancy. It was found that doubling of the sensor weight results in an approximate 2-dB reduction in the velocity response. The variations in the phase response were generally quite small, within a few degrees.

If the internal dynamics of the assembly are negligible, and the assembly moves essentially as a rigid body, then the effects of a sensor mount on the sensor performance may be easily examined. In fact, this is a well-known problem, treated by Leslie and others. If the suspension is imagined to be spring-damper combination, then the sensor

velocity response may be calculated as a function of the ratio between the signal frequency *f* and the *in-vacuo* natural frequency of the sensor-spring system, f_s. These results are shown in Fig. 2 for three different values of the damping ratio. It is clear that accurate measurement of the particle velocity requires a compliant sensor mounting system. The lowest signal frequency of interest should be at least three times greater than the *in-vacuo* mounted sensor natural frequency. This fact imposes a constraint on the sensor mounting brackets, since the brackets must be sufficiently compliant to allow the sensor package to move with the particle velocity. As shown in the following section, there are other constraints driving the mount design as well.
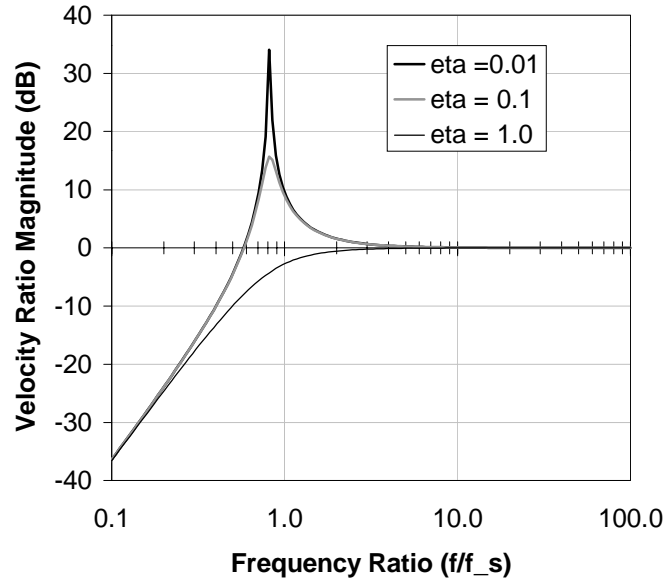
**FIG. 2. Velocity ratio magnitude vs. frequency ratio for
three values of suspension damping.**

III. SUPPORT BRACKET DESIGN

As mentioned earlier, the sensor support bracket must also provide isolation for the sensor from ship-borne vibrations. In order to address this issue, it was first necessary to determine how the necessary amount of isolation should be defined. It was decided that the sensor output due to ambient background noise in the water should be no smaller than the sensor output due to transmitted ship structural vibrations. This defines a situation that may be described as 'ambient noise limited', although this is a bit of a misnomer since there are other noise sources that are omitted from the analysis. In order to implement this analysis, it is necessary to define both the background noise levels and the levels of ship structural vibration.

Ambient ocean noise levels may be obtained from standard sources based on sea state and shipping density. For purposes of demonstrating the analysis technique, conditions corresponding to sea state 2 and shipping density 4 are assumed. Quantifying ship vibration levels at the sensor mount locations are more difficult. The existing

hydrophones are attached to a truss system that wraps around the bow of the submarine. This truss is of variable geometry depending on location, and is structurally tied to supports such as bulkheads and frames. There is limited experimental data available that measures the vibration levels at these hydrophone-mounting locations. Recent tests were performed to make some representative measurements at several ship speeds. These can be used to implement the analysis described.

The analysis proceeds as follows. The ambient noise in the ocean induces a certain output level from the sensor. This assumes that the sensor suspension provides sufficient compliance, as discussed above. Then, for a given level of ship structural vibration, one can calculate the required amount of isolation the sensor mount must provide. Alternatively, one may calculate the sensor mount stiffness or compliance necessary to achieve this ambient-noise limited condition. This calculation is then performed over the operating band of the sensor, nominally 100 – 2000 Hz. Thus, for a given sensor mass, one may calculate the largest mounting stiffness that can be tolerated.

This value of stiffness may be compared with the value necessary to satisfy the sensor operation constraints described in the preceding section. Finally, these values of stiffness may be compared against each other to develop an engineering design tool. Typical results from this analysis are shown in Fig. 3 for the case of low ship speed, and in Fig. 4 for high speed. In these figures, the solid dark line indicates the boundary between self-noise limited conditions (mounting stiffness values above the solid line) and ambient-noise limited conditions (mounting stiffness values below the dark line). Similarly, the dashed line shows the maximum allowable mounting stiffness that will allow for accurate velocity sensor performance based on the results shown in Fig. 2.
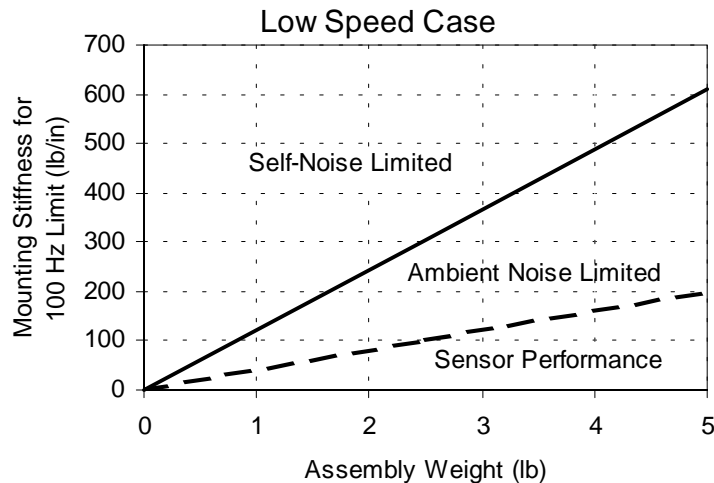
FIG. 3. Sensor mount stiffness requirement for low ship speed.
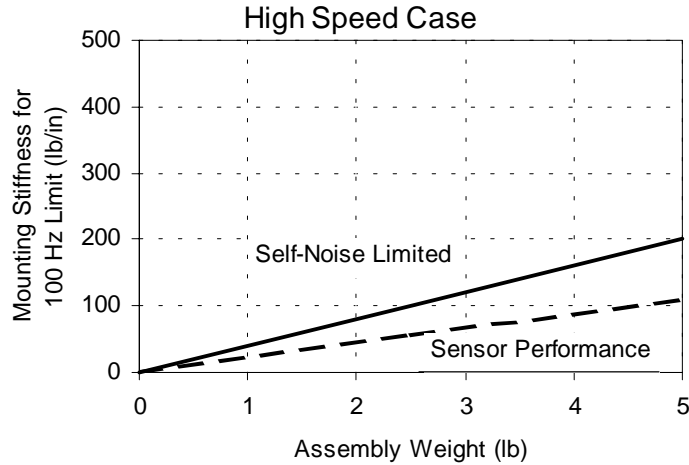
FIG. 4. Sensor mount stiffness requirement for high ship speed.

As a point of reference, the existing mounting brackets that hold the DT-276 pressure hydrophones in the conformal array have a mounting stiffness of approximately 800 lb/in. It is clear from these results that, for these two cases, the mounting stiffness is constrained by the requirement for proper sensor performance, i.e., a low mounted natural frequency. If this constraint is met, then the conditions for ambient-noise limited operation will also be met.

Using the low-speed results shown in Fig. 3, and assuming a nominal sensor assembly weight of 2.5 lb, a recommended mounting stiffness of 100 lb/in. may be deduced. To demonstrate that this stiffness may be readily achieved, a parametric redesign of the current hydrophone-mounting bracket was undertaken. Finite element models of the existing bracket were generated and validated to assure their accuracy. The critical dimensions were then systematically varied to produce a design that provided the necessary compliance. Pictures of the original mount (on the left) and the redesigned mount (on the right) are shown in Fig. 5.

**FIG. 5. Comparisons of the original and the redesigned
sensor mounting brackets.**

IV. SUMMARY

An analytical model of a neutrally buoyant, polyurethane-encapsulated velocity sensor was developed and analyzed to understand the interrelationships between the system components. Based on the results obtained from this model, it was evident that desirable velocity sensor characteristics could be achieved if the entire sensor unit was free to move essentially as a rigid body. This requirement allowed constraints on the maximum sensor mounting stiffness to be generated. In addition, another constraint on the sensor mounting stiffness was generated based on the desire to have the mount supply sufficient vibration isolation so that the sensor was ambient-noise limited rather than self-noise limited. These mounting stiffness constraints were combined to form an engineering design result that showed the mounting stiffness necessary for any given weight of the sensor assembly. Preliminary estimates using feasible sensor assemble weights identified a sensor mounting bracket stiffness of 100 lb/in. A mounting bracket redesign showed how the existing hydrophone mounting bracket (800 lb/in. stiffness) could be readily modified to provide the necessary value of stiffness.

V. REFERENCES

1. R. F. Keltie and J. W. Gregory, "Analysis of an elastically coated acoustic velocity sensor," submitted to the *J. Acoust. Soc. of Am*.

2. J. K. Kendall, C. B. Leslie, and J. L. Jones, "Hydrophones for measuring particle velocity," *J. Acoust. Soc. of Am*. **28**, 711-715, 1956.

Acoustic Pressure Gradient Sensors: Piezoelectric Motion and Fixed Types

David A. Brown*
Boris Aronov*
Larry Reinhart
Tetsuro Oishi
Acoustics Research Laboratory
University of Massachusetts Dartmouth
North Dartmouth, Massachusetts 02747

*Also: BTECH Acoustics, 1445 Wampanoag Terrace, Suite 115, East Providence, Rhode Island 02915.

ACOUSTIC PRESSURE GRADIENT SENSORS: PIEZOELECTRIC MOTION AND FIXED TYPES

David A. Brown*, Boris Aronov*, Larry Reinhart and Tetsuro Oishi
Acoustics Research Laboratory, Univ. of Massachusetts Dartmouth, N.Dartmouth, MA 02747
and *BTECH Acoustics, 1445 Wampanoag Tr., Suite 115, East Providence, RI 02915

ABSTRACT

We summarize our recent analysis and developments on acoustic pressure gradient sensors of both the motion and fixed types. Acoustical motion types generally refer to sensors whose outputs are proportional to acoustically induced motion such as acceleration (accelerometers), velocity (velocimeters) or displacement (seismometers). We also report on pressure gradient sensors that are fixed in space. One standard fixed type may be realized by using pairs of pressure sensors (hydrophones) separated in space and operating in a differential mode to determine a direct pressure gradient, $\Delta p/\Delta z$. The second, less common approach, is based on using single sensors fixed in space that respond to the pressure differences produced by the diffraction path length introduced by the sensor. We have fabricated a number of these devices including: a) the Symmtree™, a compact acoustical motion accelerometer utilizing piezoelectric plates in a bimorph cantilever tree-like fashion, b) the Aronov-Cube™, a cubical device using flexural bimorphs, c) fixed pressure gradient sensors of the differential type and d) single element diffraction type transducers.   The two acoustic (motion) accelerometers are each packaged in cylindrical near neutrally buoyant aluminum housings having attached omnidirectional hydrophones so that cardiod beam patterns may be formed. The four separate channels (3-accelerometers, 1-hydrophone) have the same co-located acoustical centers.

I. INTRODUCTION

Much attention has been directed in recent years to pressure gradient directional sensors of the first order that have a figure-of-eight (dipole) directivity pattern. For some reason, the majority of the development has been focused on one type of pressure gradient sensor, namely the acoustical motion sensor (so-called particle velocity sensor), as if they possessed significant advantages over other pressure gradient types. In designing the pressure-gradient sensor for particular applications, there exists common and unique problems that can arise and be solved in somewhat different ways for different sensor types. Therefore, we first make a brief review of the pressure-gradient transducer types.

II. IDEAL SENSORS

An analysis of sound fields requires sensors that measure both the sound pressure p (a scalar quantity) and the acoustical field motion which is most often characterized by the acoustic "particle" velocity $\bar{u}$ (a vector quantity). However, the acoustical motion of the fluid is the result of the action of a gradient in the sound pressure field as is well known and described by the linear force equation $\nabla P = -r_0 \frac{\partial \bar{u}}{\partial t}$. Therefore, it is equivalent to measure the sound pressure and sound pressure gradient. These ideal sensors are often characterized by their directivity patterns or receive sensitivity as a function of angle, which we may characterize as a sinusoidal

1

function of order n, $H(\phi) = \cos^n(\phi)$, where ϕ can represent an azimuthal angular dependence. For this reason a pressure sensor (hydrophone) is called a "zero (n = 0) order" sensor, an "omnidirectional" sensor, or equivalently a "monopole" sensor. Likewise, an ideal motion or pressure gradient sensor having maximum sensitivity in a designed direction and zero sensitivity in the perpendicular direction, $H(\phi) = \cos(\phi)$, is known as a first (n = 1) order sensor, "figure-of-eight" directional sensors, or equivalently "dipole" sensors.

Ideal Acoustic Pressure Sensor (Zero order): An ideal acoustic pressure sensor, or zero (0) order sensor, must be sufficiently smaller than acoustical wavelength such that $pd/l \ll 1$ where d is the maximum dimension of the sensor. If the sensor is not small, diffraction effects will alter the ideal response. An ideal pressure sensor has an omnidirectional beam pattern response and an electrical output that is proportional to the sound pressure only. The sensor must be fixed in the sound field or made insensitive to motion. An illustration of an ideal sensor is provided in Figure 1a.

Ideal Pressure Gradient Acoustic Motion Sensor PG-AMS (First order): An ideal acoustic motion sensor can be imagined as a small body, completely free to move in a sound field due to the action of a force arising from the gradient of the sound pressure field whereby the small body has an internal means to detect this motion such as having a small accelerometer or velocimeter inside. An ideal Acoustic Motion Sensor has a first order (figure-of-eight) directivity pattern, is only sensitive to motion in a designed direction and insensitive to motion in a perpendicular direction, and has an electrical output that is proportional to the sound pressure gradient or acoustical acceleration (velocity, or displacement). The ideal device must be insensitive to the actions of sound pressure and the possible deformation of the body arising from this action.

Ideal Pressure Gradient-Fixed Differential Sensor PG-FIX (First order): An ideal pressure gradient sensor of the fixed type can be imagined as a pair of small ($pd/l \ll 1$) ideal and identical acoustic pressure (zero order) sensors separated by a distance d also small compared to the acoustic wavelength and electrically connected in opposite as illustrated in Figure 1b. The electrical output is proportional to the pressure gradient only and the directivity pattern is of first order, $H(\phi) = \cos^1 \phi$.

Ideal Pressure Gradient – Single Element Diffraction Type Sensor PG-FIX (First order): An ideal single element diffraction type sensor consists of a single element whose boundary is fixed in the sound field but has a transduction element that responds due to the diffraction induced pressure gradient. The electrical output is proportional to the pressure gradient only and the directivity pattern is of first order.

We note that for all of these sensors, since small is defined relative to the acoustical wavelength and real bodies introduce diffraction effects that may be wavelength dependent, there is a limited frequency range where one can expect a near-ideal response. Also, that for ideal first (1) order sensors of the motion or fixed types the ideal figure-of-eight response can only be truly obtained under the assumption that the sensitivity is infinitely large because the sensitivity "off-axis" approaches zero. We will note here for future use that the linear force equation does predict that the acoustical particle acceleration of a wave, $j\omega\mathbf{u}$, is also proportional to the pressure gradient $(\nabla P = -r\,jwu)$.

Single Element
ka<<1 (small)
Output Voltage ?   Pressure only
(Device is Fixed)

$$V_P = \boldsymbol{g}_P \cdot P$$

Ideal
Monopole

V_P

$H(\phi) = \text{"1"} = \cos^0(\phi)$

d

Dual Fixed Elements
ka<<1; and kd<1

Voltage ?   Gradient in
Pressure only

$$V = \boldsymbol{g}_P (P_2 - P_1) \cong d \cdot \boldsymbol{g}_P \, \mathbf{grad} \mathbf{P}$$

Ideal
Dipole

V_{gradP}

$H(\phi) = \cos^1(\phi)$
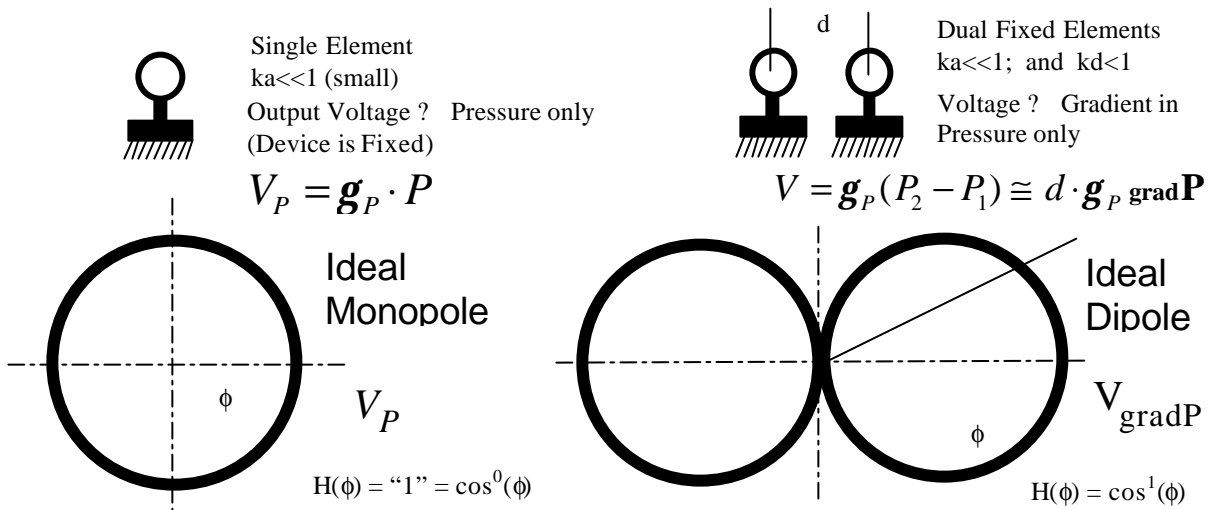
Figure 1a. Illustration of an ideal monopole (0 order) sensor and characteristic beam pattern.
b. Illustration of an ideal dipole (1 order) sensor and characteristic beam pattern.

**OMNI Hydrophone w/
influence by pressure**

**PG-AMS w/ Sensitivity to
Pressure**

**PG-AMS Sensitivity to
omni and phase**

**Low sensitivity,
Influence of Noise**

**PG-AMS Sensitivity to
perpendicular axis**

**PG-AMS Sensitivity to
perpendicular to axis**
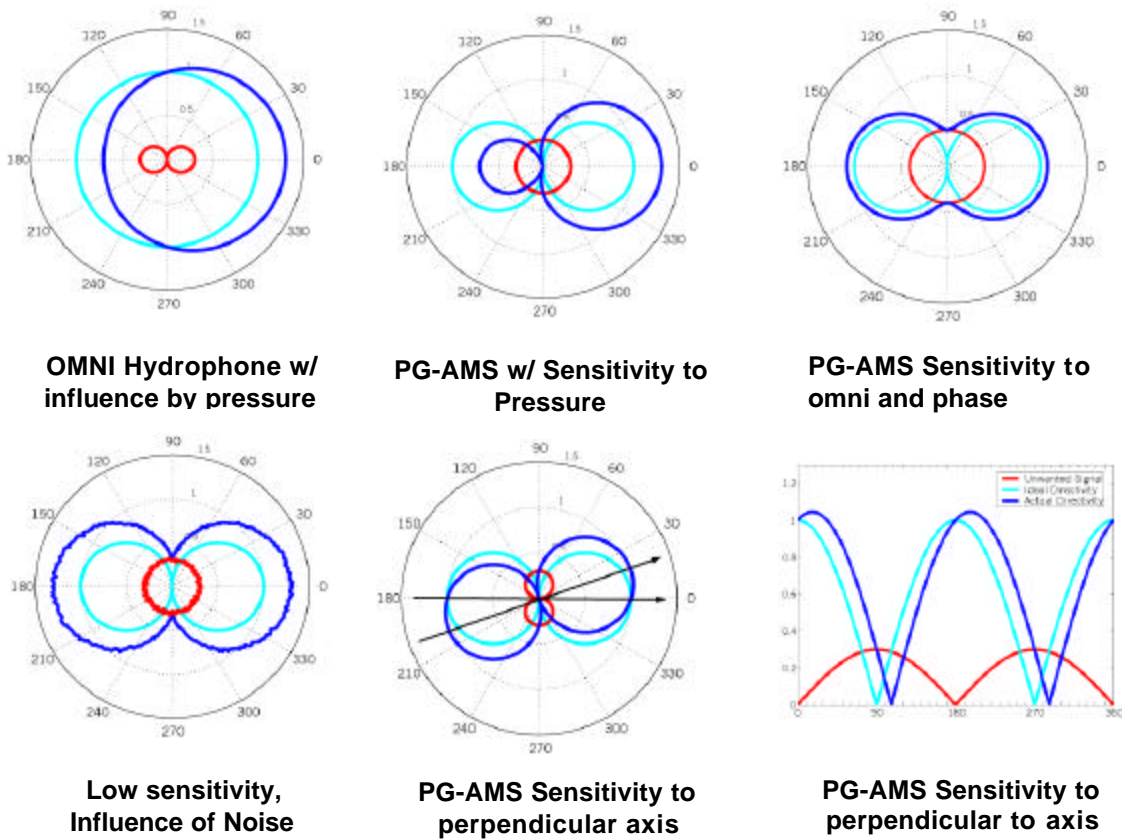
Figure 2. Illustrations of effective unwanted actions.

III. REAL SENSORS, UNWANTED ACTIONS, AND THE SYSTHESIS OF CARDIODS

Real acoustical sensors are never quite "ideal". As there can be no "point" sensors and sensitivity is proportional to the size of the element even ideal omnidirectional sensors are hard to realize. Also, it is not possible to truly "fix" a sensor in space without adding structures of significant size that will alter the sound field. In helping to understand these limits it is useful to establish the response to ideal actions and to unwanted actions. Some of the effects of unwanted noise are illustrated in Figure 2.

Combined outputs: The interest in dipole sensors comes largely from the fact, that the combination of the output of an ideal dipole (pressure gradient) sensor with the output from an ideal omnidirectional (pressure) sensors and can offer a compact means for determining the direction of an acoustical wave. Such a combination of equal weighted outputs produces a 0+1 or cardiod response (valid for one axis). This beam pattern is illustrated in Figure 3a, b for the case when the outputs of ideal sensors of equal weight are combined and in case c) when there is a mismatch in amplitude.

$$H(\phi) = 1 + \cos^1(\phi)$$
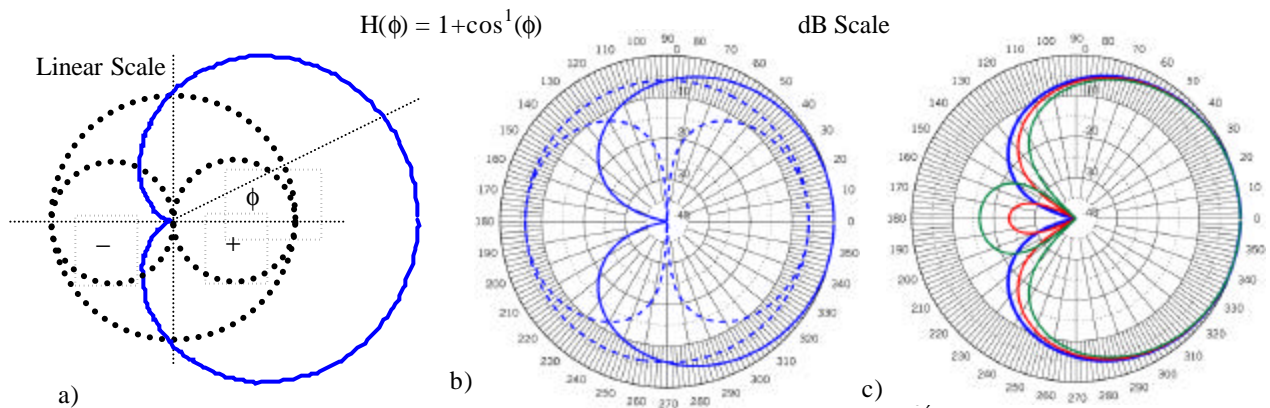
Figure 3. Illustration of an ideal cardiod beam pattern response derived from an ideal monopole (0 order) sensor and dipole (1 order) sensor on a) linear scale and b) dB Scale. It is seen that the deepness of Cardiod null is arrived at by the matching of the 0 mode and 1 mode response, and it has little to do with the deepness of the dipole null. In c) we have an ideal cardiod plotted (blue) and the case of a mismatch in amplitude matching of the omni and dipole of 1dB (red) and 2dB(Green). The plots are all re-normalized for comparisons.

IV. COMPARISON OF PRESSURE GRADIENT ACOUSTIC MOTION SENSORS (PG-AMS) WITH THE PRESSURE GRADIENT FIXED SENSORS (PG-FIX) OF THE DIFFRACTION TYPE

Introduction: Pressure gradient (PG) sensors fixed in space may be a preferred alternative to the use of acoustic motion sensors for certain acoustic low-frequency applications. In both types, the sensors are pressure gradient sensors, and the output approaches zero (or the noise floor) at low frequencies. It is well known that a pair of sensors fixed in space may be used to measure the pressure gradien,t but what is less known is that a single sensor, fixed in space, may be used as a pressure gradient device by exploiting the diffraction caused by the sensor element and its support. In certain applications this may be more desirable than using pressure gradient - acoustic motion sensors (PG-AMS) (whether accelerometers, velocimeters, or seismometers) as these devices need a "free" or soft suspension. In contrast, a pressure gradient sensor can be "fixed" (PG-FIX) rigidly to a frame or structure. We will show that motion and fixed sensors of the same size will have nearly the same sensitivity. There is no intrinsic advantage in using motion sensors over pressure gradient sensors to offset this reality. Therefore, we suggest our preference for the fixed type sensors for the applications of Low Frequency Bow Arrays (LFBA) and Integrated Bow Conformal Arrays (IBCA) as the sensors can be fixed to the structure. An analysis follows.

Consider two identical circular piezoelectric (bimorph) disks. One is configured in a near neutrally buoyant case and used below resonance (accelerometer); the second sensor will employ the same disk supported at its periphery but fixed in space and used below resonance. These two cases are shown in the Figure 1. Under action due to the acceleration of the case, the distributed uniform mechanical force is

$$f = \boldsymbol{r} t \cdot \dot{u} \tag{1}$$

The sound pressure action P may be assumed to act uniformly over the face. Therefore, we can write the specific acoustic accelerometer sensitivity $\boldsymbol{g}_{\dot{u}}$ in terms of the pressure sensitivity $\boldsymbol{g}_P$ as

$$\boldsymbol{g}_{\dot{u}} = \boldsymbol{r} t \cdot \boldsymbol{g}_P \tag{2}$$
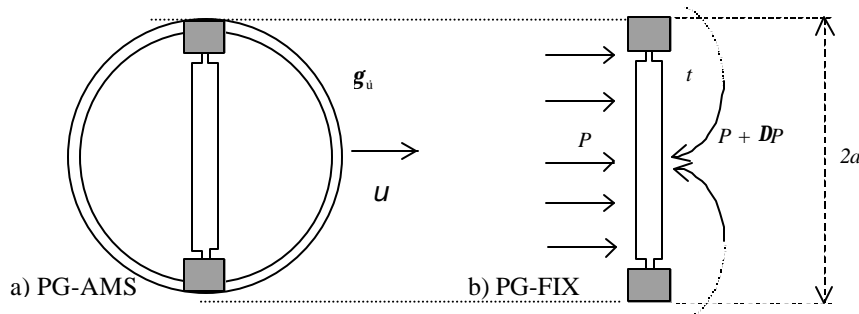
Figure 4. Illustration of the same supported disk used as a pressure gradient device in
a) a PG Acoustic Motion Sensor (PG-AMS) mounted in a moveable case and
b) a PG sensor of the Fixed (PG-FIX) and diffraction type.

We will assume the sphere vibrates in a plane wave sound field with velocity u according to
$$u = P/\rho c. \tag{3}$$
In the first case of the pressure gradient acoustic motion sensor *(PG-AMS)* (denoted A), we have the voltage output and sensitivity of in terms of pressure

$$\left|V_{output}\right| = \boldsymbol{g}_{\mathrm{\dot{u}}} \ \frac{\boldsymbol{w}}{rc} \cdot P \ ; \qquad\qquad \boldsymbol{g}_P^A = \boldsymbol{g}_{\mathrm{\dot{u}}} \cdot \frac{\boldsymbol{w}}{r_w c} \tag{4}$$

In the second case of the pressure gradient fixed (PG-FIX) diffraction type (denoted B), we have the voltage output and sensitivity in terms of pressure as

$$V_{output} = \boldsymbol{g}_P \cdot 2\frac{4}{3\boldsymbol{p}} \cdot ka \cdot P \tag{5}$$

$$\boldsymbol{g}_P^B = \boldsymbol{g}_P \cdot \frac{8}{3\boldsymbol{p}} ka \cdot \boldsymbol{p} a^2 \cdot 0.45 \ , \tag{6}$$

where $(8/3\pi)$ ka is the classical diffraction coefficient responsible for the differential path length. Thus, comparing the pressure sensitivity of the two cases we have

$$\frac{\boldsymbol{g}_P^A}{\boldsymbol{g}_P^B} = \frac{\boldsymbol{g}_w}{\boldsymbol{g}_P} \cdot \frac{\boldsymbol{w}}{r_o c} \cdot \frac{3\boldsymbol{p}}{8} = \frac{r_c t}{r_o c} \cdot \frac{\boldsymbol{w} \cdot 3\boldsymbol{p} c}{8\boldsymbol{w} a} = \frac{r_c}{r_o} \cdot \frac{t}{a} \cdot \frac{3\boldsymbol{p}}{8} \approx 1.2 \cdot \frac{r_c}{r_o} \cdot \frac{t}{a} \approx 9\frac{t}{a} \tag{7}$$

where the ratio of the density of the piezoelectric ceramic to water is approximately $r_c/r_o \approx 7.7$.

Thus, we conclude that a PG-FIX diffraction type device having relative dimensions of radius of the outer support fixture (a) to the thickness of the disk (t) on the order of 10, will have a sensitivity that is equal to the sensitivity of the acoustic motion sensor PG-AMS type. This may be expressed (for frequencies below resonance) as follows:

$$\boldsymbol{g}_P^A = \boldsymbol{g}_P^B \cdot \frac{gt}{a} \ ; \quad \text{if } \frac{a}{t} = 10, \quad \text{then } \boldsymbol{g}_P^A = \boldsymbol{g}_P^B \ . \tag{8}$$

If a PG-FIX sensor can produce comparable sensitivities as PG-AMS, the practical matters of vibration isolation and mounting may be quite advantageous. Of course if *a/t* is made larger than 10, additional advantage is achieved. Also, for the PG-AMS the case has to made to withstand hydrostatic pressure, while there is no such requirement for the PG-FIX single element diffraction type sensor.

V. REAL EXAMPLES: PRACTICAL DEVICES

Aronov has developed and prototyped a number of practical multiaxis pressure gradient sensors some of which are highlighted here and/or in the accompanying presentation. A detailed summary is beyond the scope of this summary paper. Generally, for low frequency applications, and for this context, we will define as those frequencies below 10 kHz, it is desirable to use transduction elements that are flexural devices most commonly of the piezoelectric bimorph approach. These are illustrated in the figure below.
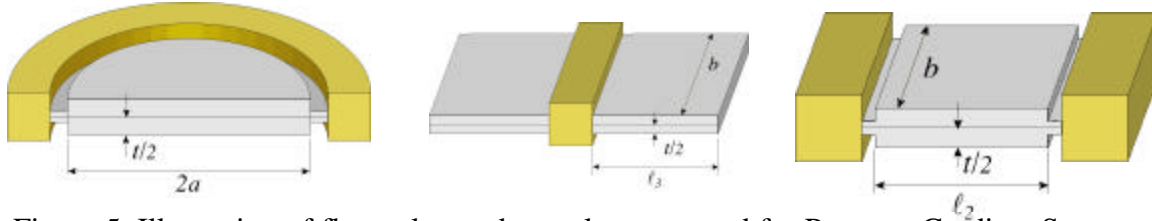
Figure 5. Illustration of flexural transducer elements used for Pressure Gradient Sensors of both motion and fixed types.

COMPACT SYMMTREE™ CANTILEVER PG-AMS:

Aronov has developed a cantilever based multiaxis PG-AMS that employs symmetrically mounted transduction elements on a common tree-like base hence the name Symmtree™. Two proof-of-concept devices have been fabricated using conventional transduction materials (PZT-4) and patents are pending. The devices also have integrated hydrophones in the form of flexural disks and the attributes that all four channels (3 accelerometers and 1 hydrophone) have the same acoustical center. The device, packaged in a neutrally buoyant housing, is compact having approximate dimensions of height 2.9 in (7.5 cm) and diameter 2.375 (5.8cm). With PZT-4 plates device BT-Sym1 has a sensitivity of $\gamma = 80$ mV/g, capacitance 1.8 nF , and resonance frequency of 5.5 kHz. A photo of a Symmtree™ accelerometer is illustrated in the figure below.

Figure 6. Photos of a BTECH Symmtree™ PG-AMS. Patents pending.

ARONOV CUBE PG-AMS (ACOUSTICAL ACCELEROMETER):

Aronov has also developed a flexural bimorph multiaxis PG-AMS that is compact and has demonstrated high sensitivity (377 mV/g). The device has integrated hydrophones in the form of flexural devices and has the attributes that all four channels have the same acoustical center. The device, packaged in a neutrally buoyant cylindrical housing, has approximate dimensions of height 2.9 in (7.5 mm) and diameter 2.375 (5.8 mm). With PZT-4 plates device BTECH-Cube-01 has a channel sensitivity of 462 mV/g @ 1kHz and a resonance frequency of 3.5 kHz. A sensor illustration is shown in Figure 7. The capacitance is 1.2 nF per channel. Beam patterns of a tested device are shown in Figure 8. Modifications of this design have produced a sensor with a sensitivity of 1250 mV/g at 1 kHz as shown in Figure 9.

7
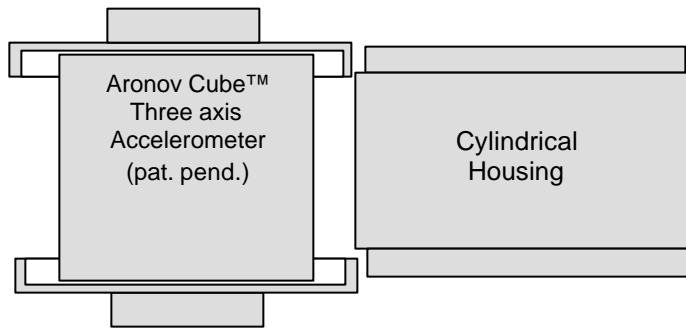
Figure 7. Illustration of a BTECH ARONOV-CUBE™ PG-AMS. Patents pending
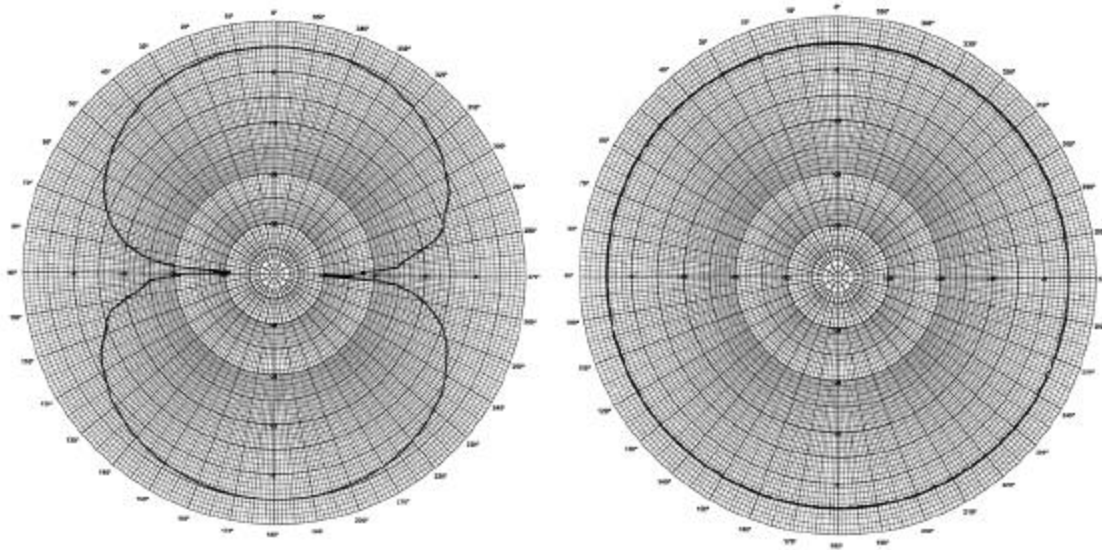
Figure 8. Beam patterns of the Aronov Cube PG-AMS for one PG-AMS channel and for the omnidirectional hydrophone.
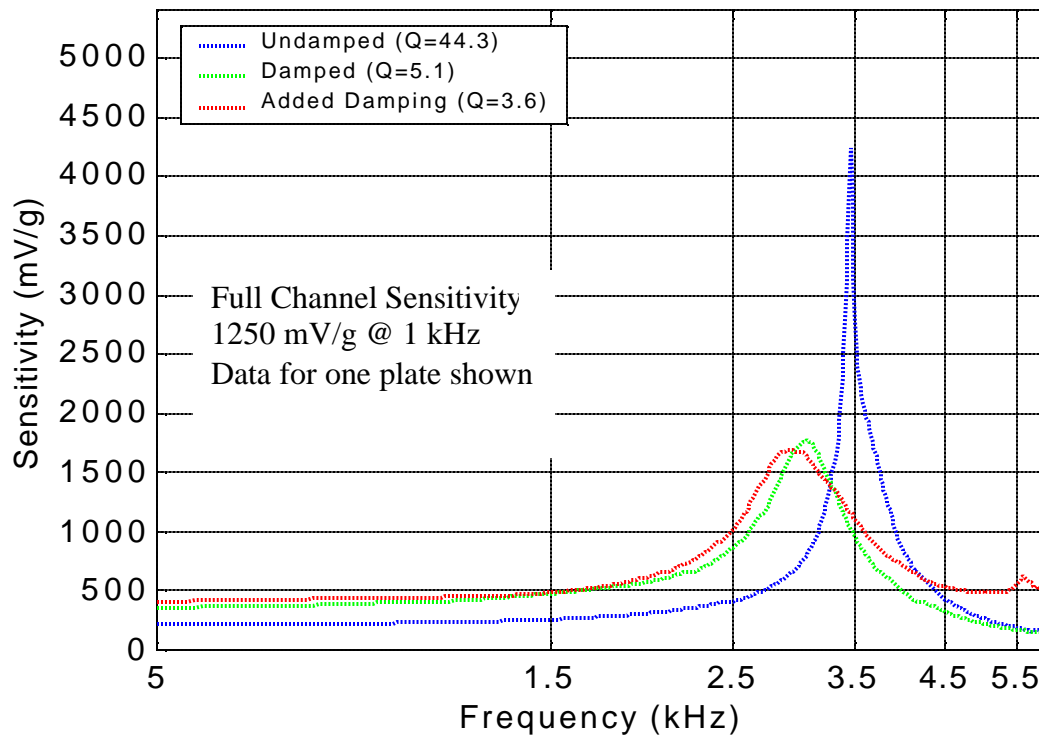
Figure 9. Frequency / sensitivity response of the Aronov Cube with different damping treatments. Data shown for one plate only. Two plates per channel produce a sensitivity of 1250 mV/g @ 1 kHz.

Regarding Quality Factor, Resonance Frequency and Damping:

Often the quality factor (Q) needs to be sufficiently low in a receiver in order to prevent the device from ringing and to extend the useable frequency range particularly when that the resonance of the transduction device is near to the frequency band of interest or operation. Increasing the receiver sensitivity while maintaining a high resonance frequency is difficult, as it can be shown that the two are inversely related, or more exactly the product of the sensitivity and square of the resonance frequency is often a configuration design constant. The Aronov Cube Accelerometer device affords means for the convenient introduction of damping materials and the application specific optimisation of this transducer is under development. Figure 9 illustrates the frequency response of the transducer with the application of damping materials.

VI. PRESSURE GRADIENT FIXED DIFFERENTIAL AND DIFFRACTION TYPES

A number of Pressure Gradient Fixed Differential and Diffraction Type Transducers are under development and will be discussed at the meeting including a three-axis accelerometer in a planar package

Advances in Acoustic Particle Velocity Sensorics

Paul A. Wlodkowski
Fred Schloss
Wilcoxon Research, Inc.
21 Firstfield Road
Gaithersburg, Maryland 20878

Advances in Acoustic Particle Velocity Sensorics

Paul A. Wlodkowski and Fred Schloss
Wilcoxon Research, Inc.
21 Firstfield Road
Gaithersburg, Maryland 20878

Abstract. The development of a high-sensitivity, low-noise acoustic particle velocity sensor in a small package remained a formidable technical challenge for many years. With the advent of single-crystal piezoelectric material, however, that goal has been achieved. Wilcoxon Research has successfully developed a Vector sensor that meets U.S. Navy requirements through a synergy of technology encompassing single piezoelectric crystals, a novel amplifier design with low-noise characteristics, and a unique method of inducing strain amplification in the piezoelectric crystal.

I. INTRODUCTION

Acoustic particle velocity transducers, also known as Vector Sensors, have a history rich in innovation. During World War II, Bell Laboratories[1] developed a pressure gradient hydrophone, comprised of electromagnetic inertia-type transducers mounted in a spherical aluminum shell. Each orthogonal pair of sensors has a figure eight or cosine pattern.[2] T. J. Schultz of the Acoustics Laboratory at Harvard University constructed an acoustic wattmeter[3] for measurements in air. Concurrently, an effort was undertaken at the Naval Ordnance Laboratory[4] in which the effect of buoyancy on the particle velocity sensor was discussed. At the Diamond Ordnance Fuse Laboratory,[5] an ingenious method was established to relate the sound intensity to temperature fluctuations in air. G. L. Boyer[6] first incorporated piezoelectric materials into an acoustic intensity meter at the David Taylor Model Basin. F. W. Desiderati[7] at the Naval Ship Research and Development Center demonstrated a *bona fide* pressure gradient transducer, consisting of two pressure-sensitive elements separated by a fixed distance. Moreover, a technique for correcting near-field effects was provided using electrical compensation in which an RC differentiating circuit was placed at the output of the pressure gradient, or acceleration channels, of the respective transducers.

The dormancy in this field for the next thirty years can be attributed to limitations in signal-processing capability. Once signal-processing technology evolved to a mature level, further requirements were placed on the sensor design. The development of a high-sensitivity, low-noise acoustic particle velocity sensor in a small package presented a formidable technical challenge to researchers for many years. By harnessing the exceptional electromechanical properties of single piezoelectric crystals[8,9] with a novel amplifier with low-noise characteristics, and a unique method of strain amplification in the piezoelectric crystal, that elusive goal was achieved.

II. DESIGN CONCEPT AND PROTOTYPE

Having recognized that the exceptional properties of single piezoelectric crystals, belonging to the relaxor group of ferroelectric materials, would be ideally suited for developing low-noise vibration transducers, engineers at Wilcoxon Research, Inc. have applied a method of strain amplification[10] to enhance the performance. The method of strain amplification utilizes a sensing structure comprised of a bending plate that has a castellated surface, which raises the piezoelectric sensing material that is mounted there above the substrate's neutral axis. Strain in the crystal is amplified via mechanical leverage. Resultantly, stress levels in the piezoelectric materials are augmented, generating more charge output and lower noise than traditional designs. Without the castellated surface, the configuration would be that of a conventional, flexural disc mode accelerometer.[11]

The castellated height is adjusted depending upon the electromechanical properties of the sensing material, and it amplifies the stress in the crystal and generates a higher charge output. Application of this technique results in the increase of the charge output for the transducer by a factor of two (6 dB), irrespective of the piezoelectric material chosen. Most significantly, this is accomplished without adding inertial mass to the sensor and by keeping the resonance frequency constant. A generalized approach to the method of strain amplification, incorporating single piezoelectric crystals, has been published recently by Wilcoxon Research, Inc.[12]

Wilcoxon Research, Inc. initiated development on its single piezoelectric crystal-based acoustic particle velocity sensor in October 2000. Five months later, in March 2001, the first prototype was assembled, and measurements were performed at the Acoustic Test Facility (ATF) at the Naval Undersea Warfare Center (NUWC) in Newport, Rhode Island. A photograph of the Wilcoxon Research Vector sensor is illustrated below in Fig. 1.

III. EXPERIMENTAL SETUP AND MEASURED RESULTS

Measurements on the Wilcoxon Research Prototype 01 Vector Sensor were taken in accordance with ANSI S1.20-1988 (Revision of S1.20-1972). The water temperature was 17°C. Projector J-9 #125 and hydrophone H-52 #101 were used to meet USRD standards. Receive voltage sensitivities and phase on all four channels were recorded. Beam patterns were generated in the XY plane for the X and Y accelerometer channels and the pressure transducer; and in the XZ plane for the X and Z accelerometer channels and the pressure transducer. The distance between the projector and Vector sensor was a constant 1.62 meters over the swept frequency range of 200 Hz to 2 kHz.

The received voltage sensitivities for the four channels of the Vector sensor are illustrated below in Fig. 2. .

FIG. 1. Vector sensor (Wilcoxon Research Prototype 01).
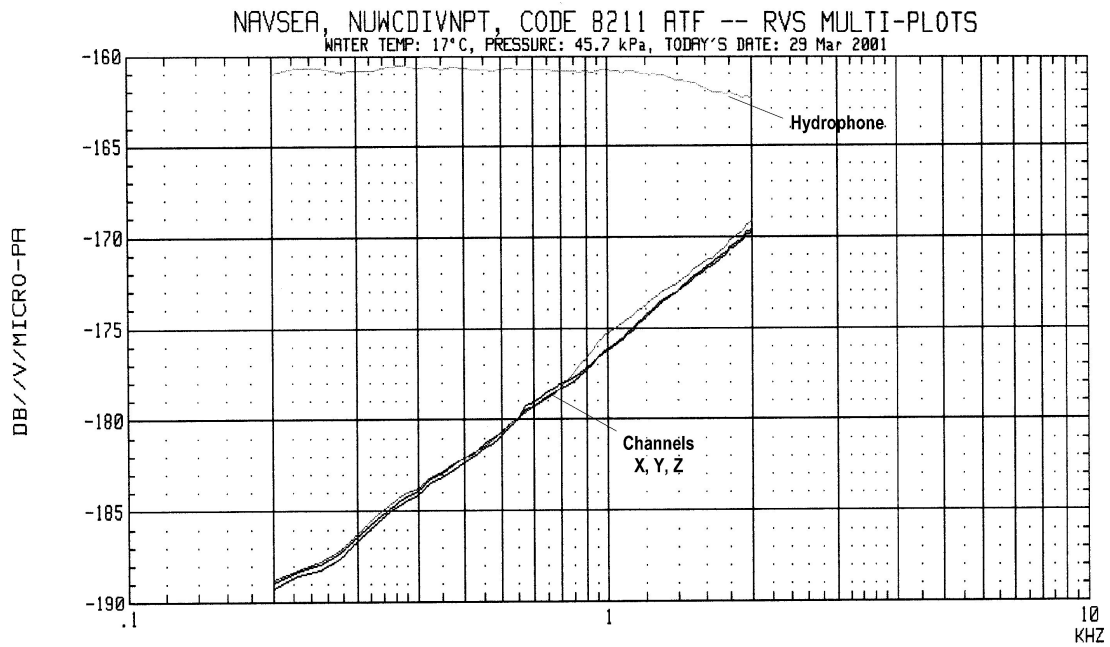
FIG. 2. Receive voltage sensitivities (Wilcoxon Research Prototype 01).

As evident from the graph in Fig. 2, the receive voltage sensitivities of the accelerometer channels differ by only a fraction of 1 dB, and the slope of the accelerometer sensitivity curve follows theory according to Newton's law for water motion.

Beam patterns in the XZ plane are shown below in Fig. 3. A typical cosine pattern was generated, and most notably nulls of greater than –35 dB were obtained. This result translates into a transverse sensitivity of less than 2%.
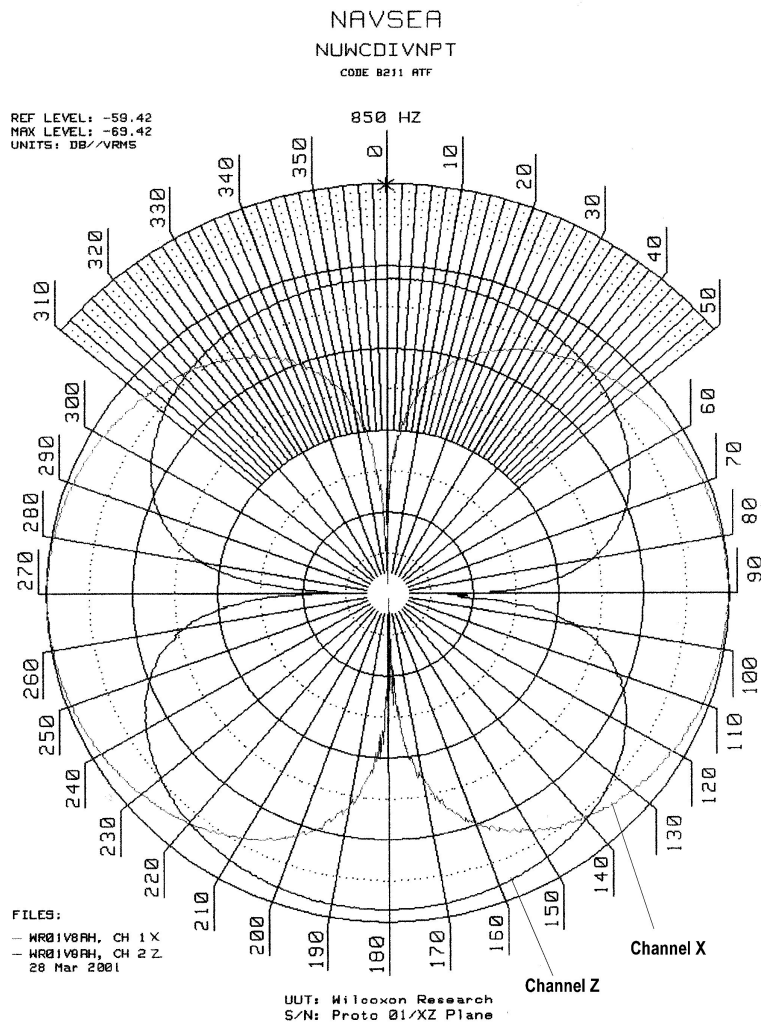
FIG. 3. Beam pattern in XZ plane (Wilcoxon Research Prototype 01).

The phase response between the Y channel of the accelerometer and the pressure transducer is depicted in Fig. 4.

4
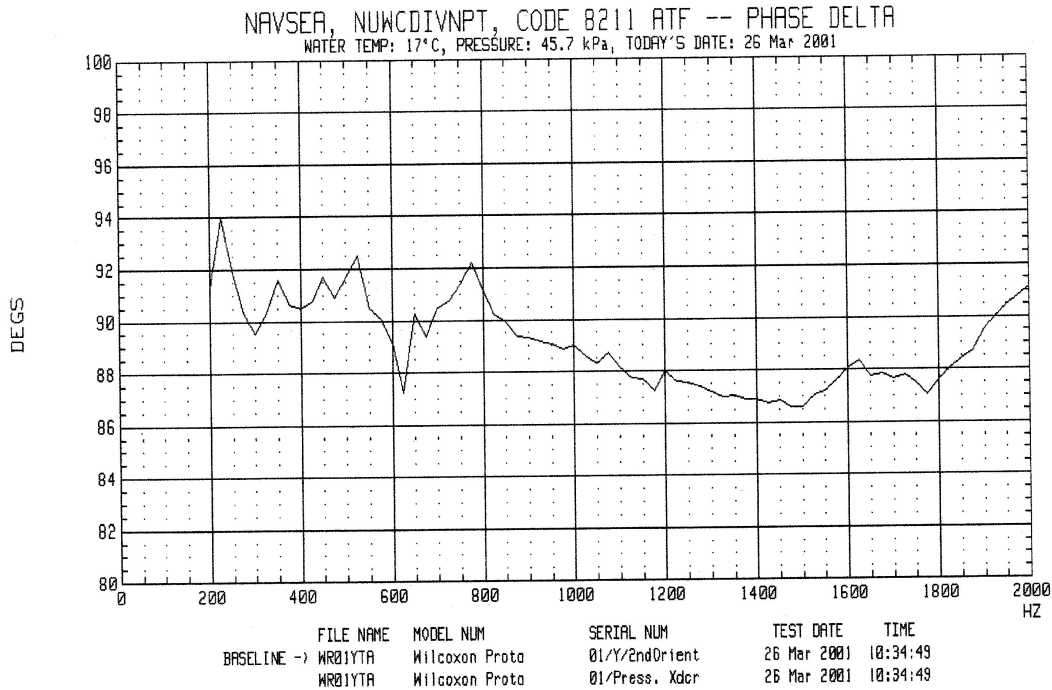
FIG. 4. Phase response of Wilcoxon Research Vector Sensor Prototype 01.

As the graph indicates, the phase response is 90°±4°, as specified by the U.S. Navy in its design objectives. Given the measurement limitations of the Acoustic Test Facility, it is expected that the phase response will be significantly improved in a free field with a continuous wave source. Low frequency phase variations may be caused by output cable restraint. Moreover, a focused effort is underway at Wilcoxon Research to enhance the transducer performance, which will further mitigate phase between the channels.

Evaluation of the inherent noise levels of acoustic particle velocity sensors is critical for a robust design.[13] It has also been shown that accelerometer noise is inversely proportional to charge output, especially at low frequencies.[14] The measured accelerometer noise of the Vector sensor, converted to the equivalent pressure level, is shown in Fig. 5 as a function of frequency. Superimposed on the graph is the Knudsen Sea State Zero level, extrapolated to 50 Hz. If necessary, it will be possible to lower the noise floor further through a combination of electrical and mechanical design efforts.
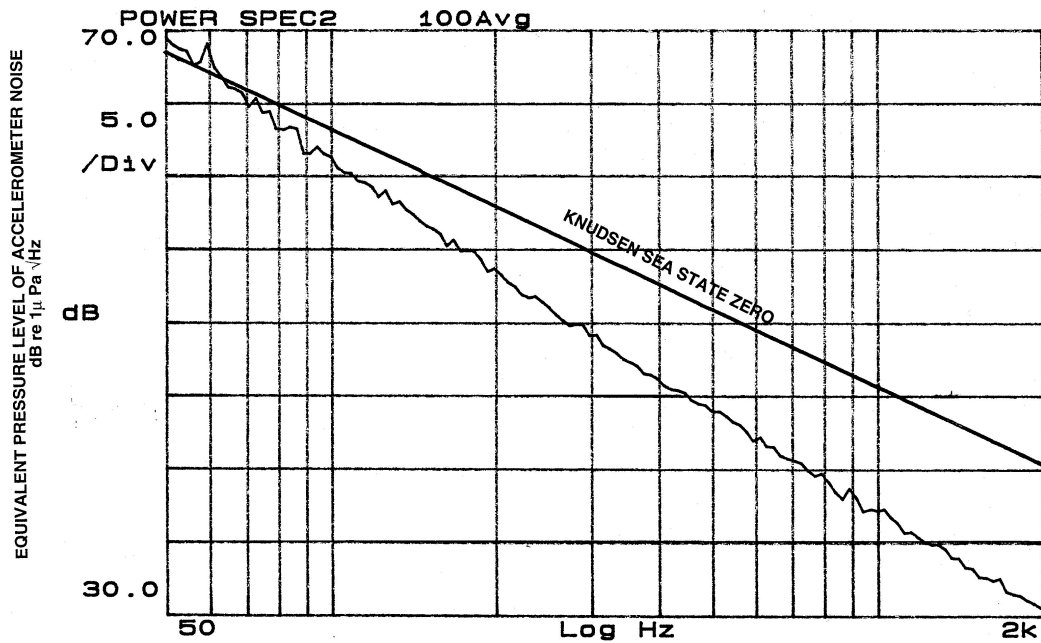
**FIG. 5. Measured accelerometer noise
(Wilcoxon Research Vector Sensor Prototype 01).**

IV. CONCLUSIONS

An advance in acoustic particle velocity sensorics has been achieved with the development of a Vector sensor, incorporating single piezoelectric crystals, a novel amplifier with low-noise characteristics, and a unique method of inducing strain amplification in the piezoelectric crystal. Directivity patterns, phase response, receive voltage sensitivities, and the equivalent pressure level of accelerometer noise demonstrate that U.S. Navy requirements have been met. This is evidenced by a Vector sensor exhibiting deep nulls exceeding 35 dB and phase response between hydrophone and accelerometer channels of 90°±4°. It is anticipated that further improvements to the performance can be expected from enhancements to transducer and amplifier design.

ACKNOWLEDGMENTS

REFERENCES

1. "Operating Notes for N.D.R.C. 1A and 2A Standard Pressure Gradient Hydrophones." Bell Telephone Laboratories, Inc. Technical Report, June 16, 1945 (Declassified).

2. "A Manual of Calibration Measurements of Sonar Equipment." Summary Technical Report of Div. 6, NDRC, Vol. II. 1946.

3. T. J. Schultz. "Acoustic Wattmeter." *The Journal of the Acoustic Society of America*. Vol. 28, No. 4, July 1956, pp. 693-699.

4. C.B. Leslie et al. "Hydrophone for Measuring Particle Velocity." *The Journal of the Acoustic Society of America*. Vol. 28, No. 4, July 1956, pp. 711-715.

5. D.R. Pardue and A.L. Hedrich, "Absolute Method for Sound Intensity Measurement." *The Review of Scientific Instruments*, Vol. 27, No. 8, August 1956, pp. 631-632.

6. G.L. Boyer. "Acoustic Intensity Meter." Technical Report. David Taylor Model Basin, December 1959.

7. F.W. Desiderati. "Underwater Acoustic Intensity Transducers." Acoustic and Vibration Laboratory Technical Note AVL-173-945, Naval Ship Research and Develoment Center, April 1967.

8. Park, S. and T.R. Shrout. "Ultrahigh Strain and Piezoelectric Behavior in Relaxor Based Ferroelectric Single Crystals." *J. Appl. Phys*. Vol. 82, No. 4, 15 August 1997, pp. 1804-1811.

9. Yamashita, Y. et al. "Recent Applications of Relaxor Materials." *Ferroelectrics*, Vol. 219, 1998, pp. 29-36.

10. K. Deng et al. "Method of Strain Amplification for Piezoelectric Transducers." Patent Pending.

11. P. David Baird. "Concept for a Low Profile Mold-in-Place Accelerometer." Acoustic Particle Velocity Sensors: Design, Performance, and Applications. *AIP Conference Proceedings 368*, M.J. Berliner and J.F. Lindberg, Eds., AIP Press, pp.431-434, 1995.

12. P.A. Wlodkowski et al. "The Development of High-Sensitivity, Low-Noise Accelerometers Utilizing Single Crystal Piezoelectric Materials." *Sensors and Actuators A*, Vol. 90, April 2001, pp. 125-131.

13. T.B. Gabrielson "Modeling and Measuring Self-Noise in Velocity and Acceleration Sensors." Acoustic Particle Velocity Sensors: Design, Performance, and Applications. *AIP Conference Proceedings 368*, M.J. Berliner and J.F. Lindberg, Eds., AIP Press, pp. 1-48, 1995.

14. Schloss, F. "Accelerometer Noise." *Sound and Vibration*. March 1993, pp. 22-23.

EDO Directional Acoustic Sensor Technology

P. David Baird
Systems Engineering Department
EDO Electro-Ceramics Products
Salt Lake City, Utah 84115

EDO Directional Acoustic Sensor Technology

P. David Baird
Systems Engineering Department
EDO Electro-Ceramics Products
Salt Lake City, Utah 84115

Abstract. EDO has developed acoustical directional sensors that address the needs of two U.S. Navy hull arrays, Conformal Acoustic Velocity Sonar (CAVES) and Low Frequency Hull Array (LFHA). These sensors are based upon a flexural disc accelerometer design. The CAVES sensor is a uni-axial, neutrally buoyant accelerometer design. The LFHA sensor consists of tri-axial accelerometers and pressure sensors. This "dyadic" configuration is capable of generating a directivity index of 9.5 dB. The MRA can be steered in any direction by adjusting the channel weights. The designs have been tested extensively at U.S. Navy test facilities. The accelerometer design passes the MIL-901-C explosive shock test.

I. DEVELOPMENT HISTORY

The development of directional acoustic sensor technology at EDO was driven by the U.S. Navy need for hull mounted motion sensors. A chronological history of events is provided in Fig. 1. A uniaxial accelerometer design was utilized in both the Conformal Acoustic Velocity Sonar (CAVES) and CAVES/Wide Aperture Array (WAA) programs. An outgrowth of this design was later implemented into vector and dyadic sensor designs.

1995 Motion Sensor Workshop
  - EDO Paper: Concept for a Low Profile Mold-in-Place Accelerometer
1996 CAVES Spherical Neutral Buoyant Accelerometer
  - Flexural Disc Design
1997/1998 CAVES Cylindrical Neutral Buoyant Accelerometer
  - Flexural Disc Design, Syntactic Foam
1998 Paper Published
  - NUWC/EDO Collaboration
  - Moffett, Trivett, Klippel, Baird, A Piezoelectric, Flexural-Disc, Neutral Buoyant, Underwater Accelerometer, IEEE Transaction on Ultrasonics, Ferroelectrics, and Frequency Control, Vol. 45, No. 5, 1998
1998 CAVES/ASTO Patch Test Accelerometers
  - Delivered 120 Accelerometer Assemblies
1998-Present LF Bow Array Vector Sensor Development
  - September 2000: NUWC Test/Technology Demonstration
  - May 2001: NUWC Dyadic Sensor Test - Seneca Lake
2000-Present CAVES WAA Preliminary Design
  - Subcontractor to General Dynamics, Electric Boat

FIG. 1. EDO Motion Sensor History

II. DIRECTIONAL ACOUSTIC SENSOR DESIGN OBJECTIVES

The development of a directional acoustic sensor is driven by applications where an artificial baffle is required. In these applications, the use of a passive resistive baffle is either impracticable or negatively impacts the performance of other sonar systems.

One such application would be the Low Frequency Hull Array (LFHA) as illustrated in Fig. 2. The LFHA is a horseshoe-shaped array of sensor staves that is conformal to the bow of a 688-class submarine. The LFHA must be acoustically trans-parent to the other sonar arrays that reside behind it. Currently, the LFHA utilizes the DT-276, an omni-directional pressure sensor. Processing against ownship self-noise can occur only at the array level. As indicated in Fig. 2, many staves are located within the ballast tanks. As a result, the self-noise field varies with position. The use of directional sensors in this application would permit the processing against local self-noise at each sensor location.
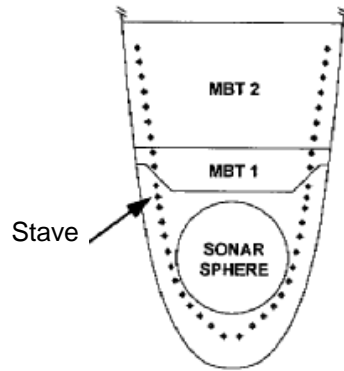
FIG. 2. Low Frequency Hull Array Configuration
(Courtesy NUWC Division Newport)

The objective of this development is to design a sensor that will be capable of generating a baffle that can be steered in a desired direction. The sensor should also be capable of generating cardioid directivity patterns at a minimum. The form factor of the sensor shall also be constrained to the existing size of the DT-276. Additional require-ments are detailed within a NUWC Division Newport motion sensor specification.

III. UNDERLYING THEORY

The dyadic or tensor sensor outputs three quantities: pressure, acceleration (proportional to gradient of pressure), and the gradient of acceleration. A scalar sensor or hydrophone utilizes only the pressure quantity. A vector sensor utilizes the pressure and the acceleration, whereas the dyadic utilizes all three quantities. The directivity index of each of these sensor configurations is provided in Fig. 3.

Sensor Type	Tensor Rank	Directivity Index (dB)
Scalar	0	0
Vector	1	4.8-6.0
Dyadic	2	7.0-9.5

FIG. 3. Sensor Directivity

The vector sensor can generate a standard cardioid directivity pattern with one null, or by selecting the weights, generate higher directivity index with two nulls. The dyadic sensor due to its spatial sensor offset can generate a higher directivity index. In order to realize the performance improvement at low frequencies, dyadic sensors must be very closely matched in sensitivity.

IV. DYADIC SENSOR DESIGN

The dyadic sensor contains both accelerometers and pressure sensors. The accelerometers are arranged to provide orthogonal outputs. The accelerometers are both co-located and distributed relative to the acoustic center of the pressure sensor. This configuration (see Fig. 4) provides the capability to generate scalar, vector and dyadic outputs.
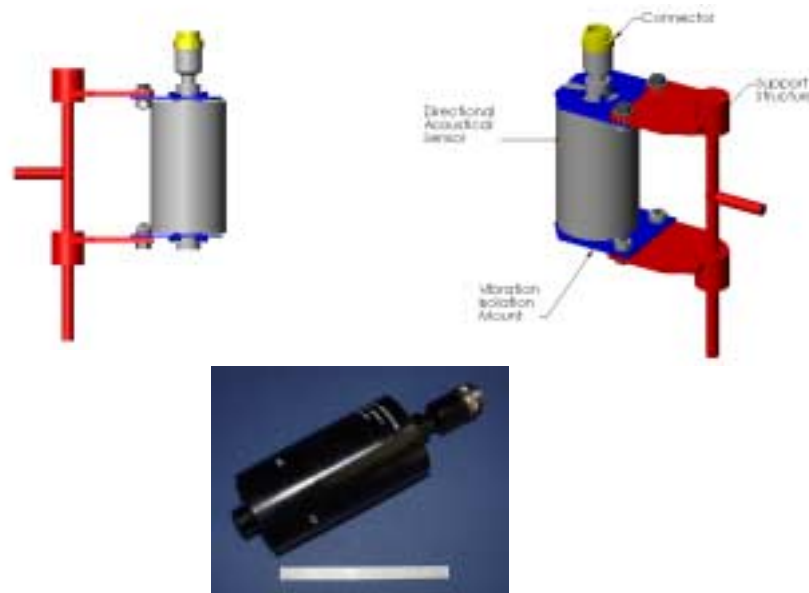
FIG. 4. Dyadic Sensor Design

V. ACCELEROMETER DESIGN

The accelerometer design, as illustrated in Fig. 5, is composed of an inertial mass substrate, two ceramic discs, and a pressure-tolerant housing. The flexural disc design is electrically terminated to provide voltage doubling.
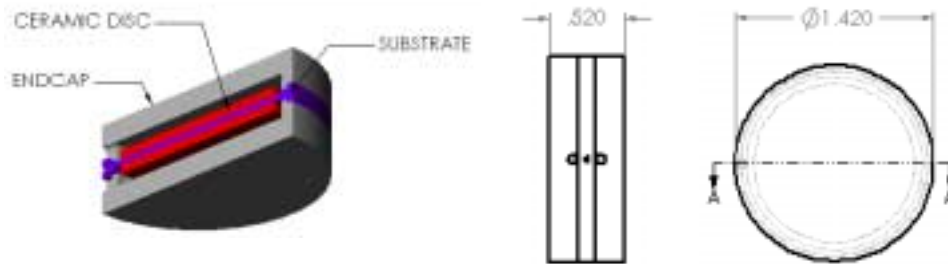
FIG. 5. Accelerometer Design

VI. ACCELEROMETER PERFORMANCE

Accelerometer performance parameters that have been measured include resonance frequency, capacitance, electrical dissipation, and sensitivity to motion and pressure. The nominal characteristics of the sensor without cable are

Capacitance:	3400 pF
Electrical Dissipation:	0.014
Resonance Frequency:	11.2 kHz
Acceleration Sensitivity:	-17.25 dB

The accelerometer's insensitivity to pressure over the operating range of hydrostatic pressure has been demonstrated using NUWC's System J. The motion sensitivity has been demonstrated using shaker head and in-water measurements. Shaker head performance at NUWC with 30 feet of cable is illustrated in Fig. 6.
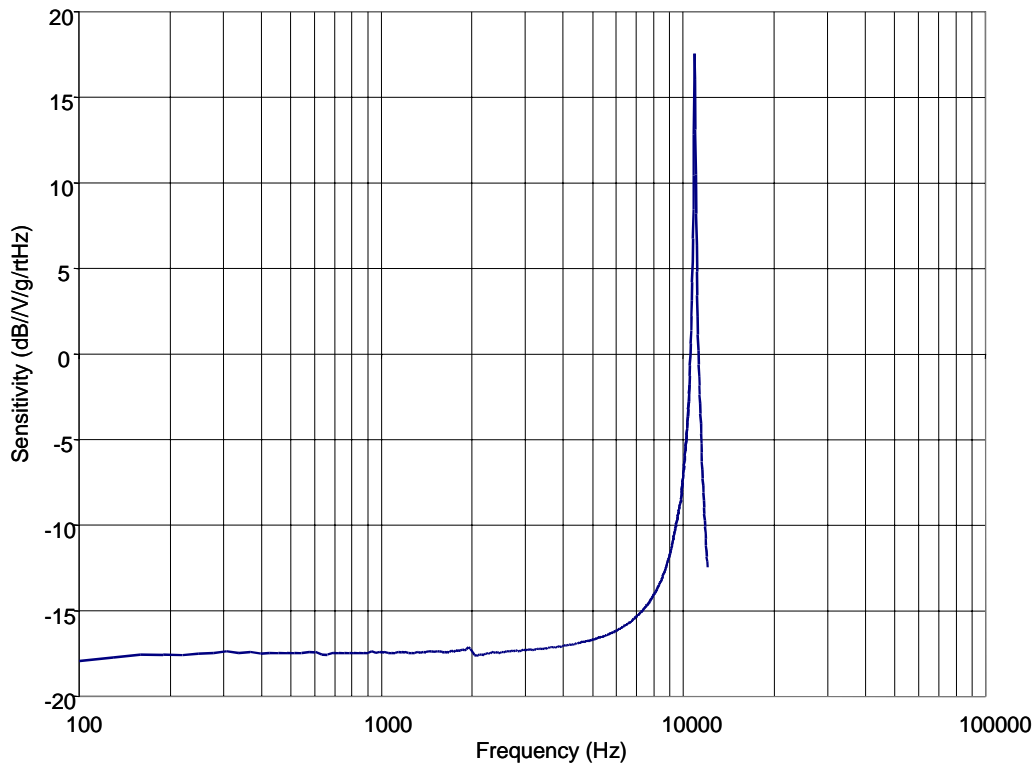
FIG. 6. Shaker Head Acceleration Sensitivity

In support of the CAVES Program, EDO manufactured 120 accelerometer assemblies. These sensors were manufactured without binning of components. The manufacturing process capability associated with that product is provided in Fig. 7.

4

Capacitance (nF)
       Standard Deviation = 0.063
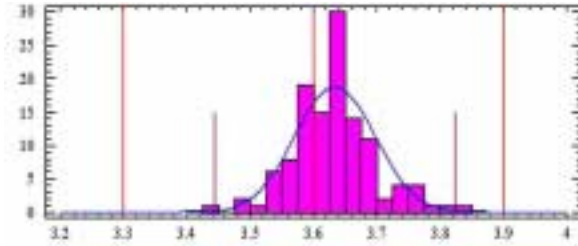
Resonance Frequency (kHz)
       Standard Deviation = 0.072
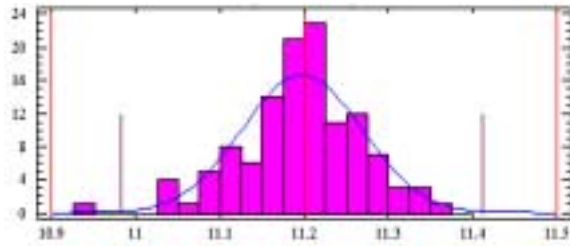
Sensitivity (dB//V/g)
       Standard Deviation = 0.19
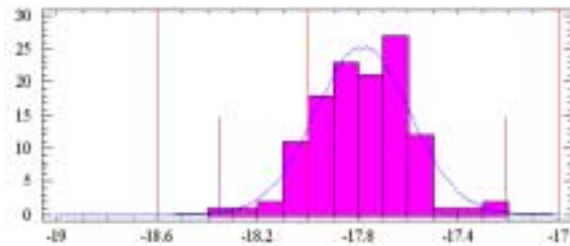
FIG. 7. Manufacturing Performance

Through the use of component selection, using characteristics such as substrate mass and ceramic, the stated performance standard deviations can be reduced by a factor of 3:1.

VII. DYADIC SENSOR PERFORMANCE

Directivity

The directivity performance of the dyadic sensor at three frequencies (200, 1000, and 5000 Hz) is provided in Figs. 8 through 10. The measurements at 200 and 1000 Hz were made at the NUWC ATF at a distance of 1.55 m. The measurements at 5000 Hz were gathered at the EDO ATF at 6 m. The sensor in all cases was attached to the mounting fixture illustrated in Fig. 4.
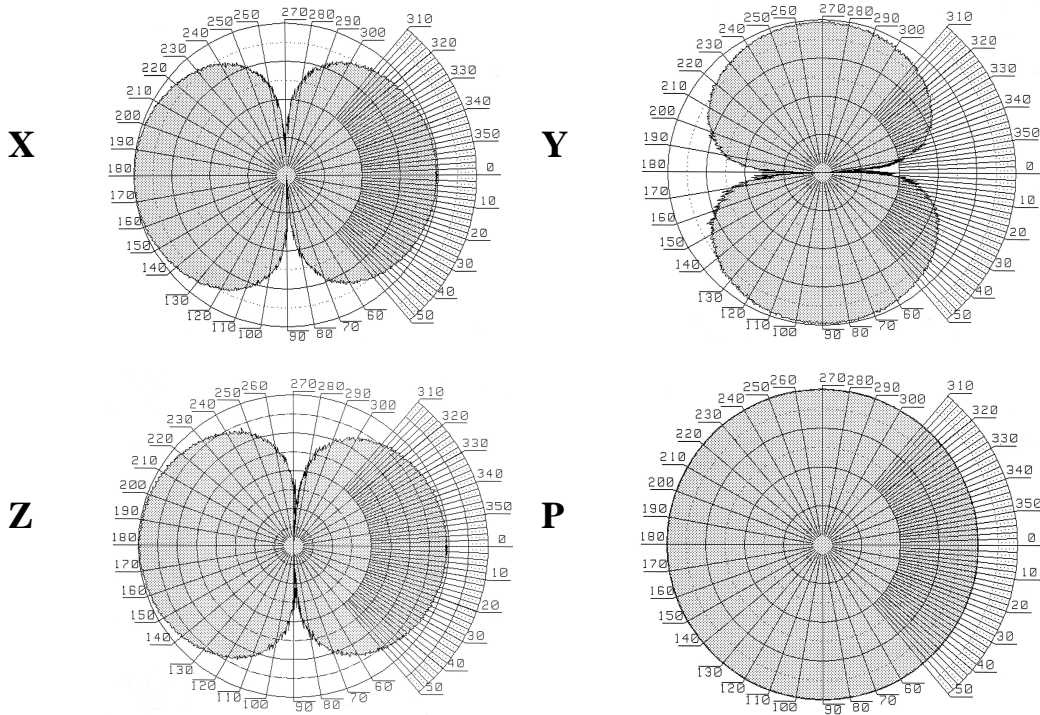
FIG. 8. Dyadic Sensor Directivity at 200 Hz
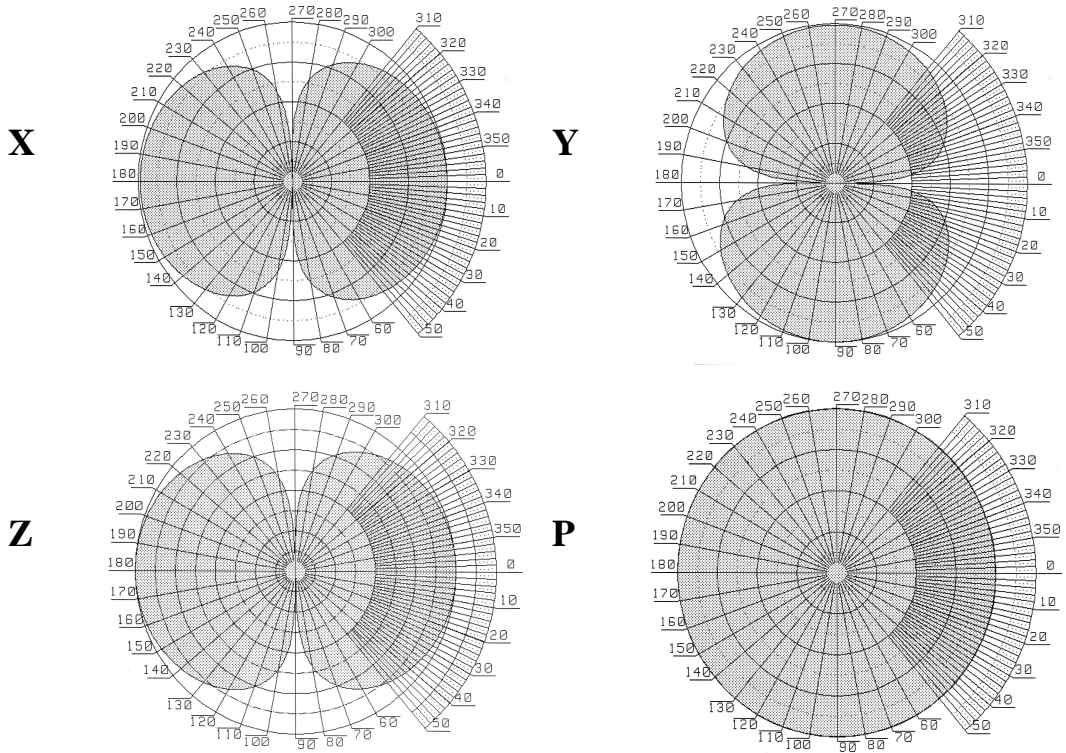
FIG. 9. Dyadic Sensor Directivity at 1000 Hz
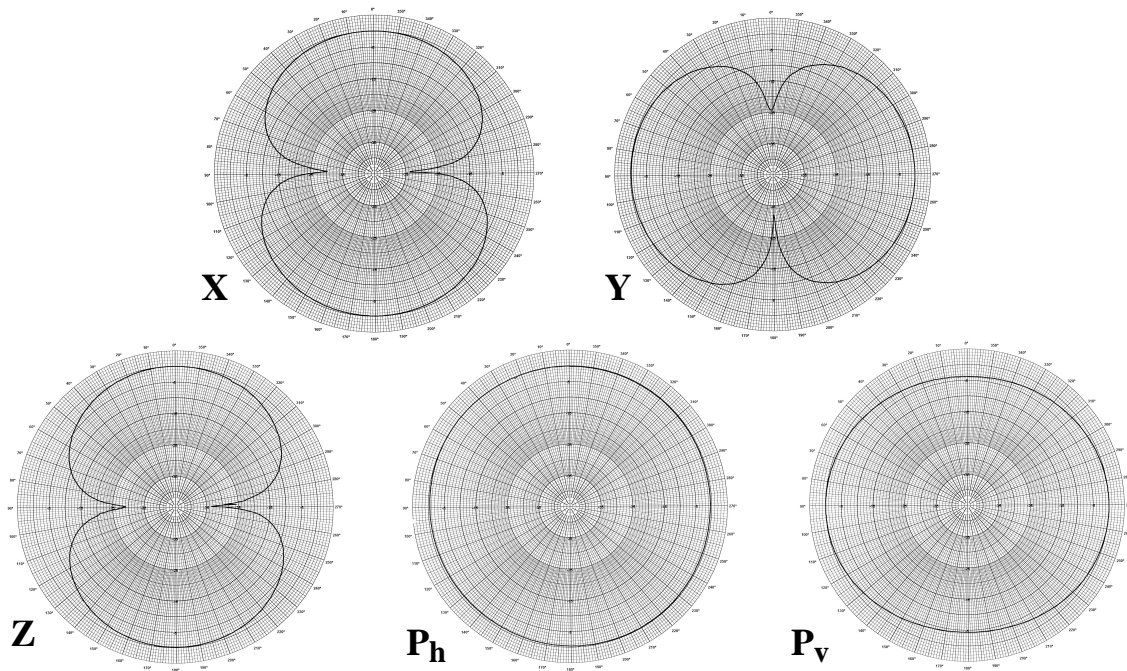
FIG. 10: Dyadic Sensor Directivity at 5000 Hz

Acoustic scattering from surfaces in close proximity to the sensor will impact the directivity performance. The LFHA mounting fixture will impact the directivity performance at higher frequencies. An example of this impact upon directivity is provided in Fig. 11. The performance without the LFHA mount is ideal dipole.

With Mount　　　　　**Without Mount**
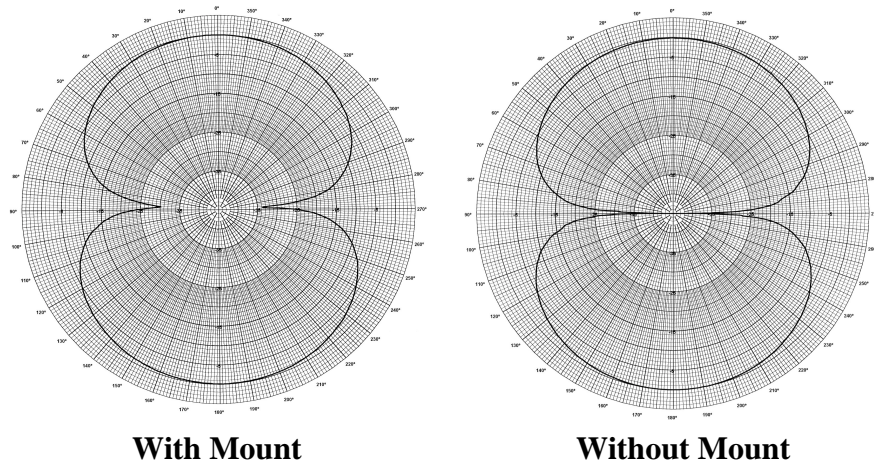
**FIG. 11. Dyadic Sensor Directivity at 5000 Hz, X-Axis,
Mounted With and Without LFHA Mount**

Receive Sensitivity

The nearfield receive sensitivity of the X, Y, and P channels is provided in Fig. 12.
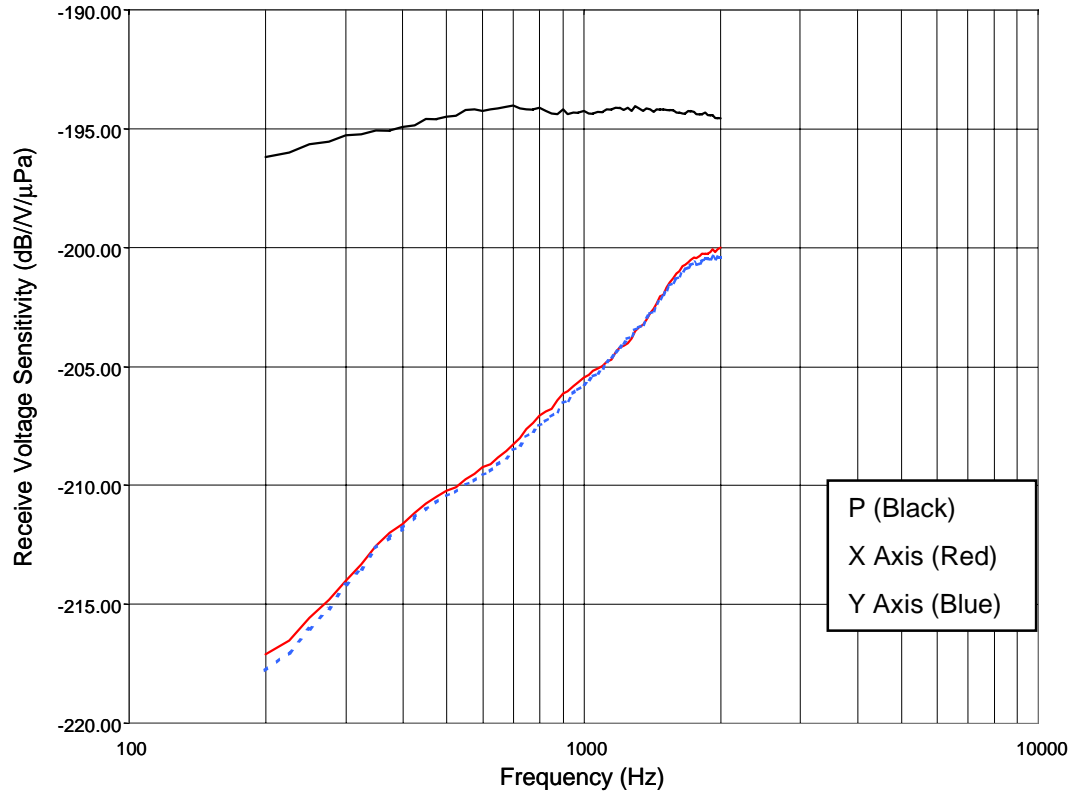
FIG. 12. Dyadic Sensor Receive Sensitivity, Horizontal Plane

The sensitivity performance below 1000 Hz does not fall off at 6 dB per octave as predicted by theory. The higher measured sensitivity is the result of the nearfield position of the sound source. The separation between sensor and sound source was 1.55 m. The nearfield particle velocity for spherical wave is given by

$$u = \frac{A}{\rho c r} \frac{\sqrt{1+k^2 r^2}}{kr} \cos(\omega t - kr - \varphi).$$

When corrected for the nearfield effect at 200 Hz, the difference between the measured and predicted is 0.4 dB.

Electronic Noise

The predicted electronic noise performance of dyadic sensor is provided in Fig. 13. The noise model used has been validated by measurements. As illustrated in the inset graph, the measured values (blue) and model predictions (red) are in close agreement.

8

The design provides compliant performance relative to the maximum acceptable level of noise specified by the NUWC requirement. At the lower frequencies the Johnson noise of the sensor dominates the performance.
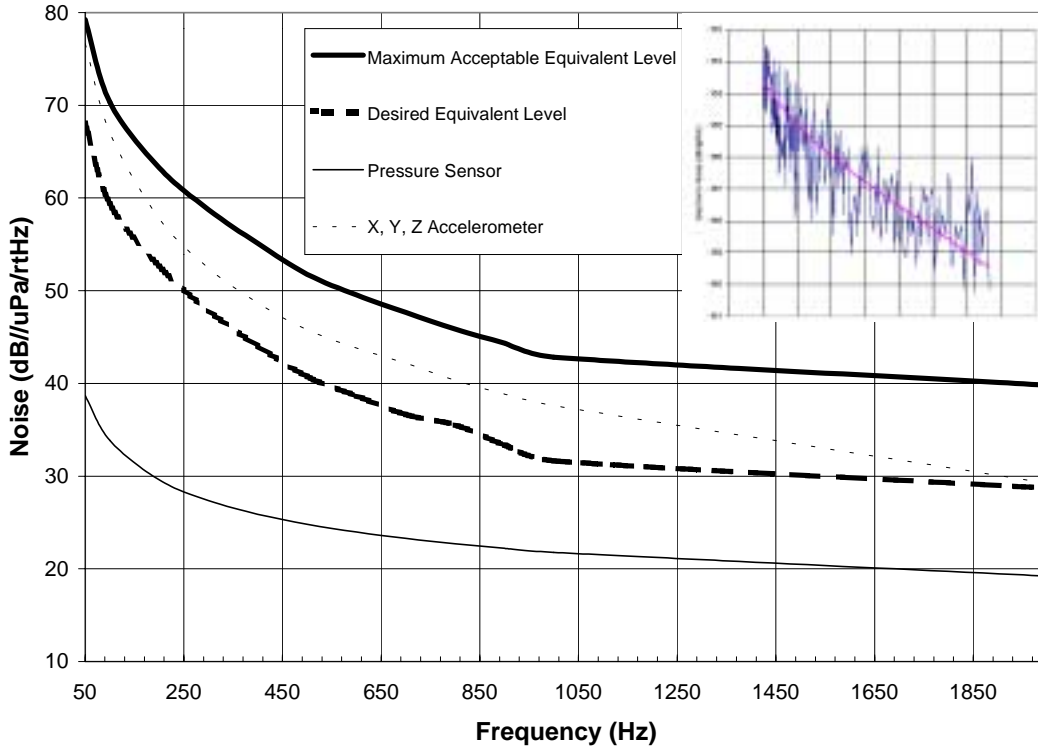
FIG. 13. Dyadic Sensor Electronic Noise versus Frequency

VIII. ENVIRONMENTAL PERFORMANCE

The accelerometer utilized in the dyadic sensor design has undergone extensive environmental testing. This testing includes hydrostatic pressure, non-operating pressure, and underwater explosive shock. Figure 14 defines the conditions under which the accelerometer has been demonstrated to operate and/or survive.

Operating Pressure Range
- 0-1000 psi

Non-Operating Temperature
- -100° to 250° F

Explosive Shock, MIL-901 C, Grade A
- Pressure Release Mount

FIG. 14. Accelerometer Environmental Performance

IX. CONCLUSIONS

EDO has demonstrated directional motion sensors based on a common building block that can be produced in a manufacturing environment, and whose performance addresses both CAVES and LFHA motion sensor requirements. The EDO dyadic sensor supports vector sensor processing. The demonstrated performance is summarized in Fig. 15.

> - Acceptable Dipole and Omni Directivity
> - Acceptable Sensitivity Matching
> - Extended Bandwidth 50-6000 Hz (50-2000 Hz Navy Baseline)
> - Acceptable Electronic Noise Performance
> - Accelerometer Insensitivity to Pressure
> - Acceptable Hydrostatic Pressure Performance
> - Broad Operating/Non Operating/Process Temperatures
> - Accelerometer Passes MIL-901 C Explosive Shock Test, Grade A

FIG. 15. Dyadic Sensor Demonstrated Performance

The extended bandwidth of the EDO dyadic sensor provides the potential to support target ranging using triangulation techniques with two or more dyadic sensors in an array. This feature in a forward-looking array may be of significant interest to provide submarines a means of maintaining tactical advantage in close encounter situations.

EDO has, in addition, demonstrated a capable manufacturing process. The process is capable of producing hardware to the very tight tolerances required by the NUWC LFHA Motion Sensor Specification.

Lastly, the EDO dyadic sensor provides the capability to support a dyadic signal process that would, in theory, provide a directivity index as great as 9.5 dB, or as much as 3.7 dB greater than a vector sensor.

Directional Hydrophones in Towed Systems

Bruce M. Abraham
Acoustics Department
Engineering and Information Technologies Group
Anteon Corporation
Mystic, Connecticut 06355

Marilyn J. Berliner
Submarine Sonar Department
Naval Undersea Warfare Center Division
Newport, Rhode Island 02841

Directional Hydrophones in Towed Systems

Dr. Bruce M. Abraham
Acoustics Department, Engineering and Information Technologies Group
Anteon Corporation
Mystic, Connecticut 06355

Dr. Marilyn J. Berliner
Submarine Sonar Department
Naval Undersea Warfare Center Division
Newport, Rhode Island 02841

Abstract. The use of directional hydrophones in towed systems is summarized. The acoustic and flow noise performance of particle velocity, particle acceleration, and pressure difference or gradient on hydrophones are compared. Primary noise mechanisms and fundamental limits for directional hydrophones in a towed array system are summarized. Approaches for noise mitigation in towed systems are presented.

I. INTRODUCTION

Directional hydrophones are those that intrinsically have a non-axisymmetric directivity pattern. Two common examples are dipole and cardioid sensors, both of which are available as commercial audio equipment. Dipole sensors respond to one component of a vector field (e.g. the particle velocity) and cardioid sensors have a maximum response at a single angle. Examples of beampatterns from omnidirectional, dipole, and two types of cardioid sensors are shown in Fig. 1.

Two salient benefits of using directional hydrophones are the ability to determine the arrival angle of an acoustic source and a directivity index greater than 0 dB. A linear array of directional hydrophones can be used in the same manner as conventional omnidirectional hydrophones to provide additional gain against ambient noise. Volumetric (e.g. multi-line towed arrays) can effectively create the performance of directional hydrophones through beamforming.

The Office of Naval Research (Code 321SS) funded the SuperDirective Array (SDA) and Multi-Mode Directional Towed Array (MMDTA) projects at the former Naval Underwater Systems Center and the Naval Undersea Warfare Center Division Newport. The Surface Ship Torpedo Defense (SSTD) program also funded the SDA effort. The primary objective of the projects was to design and demonstrate a tactical single-line towed array that used directional hydrophones. The capabilities of the array included left/right bearing discrimination and enhanced array gain. From this research came an understanding of the important noise mechanisms for directional hydrophones and ways of minimizing the non-acoustic noise to maximize performance.
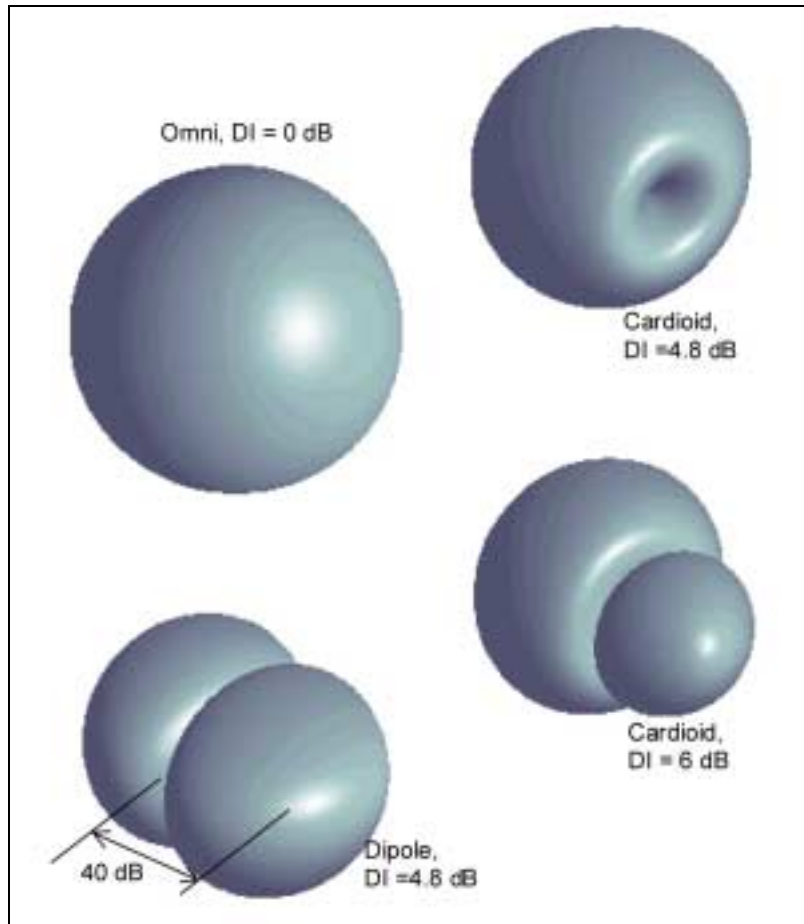
FIG. 1. Sensor beampattern examples.

Other countries have pursued development of directional towed arrays for reception of active sonar signals. This implementation is particularly appealing since the left/right position of a target can be identified using a simple omnidirectional or axis-symmetric source and a single line array of directional hydrophones.

II. DIRECTIONAL HYDROPHONE DESIGN IN TOWED SYSTEMS

The directional hydrophones developed and tested under the SDA and MMDTA projects consisted of an omnidirectional hydrophone combined with two dipole hydrophones. One such design is depicted in Fig. 2. The dipole hydrophones were oriented to measure the acoustic particle velocity along two axes (x and y) perpendicular to the array axis (z).

In this example, the dipole hydrophones consisted of geophones encapsulated in syntactic foam to achieve approximate neutral buoyancy. The geophones had a nominally flat response of 23.6 V/(m/s) above a highly damped ($\zeta = 0.33$) 28-Hz resonance. The reader is referred to Abraham[1] for further details of this sensor and to Gabrielson et al.[2] for design of a similar sensor.

Cardioid hydrophone groups can be formed in the same manner as for conventional omnidirectional hydrophones. An "extended sensor" or "high wavenumber filter" is simply a number of hydrophones distributed within half of the design acoustic wavelength ($\lambda_d/2 = c/2f_d$). Each group is wired together in either series or parallel (or a combination of both) to minimize electrical noise and maximize sensitivity. The omni and dipole outputs are digitized by three separate analog to digital converters that are part of the array telemetry system. Additionally, at least one roll sensor is needed to provide a reference to gravity. Some systems integrate the roll sensor with the dipole sensor outputs and only digitize the dipole response steered to the horizontal. This configuration preserves the left/right bearing discrimination capability but loses the full elevation angle steering capability.

Several physical mounting systems have been used for directional hydrophones in towed arrays. These designs include suspension in open-cell foam, rubber lobe-mounts, and suspension along internal axial strength members. These are illustrated in Fig. 3. The open-cell foam provides excellent mechanical isolation due to its low stiffness but the sensors may rotate with respect to the array boot leading to angular orientation uncertainty. The lobe mounts contact the boot directly, and thus sensor orientation is not an issue but a more direct coupling of the wall motion will exist compared to the foam mount. The axial strength members provide alignment of all the hydrophones in the array module at the cost of coupling axial motion into the response. The use of axial strength members with acceleration canceling omnidirectional hydrophones is appealing because the dipole sensors as oriented in Fig. 2 will have a null in the axial direction. The off-axis sensitivity of accelerometers and geophones is typically 4% (-28 dB) or less. None of the mounting systems are optimal, and sensor orientation and ultimately acoustic performance must be weighed against self-noise performance.
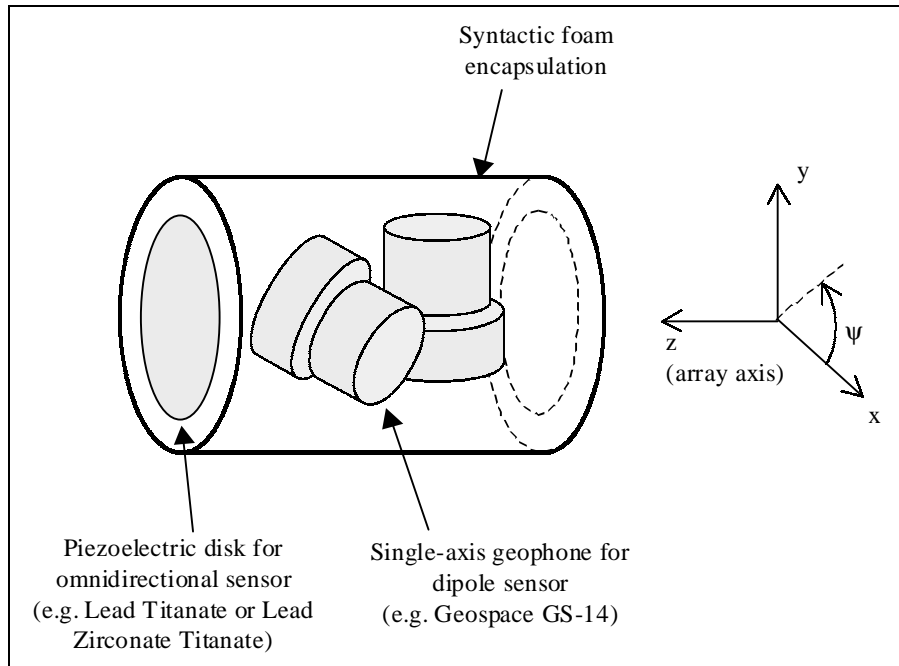
FIG. 2. Example of directional hydrophone components.
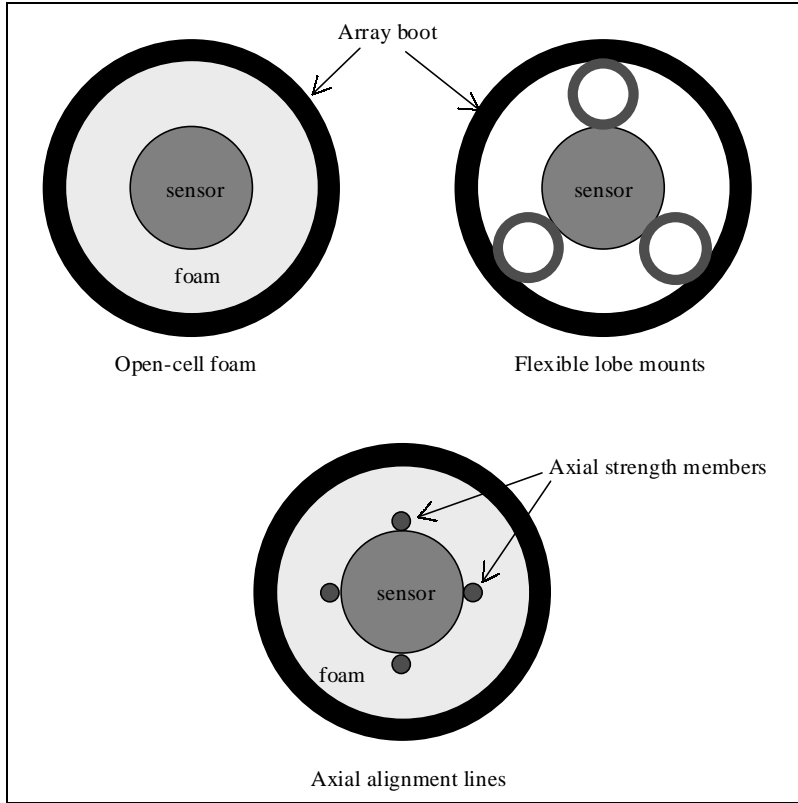
FIG. 3. Directional hydrophone mounting schemes.

III. DIRECTIONAL HYDROPHONE ARRAY ACOUSTIC OPERATION

By combining the calibrated pressure outputs from the omnidirectional and dipole hydrophones, a cardioid response at any elevation angle, ψ, can be obtained. This is expressed mathematically as,

$$P_{cardioid}(\psi) = \frac{P_{omni} + P_x \cos(\psi) + P_y \sin(\psi)}{2}. \tag{1}$$

The directivity index (DI) for a single dipole hydrophone is 4.8 dB. If a cardioid response is formed as in Eq. (1), then it will also have a DI of 4.8. Weighting the dipole response by a factor of three greater than the omnidirectional response forms a beampattern with a DI of 6. However, this is achieved at the cost of losing the uni-directional response null.

Apart from forming the cardioid (or dipole) response, array processing for the directional hydrophones parallels that of omnidirectional hydrophones. Conventional and adaptive[3] beamforming methods have been used to examine the noise field to which omnidirectional and dipole hydrophones are subject inside a fluid-filled towed array

module. The MMDTA project emphasized different modes in which a directional hydrophone array could be operated: conventional, dipole-only, or cardioid. For target searches near broadside (e.g. +/- 45°), the dipole-only mode foregoes the left/right bearing discrimination but gains excellent end- and forward-fire noise rejection. Additionally, the vertical distribution of ambient noise from wave breaking[4] generally has maxima at angles pointing towards the surface and bottom, so the horizontal dipole response can achieve a DI in excess of 4.8 on the group level.

The two-axis dipole hydrophone array discussed thus far has the obvious disadvantage that the acoustic particle velocity along the array axis is not measured. One could construct a three-axis dipole sensor for this purpose, and rejection of own-ship noise is one resulting advantage for beams steered towards end-fire.

IV. DIRECTIONAL HYDROPHONE SELF-NOISE PERFORMANCE

Self-noise is defined as any signal in the sensor response that is uncorrelated with the desired acoustic signal. For both omnidirectional and dipole hydrophones, electronic noise, cable strum, array strum, turbulent boundary layer noise, and hose wall vibration all contribute to self-noise. The electronic noise performance of dipole hydrophone parallels that of conventional hydrophones with the exception of moving coil geophones, which have a low output impedance unlike most piezoelectrics. Proper buffer electronics must be selected to ensure sensor output compatibility with the array telemetry system. Additionally, if the dipole sensor consists of a motion sensor with an in-band resonance, particular care must be taken to assure that the resonance does not electrically saturate the array analog to digital converter during towing operations.

The transverse component of cable strum that is not damped out by a Vibration Isolation Module (VIM) will be measured by dipole hydrophones as noise. Additionally if the array acoustic module itself is not neutrally buoyant, then it may strum at low tow speeds and further contribute to dipole hydrophone self-noise.

The turbulent boundary layer that develops over an array contributes significantly to the self-noise levels of both omnidirectional and dipole hydrophones. The fluctuating wall pressure and wall shear stress excite the array hose. Evanescent and propagating waves are excited in the array that contribute to sensor self-noise. Peloquin[5] gives the response of shell with inner and outer fluid loading. Examples of the ratio of outer pressure (e.g., from the turbulent boundary layer) to inner pressure (what the sensor responds to) for a 7-cm outer-diameter flexible cylinder are shown in Fig. 4. The $n = 0$ response is the fluid or breathing wave. The $n = 1$ response is a bending or shear wave. The $n = 2$ lobar response cuts on at approximately 46 Hz for this cylinder. All three of these waves are dispersive. The dipole hydrophones will response primarily to the bending wave because they are essentially uniaxial motion sensors (or equivalently pressure gradient sensors). Because the turbulent boundary layer wall pressure is homogeneous across the circumference of the array (e.g., there is no preferred orientation or statistical variation), the "X" and "Y" dipole hydrophones should have the same self-noise response.
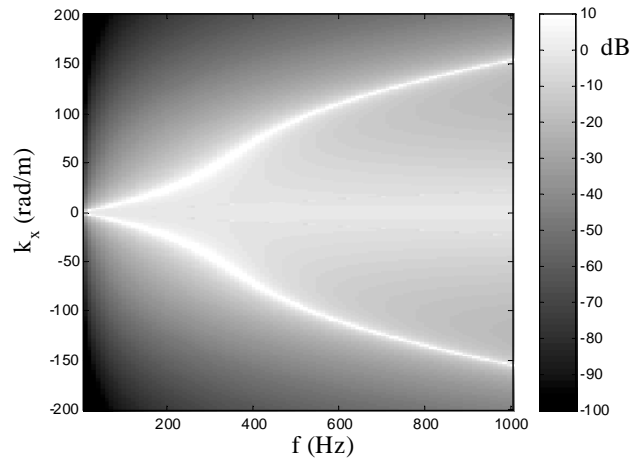
(a) n = 0
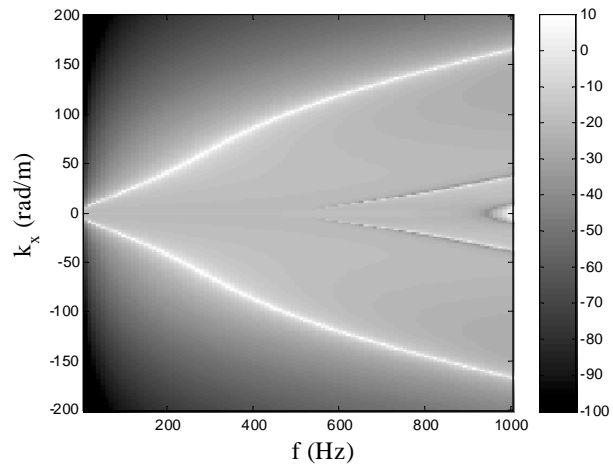
(b) n = 1
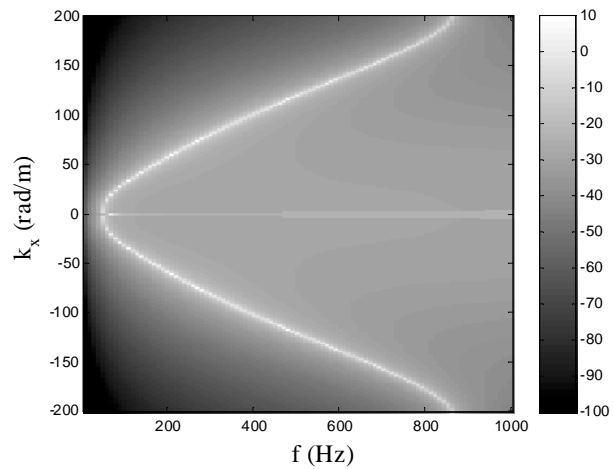
(c) n = 2

FIG. 4. Examples of ratio of inside pressure to outside pressure for infinitely-long fluid-filled cylinder.

The circumferential distribution of pressure or shear stress on the outside of an array can be represented as an infinite sum of "modes." The mode n pressure field can be defined as,

$$P_n(\psi) = \frac{1}{2\pi} \int_{-\pi}^{\pi} P(\psi)e^{-in\psi}d\psi,$$ (2)

where $P(\psi)$ is the pressure at angle ψ. A useful semi-empirical model of the turbulent boundary layer for homogenous flow over a flat plate is given by Chase[6]. This model is given in the wavevector-frequency domain. For the cylindrical array, the spanwise wavenumber at which the mode n response is centered is $k_z = n/a$ where a is the cylinder outer radius. To first order, the flat plate turbulent boundary layer model can be assumed to hold for flow over a cylinder except, perhaps for very large ratios of the boundary layer thickness to the cylinder radius, δ/a. The reader is referred to Ackroyd[7] for estimates of the boundary layer properties for turbulent flow over long cylinders. The mode n wall pressure axial wavenumber-frequency spectrum can be estimated from the wavevector-frequency spectrum as

$$\Phi_n(k_x,\omega) = \int_{-\infty}^{\infty} \Phi(k_x,k_z,\omega)|H_n(k_z)|^2 dk_z,$$ (3)

where H_n is the response function for a mode n sensor and is given by

$$H_n(k_z) = \frac{\sin[(k_z - n/a)\pi a]}{(k_z - n/a)\pi a}.$$ (4)

Figure 5 shows an example of the estimated mode 1 wall pressure field present on the outside of a 7 cm outer diameter cylinder towed at speed of 20 knots with a 140 cm boundary layer thickness. The majority of the energy from the boundary layer occurs along the convective ridge ($k_x = \omega/U_c$). This relatively high wavenumber energy is easily filtered by the array hose response and group designs. The residual levels at low wavenumbers (e.g., $|k_x| < \omega/c$) remains as the limiting self-noise (the "low wavenumber limit").

Using the mode n component of the turbulent boundary layer wall pressure excitation and the ratio of the inner to outer pressure field (in the wavenumber-frequency domain), the frequency autospectrum of the mode n response can be estimated. For a dipole hydrophone, the mode 1 pressure is related to the farfield pressure (P_{ff}) as

$$|P_{ff}| = \frac{2}{ka}|P_1|,$$ (5)

where $k = \omega/c$ and P_1 is the mode 1 pressure at the dipole hydrophone radius a. Bokde et al.[8] estimated the mode n wall pressure from measured data around the circumference of a cylinder in axial flow. They noted the mode 0 and mode 1 pressure spectra had similar levels. The equivalent farfield pressure for a dipole hydrophone, however, will inherently be noisier than for an omnidirectional hydrophone due to the scaling of (5).

By nature, the dipole hydrophones respond to the spatial gradient of the pressure field, so it is not unexpected that the dipole hydrophones will have higher self-noise levels than omnidirectional hydrophones.
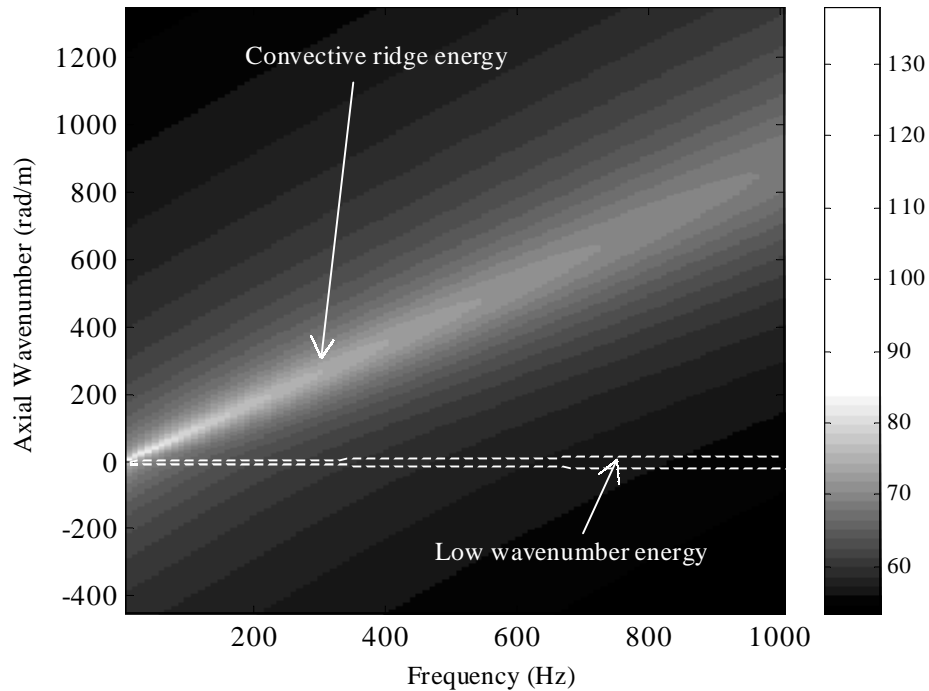
FIG. 5. Example of predicted mode 1 wavenumber-frequency spectrum for external flow over a cylinder.

An example of the predicted mode 1 self-noise is shown in Fig. 6 for tow speeds of 5, 10, 15, and 20 knots. This estimate is only for the contributions from the turbulent boundary layer wall pressure to a single hydrophone (length 5.1 cm and diameter 1.4 cm) inside a 7-cm outer-diameter flexible, fluid-filled cylinder. In general, the response is dominated by excitation of the bending wave. At higher frequencies, the sensor finite length begins to filter the high wavenumber energy of the bending wave. A longer hydrophone or a group of hydrophones has been shown to further spatially filter this wave energy. At low speeds, the dipole hydrophone response may also be limited by cable strum, ambient acoustic noise, electronic noise, or a combination of these.

Experimental measurements of the dipole self-noise in a towed array also showed the possibility of "leakage" of energy of higher order modes into the mode 1 response. Near the cut-on frequency of a lobar mode, the impedance of the cylindrical structure is very low, and the high vibration levels can bleed into other modes due to imperfect circular geometry. For example, elevated self-noise levels around the mode 5 cut-on frequency have been measured. These noise augmentations were not speed dependent but were found to decrease when the array fill fluid was pressurized to minimize geometric distortions.

Modeling and measurements of the performance of dipole hydrophones in towed arrays suggest that the self-noise field in a fluid-filled cylinder excited by a turbulent boundary layer precludes meaningful use at low frequencies. But, the exact frequencies of this usefulness depend on many factors including primarily the tow speed, array diameter, and ambient noise. Signal-free reference noise cancellation has been implemented using accelerometers designed with low acoustic sensitivity to achieve up to 20 dB of noise reduction at low frequency. To date, effective use of dipole hydrophone technology in towed systems has been with mid-frequency arrays at low tow speeds. The choice of the type of dipole sensor (e.g. accelerometer, geophone, displacement sensor) depends essentially on electronic performance and does not have an effect on the flow-induced self-noise limits. Using solid-filled towed arrays with dipole sensors is not expected to improve self-noise because the bending or shear wave would still significantly contribute to the dipole hydrophone response.
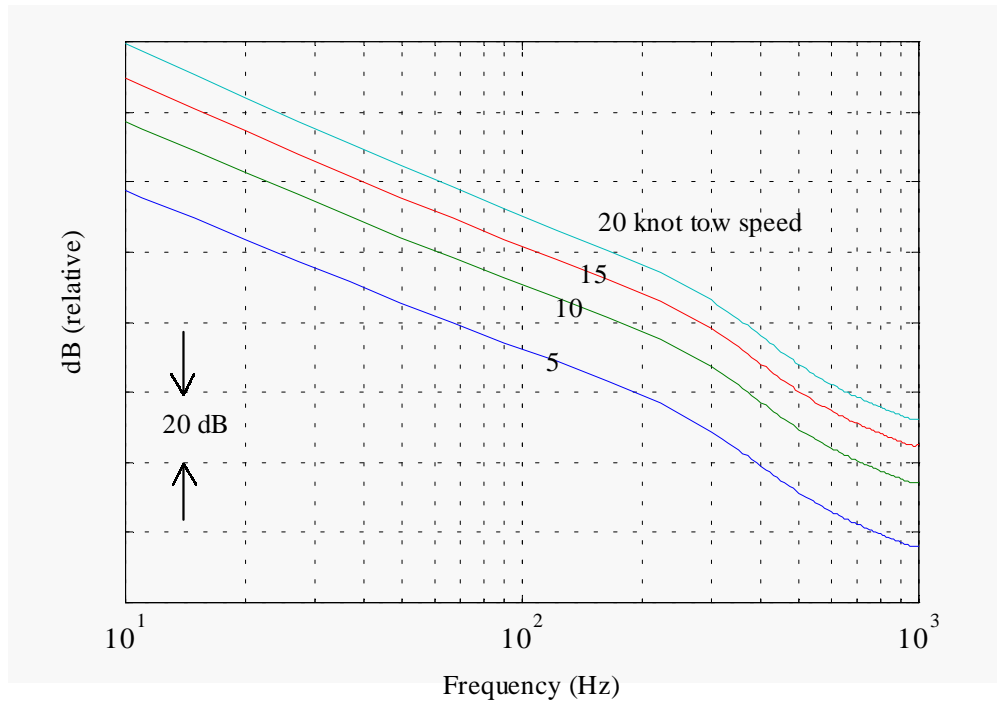
FIG. 6. Example of dipole hydrophone self-noise prediction.

V. CONCLUSIONS

The design and use of directional hydrophones for fluid-filled towed arrays was discussed. The primary noise mechanism for dipole hydrophones was shown to be a bending or shear wave in a fluid-filled cylinder. The turbulent boundary layer flow around the array excites many modes of response include the $n = 0$ breathing wave and the $n = 1$ bending wave. The dipole hydrophone responds primarily to the mode 1 pressure field inside the array (related to the fluid velocity). The self-noise is highly speed and frequency dependent. The self-noise can be minimized by using an extended

hydrophone to filter out high wavenumber energy. The dipole hydrophone performance at low frequency is fundamentally limited by the low wavenumber energy present in the towed array system.

REFERENCES

1. M. Abraham, "Low-Cost Dipole Hydrophone for Use in Towed Arrays," in <u>Proceedings of the Workshop on Acoustic Particle Velocity Sensors: Design, Performance, and Applications</u>, American Institute of Physics Conference Proceedings 368, pp. 189-201 (1996).

2. T. B. Gabrielson, D. L. Gardner, and S. L. Garrett, J. Acoust. Soc. of Am., **97**, 2227-2237 (1995).

3. D. H. Johnson and D. E. Dudgeon, <u>Array Signal Processing</u> (Prentice-Hall, Englewood Cliffs, NJ, 1993), pp. 355-358.

4. G. R. Fox, J. Acoust. Soc. of Am., **36**, 1537-1540 (1964).

5. M. S. Peloquin, "Forced Harmonic Vibration of the Generally Orthotropic Cylindrical Shell With Inner and Outer Fluid Loading," NUWC-NPT Technical Report 10,199, Naval Undersea Warfare Center Division Newport, Rhode Island (1992).

6. D. M. Chase, "The Character of the Turbulent Wall Pressure Spectrum at Subconvective Wavenumbers and a Suggested Comprehensive Model," J. of Sound and Vibration, **112**, 125-147 (1987).

7. J. A. D. Ackroyd, "On the Analysis of Turbulent Boundary Layers on Slender Cylinders," J. of Fluids Eng., **104**, 185-190 (1982).

8. A. L. W. Bokde, R. M. Lueptow, and B. Abraham, "Spanwise structure of wall pressure on a cylinder in axial flow," Physics of Fluids, **11**, 151-161 (1999).

Poster Display Information

A LOW FREQENCY MULTIMODE DIRECTIONAL TELESONAR TRANSDUCER

A. L. Butler and J. L. Butler, (Image Acoustics, Inc.,Cohasset, MA 02025)

J. A. Rice, (Naval Postgraduate School, Monterey, CA U.S. Navy Space and Naval Warfare Systems Center, San Diego, CA)

Abstract-**Directional transducers will improve the performance of undersea acoustic modems. Current designs provide only vertical directionality with omni-directionality in the horizontal plane. Horizontal directionality can yield a higher source level and higher received signal to noise through the increase in the DI or equivalently the narrower beam pattern of the device. Moreover, a horizontal steered directive beam allows selective and more secure communications between the nodes of the system. This paper reports the development of a low frequency prototype device that achieves desired directivity by the controlled combining of the three most fundamental extensional modes of vibration of a piezoelectric cylinder.**

I. INTRODUCTION

The multimode directional telesonar transducer provides horizontal directionality through extensional modal addition. Results on a high frequency, 3.5 inch diameter telesonar were presented earlier[1]. The present transducer is a vertical array which is composed of a larger quadrupole 33 mode staved cylinder, a striped tangentially poled dipole cylinder and a pair of 31 mode omni cylinders. By combining these three modes, omni-directional, dipole and quadrupole, horizontal directionality is excited through each rings extensional mode[2]. With this method identical beam patterns may be obtained over a range of frequencies. In addition to horizontal directionality the beam can be electrically steered. It has been shown that highly directive beams may be obtained from spherical transducers[3]. We extend this to the case of a cylindrical radiator. Analytical and finite element modeling were performed to verify expectations before the design was implemented to achieve cardioid and super cardioid horizontal directional patterns. Measured results are presented and are shown to agree reasonably well with calculated results.

II. TRANSDUCER OPERATION

A. Ring Modes

We consider first the transducers modes of operation and resonant frequencies. Figure 1 shows the first three extensional modes of operation. With f_0 the resonant frequency of the "breathing" omni-mode, the resonant frequencies of the higher order extensional modes are given by $f_n = f_0(1 + n^2)^{1/2}$, -where n is the mode number and
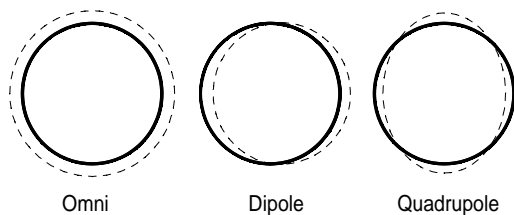
Fig. 1 First three extensional ring modes

Fig. 2 Image Acoustics, Inc. Multimode Telesonar Directional Transducer (3 ring design)

$f_0 = c/\pi D$ with c the sound speed in the ring of mean diameter D. The mode numbers n = 0, 1 and 2 give the frequencies of the omni, dipole and quadrupole modes respectively; thus, $f_1 = f_0\sqrt{2}$ and $f_2 = f_0\sqrt{5}$.

Figure 2 shows the prototype multimode transducer. A resonant frequency of 10.5 kHz was chosen for each ring. A diameter of 4.5 inches was chosen for the omni mode, a diameter of 5.45 inches for the dipole ring and a diameter of 9 inches for the quad ring. Since this transducer diameter was limited to 6.5" the quad ring was too large. To decrease the quad diameter, twelve glass-reinforced G-10 wedges along with twelve pair of 33 mode piezoelectric bars were use to construct the quad ring. The G-10 is stable with a lower sound speed than PZT and was chosen to yield a reasonably small sized 6.2 inch diameter quad mode cylinder with a resonant frequency in the vicinity of 10.5 kHz. The smaller diameter 10.5 kHz striped tangentially poled dipole ring yields high coupling and a 12 pair electrode segmentation corresponding to the quad ring allowing steering every $360/12 = 30^0$. The segmentation allows the excitation of the quad ring into the quad mode of vibration by reversing the phase in each successive quadrant. The dipole mode is achieved by reversing the phase on one half of the cylinder. The smaller diameter omni mode cylinders are resonant at nearly the same frequency and needs no segmentation for their uniform radial mode motion. Omni directional receiving response is obtained from the omni cylinders.

B. Multimode Approach

In the two-mode method the omni mode has a directivity of 1 while the dipole mode has a figure-eight directivity function cos θ where θ is the cylindrical coordinate azimuth angle in the horizontal plane. If we simply add the two, and normalize, we get

$$p(\theta) = \frac{1+\cos\theta}{2} \qquad (1)$$

which is a cardioid beam pattern function with -3dB value at $\pm 65.5^0$ and a deep back null. This may be better visualized in Fig. 2. Here the cardioid is formed by adding the omni and dipole modes. Both have unity amplitude. Since the "+" half of the dipole is in phase with the corresponding omni half, they both add, doubling the amplitude. The "-" half of the dipole is 180^0 out of phase with the corresponding omni half causing cancellation yielding the cardioid pattern.

In the three-mode method the quadrupole pattern function may be written as cos 2θ. If we combine this with an omni of strength 1 and a dipole of strength 3, we get the "super directive" beam pattern function

$$F(\theta) = 1 + 2\cos\theta + \cos 2\theta \qquad (2)$$

To better visualize the three-mode method, Fig. 4 shows the three-mode pattern synthesis. First the strength 1 omni mode pattern of (a) is added to the strength 1 quadrupole pattern (b) to get the bidirectional pattern (c) of strength 2 with lobes of the same phase. If this is now combined with a strength 2 dipole pattern (d), we get the desired resulting "super directive" pattern (e) of strength 4 which conforms to Eq. (2). The result may be normalized by dividing by 4 to yield a unity value at θ = 0. We also can use trigonometric identities to get the normalized result shown in Eq. (3).
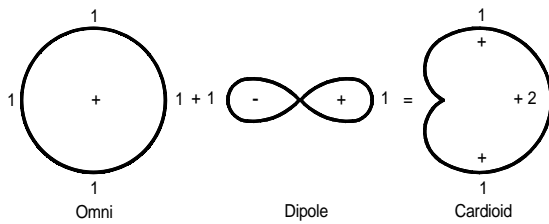
Fig. 3. Two-mode beam synthesis
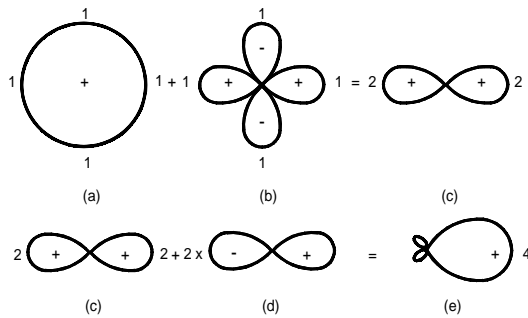
Fig. 4. Three-mode pattern synthesis

$$p(\theta) = \frac{1+2\cos\theta+\cos(2\theta)}{4} = \frac{\cos(\theta)[1+\cos(\theta)]}{2} \qquad (3)$$

As seen, the beam pattern function for this "unique" distribution is the product of a dipole and a cardioid function.

Adjusting the amplitude of the quadrupole to 0.414, while leaving an amplitude of 1 for the omni and dipole modes, results in a "minimalist" super cardioid. We call this a minimalist super cardioid, since it achieves a desirable 90^0 - 3dB beam pattern and 15 dB front-to-back ratio with minimal dependence on the higher modes. Equation (3) can be rewritten in a general form as

$$p(\theta) = \frac{1+A\cos\theta+B\cos(2\theta)}{1+A+B} \;. \qquad (4)$$

For the case of the cardioid A=1 and B=0. For the unique super cardioid A=2 and B=1 and for the minimalist super cardioid A=1 and B=0.414, our current case of interest.

III. MEASURED RESULTS

The measured Transmitting Voltage Response, TVR, for the omni, dipole and quad sections driven separately are shown in Fig. 5. The measurements on the dipole and quad units were made, for convenience, with half of each transducer driven in series with the second half. The TVR results would be 6 dB higher if the sections were all driven in parallel. A comparison with theoretical[4,5] and finite element models indicates that the measured omni response is very close to prediction. The dipole resonance is approximately 0.5 kHz higher than expected with reduced output below resonance. The quad resonance is approximately 1.0 kHz higher than expected. (The first experimental quad mode ring yielded a resonance closer to the calculated value.) The receiving free field voltage sensitivities for each ring are shown in Fig. 6. The response of the omni ring falls off above resonance and is reasonably flat below resonance as expected. These resonant frequencies are higher than the TVR values because of the open circuit conditions. All the sensitivities are above –190 dB in the range from 8 kHz to 13 kHz.
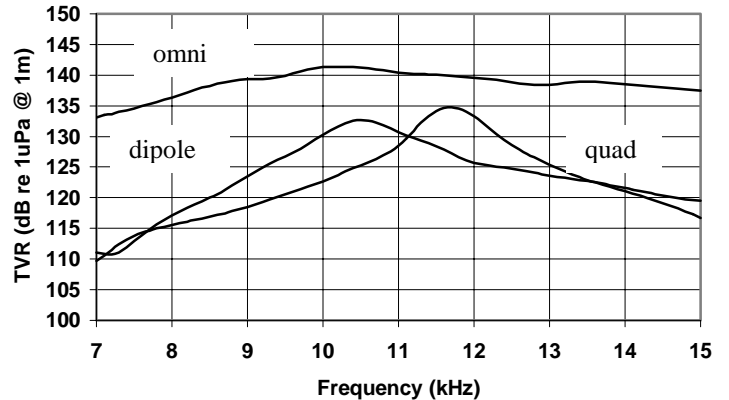
Fig. 5 Multimode Telesonar Directional Transducer (3 ring design) transmitting voltage response
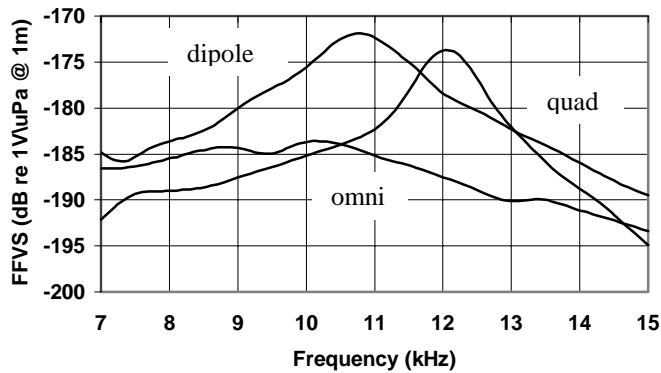
Fig. 6 Multimode Telesonar Directional Transducer (3 ring design) receiving response

The horizontal measured beam patterns, at 10.5 kHz, for the dipole and quad modes are shown in Figs. 7 and 8. As seen, the dipole and quad nulls vary from –15 dB to an exceptional –30 dB values. The lobe levels are essentially the same for the dipole case and nearly the same for the quad. The horizontal beam pattern results for summing the omni with amplitude 1, dipole with amplitude 1 and quad with amplitude 0.414 are shown in Fig. 9. As seen These results are very close to the ideal levels of -3 dB at 45^0, -12 dB at 90^0 and –15 dB at 180^0 given by Eq. (4) with A=1 and B=0.414.
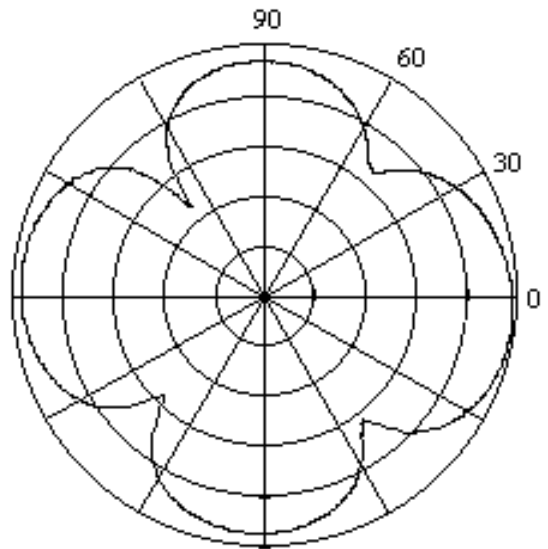
Fig. 8 Multimode Directional Telesonar Transducer Quad cylinder horizontal beam pattern at 10.5 kHz

Fig. 9 Multimode Directional Telesonar Minimalist Super Cardioid horizontal beam patterns (10 dB/div)

Fig. 7 Multimode Directional Telesonar Transducer Dipole cylinder horizontal beam pattern at 10.5 kHz

IV. SUMMARY AND CONCLUSIONS

We have presented results that have demonstrated the feasibility of achieving a constant beamwidth horizontal directional response using a combination of the omni, dipole and quadrupole extensional modes of vibration of co-resonant cylindrical transducers. The measured results substantiated predicted results. Over the frequency range of 8 to 13 kHz the beamwidths were 90° with -10 dB at 90° and a front-to-back ratio of 15 dB.

ACKNOWLEDGMENTS

REFERENCES

[1] A. L. Butler and J. L. Butler, Image Acoustics, Inc., Cohasset, MA 02025, W. L. Dalton, Acoustikos, Cataumet, MA 02534, J. A. Rice, U.S. Navy Space and Naval Warfare Systems Center, San Diego, CA 92152, "Mutlimode Directional Telesonar Transducer", Oceans 2000 Proceedings, Providence, RI

[2] S.L. Ehrlich and P.D. Frelich, "Sonar Transducer", U. S. Patent 3,290,646, December 6, 1966

[3] J. L. Butler and S. L. Ehrlich, " Superdirective spherical radiator," J. Acoust. Soc. Am., 61, 1427-1431 (1977)

[4] R. S. Gordon, L. Parad and J. L. Butler, "Equivalent circuit of a ring transducer operated in the dipole mode," J. Acoust. Soc. Am. 58, 1311-1314 (1975)

[5] "RING" Transducer design program, Image Acoustics, Inc., 97 Elm Street, Cohasset, MA 02025

Directional Hydrophones for Towed Arrays

Simon Tanner
Underwater Sensors and Oceanography
Defence Evaluation Research Agency
Winfrith Technology Centre
Dorset, United Kingdom DT2 8XJ

Abstract The poster describes the development of different hydrophones capable of measuring the vector component of the acoustic wave, thus providing directional information orthogonal to the axis of the towed array. The preferred solution is the DERA Low Profile Accelerometer (LPA) hydrophone, which comprises a biaxial accelerometer to form two orthogonal dipoles and two omnidirectional hydrophones wired in parallel to give a single high capacitance output. When matched in phase and amplitude these sensors can provide a steerable unidirectional (cardioid) output. Sea trials have shown that these hydrophones can provide instantaneous resolution of left/ right ambiguities and offer increased gain with respect to isotropic noise. This work was funded by the Ministry of Defence Corporate Research Programme contract number TG1 2.2/012/u.

Executive Summary

A number of hydrophones have been developed by DERA under the MoD sponsored Sonar Transducer Technology programme. These hydrophones have an inherent directivity despite their small dimensions and typically consist of 2 orthogonal sensors to measure the vector component of the acoustic wave, together with a conventional pressure hydrophone. When suitably matched in phase and amplitude a unidirectional (cardioid) beampattern can be obtained by combining the dipole output of the vector sensor with the monopole output of the pressure hydrophone. A key challenge is that these sensors must be compact (less than 30mm diameter), while achieving the required directivity and sensitivity, against a background of high vibrational noise, within the towed array. They must withstand hydrostatic pressures of 100 MPa (equivalent to an ocean depth of 1000m) while sensing dynamic pressures as small as 100 µPa.

Geophone, accelerometer and pressure gradient designs have been developed and have been extensively tested both in the laboratory and at sea.

Traditional pressure gradient designs offer a poor low frequency sensitivity, are susceptible to noise and are unsuitable for small diameter arrays. The geophone-based hydrophones performed well especially at lower frequencies and were the lowest cost at approximately $150 per unit using Geospace GS1L9 geophones. The accelerometer-based hydrophones offered the best bandwidth/ sensitivity product and were the preferred solution especially for use as receivers in an active sonar system. Commercial devices

were too large and expensive and a Low Profile Accelerometer (LPA) hydrophone was developed by DERA.

A Vector Towed Array was developed to demonstrate the ability of an array of directional hydrophones to resolve the bearing ambiguity and to establish their self-noise response. The array consisted of 32 LPA hydrophones each containing a pressure hydrophone and a pair of orthoganal accelerometer outputs.

This array was evaluated during a trial at the Naval Surface Warfare Centre facility in Idaho, USA. The self-noise response of vector hydrophones is critical to their application. A detailed analysis of their self–noise performance is beyond the scope of this paper, however analysis of the trials data show that the array is clearly able to resolve both port and starboard contacts instantaneously and under realistic operational conditions. The beamformed array resolves the target ambiguity with discrimination between port and starboard targets of up to 20 dB

a) Conventional array response

b) Directional array response
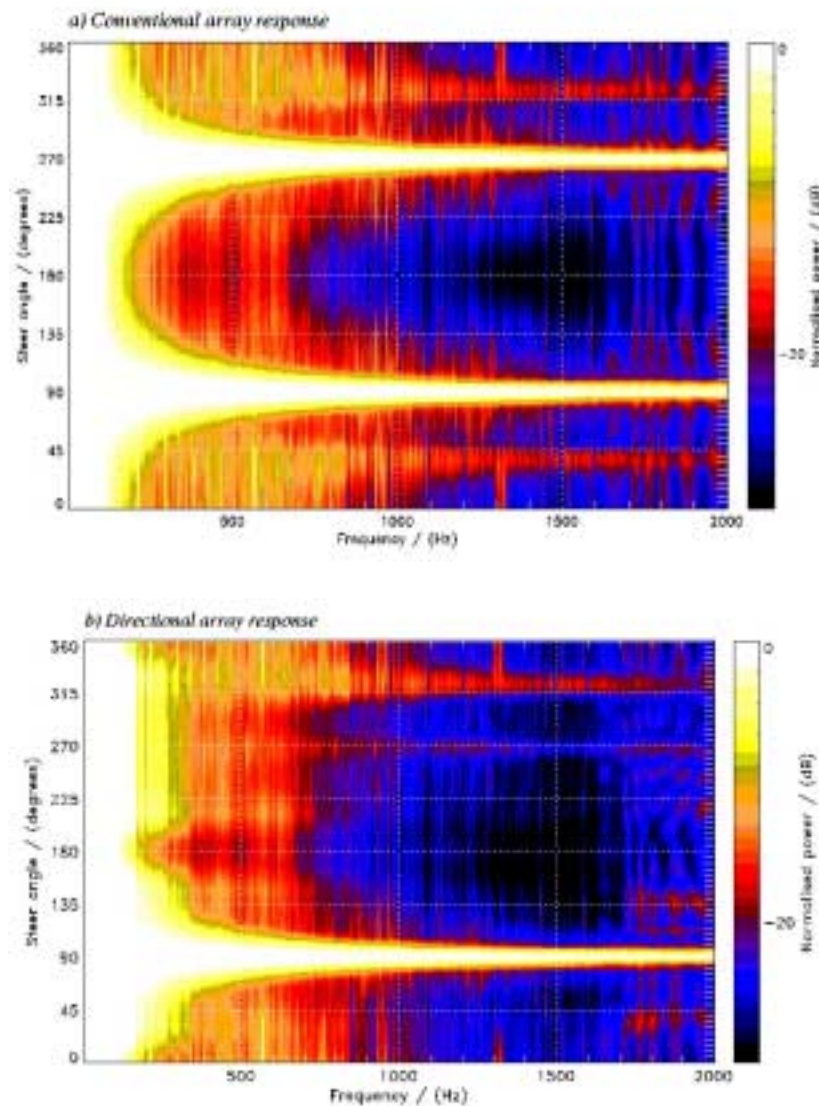
Beamformed response to a starboard target of 16 LPA hydrophones in omni and cardioid modes

The DERA LPA hydrophone is the smallest, high-performance directional sensor tested under this programme and its ability to instantaneously resolve left right ambiguities has been successfully demonstrated at sea. The ability to resolve bearing ambiguities could provide the Navy with an obvious operational advantage particularly in shallow water where manoeuvring constraints may be greater.

Acknowledgments

List of Attendees

LIST OF ATTENDEES

Bruce M. Abraham (Speaker)
Anteon Corp.
240 Oral School Road
Mystic, CT 06355-1208
Tel: (860)572-9600
Email: babraham@anteon.com

Boris Aronov (Speaker)
U. of Mass., Dartmouth (also BTECH)
Acoustics Research Laboratory
22 Seabeds Way, #12.
Needham, MA 02494
Tel: (781) 455-6949
Email: BAronov@Mediaone.net
Fax: (508) 999-9262

P. David Baird (Speaker)
EDO Corporation
2645 South 300 West
Salt Lake City, UT 84115
Tel: (801) 486-7481 Ext. 311
Email: dbaird@edoceramic.com

Kim C. Benjamin
NUWC Division Newport
1176 Howell Street
Newport, RI 02840
Tel: (401) 832-5320
Email: benjaminkc@npt.nuwc.navy.mil

Jeffrey E. Boisvert
NUWC Division Newport
1176 Howell Street
Newport, RI 02841
Tel: (401) 832-2498
Email: boisvertje@npt.nuwc.navy.mil

David Brown (Speaker)
U. of Mass., Dartmouth (also BTECH)
Dept. of Electrical and Comp. Engineering
285 Old Westport Road
North Dartmouth, MA 02747-2300
Tel: (508) 999-8479
Email: dbrown@umassd.edu
Fax: (508) 999-9262

Alex Butler
Image Acoustics
97 Elm Street
Cohasset, MA 02025
Tel: (781) 383-2002
Email: butler@imageacoustics.com

Steven Butler
NUWC Division Newport
1176 Howell Street
Newport, RI 02841
Tel: (401) 832-5101
Email: butlersc@npt.nuwc.navy.mil

John Cannon
Office of Naval Intelligence
1708 Cody Drive
Silver Springs, MD 20902
Tel: (301) 669-4787
Email: jcannon@nmic.navy.mil

Donna Y. Chapman
NUWC Division Newport
1176 Howell Street
Newport, RI
Tel: (401) 832-8337
Email: chapmandy@nuwc.npt.navy.mil

Mark Chase
Naval Research lab
4555 Overlook Avenue, SW
Washington, DC 20375
Tel: (202) 767-3313
Email: chase@anvil.nrl.navy.mil

Cathy Ann Clark
NUWC Division Newport
1176 Howell Street
Newport, RI 02841-1708
Tel: (401) 832-8182
Email: clarkca@npt.nuwc.navy.mil

Pierre Corriveau
NUWC Division Newport
1176 Howell Street
Newport, RI 02841
Tel: (401) 832-2724
Email: corriveaupj@npt.nuwc.navy.mil

Donald Cox
NUWC Division Newport
1176 Howell Street
Newport, RI 02841
Tel: (401) 832-7438
Email: coxdl@npt.nuwc.navy.mil

Glenn Cox
NUWC Division Keyport
610 Dowell Street
Keyport, WA 98345
Tel: (360) 315-7405
Email: cox@kpt.nuwc.navy.mil

Benjamin Cray (Speaker/Co-Chair)
NUWC Division Newport
1176 Howell Street
Newport, RI 02841-1708
Tel: (401) 832-8454
Email: crayba@npt.nuwc.navy.mil

Alan Curtis
MSI
521 Great Road
Littleton, MA 01460
Tel: (978) 486-0404 Ext. 208
Email: curtis@matsysinc.com

Scott Dobson
Electric Boat Corporation
75 Eastern Point Road
Groton, CT
Tel: (860) -433-7927
Email: sdobson@ebmail.gdeb.com

Barry Doust
BAE Systems
115 Bay State Drive
Braintree, MA 02184
Tel: (781) 848-3400 Ext. 561
Email: barry.doust@baesystems.com

Gerald D'Spain (Speaker)
Marine Physical Laboratory of the
Scripps Institution of Oceanography
291 Rosecrans Street
San Diego, CA 92106
Tel: (858) 534-5517
Email: gld@mpl.ucsd.edu

Joe Ducas
Lockheed Martin
25 Enterprise Center
Middletown, RI 02842
Tel: (401) 848-8154
Email: joseph.ducas@lmco.com

Roy Elswick (Session Chair)
Office of Naval Research
800 N. Quincy Street
Arlington, VA 22217
Tel: (703) 588-1036
Email: elswick@onr.navy.mil

Victor F. Evora
NUWC Division Newport
1176 Howell Street
Newport, RI 02841
Tel: (401) 832-8475
Email: evoravf@aol.com

Kurt Eyster
NUWC Division Newport
1176 Howell Street
Newport, RI 02841
Tel: (401) 832-3020

Sezin Feher
Johns Hopkins U./APL
11100 Johns Hopkins Road
Laurel, MD 20723
Tel: (443) 778-8913
Email: sezin.feher@jhuapl.edu

David Feit
NSWC Carderock Division
9500 MacArthur Blvd.
W. Bethesda, MD 20817
Tel: (301) 227-1293
Email: feitd@nswccd,navy.mil

Patrick Ferat
Johns Hopkins U./APL
11100 Johns Hopkins Road
Laurel, MD 20723
Email: patrick.ferat@jhuapl.edu

Glen Ferguson
Benthos
49 Edgerton Drive
N. Falmouth, MA 02556
Tel: (508) 563-1000
Email: gferguson@benthos.com

Stephen E. Forsythe
NUWC Division Newport
1176 Howell Street
Newport, RI 02841
Tel: (401) 832-8963
Email: forsythese@npt.nuwc.navy.mil

Ryan Franklin
Sittel Corporation
1206 Foothill Road
Ojai, CA 93023-1727
Tel: (805) 646-0700
Email: ryanf@sittelcorp.com

Tim French
DERA, Dera Winfrith
Winfrith Technology Centre
Dorchester, UK DT2 8X5
Tel: (44) 01305-212470
Email: tafrench@dera.gov.uk

Bernard Fromont
Thomas Marconi Sonar
525 Route des Dollines, BP A57
06903 Sophia Autipolis, France
Tel: (33) 49296-3061
Email: bernard.fromont@
          tms.thomson.csf.com

Thomas B. Gabrielson (Speaker)
Applied Research Laboratory
Penn State University
P.O. Box 30
State College, PA 16804
Tel: (814) 865-1370
Email: tbg3@psu.edu

Jim Glynn
MSI
521 Great Road
Littleton, MA 01460
Tel: (978) 486-0404
Email: glynn@matsysinc.com

Jim Hardiman
Benthos
49 Edgerton Drive
N. Falmouth, MA 02556
Tel: (508) 563-1000 Ext. 605
Email: jhardiman@benthos.com

Mike Higgins (Speaker)
RDA Incorporated
P.O. Box 49
Doylestown, PA 18901
Tel: (215) 340-9514
Email: mehiggs@voicenet.com
Fax: (215) 340-9515

Robert S. Janus
NUWC Division Newport
Newport, RI 02841
Tel: (401) 832-5113
Email: janusrs@npt.nuwc.navy.mil

Kirk Jenne
NUWC Division Newport
1176 Howell Street
Newport, RI 02841
Tel: (401) 832-5319
Email: jenneke@npt.nuwc.navy.mil

Ted Kazmar
BAE Systems
115 Bay State Drive
Braintree, MA 02184
Tel: 781/848-3400
Email: ted.kazmar@baesystems.com

Richard Keltie (Speaker)
North Carolina State University
Dept. of Mechanical and Aerospace Eng.
Box 7910, 3211 Broughton Hall
Raleigh, NC 27695
Tel: (919) 515-5258
Email: keltie@eos.ncsu.edu

Gerald C. Lauchle (Speaker)
APL, Penn State University
P.O. Box 30
State College, PA 16804
Tel: (814) 863-7145
Email: gcl1@psu.edu
Fax: (814) 865-3119

John Law
NUWC Division Newport
1176 Howell Street
Newport, RI 02841
Tel: (401) 832-8189
Email: law_j@nuwc.npt.navy.mil

Gordon Lee
2118 N. Monroe Street, # 56
Arlington, VA 22207

Jan Lindberg
Office of Naval Research
800 N. Quincy Street
Arlington, VA 22217
Tel: (703) 696-7116
Email: lindbej@onr.navy.mil

L. Dwight Luker
NUWC, Code 2161, Bldg. 1171B
1170 Howell Street
Newport, RI 02841
Tel: (401) 832-8962
Email: lukerld@npt.nuwc.navy.mil

Gordon Marshall
Naval Air Systems Command
Cedar Point Road, Bldg. 2185, Suite 1144
Patuxent River, MD
Tel: (301) 342-0905
Email: marshallgk@navair.navy.mil

James McConnell (Speaker)
Acoustech Corporation
P.O. Box 139
State College, PA 16804-0139
Tel: (814) 867-2629
Email: Jamesamcconnell@hotmail.com
Fax: (814) 867-2760

James McEachern (Workshop Sponsor)
Office of Naval Research
800 N. Quincy Street
Arlington, VA 22217-5660
Tel: (703) 696-6462
Email: james_mceachern@onr.navy.mil
Fax: (703) 696-3390

Ray Melusky
Office of Naval Intelligence
4251 Suitland Road
Washington, DC 20395
Tel: (301) 669-3973
Email: rmelusky@nmic.navy.mil

Mark Moffett
NUWC Division Newport
Newport, RI 02841
Tel: (401) 832-5116
Email: moffettmb@npt.nuwc.navy.mil

Thomas R. Morgan
4916 Gainsborough Drive
Fairfax, VA 22032
Tel: (703) 323-5270
Email: parktrent@earthlink.net

Richard Nadolink (Workshop Sponsor)
NUWC, Code 10, Building 990-6
Newport, RI 02841
Tel: (401) 832-6760
Email: nadlinkrh@npt.nuwc.navy.mil
Fax: (401) 832-3927

Tetsuro Oishi
U. of Massachusetts, Dartmouth
291 Allen Street, 2nd Flr.
New Bedford, MA 02740
Tel: (508) 990-8343
Email: toishi@umassd.edu

Stephane Pairault
Thomson Marconi Sonar
525 Route des Dollines BP AST
06903 Sophia Antipolis, Cedex, France
Tel: (33) 492964065
Email: stephane.pairault@
            tms.thomson.csf.com

Jean Piquette
NUWC Division Newport
1176 Howell Street
Newport, RI 02871
Tel: (401) 832-8468
Email: piquettejc@npt.nuwc.navy.mil

John H. Pierse
Johns Hopkins University/APL
Submarine Development Squadron 12
Naval Submarine Base
Groton, CT 06349
Tel: (860) 694-3169
Email: jpierse@csds12.navy.mil

Jim Powers
NUWC Division Newport
Newport, RI 02841
Tel: (401) 832-5091
Email: powersjm@npt.nuwc.navy.mil

Deepak Ramani
NUWC Division Newport
1176 Howell Street
Newport, RI 02841
Tel: (401) 832-2819
Email: ramanidv@npt.nuwc.navy.mil

Lawrence Reinhart
U. of Massachusetts, Dartmouth, ECE Dept.
285 Old Westport Road
Dartmouth, MA 02747
Tel: 508/910-6978
Email: lreinhart@umassd.edu

Russ Roberts
Enigmatics, Inc.
P.O. Box 537
New Harmony, UT 84757
Tel: (435) 865-7822
Email: k7usn@ieee.org

Pete Scala
ASTO
2531 Jefferson Davis Highway
Arlington, VA 22242
Tel: (202) 781-1218
Email: scalapa@navsea.navy.mil

Dean J. Schmidlin
U. of Massachusetts, Dartmouth
285 Old Westport Road
North Dartmouth, MA 02747
Tel: (508) 999-8469
Email: dschmidlin@umassd.edu

Howard H. Schloemer
OASIS
12 Laurel Hill Drive, South
Niantic, CT 06357
Tel: (860) 739-6506
Email: hhjischloemer@msn.com

Fred Schloss (Speaker)
Wilcoxon Research
21 Firstfield Road
Gaithersburg, MD 20878
Tel: (301) 330-8811
Email: senors@wilcoxon.com or
frschloss@starpower.net

Manuel Silvia (Speaker)
SITTEL Corporation
1206 Foothill Road
Ojai, CA 93023-1727
Tel: (805) 646-0700
Email: msilvia@sittelcorp.com
Fax: (805) 646-0055

Jim Smith
EDO Corporation
1444 E. Sherman Ave.
Salt Lake City, UT 84105
Tel: (801) 541-4512
Email: jsmith@edoceramic.com

Murray Strasberg
NSWC Carderock Division
West Bethesda, MD
Tel: (301) 227-1389
Email: strasbergm@nswccd.navy.mil

Mike Sullivan
Electric Boat
33 Simpson Lane
Oakdale, CT 06370
Tel: (860) 848-1404

Simon Tanner
DERA
Dera Winfrith Technology Centre
Dorchester, UK DT2 8XJ
Tel: (46) 1305-212476
Email: stanner@dera.gov.uk

Frank Tito
NUWC Division Newport
1176 Howell Street
Newport, RI 02841
Tel: (401) 832-5090
Email: titofa@npt.nuwc.navy.mil

Glenn Volkema
U. of Massachusetts, Dartmouth
285 Old Westport Road
North Dartmouth, MA 02747
Email: gvolkema@umassd.edu

John R. Welch
NUWC Division Newport
1176 Howell Street
Newport, RI 02841
Tel: (401) 832-2089
Email: welchjr@npt.nuwc.navy.mil

Fred Wilcoxon
Wilcoxon Research
21 Firstfield Road
Gaithersburg, MD 20878
Tel: (301) 330-8811
Email: fred@wilcoxon.com

Paul Wlodkowski (Speaker)
Wilcoxon Research
21 Firstfield Road
Gaithersburg, MD 20878
Tel: (301) 947-7964
Email: paulw@wilcoxon.com

Paul W. Wynn
NUWC Division Newport
1176 Howell Street
Newport, RI 02871
Tel: (401) 832-4345
Email: wynnpw@npt.nuwc.navy.mil

Joseph F. Zalesak
NUWC Division Newport
1176 Howell Street
Newport, RI 02842-1708
Tel: (401) 832-9202
Email: zalesakjf@npt.nuwc.navy.mil

Jon Zilius
Office of Naval Intelligence
4956 Swinfor Drive
Fairfax, VA 22032
Tel: (301) 669-3848
Email: jonfxst01@hotmail.com